ALGORITHMIC TECHNIQUES FOR THE ACOUSTICAL ANALYSIS OF EXHAUST SYSTEMS

by

John F Dowling

A Doctoral Thesis
Submitted in partial fulfilment of the requirements
for the award of
Doctor of Philosophy of Loughborough University

April 2005

Acknowledgements

Dr K S Peat, the supervisor for the author of this thesis has shown a deep understanding of the difficulties involved in this research work. The academic and constructive suggestions made by Dr Peat have enabled the author to obtain invaluable skills. The author would like to show his appreciation for all the advice that his supervisor has provided; without this considerable, helpful supervision, the thesis could not have been completed.

The author would also like to thank the commercial company Arvin Meritor for the use of experimental data as a comparison to the theoretical predictions achieved in the thesis. Also, thanks to Sabry Allam and Hans Boden of KTH, Stockholm, for the use of their measurement results from the European Artemis Project concerning a Volvo truck engine. The results obtained through the project have provided a valuable experimental comparison for the theoretical results gained in the thesis.

In particular I wish to convey my sincere thanks to my family and friends who have provided valuable, emotional support throughout the years of research. They have consistently supported and encouraged me during the highs and lows that inevitably come in an undertaking of this nature.

The author would also like to thank the States of Guernsey Education Department and the Disability and Additional Needs Service at Loughborough University for enabling him to realise his potential despite his disability. Finally, the author is grateful for the student sponsorship from Loughborough University that has aided him to complete his doctorial thesis.

Abstract

One dimensional, linear, plane-wave modelling of silencer systems in the frequency domain provides an efficient means to analyse their acoustic performance. Software packages are available to analyse silencers within these modelling parameters; however, they are heavily restricted. The thesis develops an algorithm that increases the computational efficiency of the silencer analysis.

The thesis concentrates on how data, within a software package, is stored, retrieved and analysed. The computational efficiency is increased as a result of the predictable patterns caused by the repetitive nature of exhaust system analysis. The work uses the knowledge gained from the construction of two previous algorithms of similar parameters; it isolates and maximises their advantages whilst minimising their associated disadvantages. The new algorithm is dependent on identifying consecutively sequenced exhaust components and sub-systems of such components within the whole exhaust system.

The algorithm is further generalised to include multiple time-variant sources, multiple radiation points and exhaust systems that have a balance pipe. Another feature of the improved algorithm encompasses the option of modelling secondary noise sources such as might arise from flow generated noise or be included for active noise cancellation systems.

The validation of these algorithmic techniques is demonstrated by comparison of the theoretical noise predictions with experimental or known results. These predictions are achieved by writing computational code using object orientated programming techniques in the language of C++ to implement the algorithms.

Keywords Linear acoustics, Silencer, Algorithm, Transfer matrix, Time-variant Sources, Tailpipe configurations

Symbols

A_j	= Admittance matrix coefficient
A_{max}	= Maximum open area of valve
$A_{\eta d}$	= Area of orifice in the first valve stage
A_p	= Area of pipe
A_v	= Area of the valve
A_w	= Admittance
$\widetilde{A}$	= Open valve area
$\overline{A_v}$	= Mean open area of the valve
a, b, c, d	= Transfer matrix coefficients
[A]	= Admittance matrix
[a], [b]...[j]	= Diagonal matrix of coefficients
B, f, p, q, r	= Integer counter
[B]	= Diagonal load matrix
C, L	= Boolean variable
C_d	= Discharge coefficient
$C_{\bar{d}}$	= mean discharge coefficient
C_v	= Coefficient for the non-dimensional valve open area function
$\overline{C_v}$	= Mean of C_v
$\bar{c}$	= Mean speed of sound of the gas flow
[c]	= Diagonal matrix modelling a Helmholtz resonator
[D], [F]	= Matrices concerning Fourier coefficients of the valve lift curve
{d}	= Pressure vector used to model injected source
E, G	= Reduction matrix coefficients
e	= Integer label denoting a branch or valve of the manifold
e	= Matrix coefficients in Chapter 5
F	= Fork
f	= Matrix coefficients
f_{ig}	= Path fraction variable
f_r	= Resonant frequency
[G], [H]	= General matrices

h,k,m,q,r,u,w,z = Integer counters

h,g = Matrix coefficients in Chapter 5

I_e = Inlet point on a junction

i = $\sqrt{-1}$

[I] = Identity matrix

J = Junction

j = Counter

[J] = Diagonal matrix used in single value decomposition

k = Wave number

L = Length

l = Length of the valve neck

l = Length of pipe in Chapter 5

l_I = Length between source and injected sound

l_P = Length between evaluated source point and the radiation point

l_a = Length between source and microphones one

l_b = Length between source and microphone two

l_r = Radius of valve port

$l_r\eta$ = Distance used to calculate valve open area n

[L] = Set of linear equations

M = cell values of **[M]**

M = Integer counter in Chapter 5

[m], **[n]** = Diagonal matrix of coefficients

[M] = Matrix used in direct measurement of source impedance, post analysis

N = Number of harmonics

n = Number of unknowns

N,n = Integer counter in Chapter 5

n_c = Number of valves, path fraction application

P = Acoustic pressure

P_E = Pressure at an effective source point

P_r = Acoustic pressure at a radiation point

P_s = Acoustic source pressure

P_M = Measured pressure within the atmosphere

P_{max} = Maximum acoustic pressure

$\{\mathbf{P}\}$ = Pressure vector

$\{\mathbf{Q}\}$ = Set of known values

Q = Integer counter

R = Radiation point

$\{\mathbf{r}\}$ = Residual vector used in single value decomposition

S = Source pressure vector coefficient

SID = Integer variable for flowcharts

s = Valve lift

$\{\mathbf{S}\}$ = Source vector

T = Period

t = Time

$[\mathbf{T}]$ = Transfer matrix

U = Acoustic velocity

uo = Number of unmarked outlet associated with the resonator

$[\mathbf{U}]$, $[\mathbf{V}]$ = Orthonormal matrices used in single value decomposition

V = Acoustic mass velocity

V_r = Acoustic mass velocity at a radiation point

V_e = Acoustic mass velocity at an effective source

V_s = Acoustic mass velocity at a source

V_c = Fluid volume of cylinder

v = Acoustic mass velocity associated with the velocity vector

v_{IN} = Injected acoustic mass velocity

$\{\mathbf{V}\}$ = Acoustic mass velocity vector

W = Acoustic power

X, Y = Arbitrary points in a duct

X_v = Point of valve outlet

x = Thickness of valve seat

$\{\mathbf{x}\}$ = vector of unknown values

y = Distance between valve head and valve seat

y_1 = y in the first stage of the valve lift

y_2 = y in the second stage of the valve lift

y_{2h} = Horizontal component of y_2

y_{2v} = Vertical component of y_2

Z = Acoustic impedance

Z_E = Impedance at source evaluation point

Z_L = Load impedance

$[\mathbf{Z}]$ = Diagonal impedance matrix

α = Admittance

β = Number of engine strokes in a cycle

Γ = Cell reference of the admittance matrix

γ = cell value vector $\{\mathbf{d}\}$

η_d = Length of the normal used to calculate valve open area

θ = Crank angle

λ = Wavelength

ξ_E = Non-dimensional source impedance

$\overline{\rho}$ = Mean density of the gas flow

σ = Angular adjustment variable

τ = Time parameter

ϕ = Path fraction

χ_j = Cell values of matrix [**c**]

ψ = Cell value of matrix [**B**]

φ = Valve seat angle

Ω_f = Injected angular frequency

ω = Angular frequency

Contents

Chapter 1 Introduction

Chapter 2 An Algorithm for the Efficient Acoustic Analysis of Silencers of any General Geometry

Chapter 3 Modelling Multiple Time-Variant Sources

Chapter 4 Modelling of Source Impedance Measurement Methods

Chapter 5 Modelling Multiple Radiation Points, Monopole and Dipole Sources

CHAPTER 1

Introduction

1.1 Problem definition

One of the biggest modern day pollutants in the environment is noise, for which road vehicles are a predominant contributing factor [1,2]. Noise produced by automotive vehicles affects the driver, passengers and the general public in the vicinity of the vehicle.

The noise is generated primarily by the engine, or as a result of the vehicle moving [3]. At low speeds the most significant noise is produced fundamentally by the engine and originates from the explosions in the combustion chambers [4]. Vibrations of the cylinder block due to in-cylinder explosions give rise to combustion noise. The explosions cause the moving parts of the engine to impact upon the stationary parts giving rise to mechanical noise such as piston-slap and bearing rumble. The high pressure gas in the cylinders following combustion is released through the exhaust valves and gives rise to significant noise which propagates in the gas flow through the exhaust manifold of the engine and then through the exhaust system [1]. Within the exhaust the propagating noise is silenced, as much as possible, via the use of a network of acoustic elements that have reflective and dissipative properties [5]. Lower level pressure oscillations on the intake cycle of the engine give rise to intake noise which propagates against the mean flow of clean air into the engine and radiates from the intake snorkel. Although the initial level of intake noise is much less than exhaust noise, intake silencers tend to be much more rudimentary than exhaust silencers. At low engine speeds, the sources that contribute most to the overall external vehicle noise are combustion noise, exhaust and intake noise. Tyre noise and aerodynamic noise generated by flow past the vehicle structure become more significant as the vehicle speed increases and eventually become the dominant noise sources [3]. There

are many other primary noise sources which are ordinarily of lesser significance, such as mechanical noise from the transmission system and aerodynamic noise from the cooling fan. There are many other secondary noises caused when undamped vibrations from the engine, transmission and suspension systems cause vibrations in other components, such as the sump, rocker cover and the entire vehicle shell. This thesis is concerned solely with exhaust and intake noise. In particular it addresses aspects of the acoustic analysis and design of exhaust and intake systems.

Noise propagates as a wave through a medium, thus it is modelled as a wave motion [1,4]. Since the evolution of computer technology, the advancement in numerical and computational procedures has aided the predictive capability of sound transmission in general. Nowadays the initial acoustic design and analysis of exhaust and intake systems is routinely done by computer. An iterative design and analysis cycle is followed until an acceptable solution is predicted, at which stage a system is manufactured and tested. The reduction of time required to design an exhaust is vitally important as the industry is commercially driven by launch dates. Failure to produce a fully tested and validated vehicle within the date will have large economic consequences. Thus it is essential in the iterative design process that the computational analysis of a given system is fast and that design changes can be implemented very quickly. Furthermore, recently the iterative design and analysis cycle for exhaust systems has been automated by mathematical optimization studies that analyse vast numbers of potential designs [7,8]. Even with computational advances, in particular the increase of calculation speed, optimization studies still require ever faster solutions in order to achieve their potential [9,10]. Thus the computational speed of analysis is extremely important and figures largely in this thesis.

As manufacturers develop new exhaust designs, then the associated predictive, acoustic software has to acquire the capability to analyse them. As noted, such commercial software for the automotive industry also has to be able to analyse the exhaust designs quickly and efficiently. The common practices used to reduce computational execution time are the reduction of the accuracy or generality concerned with an algorithm. Commercial software for silencer analysis [11,12] tends to adopt the latter technique, such that the types and connectivity of the basic acoustic elements that comprise the silencer are highly restricted. More recently a general form

of software has been released [13-15] that allows for totally general connectivity between acoustic elements of a more general nature. The resultant increase in computational time is a problem, however, particularly in optimization studies. Investigation into the procedural processes within an algorithm can identify areas where execution time can be reduced without affecting accuracy [9,10]. Thus a fast and general algorithm for silencer analysis for yet more generality, with the option of adding subsequent capability, needs to be investigated and forms the basis of this thesis.

1.2 An overview of exhaust system analysis

Research into wave propagation within exhaust systems can be divided into two main areas, namely time-domain [6] and frequency-domain [1] analysis. Both areas are derived from the conservation laws of mass, momentum and energy. Time domain or finite wave theory retains the non-linear terms in the conservation equations and thus remains valid for waves of any amplitude [1,6]. In contrast, frequency domain analysis assumes that the waves consist only of small amplitude disturbances of the fluid properties about their mean values, such that one can linearise the conservation equations [1]. In particular, if the wave amplitude is of such a magnitude that the sound wave changes appreciably in shape as it propagates, the frequency domain analysis will be subject to significant error. However, the advantage of frequency domain analysis is that separate solutions of the linearized conservation equations can be summed to form a general solution. Thus linearization of the conservation equations allows a solution to be generated for a single frequency of the wave at a time and therefore the solution is significantly faster and simpler than for non-linear time-domain analysis. The advantage of time domain analysis is that changes of wave shape with time are observed and therefore there is an associated greater accuracy for large amplitude waves. This is particularly useful for modelling shock waves in exhaust valves that pertain to engine performance [6]. The wave amplitude tends to diminish with distance along the exhaust system, firstly as a result of the smoothing effect as the out-of-phase pressure pulses from the various cylinders are merged within the manifold. Most elements of the exhaust system serve to reduce the amplitude of the

pressure pulses, even though their primary purpose might be quite different. The turbine of a turbocharger, a catalytic converter and a diesel particulate filter all fall into this category. Furthermore they are located upstream of the dedicated silencer units, hence the wave amplitudes in the silencer units are low enough for linearized frequency domain analysis to be reasonably accurate. However, within the engine manifold section, the pressure fluctuations above and below the mean are of the same order as the mean and therefore non-linear, time domain analysis is ordinarily used within the manifold analysis [6,16]. The dominant frequency component of the pressure wave is the engine firing frequency, which is low, such that the manifold branches are acoustically short. Thus nonlinear effects on wave propagation within the manifold are not as noticeable as the wave amplitude would imply. A combination of time domain analysis for the manifold and frequency domain analysis for the exhaust is referred to as the hybrid approach [17-19].

The work presented in this thesis advances the capability of automotive exhaust noise prediction software within the frequency-domain. The theory is also valid and can be applied to engine intake, ventilation and compressor systems [1,6,20-22].

Propagation of waves that may have large amplitudes are usually evaluated in the non-linear time domain [23]. This method ensures that the wave shapes are correctly modelled in relation to time [6]. The time-domain or finite wave theory is especially useful in modelling blow-down conditions; these occur in the intake and exhaust manifolds of an internal combustion engine. Blow-down conditions occur when the intake or exhaust valves are open, hence causing a vast difference in the pressure and the balance of temperature between the cylinder and manifold [1]. This creates an unsteady flow within the manifold. Time-domain analysis is also used to model the effects of wave patterns that only occur when there are large disturbances, such as shock waves.

In summary, time-domain analysis of acoustic waves propagating through ducts requires considerable computational effort, but remains accurate whatever the wave amplitude. In contrast, frequency-domain analysis is computationally very efficient and is preferred for modelling waves that have small pressure disturbances. The hybrid approach uses time-domain analysis for the acoustic evaluation of large disturbances

within the manifold and downpipe with the addition of frequency-domain analysis for the acoustic wave propagating through the exhaust section. However, the merging of these two forms of modelling acoustic wave propagation through the manifold and exhaust has not yet yielded any significantly better results than the use of solely time-domain or frequency-domain analysis.

1.3 Time-domain analysis of manifolds and exhausts

Time-domain analysis of acoustic waves propagating within ducts is mainly evaluated by the method of characteristics developed initially by Riemann [6,23]. Essentially, the governing partial differential equations of conservation of mass, momentum and energy are reduced to much simpler algebraic equations, characteristic equations, that are valid along particular paths, or characteristic lines, that must be calculated. This method is exceptionally general and is capable of modelling wave behaviour that has large pressure disturbances, including shock waves.

A shock wave is basically a sudden change of pressure and occurs when the local pressure gradient within part of a wave tends to infinity. Since the local wave speed in a non-linear wave is a function of the local pressure amplitude, a non-linear harmonic wave would steepen locally as it travels until eventually it would assume the characteristic N-shape of a shock wave. In an exhaust system, a shock wave would occur eventually as a result of a long downpipe and can be eliminated by designing the exhaust system with a short downpipe. Shock waves also occur at the exhaust valves as they first open, when the magnitude of the cylinder pressure is vastly greater than the pressure in the manifold on the other side of the valve. Manifold and exhaust systems are now generally designed to avoid shock waves in downpipes, although in some high performance vehicles where radiated noise is not an issue, they do occur. The only area in which shock waves should appear, unless there is a poor exhaust/manifold design, is at the exhaust valves [6,23].

The method of characteristics is divided into two main areas, homentropic and non-homentropic flow. The assumption of homentropic flow implies that heat transfer

effects and irreversible effects such as wall friction are negligible, otherwise the entropy will be non-uniform. This assumption allows the wave to be modelled mathematically by two characteristic equations. These characteristics and the initial starting conditions provide enough information to model the wave travelling along a one dimensional pipe. Therefore, characterization of non-linear wave theory can be modelled numerically via two characteristics or path lines. The accuracy of the method of characteristics depends on the spatial and time intervals between path lines. However, the smaller the intervals, the greater the computational time needed to solve a particular problem.

The method of characteristics, assuming homentropic flow, is a useful analytical tool to evaluate one-dimensional gas dynamics within manifolds [1,6]. A more general method of characteristics incorporates fully non-homentropic flow, allowing for heat transfer and irreversible processes such as wall friction [24]. This method encompasses all three partial differential equations of mass, momentum and energy. As a result of the generality of the non-homentropic flow method, the Riemann variables are not constant, adding to the computational time required to solve the characteristic equations numerically [6]. The addition of a third path line also increases the computational time required to solve a non-homentropic, time-dependent problem via numerical analysis [1,6,23,25].

The non-homentropic form of the method of characteristics can be applied to evaluate the effect of scavenging of air due to the pressure drop within cylinders [26]. The behaviour of wave action in two-stroke engines and their manifolds is generally modelled by this method of characteristics [26,27], especially when the engine is supercharged [28].

The computational time required for solving one-dimensional gas dynamic equations of an internal combustion engine manifold is dependent on both the finite time interval and the distance along the pipes [1,6]. The method of characteristics can also be applied to two or three dimensional flow problems. The inclusion of other dimensions increases the accuracy of the model, but also greatly increases the computational time required and the user time in creating the mesh [6].

The Courant, Isaacson and Rees (CIR) [6] method is a finite difference technique, similar to the mesh method of characteristics, which characterizes the flow behaviour of a compressible fluid by using special formulations of the equations which characterise the flow of a compressible fluid. The similarities to the mesh method of characteristics are apparent as all the path lines can be traced back to the initial time level. The CIR method has a one step iterative procedure for non-homentropic flow conditions. It consists of three characteristic equations which are discretized. The mesh method of characteristics and CIR both have linear interpolation characteristics and therefore they are first order accurate in space and time. Methods such as CIR are based on conservation laws. It has been shown that at discontinuities the waves do not travel at the correct speeds [6], which is a disadvantage. Therefore, the method of characteristics and CIR can become numerically unstable and unable to converge to consistent solutions when there are discontinuities present [6]. Nevertheless, the CIR method is used to model the gas dynamics of engine manifolds [29].

With the method of characteristics and CIR methods, it is important to achieve a suitable time step or mesh size. If the time step is too small, the computational time is too large, or else the accuracy is not effective enough. Courant, Friedrichs and Lewy (CFL) [6] have evolved a formulation to calculate a suitable time step. It is based upon the distance between mesh points, the maximum possible wave speed within the solution process and a CFL parameter [6].

Finite difference methods cannot readily cope with discontinuities. Explicit schemes are required to enable tracking of the discontinuities that occur within shock waves. Numerical integration schemes can characterize both smooth and discontinuous areas of wave propagation. These methods are called shock capturing schemes [6,30]. Although CIR and the method of characteristics are based on a special formulation of a compressible fluid, they do not explain fully the behaviour of those partial differential equations. However, the development of CIR has enabled simulations of compression ignition engines [6].

Control volume approaches are used to characterize wave propagation where shock waves are present and they adhere to Rankine-Hugoniot equations. These equations are a combination of the conservation laws in an integral format. Rankine-Hugoniot

equations were developed to govern flow through shock waves [6]. There are many numerical integration schemes, but the Lax-Wendroff method is used as the basis for many others [31]. Although the first Lax-Wendroff attempt at developing a shock capturing scheme resulted in poor resolution, subsequent schemes were an improvement and inspired more accurate schemes, such as the MacCormack method [6]. This method is a second order accurate scheme that can be applied for use as a predictor-corrector algorithm [6]. This method is shown to be a less dispersive and slightly faster predictor-corrector algorithm than the Lax-Wendroff method [33].

Godunov [6] developed an inter-cell, initial value problem based on the conservation laws, where the inter-cell fluxes could be calculated by solving a sequence of local Riemann problems. It is based on the physics of wave propagation phenomena, it is first order spatially accurate, and generally has more accuracy than most space centred first order accurate schemes, such as the Lax-Friedrichs scheme. It was shown that if the scheme was extended to involve higher orders, failure would occur with steep gradients [6]. Therefore, this presented large problems for solving hyperbolic equations with numerical methods, which are needed for shock wave capturing schemes. A total variation diminishing (TVD) concept or criterion was developed [6,31] to ensure that an applied predictor-corrector algorithm would not fail.

A flux-corrected transport (FCT) method was also developed [6,34] to ensure that shock wave capturing schemes could be implemented. FCT uses a higher-order difference scheme for the initial stage, which allows for spurious wave oscillations to appear, then it uses a global diffusion processes to eliminate them. It has been shown that FCT is computationally more efficient than TVD [33].

The mathematical techniques that have been reviewed within this section are used to tune and design efficient manifolds. The volumetric efficiency of a four-stroke engine is modelled routinely with a wide range of manifold pipe configurations before manufacturing occurs [6,25,34]. Wave propagation in the manifold affects the performance of the engine, but creating physical models of manifolds are expensive and time-consuming. Therefore, computational fluid dynamic codes are used to reduce the research and development costs.

Designers of high performance vehicles, such as Formula One racing cars, use time-domain analysis and computational fluid dynamics to achieve different objectives. High performance engines require the maximum possible power output regardless of efficiency and noise levels. In this area of research engine performance and air flow is maximised [6].

Lawn mowers, mopeds, chainsaws etc. generally use two-stroke engines, along with some more sophisticated high performance machinery, such as motor-cycles, outboard motors and snowmobiles. These engines commonly have a single cylinder, however, more high-powered machinery can have multiple cylinders. As a result of engines only having two-strokes, the exhaust and intake strokes are less well defined. Therefore, their performance is more dependent on the manifold configurations. Time-domain analysis is used to optimise the performance of two-stoke engines [35-37].

There are time-domain, computational fluid dynamic (CFD) codes which are available commercially, an example of this being AVL BOOST software. AVL BOOST analyses one dimensional pipe flows with an adapted Godunov scheme. The software is able to analyse the thermodynamics within internal combustion engine cylinders, intake and exhaust manifolds. It has many features, such as the ability to analyse the effects of perforated pipes, flow restrictions, plenums and crankcases, amongst others [38].

Wave Software produced by the Ricardo Plc [39] is another time-domain code. This software includes engine management systems, 1D/3D hybrid flow simulation codes and thermodynamic analysis of cylinder chambers, along with acoustic analysis codes for intake/exhaust analysis.

Another commercial CFD code is GT-Power which solves 1D/3D flow and thermodynamic problems. This software calculates within the time-domain and acoustically analyses intake/exhaust noise. Therefore, the software is also capable of analysing acoustically mufflers using three-dimensional meshing techniques [40].

Some automotive vehicle companies invest in their own CFD codes. For example, Lotus have developed their own time-domain code, LES [41,42], a one-dimensional

gas dynamic CFD code. It can interact with STAR-CD [41] software products for three-dimensional thermodynamic analysis of internal combustion engines.

These time-domain codes are used principally for engine performance calculations. The intake and exhaust systems are represented within them and a prediction of radiated noise can be obtained from the analysis. However, these codes are generally unable to represent correctly the detailed geometry of a commercial exhaust silencer and the silencer modelling is grossly simplified. The principal concern is to represent correctly the backpressure of the exhaust and intake systems in order to predict the engine performance accurately. The acoustic representation is relatively poor and hence the noise predictions are unreliable. Thus, in most cases a hybrid capability to link to frequency domain analysis of silencer systems is either offered, or is in development, in order to enhance acoustic prediction capability.

1.4 Frequency-domain analysis of exhausts

An acoustic wave is characterised by three conservation laws, mass continuity, dynamic equilibrium and isentropic continuity. If there are only small disturbances of the acoustic wave about the mean, then linearisation can occur. Thus the conservation of mass continuity and dynamic equilibrium can be rearranged to yield the classic wave equation. The time dependency of the linear partial differential wave equation can then be assumed to be harmonic without loss of generality.

Linear frequency domain modelling via the scattering or transfer matrix methods is possible at low frequencies [1,43], below the cut-on frequency of non-planar wave modes. The cut-on frequency is determined by the cross-sectional dimensions of a uniform pipe and the speed of sound. At low frequencies, only plane waves propagate continuously through a duct network as the higher order modes are evanescent [43].

Primarily, there are two systems of representing acoustic parameters in ducts within the plane-wave frequency domain, namely scattering matrices and transfer matrices [44-46]. Systems that use transfer matrices and scattering matrices are good

at modelling acoustic behaviour within ducts [5,43]. The scattering matrix system represents the acoustic pressure within a duct as a sum of two wave components, one propagating in the one-dimensional positive 'x' direction and a second propagating in the negative 'x' direction. The combination of evaluating the interaction between the two pressure waves characterises completely a propagating linear wave in an acoustic duct section via four parameters. These four parameters are entered into a two-by-two scattering matrix which relates the components of the wave pressures propagating in the negative direction, to those propagating in the positive direction at either end of the duct section. Scattering matrix modelling is applicable to the computational modelling of low frequency duct networks [43].

A transfer matrix is very similar to a scattering matrix. It is used to relate acoustic properties at the inlet of a duct section to similar properties at the outlet. Typically, the acoustic mass velocity and acoustic pressure at the inlet and the outlet are related by a two-by-two transfer matrix. More generally, two acoustic properties are defined for every inlet or outlet, otherwise known as ports, of a duct section and the corresponding transfer matrix relates the inlet to the outlet properties. Transfer matrix analysis of ducts has proven to be exceptionally useful for modelling individual exhaust components [45-47]; these systems are versatile at modelling low frequency networks [1,48]. The use of transfer matrix modelling leads to a condensed, two-by-two matrix to describe the overall acoustical behaviour of exhaust systems with a sole inlet and outlet [15,43]. The coefficients of transfer matrices are generally frequency dependent.

1.4.1 Transfer matrices for different acoustic elements

An acoustic element is any single basic component of a silencer system for which a transfer matrix can be derived. The most common acoustic element of a silencer system is a uniform pipe, characterised by its length and cross-sectional area. The coefficients of the transfer matrix, the four-pole parameters, are a function of the geometry, the frequency, background fluid properties and mean flow conditions within the pipe [49-51]. It is also possible to account for the acoustic effect of linear

temperature variation [50] within an element. For any acoustic element which has a sole inlet and outlet, a two-by-two transfer matrix can be constructed to relate the acoustic properties at the inlet to those at the outlet. Many acoustic elements have two ports, a single inlet and outlet, and corresponding transfer matrices have been derived for conical pipes [52], area changes [46,53], and porous hoses [55], for example. Catalytic converters [5,55] and diesel particulate filters [56] are not primarily within exhaust systems to reduce noise, but they do have a significant acoustic effect and transfer matrices for these elements can be derived and used within linear acoustic network modelling. Hole arrays [10], a grouping of similar orifices in parallel through which an acoustic wave propagates, are modelled from the impedance of single orifices [57] with interference effects as given by the Fok function [58]. The net impedance of the array is incorporated in a transfer matrix of a hole array element. Closed ends or termination are simply modelled by evaluating the wall impedance/admittance [1], a ratio between the pressure and acoustic mass velocity.

If all acoustic elements had two ports there would no problem in overall analysis of a silencer system, since all the elements would be linked consecutively [10] and would have two-by-two transfer matrices. These matrices could then be multiplied in consecutive order to yield an overall two-by-two transfer matrix for the entire system. However, most silencer systems have some form of multi-port element within them, where the acoustic waves can diverge along and/or converge from two or more separate paths. The transfer matrix of any multi-port element contains more than two rows and/or columns. Thus consecutive multiplication of transfer matrices is no longer possible and reduction of the overall system into a single transfer matrix is very complicated and requires dedicated algorithms.

The simplest form of multi-port element is the fork element which can have three or more ports. These elements are used to connect different elements together to form closed end branches, extended inlets/outlets [5], overlapping paths [10] and many other network configurations. Forks can be characterised in their most basic form as the sum of the acoustic mass velocities into the element equalling the sum of mass velocities out, whilst the acoustic pressure within the element is constant [1].

Another multi-port element that is common to all exhaust silencers is the perforated pipe, which is used primarily to guide the mean flow, for minimal back-pressure, while allowing acoustic energy to propagate through the perforations. Initial analysis of 'straight through' resonators, namely one perforated 'flow' pipe within an outer casing was investigated by Sullivan and Crocker [59]. The basic element is then a four-port, with a four-by-four transfer matrix relating the acoustic properties at the inlets to the perforated tube and casing to those at the outlets [1,5,60]. The theory and application of acoustic elements with perforated pipes was researched further by Sullivan [61,62]. In all of these cases a segmented approach was used to model the interaction between the inner tube and the outer cavity. Numerical decoupling of perforated pipe silencer elements [60] enabled a more accurate distributed modelling approach to be used for a straight-through resonator. This modelling of a single pass resonator [63,64] obviously leads to the investigation of three-duct or two-pass resonator elements. These elements consist of two perforated pipes within the silencer casing [65], a six-port element. The extension to triple-pass, eight-port, resonators [5] and beyond is obvious. It is not unusual for an exhaust silencer to have four or five perforated pipes within the casing and triple-pass resonators may be regarded as the norm.

1.4.2 Linear codes for silencer analysis

Linear codes were written to assemble complicated network systems of acoustic elements and to predict their overall acoustic properties. Once the linear codes have assembled the network systems, the elements are reduced to a single overall transfer matrix [10,11]. The availability and capability of commercial software modelling of exhaust ducts and silencer systems in the frequency domain is small compared to time-domain analysis of engine manifolds [38,40,41,65]. Sound In Ducts (SID) software is available commercially for the acoustical analysis of ducts and uses frequency domain evaluation techniques [12]. Loughborough And Mira Program for Silencer (LAMPS) software [11,15] is also currently available commercially. The two key features of any linear code are the variety of basic elements which can be used to create silencers and the generality with which these can be assembled into a network.

SID [12] was designed and engineered specifically for HVAC systems [20]. The only multi-port acoustic elements which are supported are three-port fork elements. HVAC systems do not have resonator elements within their network. Thus SID cannot be used for vehicle exhaust acoustic analysis without considerable simplification in the modelling of the silencers. The code does, however, allow for any general assemblage of the acoustic elements that it supports.

In contrast to SID, LAMPS was developed specifically to analyse exhaust and intake systems. Thus, in addition to three-port fork elements, LAMPS allows resonator elements up to triple-pass, or eight-port elements. The software has a number of algorithms that are used to reduce the overall network of acoustic elements to a single transfer matrix. However, although LAMPS allows for an infinite number of potential network designs, the connectivity between multi-port elements is limited by the number of different reduction algorithms. This software is also constricted by the assumption that the overall systems have a single inlet and outlet. In 2003 LAMPS3 was released, a new version that used a global approach with a general algorithm that could solve for any connectivity of elements [14,15]. The overall system was again restricted to one with a single inlet and outlet. This general code suffers from the fact that it is very slow compared to conventional codes. The one-dimensional software analysis package LAMPS has proven to be a valuable predictive tool for design and optimisation studies for the intake and exhaust of an internal combustion engine [66,67]. Genetic algorithms are used in conjunction with LAMPS to improve silencer design. A typical, full factorial analysis of a silencer consists of 800 million changes. For each variant, analysis at 1000 different frequencies may be required. Thus the computational time required for a single analysis is absolutely critical. The development of a general code for any connectivity of silencer elements is very beneficial in that it extends the capability of the software to model more complex systems, but the general code is too slow to be used within optimisation studies. Thus a hybrid code [9,10] that encompasses the algorithmic generality of the general code [14,15] and speed of the conventional code [11] was required. Such a code has now been developed and details of its key features are explained in Chapter 2 of the thesis. The hybrid code identifies any consecutive sequence of two-port elements and reduces characteristic parameters by matrix multiplication. This code also recognises sub-

systems within whole networks and reduces them to equivalent two-port systems by a global matrix approach. The hybrid code also logs the order of individual, acoustic element transfer matrix calculations and sub-system reduction for rapid calculation at subsequent frequencies.

1.4.3 Source modelling

As noted above, a complete silencer system with a single inlet and outlet can be reduced to an equivalent overall two-by-two transfer matrix. Knowledge of the source and radiation impedances is then needed in order to evaluate the overall acoustic effectiveness of a silencer system. The radiation impedance from a uniform pipe into free space is well documented [1,43,49,66]. In contrast, the source impedance is very poorly characterised and needs to be investigated further. It is generally assumed to be a constant [66,67,69], or even infinite.

The LAMPS software packages use an empirically derived constant for the source impedance of exhaust systems and an infinite source impedance for intake systems. These values have been found to give the best overall correlation between measured and predicted insertion loss for silencer systems on a wide variety of engines. Alternatively, the user may specify their own constant or frequency-dependent values of source impedance. This facility is generally used when a user has attempted to measure the source impedance of a given engine. The source location is generally taken to be at the outlet of the manifold, since the overall system is assumed to have a single inlet. The source and radiation elements may be regarded as one-port elements. The only way in which the acoustic effect of manifold branches can be included is to regard one valve as the active source and the other valves as passive terminations at the end of side-branches. It may be noted that the effects of valve-timing and the phase relationship between different cylinders are entirely ignored in such an approach. Linear, time-variant models of multi-cylinder intake [70] and compressor systems [22] have been studied. Discharge through the exhaust valves of an IC engine is fundamentally nonlinear, however. A simplified linear model of flow through an exhaust valve [71,72] is used as a basis for the development of a time-dependent source model of a multiple-cylinder engine in Chapter 3 of the thesis. Its use precludes

the necessity for a source impedance. It is not expected to be an accurate representation of the source, but it does account for phase differences between cylinders and may be expected to be at least as accurate as the use of a constant source impedance.

One-port acoustic sources are assumed to be linear and time-invariant when modelling within the frequency domain [73]. Whilst this assumption may be valid for fan sources in HVAC systems [74], it is of questionable validity for IC engines and indeed this matter has been studied extensively, especially with respect to the measurement of the source impedance [74-81]. Source impedance is measured by one of two different techniques, either the indirect [71] or the direct [72] method. The former is most suitable for IC-engines, but gives implausible negative values for the resistance. It has been shown by analysis, using a simplistic single-cylinder linear source, that the time-variance of the valve is sufficient to cause these negative values. Non-linearity in the valve may be another factor. Indeed, the analysis shows that the entire concept of a source impedance which is defined by a single value at a given frequency is fundamentally flawed for even a linear time-variant source. However, the effective source impedance as measured by either method, or the constant values used ordinarily within LAMPS, can give rise to reasonably accurate predictions of insertion loss [1]. The correct source characterization in the case of a linear time-variant source gives rise to a full impedance matrix that describes the relationship between source pressure and mass velocity with full modal coupling included [71]. In Chapter 4 of the thesis, previous work on analysis of the indirect and direct measurement methods of source impedance is extended to multi-cylinder engines. Earlier conclusions from the single-cylinder work are reaffirmed for multi-cylinder engines. The effective single-value source impedance and the correct source impedance matrix are derived for a simplistic linear multi-cylinder engine. The results are used to compare measured and calculated source impedance and to derive overall insertion loss results for various systems.

1.4.4 Additional features

The high pressure gas in the cylinders that vents through the exhaust valves is the primary source of sound waves that propagate through the exhaust system [1,6]. However, not all the noise that is radiated at the outlet of the exhaust system is attributable to this primary source [82]. High velocity exhaust gas flow over various types of discontinuities within the exhaust system gives rise to self-noise, or flow-generated noise (FGN). In respect of more general applications, FGN caused by spoilers was researched initially by Iudin [83] and later by Gordon [84,85]. The strength of various forms of FGN sources and the net effect on overall systems has been studied [86-89]. Clearly, there is a need for linear, plane-wave software for the acoustic analysis of silencers to include any FGN that is significant at low frequencies. There is evidence that the accuracy of such software is now limited by the neglect of FGN at high engine speeds [15]. If the strength and location of a FGN source were known, then in principle it can be modelled as a dipole source [13] within the assemblage of acoustic elements and its overall effect on radiated noise can be determined.

In Chapter 5 of the thesis, the capability of the software is extended to include analysis of the effect of monopole and dipole sources of known strength placed anywhere within a silencer system. The latter allows for inclusion of FGN sources as noted. Inclusion of monopole sources, for instance the output of a loudspeaker, allows the software to be used for studies on active noise cancellation systems.

Engineering of automotive exhaust systems is evolving as the knowledge and creativity of designers and engineers expand [15], subsequently the software capability has to encompass an ever increasing set of features. Research into exhausts within the linear, plane wave, frequency domain have concentrated largely on systems with a sole inlet and outlet [1,5,43]. However, twin tailpipe exhaust systems are becoming increasingly popular. Although this does not present any great analytical challenge in principle, it does present a significant problem with regard to a general algorithm for analysis. Furthermore, vee-engine designs often have twin exhaust systems joined by a balance pipe and there are even twin exhaust, twin tailpipe systems. None of these

types of system can be modelled by LAMPS, SID or, to the author's knowledge, any silencer analysis code. In Chapter 5 algorithms are developed to include all of these effects in the hybrid model.

CHAPTER 2

An Algorithm for the Efficient Acoustic Analysis of Silencers of any General Geometry

2.1 Introduction

Silencers can be modelled by a system of acoustic elements [1]. Each part of an exhaust can be modelled by an individual element [5]. Once the physical properties of an element are known, the mathematical relationship between the acoustic behaviour at the inlet and outlet can be calculated. There are many different types of elements, such as uniform pipes, conical pipes, hole arrays, area changes, catalytic converters, closed ends, forks and resonators, etc, see Section 1.4.1.

Since the acoustic effect of a silencer system can be calculated with linear, plane-wave analysis at low frequency, these elements can be characterized by transfer matrices which relate the convective acoustic pressure and mass velocity [1,49] between the inlets and outlets. The various acoustic elements within a system can be grouped into three distinct sets [9,10]; those which have one port, exactly two-ports, or more than two-ports. Note that a port is an alternative name for an inlet or an outlet.

Figure 2. 1. illustrates a simple silencer sub-system consisting solely of two-port acoustic elements. The acoustic behaviour of any two-port element can be expressed by a simple two-by-two transfer matrix, for example the first element of the expansion chamber, i.e. a pipe, can be characterized mathematically as:

$$\begin{bmatrix} P_0 \\ V_0 \end{bmatrix} = \begin{bmatrix} a_{01} & b_{01} \\ c_{01} & d_{01} \end{bmatrix} \begin{bmatrix} P_1 \\ V_1 \end{bmatrix}. \tag{2.1}$$

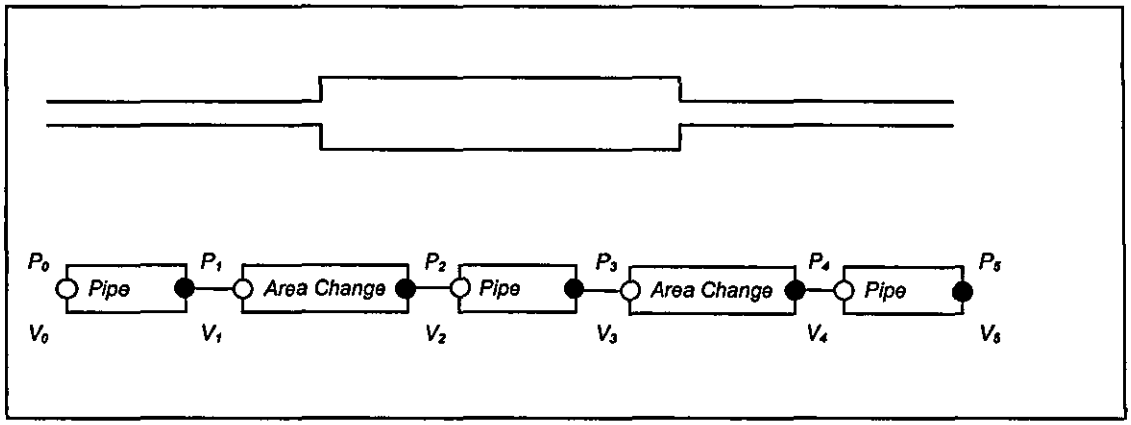

Figure 2. 1 An expansion chamber consisting of five two-port elements

Here a, b, c and d are the coefficients that constitute a four-pole matrix, whilst P and V are the convective acoustic pressure and mass velocity respectively. The numerical subscripts denote the ports. Equation (2.1) is known as a transfer matrix equation and is fundamental to the analysis of silencers. For any element that has only two ports, all four coefficients can be found from considering the conservation equations of mass, momentum and energy [1]. Transfer matrices for different acoustic elements can be multiplied sequentially to give an overall two-by-two transfer matrix. This relates the acoustic properties between the inlet and outlet of the overall system, since

$$\begin{bmatrix} P_0 \\ V_0 \end{bmatrix} = \begin{bmatrix} a_{01} & b_{01} \\ c_{01} & d_{01} \end{bmatrix} \begin{bmatrix} a_{12} & b_{12} \\ c_{12} & d_{12} \end{bmatrix} \begin{bmatrix} a_{23} & b_{23} \\ c_{23} & d_{23} \end{bmatrix} \begin{bmatrix} a_{34} & b_{34} \\ c_{34} & d_{34} \end{bmatrix} \begin{bmatrix} a_{45} & b_{45} \\ c_{45} & d_{45} \end{bmatrix} \begin{bmatrix} P_5 \\ V_5 \end{bmatrix}, \tag{2.2}$$

can reduced to a single two-by-two matrix equation.

Successive multiplication of sequentially ordered transfer matrices provides exceptional computational efficiency that can only be used for the simplest of silencer systems [1,11].

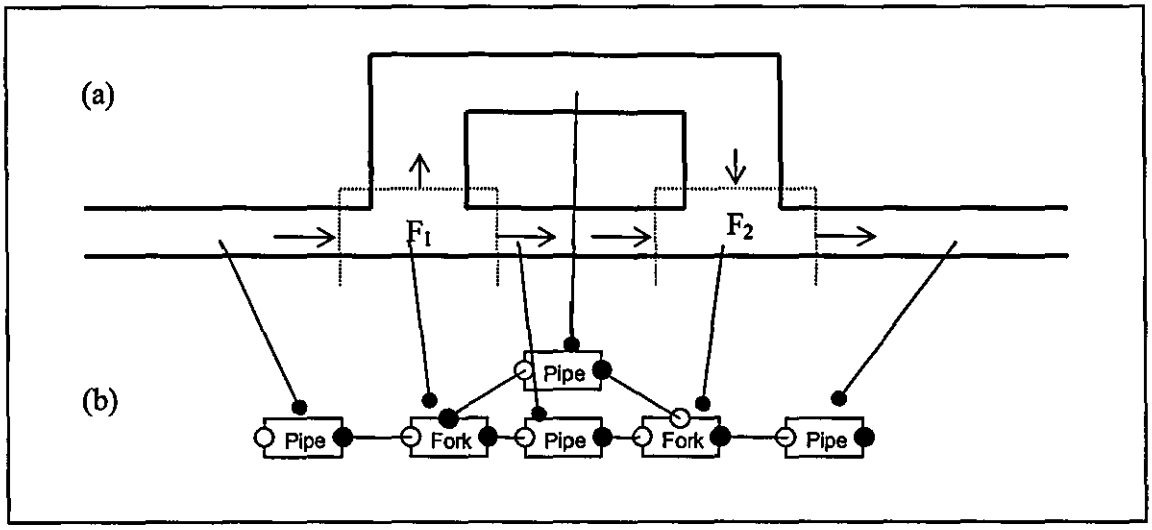

Figure 2. 2 A Quincke tube system

Figure 2. 2a shows a pair of parallel pipe elements between two, two-port pipe elements, formally known as a Quincke tube system. The conventional multiplication of sequential transfer matrices does not work as a result of the three-port fork elements. It is very easy to create an algorithm to calculate the acoustic effect of a simple Quincke tube as given in Figure 2. 2. [20,21]. However, there are many variations of the Quincke tube system, such as a set of parallel expansion chamber silencers between two, two-port elements or a set of nested parallel elements, as shown in Figure 2. 3.

There are an infinite number of such different silencer designs that could be postulated [7,8]. However, for every new design another algorithm has to be developed. This implies that there needs to be a generic algorithm that can calculate any silencer with any geometric design. The complexity of a typical silencer design is illustrated in Figure 2. 4. The element linkage of a silencer that constitutes a triple-pass with coupling [58,62] between the flow returns and the inlet and outlet pipes, as shown in Figure 2. 4c, is highlighted in Figure 2. 5.

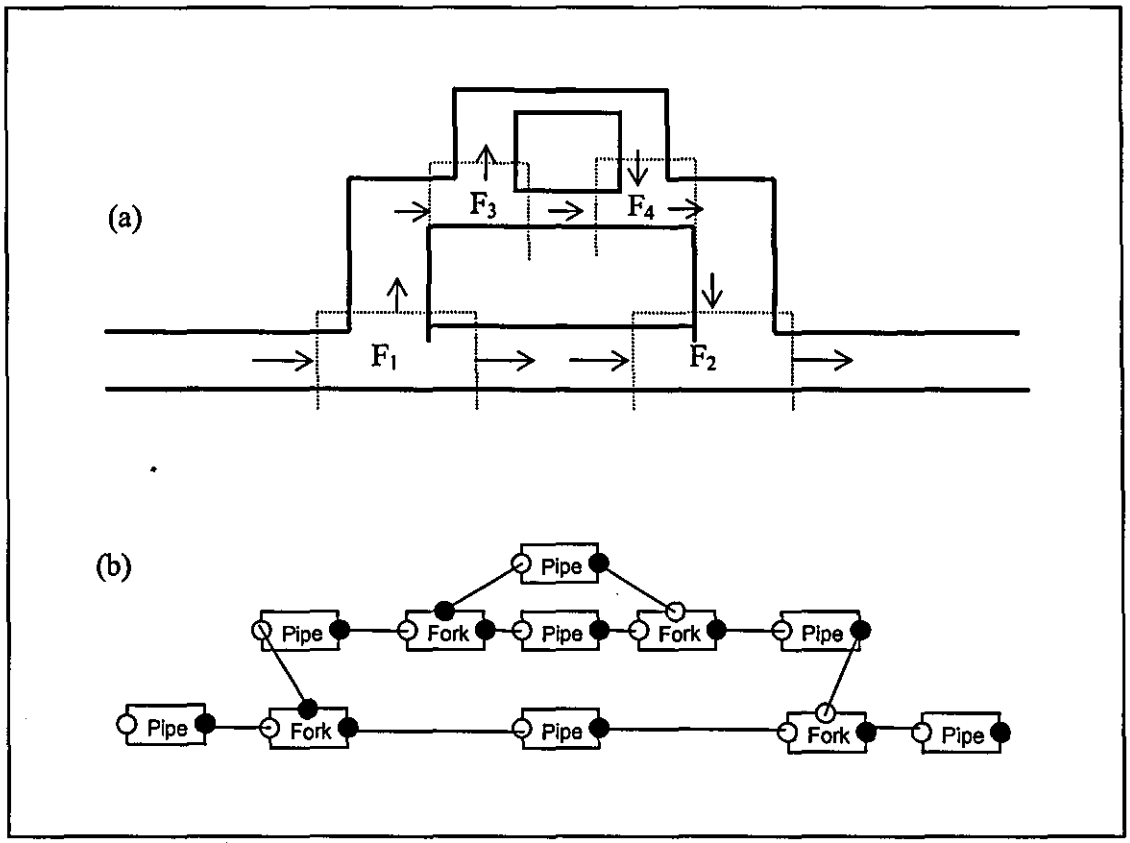

Figure 2. 3 Nested parallel elements system

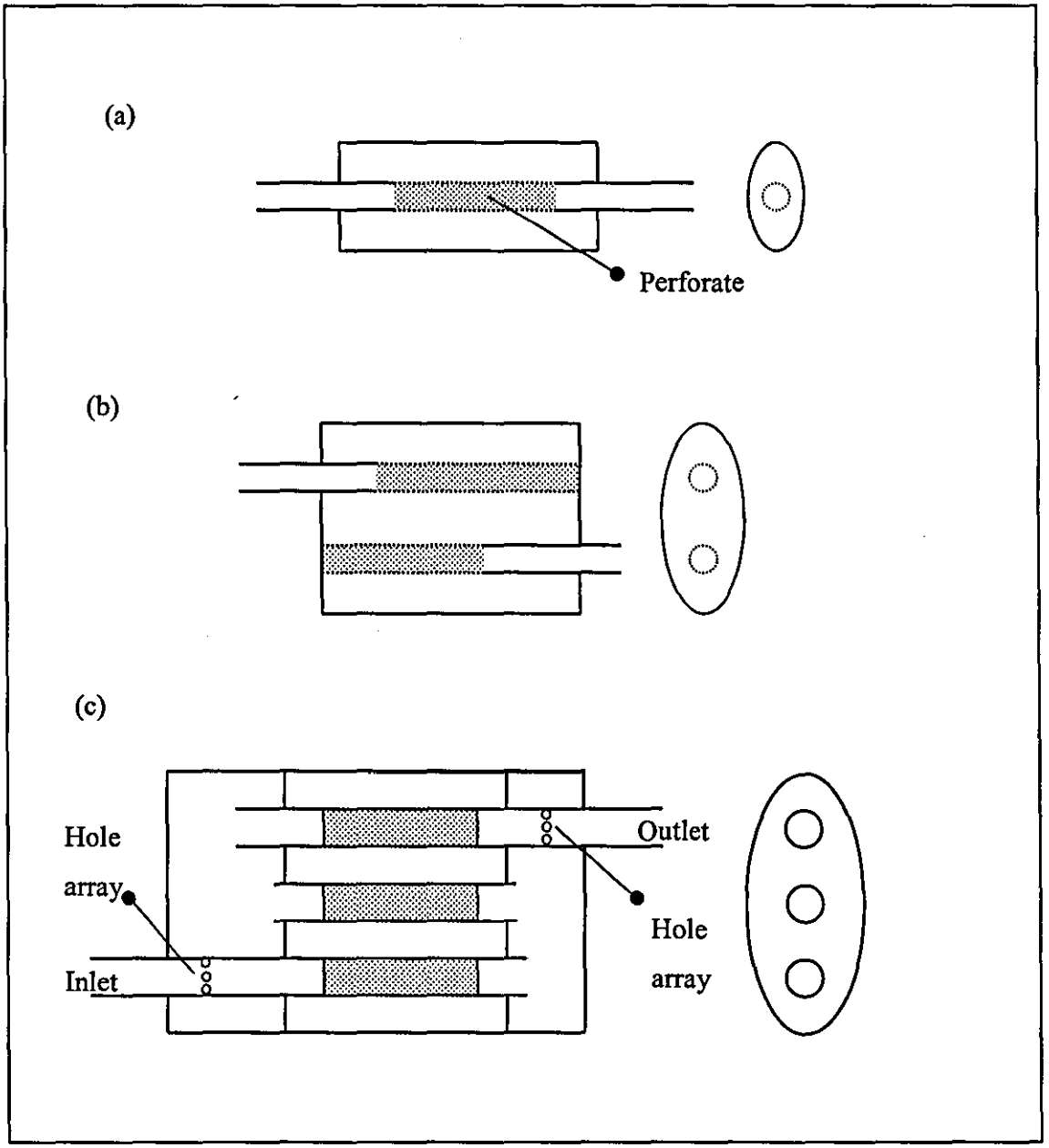

Figure 2. 4 Various types of silencer box: (a) straight-through, single-pass; (b) two-pass, cross-flow; (c) triple-pass with coupling between the flow returns and the inlet and outlet pipes.

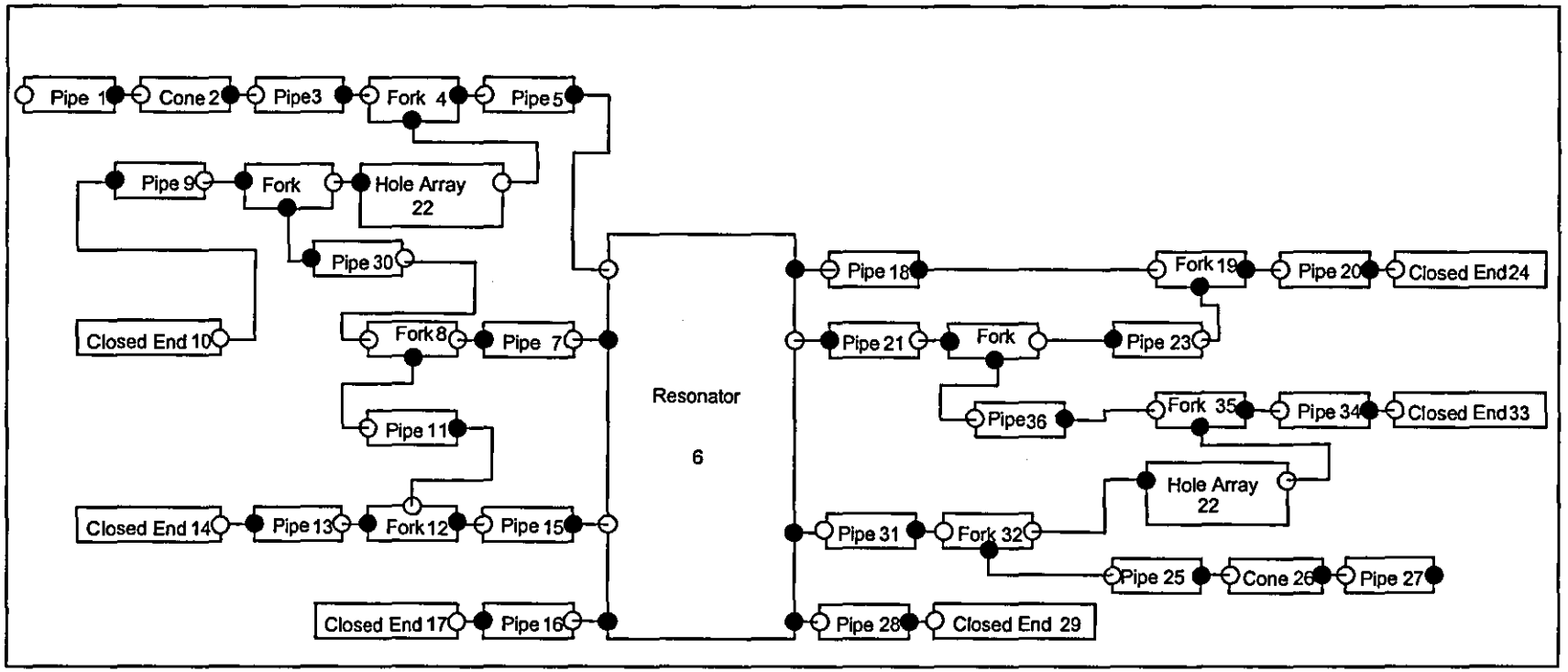

Figure 2. 5 Acoustic element representation of a silencer which has a triple-pass with coupling between the flow returns and the inlet and outlet pipes

2.2 Computational code techniques

2.2.1 Conventional code

Lamps [11,15] is an example of 'conventional' plane-wave, linear acoustic code that can analyse many different designs of silencers. It can reduce many non-sequential groups of elements to a two-by-two transfer matrix. However, neither this code, nor any of its competitors can reduce any general set of non-sequential acoustic elements to a single, overall transfer matrix. Therefore, even small adaptations in the geometry of a given design can cause significant problems for the code. An example is the silencer shown in Figure 2. 4c. In the absence of the hole arrays on the inlet and outlet tubes, the conventional Lamps code can reduce this system. However, with the hole arrays present, there is no standard code in existence that can analyse the resulting silencer. It would be perfectly possible to develop an algorithm that could analyse such a silencer, but then a designer could make another small modification that would require yet another algorithm. Clearly what is required is an algorithm that can handle any general linking of acoustic elements.

2.2.2 General code

A first attempt at such a 'general' [10,15] code has been attempted recently and developed sufficiently to have been released as a new variant of LAMPS. Although this code satisfies the requirement for generality, the cost of this is considerable in terms of computational efficiency. Therefore, there is a need for a 'hybrid' algorithm that encompasses the advantages of both the conventional and the general codes, whilst minimizing the disadvantages. This hybrid will satisfy two major criteria, firstly the ability to reduce any silencer system which has a single source and a single radiation element to an overall two-by-two transfer matrix. Then secondly, the ability to reduce that system as fast as possible. This is achieved by identifying sequential two-port elements

and sub-systems. A sub-system is a group of elements with a single inlet and outlet, e.g. Figure 2. 3.

To illustrate the inefficiency of the general approach to silencer analysis, consider a simple expansion box silencer, see Figure 2.1. This approach numbers each port, as on Figure 2.1, and then it numbers the coefficients of the transfer matrix for each element accordingly. For example, element 2 in Figure 2.1 is characterized as

$$\begin{bmatrix} P_1 \\ V_1 \end{bmatrix} = [\mathbf{T}]_{12} \begin{bmatrix} P_2 \\ V_2 \end{bmatrix}. \tag{2.3}$$

Let the two-by-two transfer matrix $[\mathbf{T}]_{12}$ be:

$$[\mathbf{T}]_{12} = \begin{bmatrix} a_{12} & b_{12} \\ c_{12} & d_{12} \end{bmatrix} \tag{2.4}$$

Alternatively, equation (2.3) can be rearranged to give;

$$\begin{bmatrix} 0 \\ 0 \end{bmatrix} = \begin{bmatrix} -1 & 0 & a_{12} & b_{12} \\ 0 & -1 & c_{12} & d_{12} \end{bmatrix} \begin{bmatrix} P_1 \\ V_1 \\ P_2 \\ V_2 \end{bmatrix} \tag{2.5}$$

Similar equations to (2.3) to (2.5) can be constructed for all of the elements 1 to 5 shown in Figure 2.1. These equations can then be inserted into a 'global' reduction matrix equation

$$\begin{bmatrix} -1 & 0 & a_{01} & b_{01} & 0 & 0 & 0 & 0 & 0 & 0 & 0 & 0 \\ 0 & -1 & c_{01} & d_{01} & 0 & 0 & 0 & 0 & 0 & 0 & 0 & 0 \\ 0 & 0 & -1 & 0 & a_{12} & b_{12} & 0 & 0 & 0 & 0 & 0 & 0 \\ 0 & 0 & 0 & -1 & c_{12} & d_{12} & 0 & 0 & 0 & 0 & 0 & 0 \\ 0 & 0 & 0 & 0 & -1 & 0 & a_{23} & b_{23} & 0 & 0 & 0 & 0 \\ 0 & 0 & 0 & 0 & 0 & -1 & c_{23} & d_{23} & 0 & 0 & 0 & 0 \\ 0 & 0 & 0 & 0 & 0 & 0 & -1 & 0 & a_{34} & b_{34} & 0 & 0 \\ 0 & 0 & 0 & 0 & 0 & 0 & 0 & -1 & c_{34} & d_{34} & 0 & 0 \\ 0 & 0 & 0 & 0 & 0 & 0 & 0 & 0 & -1 & 0 & a_{45} & b_{45} \\ 0 & 0 & 0 & 0 & 0 & 0 & 0 & 0 & 0 & -1 & c_{45} & d_{45} \end{bmatrix} \begin{bmatrix} P_0 \\ V_0 \\ P_1 \\ V_1 \\ P_2 \\ V_2 \\ P_3 \\ V_3 \\ P_4 \\ V_4 \\ P_5 \\ V_5 \end{bmatrix} = \begin{bmatrix} 0 \\ 0 \\ 0 \\ 0 \\ 0 \\ 0 \\ 0 \\ 0 \\ 0 \\ 0 \end{bmatrix} \tag{2.6}$$

This matrix equation can be re-arranged so that P_0 and V_0 are on the right hand side of the equation to give a square 10 by 10 matrix. A relationship between P_0, V_0 and P_5, V_5 can then be evaluated by a modified Gauss-Jordon method [90]. Equation (2.6) shows that there is considerable amount of calculation required to reduce a simple expansion box silencer to an equivalent, overall two-by-two transfer matrix. Equation (2.6) illustrates the sparseness of the global matrix showing that this method, although general, is inefficient. This approach can be applied to any general silencer. However, if a silencer has n ports, the global matrix will be $2n$ by $2n$ regardless of any sequential elements. The computational effort required by the modified Gauss-Jordan method increases in proportion to $(2n)^3$, whereas the effort for multiplication of successive transfer matrices increases linearly with n. Thus, as the number of ports in an overall silencer system increases, the computing time required by the general method soon becomes excessive.

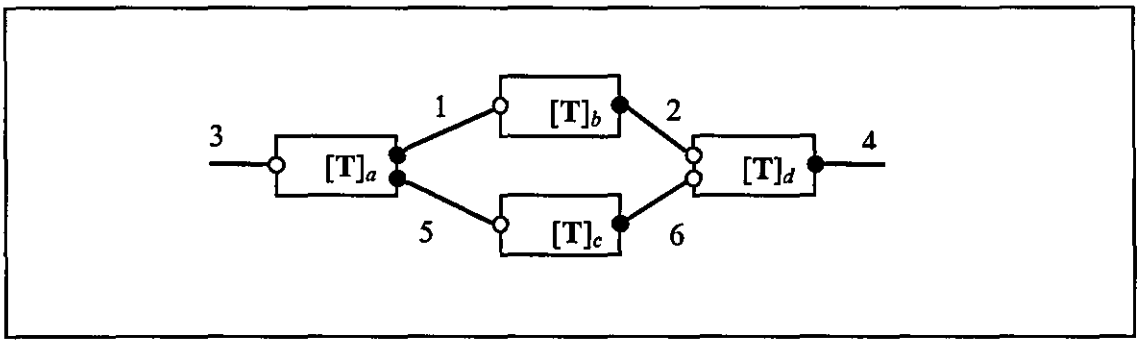

Figure 2. 6 Numbered reduction sub-system which is found in a Quincke tube

The general code is able to reduce any system whether conventionally sequenced or not. Figure 2. 6 illustrates a sub-system with one inlet and outlet which is geometrically similar to the Quincke tube system as shown in Figure 2. 2. Before the reduction occurs, all the ports are numbered; the ordering of numbers is irrelevant. Each acoustic pressure and velocity at each port is related by the numbering. At a three-port fork element, the inlet and outlet variables are related by three equations, one for conservation of convective acoustic mass velocity and two for constant acoustic pressure [1], thus for example

$$\begin{bmatrix} P_3 \\ V_3 \\ 0 \end{bmatrix} = \begin{bmatrix} 1 & 0 & 0 & 0 \\ 0 & 1 & 0 & 1 \\ 1 & 0 & -1 & 0 \end{bmatrix} \begin{bmatrix} P_1 \\ V_1 \\ P_5 \\ V_5 \end{bmatrix}. \tag{2.7}$$

This can be re-arranged to give

$$\begin{bmatrix} 0 \\ 0 \\ 0 \end{bmatrix} = \begin{bmatrix} 1 & 0 & -1 & 0 & 0 & 0 \\ 0 & 1 & 0 & -1 & 0 & 1 \\ 1 & 0 & 0 & 0 & -1 & 0 \end{bmatrix} \begin{bmatrix} P_1 \\ V_1 \\ P_3 \\ V_3 \\ P_5 \\ V_5 \end{bmatrix}. \tag{2.8}$$

From equation (2.5),

$$\begin{bmatrix}0\\0\end{bmatrix}=\begin{bmatrix}-1 & 0 & a_{12} & b_{12}\\ 0 & -1 & c_{12} & d_{12}\end{bmatrix}\begin{bmatrix}P_1\\V_1\\P_2\\V_2\end{bmatrix}, \tag{2.9}$$

since $[\mathbf{T}]_{12}$. A similar expression follows for the other two-port element, $[\mathbf{T}]_c=[\mathbf{T}]_{56}$. Therefore, by letting every number in Figure 2. 6 represent a link, and noting that each fork with n ports enable n equations to be formulated, a reduction matrix can be created. For an overall system with a single inlet port, a single outlet port and n ports in total, there will be $2n$-2 unknowns. Thus, in this example with 6 ports, the reduction matrix is of size 10 by 12 with general form:

$$\begin{bmatrix}0\\0\\:\\:\\0\\0\end{bmatrix}=\begin{bmatrix}E_{1,1} & \cdots & \cdots & \cdots & \cdots & E_{1,12}\\ : & \ddots & & & & :\\ : & & \ddots & & & :\\ : & & & \ddots & & :\\ : & & & & \ddots & :\\ E_{10,1} & \cdots & \cdots & \cdots & \cdots & E_{10,12}\end{bmatrix}\begin{bmatrix}P_1\\V_1\\:\\:\\P_6\\V_6\end{bmatrix}. \tag{2.10}$$

The equations that involve variables at the single inlet of the sub-system, namely P_3 and V_3 in this example must have their rows exchanged with the bottom two rows. Likewise the coefficients for the variables of the single outlet of the sub-system, in this case P_4 and V_4, are exchanged with those in the last two columns to re-order the outlet variables at the bottom of the overall vector of variables. This matrix manipulation allows the 10 by 12 matrix equation to be converted to a 10 by 10,

$$\begin{bmatrix} 0 \\ : \\ : \\ 0 \\ P_3 \\ V_3 \end{bmatrix} = \begin{bmatrix} G_{1,1} & .. & .. & .. & .. & G_{1,10} \\ : & & & & & : \\ : & & & & & : \\ G_{8,1} & .. & .. & .. & .. & G_{8,10} \\ G_{9,1} & .. & .. & .. & .. & G_{9,10} \\ G_{10,1} & .. & .. & .. & .. & G_{10,10} \end{bmatrix} \begin{bmatrix} P_1 \\ V_1 \\ : \\ V_6 \\ P_4 \\ V_4 \end{bmatrix}. \qquad (2.11)$$

The final step is to find a two-by-two transfer matrix relationship between P_3, V_3 and P_4, V_4 by row operations. This can always be achieved since the variables of each inlet and outlet of the sub-system only appear once, each in a separate equation. This final step of matrix manipulation starts with finding the maximum value within the first *n-2* rows in the first column. Let the largest value be in row 4, say $G_{4,1}$; now interchange rows 4 and 1. This partial pivoting is vitally important as many of the coefficients are zero. The last two rows in equation (2.11) cannot be interchanged. The factors within row 1 are now subtracted from rows 2 to n to force the coefficients in the first column, except the first row, to have the value zero. This is the Gauss-Jordan method with partial pivoting. The method is repeated in column 2 to force the coefficients in rows 3 to *n* to equal zero, this is done until column *n-2*. The method is general and will work on any square matrix which describes a sub-system with a single inlet and outlet, hence

$$\begin{bmatrix} 0 \\ : \\ : \\ 0 \\ P_3 \\ V_3 \end{bmatrix} = \begin{bmatrix} G'_{1,1} & .. & .. & .. & .. & G'_{1,10} \\ 0 & . & & & & : \\ : & 0 & . & & & : \\ 0 & .. & 0 & G'_{8,8} & G'_{8,9} & G'_{8,10} \\ 0 & .. & .. & 0 & G'_{9,9} & G'_{9,10} \\ 0 & .. & .. & 0 & G'_{10,9} & G'_{10,10} \end{bmatrix} \begin{bmatrix} P_1 \\ V_1 \\ : \\ V_6 \\ P_4 \\ V_4 \end{bmatrix}. \qquad (2.12)$$

The Gauss-Jordon method as applied to this problem results in equation (2.12), hence the last two rows can be used to create a two-by-two transfer matrix,

$$\begin{bmatrix} P_3 \\ V_3 \end{bmatrix} = \begin{bmatrix} G'_{9,9} & G'_{9,10} \\ G'_{10,9} & G'_{10,10} \end{bmatrix} \begin{bmatrix} P_4 \\ V_4 \end{bmatrix}. \tag{2.13}$$

This implies that the whole sub-system can be modelled as a sub two-port element, hence sequential multiplication of two-by-two transfer matrices either side of the sub-system can occur.

2.2.3 Data logging

The computational cost of the path fraction technique, see Section 2.5, is high because it has general capabilities to analyse any geometric design of silencers that consist of a sole inlet and outlet. Acoustical studies of silencers require analysis over hundreds or thousands of discrete frequencies [66,67]. When analyzing a silencer at a different frequency, the acoustic element linkage remains the same as for the initial frequency, it is only the coefficients of the transfer matrices that change. Likewise, even optimisation studies [7,8] only require alterations to the geometric data of acoustic elements, for example the length and/or diameter of a given pipe. Again, such changes only alter the actual coefficients of the transfer matrices and do not affect the linkage of the silencer elements. This implies that the path fraction analysis need only be done once, since the order of reduction and the location of consecutively sequenced transfer matrices and the definition of sub-systems remains exactly the same. However, the results of the path fraction analysis must be logged for use in every analysis of the same basic system. For instance, since the reduction of sub-systems remains exactly the same and only the value of the coefficients may change, then the formal construction of sub-system matrices for subsequent analyses can be avoided. Instead, a data log is used immediately to position a coefficient within a sub-system matrix, rather than creation of the matrix through a decision making process which is computationally expensive.

The data logging aspect of the hybrid algorithm is fundamentally important to the overall saving of computational time, as the analysis at the initial frequency requires a significant

amount of time. The logging techniques are complex, but they are all based on Section 2.6.9.

The first technique requires the data logging as explained in Section 2.6.9. In this procedure, elements may enter 'logging an element' algorithm more than once. Therefore, the algorithm sorts the most recently visited elements to the end of the list, see Flowchart 2.9. This is required for the reduction of sub-systems to occur in the correct order compared to other reduction routines. This log is used to navigate through the silencer design when the subsequent frequencies are being analysed. It is also used in Flowchart 2.8, see Section 2.6.8, the 'Searching for an element' algorithm also uses the log to locate a previously analysed element that has an unmarked outlet.

The second data logging technique only occurs in the initial frequency analysis; this log, referred to as the 'problem' data log, records the most probable elements to cause a failure in the algorithm. If the algorithm has a problematic element, such as a resonator, it is logged, then the algorithm analyses the elements around the problematic element subsequently returns to that element. This always results in a successful analysis of the whole silencer. The log is used in Flowchart 2.8, see Section 2.6.8, when the general data log does not return a suitable element, i.e. one with an unmarked outlet. When a problematic element is retrieved from the 'problem' data log, the reference is subsequently deleted. This enables tracking of problematic elements, i.e. if one is retrieved and all the inlets and outlets become marked, it is no longer a problematic element and is subsequently removed from the log.

The third technique is to data log the reduction matrix in the form of equation (2.11) prior to the initiation of the Gauss-Jordan method, i.e. it records the entire square matrix. During the initial frequency analysis of the silencer system, the technique also records the ID number of the element associated with each transfer matrix, see Section 2.4, and the placement of their coefficients in the sub-system reduction matrix. These IDs and coefficient placing coordinates can be recalled in subsequent frequency analysis to enable the reduction matrix to be constructed with greater computational speed. Hence, reduction

via the Gauss-Jordon method of the adapted matrix can proceed. This enables fast adaptation of the reduction matrices at subsequent frequencies as opposed to the slow matrix construction for the initial frequency, as explained in Section 2.7.

The fourth data log enables sub-systems to be identified during frequency analysis subsequent the initial one. Since the general data log, which is used during the subsequent frequency to navigate throughout the silencer, only records individual elements once, this can be used to identify a sub-system. Flowchart 2.9 shows that the most recent element is stored within the general log at the end of the list. Within a sub-system the last element to be visited by the hybrid algorithm is always the element which holds the sole outlet of that system. Therefore, if the fourth log holds IDs of these elements, since the 'multi-port' algorithm can check the IDs of multi-port elements during subsequent frequencies, it can be used for a fast method of sub-systems identification, see Flowchart 2.4.

The computational efficiency of the hybrid algorithm is strongly dependent on detailed comprehensive data logs.

2.3 Objectives of the hybrid algorithm

The hybrid algorithm needs to satisfy the two main criteria; identification of two-port sub-systems and the use of data logs. Firstly, the algorithm identifies the simplest form of element linkage, namely consecutively sequential two-port elements. Whenever the outlet of a two-port element is connected to the inlet of another two-port element, then multiplication of their respective transfer matrices can occur. This is the first objective for the hybrid algorithm to achieve, namely to identify and reduce consecutive two-port elements. A full explanation of the many sub-algorithms that constitute the complete hybrid algorithm is detailed in Section 2.6.

The second objective is to use Gauss-Jordan elimination [90] of sub-systems only when it is absolutely necessary, on as small a system of elements as possible. This involves the identification of the most basic of sub-systems. For example, there is one sub-system in Figure 2. 2 and two sub-systems in Figure 2. 3. The identification of sub-systems is achieved by using the path fraction technique see Section 2.5.

The acoustic effect of a silencer system is usually calculated over a range of frequencies. The algorithm now uses the knowledge gained within the analysis of the first frequency to decrease the time required to analyse at subsequent frequencies. This is achieved by the algorithm keeping a log of all the relevant decisions that it has made during the analysis of the silencer at the first specified frequency, see Section 2.2.3.

2.4 Analysis Structure

The mathematically modelling of the acoustics of silencer systems involves a vast amount of repetitive calculations; hence computational code has already been used. Since there are similarities between different acoustical elements, correct grouping of these will enable the computational efficiency to be increased significantly. The use of object oriented programming (OOP), in conjunction with polymorphism, by using the C++ [91,92] programming language simplifies the grouping and classification of different elements. Inheritance [91] will ensure that all elements consist of exactly the same fundamental properties. This occurs through the precise building of individual objects through the use of classes [91]. Therefore, elements can be grouped and processed according to their most common properties, for example:

- All elements will have a base class [91] called 'general element'.
- All single port elements will inherit a class that consists of functions and data members [91] that processes sub-routines which only concern these types of elements.
- Similarly, a two-port element will inherit a specific class which itself inherits a class that will process two-by two-transfer matrices.
- All multi-port elements will inherit a class that will process the path fraction technique.

Since the type of mathematical analysis used allows the acoustic behaviour of each element to be calculated separately, the computational model of each element will be modelled by a separate object [91]. Every element will be linked to another element by pointers [91]. These pointers will be adapted as reduction of sequential elements and sub-systems occur. Since pointers rely on computer address systems [91], retrieval of objects will rely on an individual identification system created by the programmer. This is a result of each computational object of an individual acoustic element requiring construction and destruction [91] for each individual frequency of analysis. Every computational model of an element will have a different identification number (ID) which will be issued when the silencer model file is read. The elements can be retrieved via a dynamic array [91] of pointers in the cast [91] format of the base class 'general element' called 'index'. The ID will relate to the position within the dynamic array where the address of that individual element is located.

As the hybrid algorithm proceeds through a given silencer, the algorithm is not aware of the overall geometry of the silencer. At any given point within the analysis, the algorithm is only aware of the immediate properties of the acoustic element which is currently being processed. Any other information which the algorithm is allowed to use is constituted by the decisions that have been made previously and the elements which it has visited. This documentation is kept in the log, which is internally stored by the computer memory. The log is referred to in the analysis of the silencer at the first specified frequency and at

subsequent frequencies. Therefore, the log stores IDs to reference elements and lists of integers to represent decisions that the algorithm has made.

Many areas of recording and copying information require the copying of complex objects. These objects often contain dynamic arrays that are referred to by pointers, thus the objects need individual copying functions. This implies the use of lists [92], however C++ library lists cannot be used as a result of the complexity of the class structure. Individual list and copying functions have to be written because classes consist of dynamic arrays which change in size throughout the algorithm.

2.5 Path fraction technique

The path fraction technique is used to identify sub-systems. These sub-systems can have any number of any type of elements. Overall, they must have one inlet and outlet and they must also start and finish with a multi-port element. They do not have to be sequentially ordered. The reduction of a sub-system relates the acoustic behaviour of a single inlet on a multi-port element, to a single outlet of another, or the same, multi-port element via a two-by-two transfer matrix. Once a system is identified, Gauss elimination can reduce the system to a two-by-two transfer matrix, therefore it can be modelled as a two-port element. Sequential transfer matrix multiplication between two-port elements either side of the system can proceed.

Identification of sub-systems commences when the hybrid algorithm encounters a multi-port element. At this point, a path fraction, say ϕ, is introduced which is unique to that multi-port element. Initially ϕ=1 and it is then divided by the number of outlets within the multi-port element. The identification is completed when the value of the path fraction is restored to ϕ=1.

2.5.1 Example 1, A pair of parallel paths (Quincke tube)

Figure 2. 2 represents a pair of two-port elements in parallel which are situated between two other two-port elements in conventional sequential order. All of the two-port elements may represent any conventional sequence of two-port elements, or indeed, any other reducible sub-systems, without loss of generality to the algorithm. When the algorithm encounters an inlet port, or an outlet port, it flags the port concerned, thus enabling the algorithm to track where it has been. The algorithm departs the first two-port element and acknowledges that the subsequent element is a multi-port element which has two outlet ports. Therefore, the algorithm issues a path fraction of ϕ_1=1 for this multi-port element, say element 1, and subsequently divides it by the number of outlets, such that ϕ_1=0.5 at both outlet ports. The algorithm takes either of the two outlet paths, each of which leads to a two-port element, analyses it and then proceeds from the outlet port to the inlet port of the next multi-port element. Thus the algorithm is now at F_2, with respect to Figure 2. 2. The inlet port at which it arrives is marked and the associated value of ϕ_1 is set as ϕ_1=0.5, having been carried along the path through the preceding two-port. The algorithm notes that the other inlet port is not marked. Hence, the algorithm retraces its path back to the first multi-port, where it searches for an unmarked outlet port. It then follows through this outlet port in the same manner as described above, until it progresses to F_2 again. At this point both the inlet ports of the fork are marked, hence addition of path fractions can occur. Both of the path fractions at the inlet ports of the fork come from F_1 and therefore refer to the same path fraction, i.e. ϕ_1. The value of ϕ_1 is 0.5 at each inlet port, thus when these quantities are added together, ϕ=1. Therefore, a complete sub-system has been identified and the reduction of that sub-system, to an equivalent sub two-port, can proceed. This reduction procedure is explained in Section 2.7. It results in a single two-by-two transfer matrix that describes the acoustic behaviour of the two parallel, two-port elements and the multi-port elements. This equivalent two-port element is now in sequential order with the first two-port element as shown in Figure 2. 2, hence their transfer matrices are multiplied together to give a single equivalent two-port element. The algorithm now proceeds through the single outlet port of this reduced system and notes that the final element shown in Figure 2. 2 is yet another two-port element.

Thus, the transfer matrices of these sequential two-ports are multiplied together to give an overall two-by-two transfer matrix for the single equivalent two-port element of the entire system.

2.5.2 Example 2, Nested parallel paths

Figure 2. 3 illustrates a set of nested parallel paths. In this example there is one pipe element between each fork, however, there can be any number of consecutively sequenced two-port elements or reducible sub-systems without loss of generality. The hybrid algorithm starts as in Section 2.5.1 and progresses past F_1, the first fork or a multi-port element, which has two outlet ports, hence ϕ_1=0.5 at each outlet. The algorithm then randomly chooses an outlet path, say the path from F_1 to F_3. The algorithm analyses the two-port element as it travels along the path and conveys the path fraction ϕ_1=0.5. At F_3, the second fork, another multi-port element is encountered that has a single inlet and multiple outlets. Thus another path fraction, say ϕ_2, is created for this element, where ϕ_2=1. All of the path fractions relevant to this element are divided by the number of outlets, therefore ϕ_1=0.25 and ϕ_2=0.5 at each outlet port of the element. The algorithm progresses to analyse the two two-port elements between F_3 and F_4, as shown in Figure 2. 3, in a similar process to that of Section 2.5.1. When both of the inlets associated with the fork element at F_4 become marked, addition of the path fractions occurs. This results in ϕ_1=0.5 and ϕ_2=1, which identifies a reducible sub-system between F_3 and F_4. The sub-system identified is exactly the same as in Section 2.5.1 and results in a single transfer matrix characterizing the acoustic behaviour between and including F_3 and F_4. This procedure terminates the need for path fraction ϕ_2 which is subsequently discounted. Now the algorithm analyses the multi-port element at F_2 and observes that it has one marked and one unmarked inlet. Therefore, the algorithm subsequently retraces the steps it has made to the multi-port element at F_1 to find an unmarked outlet and proceeds along that path. The algorithm analyses the two-port element on the path and re-enters the fork element F_2. The algorithm now observes that both of the inlets associated with the fork are

marked, hence addition of the path fractions occurs. The only path fraction at these inlets is ϕ_1 and after addition, ϕ_1=1. Therefore, a second reducible sub-system has been found and the reduction procedure is used to create a two-by-two transfer matrix that describes the acoustic behaviour between F_1 and F_2. This results in three conventionally sequenced transfer matrices that are multiplied together to give a transfer matrix that acoustically characterizes the behaviour of the overall system.

2.5.3 Example 3, Overlapping paths

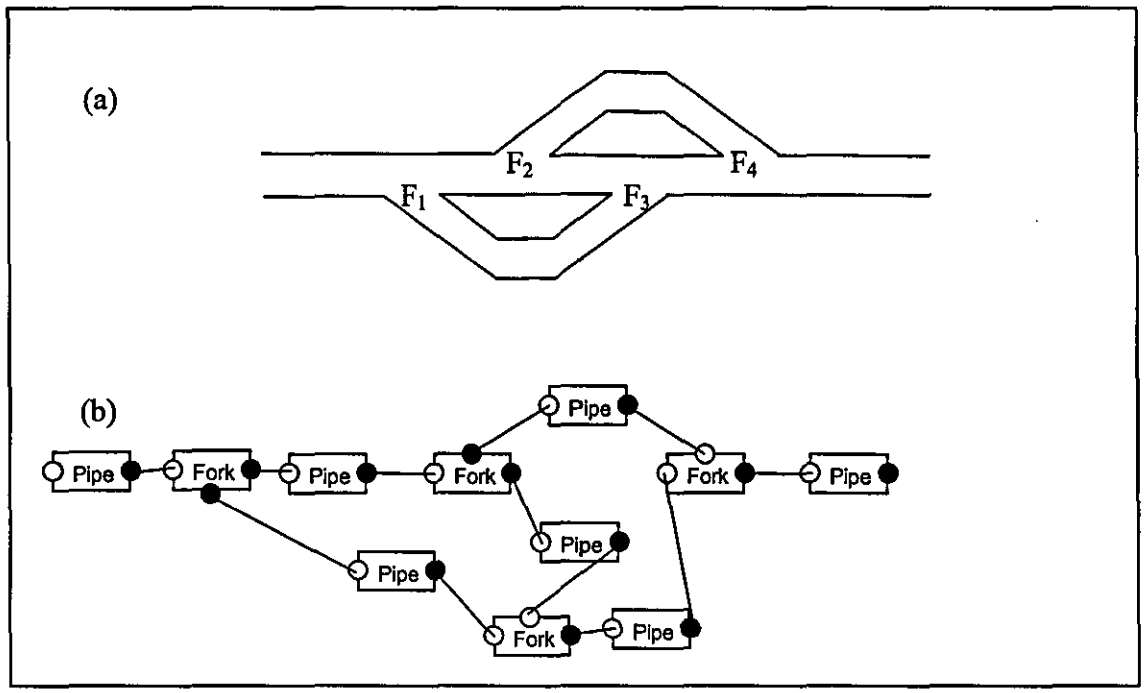

Figure 2. 7 Over lapping paths

A more complicated system to analyse is shown in Figure 2. 7. As in the previous examples, the path fraction value at the outlet ports of F_1 is ϕ_1=0.5. The algorithm then proceeds through an outlet, say from F_1 to F_3 and analyses the two-port element along that path. As before, only one pipe element is shown between the fork elements, however, each could be regarded as any number of consecutively sequenced two-port elements or reducible sub-systems without loss of generality. When the algorithm first arrives at the fork element at F_3, it marks one inlet port and associates ϕ_1=0.5 with this port. The other

inlet port is unmarked and so the algorithm retraces the steps which it has made. It then progresses along the path from F_1 to F_2, while analyzing the elements along that path. The algorithm enters the fork at F_2 and creates another path fraction, resulting in ϕ_1=0.25 and ϕ_2=0.5 at both outlet ports of F_2. Suppose the algorithm next proceeds from F_2 to F_3, as shown in Figure 2. 7, analysing the two-port elements along the path. At F_3, the second inlet port is marked which results in addition of the path fractions to give ϕ_1=0.75 and ϕ_2=0.5 at the outlet port of F_3. Since there is a new junction, there will be another path fraction ϕ_3=1, the unity value being due to the fork element having a single outlet. The algorithm proceeds to F_4, as always analysing the two-port elements along the path, where it subsequently retraces to F_2, because there is only one marked inlet. The algorithm now chooses the path from F_2 to F_4 indicated by the unmarked outlet port on the fork element at F_2. When the algorithm reaches F_4, all of the inlets are marked, therefore addition of the path fractions occurs. At F_4 there are two inlets; one with ϕ_1=0.25 and ϕ_2=0.5, the other inlet has ϕ_1=0.75, ϕ_2=0.5 and ϕ_3=1. Hence, the resulting summation leaves all the path fraction with unity value. Subsequently, the entire sub-system from F_1 to F_4 is reduced as a single entity, leaving three consecutively sequenced two-by-two transfer matrices that can be multiplied together.

2.5.4 Example 4, A side branch

The path fraction technique is also applicable to side branches. As previous examples have shown, the path fraction algorithm creates a path fraction with value ϕ_1=0.5 at both outlet ports of F_1, with respect to Figure 2. 8. The algorithm then randomly picks the path which is attached to the closed end and proceeds along the path. Between the fork element and the closed end, there could be any number of sequential ordered two-port elements or reducible systems without loss of generality. If the algorithm picks the path which leads to the outlet and ϕ_1 is non-unity, the algorithm retraces the steps it has made and subsequently finds the other path.

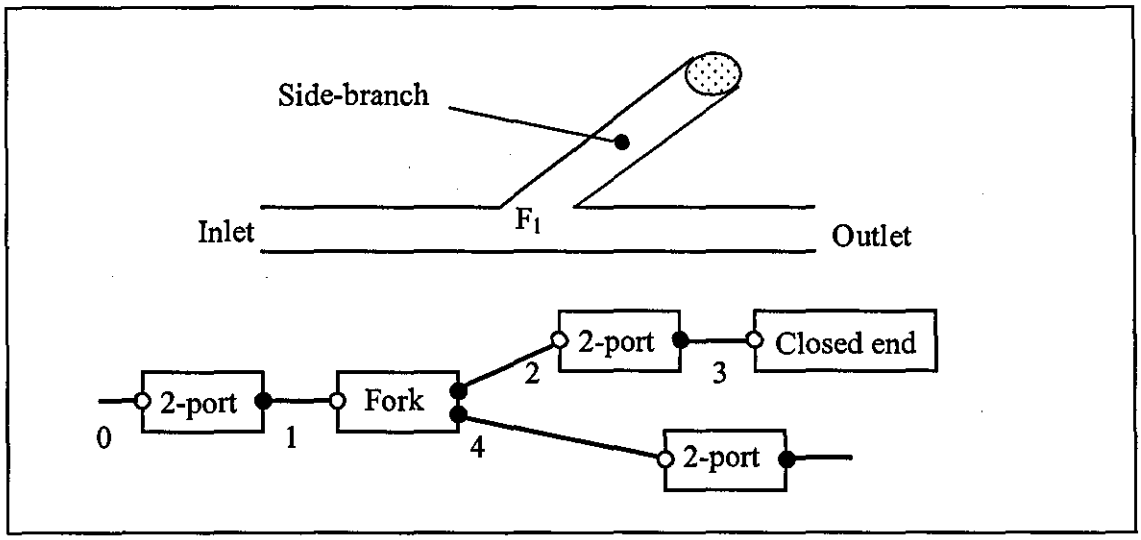

Figure 2. 8 A side branch

When the algorithm reaches the closed end, it evaluates a wall admittance, say $A_w=V/P$. When the hybrid algorithm eventually reaches a closed-end there are only two possibilities. Either, there is one equivalent two port element between the closed-end and the multi-port element, or else there is no element at all. Let A_{w3} be the wall admittance at the closed-end. With respect to the numbering system of the ports given in Figure 2. 8, let

$$\begin{bmatrix} P_0 \\ V_0 \end{bmatrix} = \begin{bmatrix} a_{01} & b_{01} \\ c_{01} & d_{01} \end{bmatrix} \begin{bmatrix} P_1 \\ V_1 \end{bmatrix}. \tag{2.14}$$

Now

$$V_1 = V_2 + V_4 \tag{2.15}$$

and

$$P_1 = P_2 = P_4. \tag{2.16}$$

If an admittance [1], A_{w2}, can be found at position *2*, the side-branch and closed end can be reduced. Let

$$\begin{bmatrix} P_2 \\ V_2 \end{bmatrix} = \begin{bmatrix} a_{23} & b_{23} \\ c_{23} & d_{23} \end{bmatrix} \begin{bmatrix} P_3 \\ V_3 \end{bmatrix}, \tag{2.17}$$

then

$$A_{w2} = \frac{c_{23} + d_{23} A_{w3}}{a_{23} + b_{23} A_{w3}}. \tag{2.18}$$

Hence, an overall admittance, A_{w2}, can be calculated for the combined effect of the two-port and termination elements using equation (2.18). Therefore, the relationship between *0* and *4* is

$$\begin{bmatrix} P_0 \\ V_0 \end{bmatrix} = \begin{bmatrix} a_{01} + b_{01} A_{w2} & b_{01} \\ c_{01} + d_{01} A_{w2} & d_{01} \end{bmatrix} \begin{bmatrix} P_4 \\ V_4 \end{bmatrix}. \tag{2.19}$$

The reduced acoustic characteristic of the side branch is often left until a Gauss elimination routine is used to reduce the whole sub-system. This is common when analysing complex silencer systems consisting of resonator walls as shown in Figure 2. 4 and Figure 2. 5. However, within silencer systems, 'specific' side-branch systems occur, as shown in Figure 2. 8. This type of system can incorporate wall admittance A_{w2} into the two-port element prior to the fork, as shown in equation (2.19). Since the side branch has been reduced to leave a net two-by-two transfer matrix, the path fraction, which was associated with the fork element, is disregarded.

2.5.5 Example 5, Loop-back path

An example of a multi-port element which contains a loop-back path is the simple flow-reversal, two-pass resonator system shown in Figure 2. 9. A multi-path resonator element consists of any number of parallel, perforated tubes within an outer casing which is impervious. If a resonator element has n-1 perforates, a $2n$ x $2n$ transfer matrix can be evaluated, which relates the n distinct plane-wave acoustic pressure and velocity values at one end of the element, to those at the other end [5,60,65]. Thus, unlike a fork element, the inlet and outlet ports are not grouped at each side of the element, but each port is marked as being an inlet or an outlet. In Figure 2. 9, as in previous examples, an open circle denotes an inlet port and a filled circle an outlet port. In this particular example, the outer casing is terminated at the extremes of the two perforates by the end walls of the silencer box, hence the casing has outlet ports at both ends which lead directly to closed end elements.

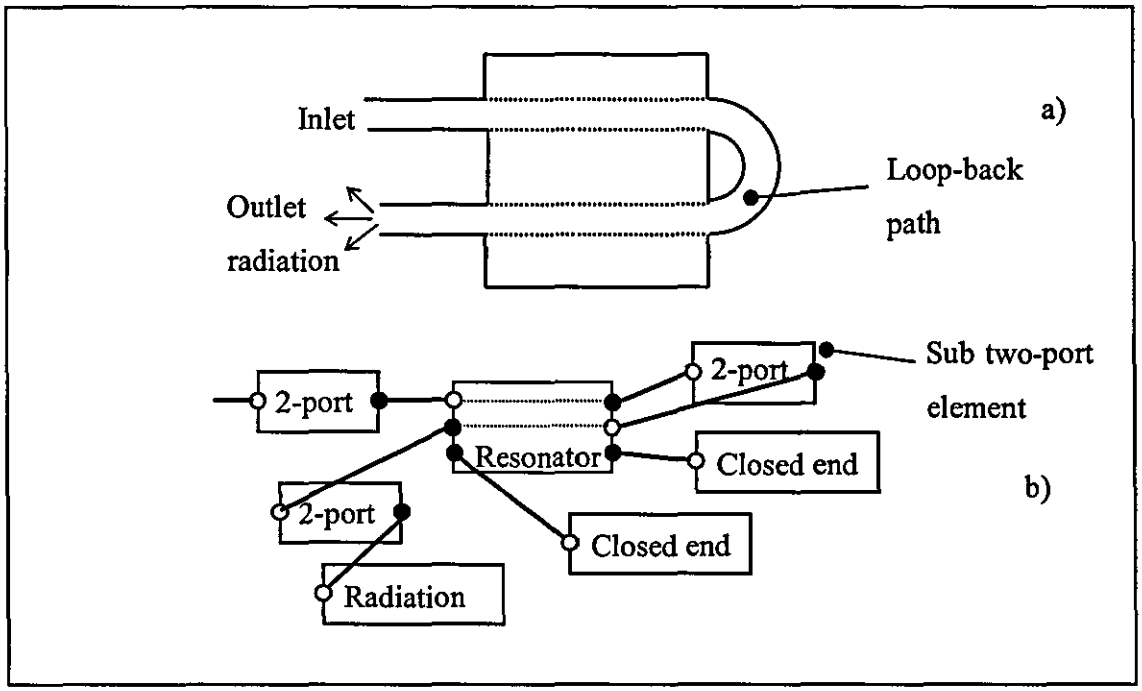

Figure 2. 9. Two-pass flow-return resonator with loop-back path

The algorithm evaluates the two-by-two matrix of the first two-port element and then proceeds along the link from the outlet port to the resonator element, where it sets the flag at the first inlet. There is also an un-flagged inlet port for the element, but the only current path fraction is the new one for the resonator element, say ϕ_1 where ϕ_1=1. Hence, rather than retrace the inlet path, the algorithm switches mode and follows the outlet paths. The flagged inlet is marked as the single overall inlet port to the multi-path element and then the path fraction of the resonator element is divided by the total number of outlet ports, such that $\phi_1 = 1/4$.

Although it is irrelevant to overall functionality, outlet paths are treated in the order of top to bottom, left to right hand sides of an element. In this case, therefore, the algorithm follows the link to a two-port element, then evaluates the associated two-by-two transfer matrix, and proceeds to the radiation element. The latter marks the end of the silencer system, but since the path fraction is less than one, the algorithm retraces the path back to the resonator element, where it marks the outlet port as the single overall outlet of the element. The link from the next outlet port is followed to a closed end element. This is a very simple case of a side-branch path as discussed in Section 2.5.4. The path is retraced and at re-entry to the resonator element, the outlet port is eliminated, such that now ϕ_1=1/3.

The link from the next outlet port leads to a two-port element then back into the resonator element at an inlet port. This is the loop-back path. The intermediate two-by-two matrix gives sufficient equations to eliminate effectively the acoustic variables associated with the outlet port, so again this becomes redundant and now ϕ_1=1/2. Finally, the algorithm follows the link from the last outlet port to another closed end element, the path is retraced and now ϕ_1=1. Unification of the path fraction signals that a complete sub-system has been identified. This can be reduced to a two-by-two transfer matrix of an equivalent two-port element between the single overall inlet and outlet ports of the resonator element, see Section 2.2.2. The entire system is now composed of three sequential two-port elements which are reduced into one, see Section 2.2.1.

2.5.6 Example 6, Triple pass with flow returns

This example is a commercial silencer designed by Arvin Meritor [93]. The hybrid algorithm starts with analysing element 1, as shown in Figure 2. 10 and then proceeds through the outlet of that two-port element. Since both elements 1 and 2 are two-port elements, their transfer matrices are multiplied together and the algorithm proceeds through the outlet of element 2. This transfer matrix multiplication happens with the two-by-two transfer matrices associated with elements 1-5, as they are all in sequential order.

The hybrid algorithm reaches element 6 and observes that it is a multi-port element with only one marked inlet, the port through which the algorithm has entered. The algorithm now creates a path fraction for this multi-port element and divides it by the number of unmarked outlets, so ϕ_1=0.2.

The algorithm now selects the first outlet on the left hand side of the resonator nearest the top, as shown in Figure 2. 10, and proceeds to analyse pipe element 7. At the fork element 8 a new path fraction is created and both the path fractions are divided by the number of unmarked outlets, such that ϕ_1=0.1 and ϕ_2=0.5 at the outlet ports of this element. Here the algorithm randomly picks an outlet, say element 11 and proceeds to analyse it. At fork element 12 another path fraction is created and the path fractions at the outlet ports are now ϕ_1=0.05, ϕ_2=0.25 and ϕ_3=0.5. The algorithm proceeds to analyse elements 13 and 14, which constitute a 'side branch' that is reduced in the manner given in Section 2.5.4. Subsequently, the algorithm reduces elements 11-15 into one equivalent two-by-two transfer matrix and two-port element, which is associated with element 11. The outlet link of element 11 is realigned with the inlet of the resonator element, hence replacing element 15. The path fractions here are now ϕ_1=0.1 and ϕ_2=0.5 and ϕ_3 has become redundant. The algorithm proceeds through the outlet of element 11 to the resonator element and observes that all of the inlets associated with that element are not marked. Consequently, the algorithm retraces the steps that it has made until it reaches the fork element 8, where there is an unmarked outlet. It proceeds to analyse elements 9 and 10. When the algorithm reaches element 10, it realises that elements 7-11 constitute a

sub two-port element and that elements 9 and 10 form a side-branch, thus, the algorithm reduces them to a single equivalent two-by-two transfer matrix associated with element 7. Path fraction ϕ_2 has now become redundant. The revised elements 7 and 11 now form two successive two-port elements which are multiplied together and at their outlet port, ϕ_1=0.2. The outlet port of element 7 now links to the inlet of the resonator where element 15 was originally connected.

The algorithm has discovered a loop-back path and reduced all the elements associated with it into one sub two-port element. Thus, as in Section 2.5.5, the number of outlet ports is reduced by one and now ϕ_1=0.25 at the remaining outlet ports of element 6. The algorithm proceeds to analyse the path associated with the next outlet towards the bottom of the resonator on the left hand side, namely elements 16 and 17. The overall admittance of the two elements can be calculated, see Section 2.5.4. These elements do not constitute a 'specific' side-branch, see Section 2.5.4, as it is attached to a resonator and not a fork. Therefore, the evaluated wall admittance associated with element 17 is left. The inlet of element 17 is linked to the resonator where the link to inlet of the element 16 used to be, ϕ_1 is re-evaluated to give ϕ_1=0.33.

The algorithm now proceeds to the outlet port at the top right hand side of the resonator to find and reduce the second loop-back path in a similar manner to that already described, leaving ϕ_1=0.5. The algorithm then moves to the next outlet port on the right hand side of the resonator and reduces the consecutively sequenced elements 25-27. It realises that element 27 is the last element, but since $\phi_1 \neq 1$, the algorithm searches for an unmarked outlet. Element 28 is found via the search and after analysing that element and element 29, ϕ_1=1. Subsequently, reduction between the original outlet of the element 5 and inlet of element 25 results in three sequenced transfer matrices and hence an overall transfer matrix for the silencer system.

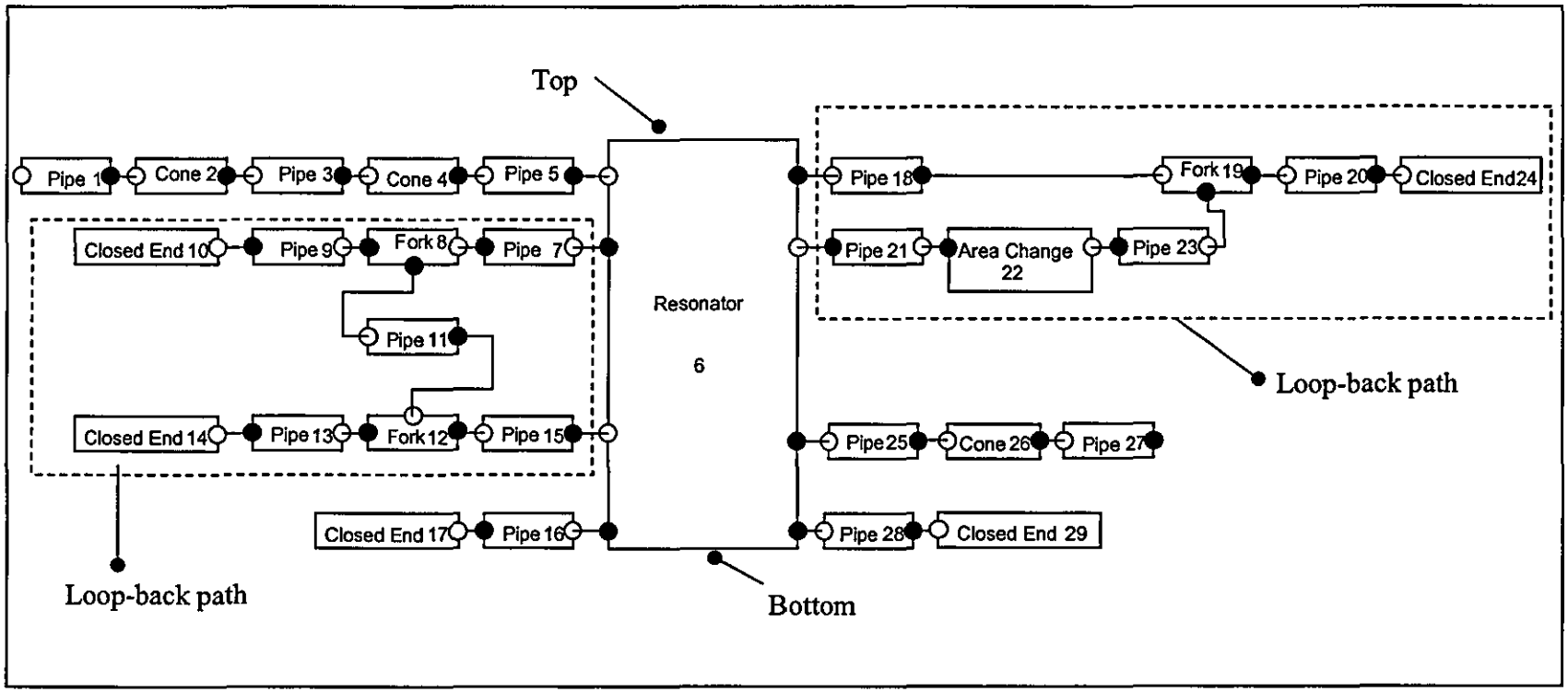

Figure 2. 10. Acoustic element representation of a silencer which has a triple pass with flow returns

2.6 Algorithms

2.6.1 Main algorithm, Flowchart 2.1

(All the flowcharts are at the end of the chapter, and can be referenced by their flowchart numbering. The flowcharts are linked together via distinctive boxes, for example if a box has 'F2.3' then it links to Flowchart 2.3. On the linked flowchart, say Flowchart 2.3 the algorithm will commence at box 'Link F2.3'.)

The main algorithm as shown in Flowchart 2.1 is concerned with retrieving and recording data combined with grouping elements ready for processing. The first process which this algorithm achieves is to acquire the data from a file and build an internal computational model of the system. This requires objects to be constructed and the properties of each individual acoustic element to be stored in these elements. Then the process sets the links between objects using pointers. When the file is read, dynamic arrays of pointers in the form of base casts [91,92] are compiled; this enables rapid retrieval and copying of internal data. At this point the initial frequency is set and a Boolean variable L is set to true. This variable distinguishes the first frequency from the subsequent ones. The variable is needed to allow subsequent algorithmic routines to ascertain whether data logs have to be compiled or referenced.

The 'main' algorithm then proceeds to make a totally separate copy of the internal computational model of the silencer. This is required because the pointers linking the elements change throughout every individual frequency analysis. Hence, when a frequency has been analysed, a new copy of the original silencer design is required. As a result of careful logging, as the file is read, data is recorded for memory space allocation. This log is kept to enable rapid copying functions. When the copying procedure has been completed, the first element is retrieved from the memory, namely the element pointed to by the outlet of the source element.

Since the analysis is considering the initial frequency, the first element is logged in the 'general' log as explained in Section 2.6.9. Then the algorithm proceeds to assess the number of ports that are in the first element. Thereafter the appropriate sub-algorithm is called:

- For a two-port element, the sub-algorithm is explained in Section 2.6.2.
- For a single-port element, the sub-algorithm is explained in Section 2.6.3.
- The multi-port element sub-algorithm is explained in Section 2.6.4.

If the current element being analysed is not a radiation element, the 'Main' algorithm proceeds to acquire the next element to analyse. Since the initial frequency is still being analysed, the sub-algorithm 'Locating an element' algorithm is called. This is explained in Section 2.6.7. If the frequency is not the initial frequency, the next element can be located by using the log, Section 2.6.10. At this point the 'Main' algorithm loops back on itself as shown in Flowchart 2.1. The loop breaks when the radiation element is found. When this happens, the overall two-by-two transfer matrix, which describes the acoustic characteristics of the whole silencer system at a specific frequency, is recorded. If the frequency is not set to the maximum frequency, the Boolean variable L is set to false and the frequency is increased. After this, the algorithm loops back and analyses the silencer at the new frequency, as shown on Flowchart 2.1. Hence a copy of the original silencer design is made and analysis proceeds. On this loop and subsequent loops, the 'general' log has already been built, therefore, at the new frequencies, the system will be analysed rapidly.

2.6.2 Two-port algorithm, Flowchart 2.2

This algorithm is devised essentially to construct the two-by-two transfer matrix of any given two-port element and it identifies two consecutively sequenced four-pole transfer

matrices. This algorithm receives a two-port element and then evaluates the transfer matrix according to the type of element. This is achieved by casting [91] the element and calling an evaluation function that depends only on the angular frequency. The other parameters do not vary with frequency and therefore are held in the object according to the acoustic element type.

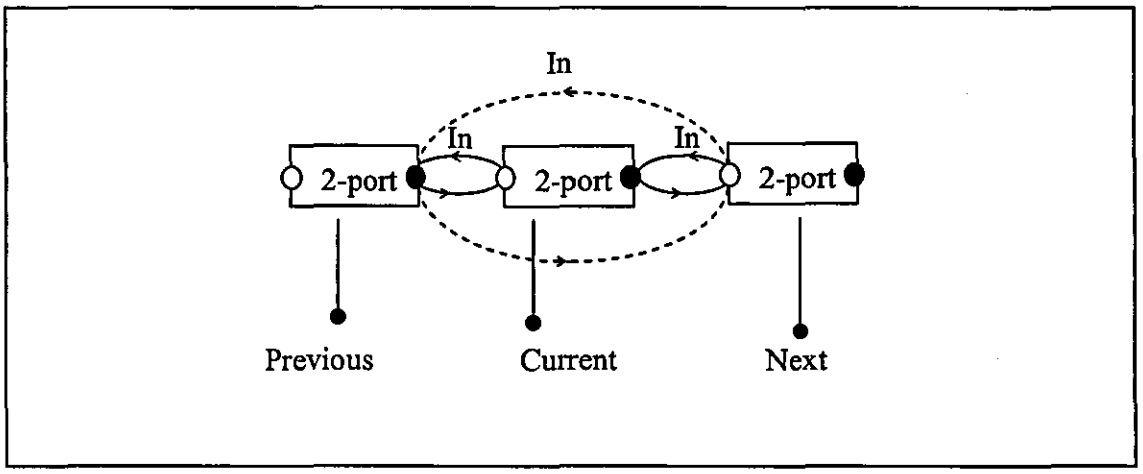

Figure 2. 11 Three sequential two-port elements illustrating pointer linkage

The total number of ports within the previous element is checked, see Figure 2. 11, once the transfer matrix of the current two-port element is evaluated. If the previous element has two ports, then multiplication of transfer matrices can proceed. When this happens, the pointers that belong to the previous, current and next elements are realigned.

The class 'general element' has two dynamic arrays consisting of 'node' classes. These classes have a pointer within them; either an inlet pointer, or an outlet pointer. With reference to Figure 2. 11, a hollow circle denotes an inlet and a solid circle denotes an outlet. The solid lines between the inlet and outlet refer to a pointer linking the objects/elements prior to pointer realignment. Hence, the dotted lines relate to the pointer redirection after the 'Realign pointers' process box, with reference to Flowchart 2.2. Let the 'Out' pointers in Figure 2. 11 belong as a data member to the outlet 'node' class, which points to the inlet node/port of the following element. Similarly, the 'In' pointer is

a data member of the inlet 'node' class and it points to the outlet node/port of the preceding element.

Let the resultant transfer matrix that arises after multiplication of the transfer matrices of the 'previous' and 'current' two-port elements be stored as the new transfer matrix of the 'previous' element. The 'current' element is now redundant. Thus, let the outlet pointer belonging to the outlet 'node' of the 'previous' element be redirected to point to the inlet node of the 'next' element, see Figure 2. 11. Similarly, let the pointer belonging to the inlet node of the 'next' element be redirected to point to the outlet node of the 'previous' element. Subsequently, the 'current' element has disappeared from the computational model, but the object has not been destructed. The 'previous' element is renamed as 'current' and returned to the 'main' algorithm.

If the total number of ports in the 'previous' element was not equal to two, the matrix multiplication and pointer realignment would not occur. This is shown on Flowchart 2.2.

2.6.3 Single port algorithm, Flowchart 2.3

This algorithm receives a single port element from the 'Main' algorithm. Within this explanation of the hybrid algorithm, the 'Single port' algorithm will only encounter a closed end or a radiation. Note that a termination/closed end is referred in the hybrid algorithm as a 'closed end' object [91]. The 'Single port' algorithm will verify if the single port element is a closed end and, if not, the radiation element will simply be returned to the 'main' algorithm, see Flowchart 2.3.

Assume then that the received element is a closed end. The 'Single port' algorithm will proceed to calculate the wall admittance. This admittance depends on the angular frequency set in the 'main' algorithm and the parameters which are stored internally in the computational object class 'closed end'. Once this admittance has been calculated, the

'single port' algorithm identifies whether or not the previous element, indicated by the inlet 'node' class, has two ports. If this is true, then A_{w2} is calculated, see equation (2.18). If it is not true, the single port element is returned to the 'main' algorithm. In the former case, pointer realignment will occur between the closed end and the node pointed to by the inlet node pointer of the two-port element. This is done in the same way as described in Section 2.6.2.

The 'Single port' algorithm proceeds to verify if the element pointed to by the pointer within the inlet 'node' is a three-port fork element. If the configuration is exactly the same as in Figure 2. 8, then equation (2.18) is used to incorporate A_{w2} into the preceding two-port element. This is pointed to by the pointer in the inlet 'node' of the fork. If not, then the closed end is returned to the 'Main' algorithm. If the element configuration is the same, then the elements either side of the closed fork, ignoring the closed end branch, have their pointers realigned to point to each other, such that the fork element and closed-end branch disappear from the computational model. The overall transfer matrix is associated with the two-port element which is connected to the inlet of the fork and this is returned to the 'Main' algorithm.

2.6.4 Multi-port algorithm, Flowchart 2.4

This algorithm essentially accesses the different types of multi-port elements and refers them to appropriate sub-algorithms. As Section 2.6.7 explains in detail, each 'node' class has a Boolean variable which is initially set to false. The hybrid algorithm encounters a 'node', this variable is set to true. It is used to detect which groups of path fraction need adding together, as explained in Section 2.6.6. Within the 'Multi-port' algorithm the integer value B is given a specific value which will enable the 'Resonator path fraction' algorithm to process the path fractions appropriately.

With reference to Flowchart 2.4, the 'multi-port' algorithm receives a multi-port element and firstly sets B to zero. It then enquires whether or not L is true. If L is false, then a data log has already been created. The algorithm then checks if the multi-port element is a resonator and if the associated transfer matrix needs evaluating, if so, the matrix is evaluated. The algorithm checks if the ID of the multi-port element is the same as the ID of the next element recorded in the reduction log. This log records the last element ID of sub-systems that have to be reduced by Gauss elimination. If the IDs are the same, then there is a sub-system ready for reduction, hence reduction takes place. After this the received element is returned to the 'Main' algorithm.

If 'L' is true, as in Section 2.6.1, hence the data log has yet to be created, the type of the multi-port element is first checked. If the element is a fork, it is passed to the 'Path fraction for forks' algorithm, see Section 2.6.5. Otherwise, the multi-port element is a resonator. If the transfer matrix of the resonator has not yet been evaluated, it is evaluated now. The next step is to set the value of an integer variable B which is used to control the flow of the subsequent steps. If the previous element which is held in the general log:

- Is attached to the source element, then B equals 1.
- Is a closed end, then B equals 2.
- Is a sub two-port, element then B equals 2.

If these equality checks, as shown above, all fail, then the inlets on the left hand side of the resonator are checked to see whether more than 2 are marked and that there are none on the right hand side. If true, the value of B is set to 3. If false, the ports on the left hand side of the resonator will be tested to see if all the ports are marked. If this verification is true, B is set to 4, if not, B is set to the default of 1. Then the resonator element is passed to the 'resonator path fraction' algorithm with reference to Flowchart 2.11. When the element is passed back to the 'multi-port' algorithm, the path fraction corresponding to the element is checked. If the value is unity, then this means that a sub-system has been found; hence the system is sent to be reduced. If not, the element is returned to the 'Main' algorithm.

2.6.5 Path fraction for forks algorithm, Flowchart 2.5

This algorithm decides if a path fraction needs to be created, or if the path fractions that are entering the fork element need to be added together. The algorithm receives a fork element, it then checks whether or not all the outlets are marked except for one. If so, the 'Path fraction addition' algorithm is called, see Flowchart 2.5. If not, then a new path fraction is added to the algorithm and then all the path fractions are divided by the number of outlets.

2.6.6 Path fraction addition algorithm, Flowchart 2.6

This algorithm compiles two or more lists of path fractions into one and from that new list it accesses whether or not there is a sub-system that can be reduced. Let ϕ denote a path fraction label and an associated subscript relates to an individual, multi-port element. Also let the Boolean variable L be set to false, this variable is true when there is a path fraction with the same label in two or more lists.

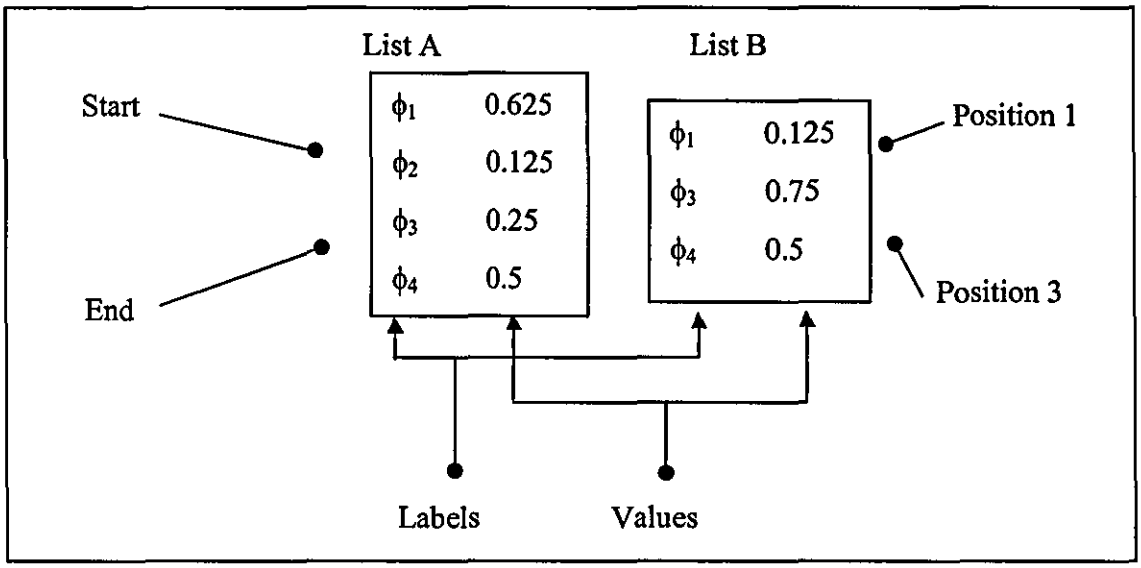

Figure 2. 12 List of path fraction labels and values

The algorithm receives a collection of path fraction lists referring to specialized lists rather than C++ library list, see Section 2.6.9. It sorts the list order according to the length of the lists, let 'List A' be the largest list where p is the length of the list, see Figure 2. 12. Then it sets r to the number of received lists.

The algorithm checks if there are more than two path fraction lists to add together, see Flowchart 2.6. Then the algorithm selects another list, 'List B', where q is the length of the list. The list is checked to see whether or not it has any members that require adding or inserting into 'List A'. If not, the algorithm loops back to access another list. If so, it continues to add 'List B' to 'List A'.

When the algorithm adds two lists, it sums the path fraction values which have the same labels. It then inserts path fractions that appear in the smaller list, but not in the larger one. Therefore, when adding the path fraction lists, the algorithm initially sets f to equal p and passes through a decision that checks if f is larger than 0. Then the algorithm checks if the label at position q in 'List B' has the same label in position f in 'List A', see Figure 2. 12. If so, the associated values are added together and replace the value in 'List A' and L is set to true. Now f is decreased by one. If not, f is just decreased by one. The algorithm returns to the decision box, this ensures that the member at position q in 'List B' is checked with every member in 'List A'. If a data member appears in 'List B' and not in 'List A', L remains false. Hence, if L remains false, the member at position q in 'List B' is inserted into 'List A' after position q, and then p is increased by one. If L is true, it is reset to false. Now q is decreased by one regardless of the state of L.

The algorithm returns to verify if q is larger than 0. If so, the member at position q is checked against list members in 'List A', as stated. If not, r is decreased by one as a complete list has been checked against 'List A'. Now, suppose that a list has been checked, the algorithm verifies if there is another list to check against 'List A'. If r is not larger than one, then all the lists have been combined into one list, 'List A'. Now 'List A' is checked for path fractions of value l. If one or more of the members of 'List A' has an

associated path fraction of 1, the labels associated with the members relate to the multi-port elements within a sub-system that can be reduced. Therefore, this sub-system is subsequently reduced. If there are no path fractions that equate to 1, a new path fraction is added. This accounts for the multi-port element that brings the path fractions together. Lastly, all the path fractions in 'List A' are divided by the number of outlets of that element.

2.6.7 Locating an element algorithm, Flowchart 2.7

The purpose of this algorithm is to locate the next element quickly. If it cannot, it will call another algorithm which will search thoroughly for an element. Hence it will reduce computational time when elements are ordered sequentially. This is done to ensure rapid processing.

Each inlet or outlet node/port is modelled by a 'node' class, which has a pointer to the next element and a marker. The marker is either true or false, where true denotes that the algorithm has already visited that port.

The algorithm receives from the 'Main' algorithm an element that has been analyzed and first checks whether or not there is an unmarked outlet. If not, the algorithm will call the 'Search for an element' algorithm, see Section 2.6.8. Alternatively, if there is an unmarked outlet, the algorithm will mark the outlet of the 'current' element and the inlet of the 'next' element. The 'next' element is pointed to by the pointer associated with the outlet of the 'current' element. Then the algorithm will test if the 'next' element is pointing to a resonator. If so, it will log the resonator in the 'problem' log, see Section 2.6.9. The algorithm will only select a resonator if it is absolutely necessary. Reduction of a silencer system is simpler if the elements surrounding the resonator are analysed prior to the involvement of the resonator within the algorithm.

Now the algorithm will then test if the 'next' element which is pointed to by the marked outlet has an unmarked inlet. Providing this test is false, the element, which is pointed to by the outlet, is retrieved. Otherwise, the 'search element' is used to find the 'next' element. After finding the next element, the 'locating an element' algorithm logs that element in the problem log, if it is a resonator. Then the element is returned to the 'main' algorithm. Resonators often cause problems with conventional code and therefore are logged in a problem log. If the 'search element' algorithm has a problem, it will revert back to the problem log, see Section 2.6.8.

The first logging of a resonator enables the 'Search element' algorithm to retrieve the resonator if it cannot find another element to analyse. On element retrieval the entry in the 'problem' log is removed. However, the resonator may cause reduction problems in the future, therefore it is re-entered.

2.6.8 Searching for an element algorithm, Flowchart 2.8

This algorithm retrieves the next element which is not immediately within the local area of the current element. Hence, the object of the algorithm is to search the 'general' and 'problem' logs to locate a probable next element. These logs are different to the arrays in which the elements are stored. A log is a specialist list [91] that holds references to an element and associated information about that element within the context of the list. The C++ library has a list class. However, if a class has an associated dynamic array, the C++ list does not make a total separate copy of the class and the associated dynamic array. For this reason specialist lists have to be written. These specialist lists are based fundamentally on the C++ generic list class, but account for the dynamic arrays held within classes. A specialist list has to be written for each class that requires a list function because some classes have multiple dynamic arrays.

The procedure starts by setting r to the number of elements in the general log. This log records all the elements that the hybrid algorithm has analysed. The 'retrieving an element from a log' algorithm then retrieves the element from the 'general' log, which is located by the value r, see Section 2.6.10. After retrieval, that element is tested to verify whether or not it has an unmarked outlet. If so, then the element pointed to by the outlet is returned and then is given the label 'next'. If not, then the algorithm checks if r equals 1. Assuming that r is larger than 1, it loops back to retrieve another element from the general log. If r=1, then the algorithm has failed to find the element in the 'general' log. This loop searches for an analysed element with an unmarked outlet. However, the loop can fail as problem elements, such as resonators, are logged in the problem log. Therefore, if r=1 the 'problem' log, which stores awkward elements, needs to be accessed to enable progression of the hybrid algorithm.

Silencer systems which have resonator elements are awkward in that they include non-sequential elements which are difficult to analyse. Therefore, when the hybrid algorithm encounters a resonator, it is logged in the 'problem' log. If the algorithm fails to find an element in the 'general' log, then the 'problem' log is searched in a similar manner to that described above for the 'general' log. When the 'problem' element is found and given the label 'next', it is subsequently removed from the 'problem' log. Then similarly, the element pointed to by the outlet is returned to the algorithm which is called 'Locating an element' algorithm.

2.6.9 Logging an element algorithm, Flowchart 2.9

The logging algorithms act essentially as lists, but as these involve complicated objects that need separate copying functions, C++ lists cannot be used, therefore specialized lists are used. The 'general' and 'problem' logs keep a list of ID numbers and associated data that is specific to that data member. However, other logs can keep any kind of data, as long as each data member can be identified individually.

The object of this algorithm is to check whether or not the element is in the specialized list, if not, it is added. The algorithm receives an element and sets *a* to the current size of the list; it also sets a pointer to the top of the list. Then it checks if *a* is equal to 0, if not, it then verifies if the ID of the object in the list pointed to matches the ID of the object received. If so, the algorithm moves the object to the top of the list. When the IDs do not match, the pointer is moved down the list and *a* is decreased by 1 and the algorithm loops back with reference to Flowchart 2.9. The loop continues until r equals 0, this means that the received element does not appear in the list; hence it is added to the list. Lists are just dynamic arrays of objects, therefore when an object is added, the present array is copied into a temporary array and then the present array is deleted [91]. Then a new dynamic array is created with the size increased by one; the temporary version is copied back into the new array. Now the received object is copied into the new array, then the temporary array is deleted. Finally, the algorithm returns to where it was called.

2.6.10 Retrieving data from a log algorithm, Flowchart 2.10

The algorithm concentrates on an element object, however, it remains valid for any form of data object and its associated log. The log stores a list of integers which relate to the IDs of the elements, see Section 2.4. This algorithm receives a number that specifies a particular member of the specialized list. This member is an integer object and relates to a member in the 'index' array. Therefore, if the ID of a particular element is 5, it will have a base class pointer to it in the fifth member of the dynamic array 'index'. Hence, this algorithm can retrieve the element via the 'index' array and return it to the previous algorithm, with reference to Flowchart 2.10.

2.6.11 Resonator path fraction algorithm, Flowchart 2.11

This algorithm receives a resonator together with a value for a control variable B, see Flowcharts 2.4 and 2.11.

If B=1, this means that all the path fractions are entering the resonator object through a single inlet. Hence, the new path fraction, which will be associated with the resonator, is calculated by creating a new path fraction with value one which will be added to the list of path fractions received through that single inlet. Then all the path fraction values within the list will be divided by the number of unmarked outlets.

If B=2, then the hybrid has encountered a loop-back path or a closed end, see Figure 2. 9. These types of links need to be neglected by the path fraction as they do not link the outlet of a sub-system to the inlet, however, they do need to occur in the reduction of a sub-system. When the algorithm encounters these types of linkages, the path fraction associated with the resonator has already been created. There may also be a list of path fractions associated with it, see Sections 2.6.5 and 2.6.6. When this occurs, the list has to ignore the associated inlets and outlets. This is achieved by multiplying each path fraction value by

$$f_{ig} = \frac{uo+1}{uo}, \tag{2.20}$$

where uo is the number of unmarked outlets associated with the resonator.

If B=3, the path fractions that enter through the inlets of the leftt hand side of the resonator need adding together. This occurs because multiple path fractions enter one single element as with forks, see Sections 2.6.5 and 2.6.6. Therefore, the 'path fraction addition' algorithm is used to compile the associated lists, see Section 2.6.6.

If B=4, the lists that enter through the inlets on the right hand side of the resonator are added to the list associated with the resonator via the 'path fraction addition' algorithm, see section 2.6.6. This occurs when resonators have hole-arrays on the right hand side, as in Figure 2. 5, the path fraction exits through the right hand side and returns partially to that side. Consequently, the path fractions have to be summed, see Section 2.6.6.

2.7 Sub-systems reduction

When the path fraction technique has found a sub-system, it is known that it has a sole inlet and outlet. It is implied that there are enough equations to link the acoustic pressure and velocity between the inlet and outlet via a two-by-two transfer matrix. Therefore, there are n-2 equations in n unknowns, so exactly the same general code/method [15] is used to reduce the known information, hence the Gauss-Jordon method with partial pivoting. The general code is used to reduce the sub-system, see Section 2.2.2. This occurs when all consecutively sequenced elements within the sub-system have been reduced.

As shown by Section 2.6.6, the multi-port elements are identified once a collection of two or more of those elements have path fractions values of 1. The general code is used to reduce the sub-system to a two-by-two transfer matrix. Therefore, there arises three two-by-two transfer matrices which are multiplied sequentially, i.e. the two matrices, one before and one after the reduced system, plus the transfer matrix belonging to the reduced sub-system. The information that belonged to the sub-system can now be disregarded for that individual frequency analysis, as all the relevant information is now held within one transfer matrix.

The general code is only used when it is absolutely necessary as the computational time required by general code is a cubic function of n unknowns. This means that it is

computationally advantageous to solve many smaller sub-systems as opposed to a whole system with Gauss-Jordon/general code technique.

2.8 Results

Five silencer designs of varying complexity were analysed on three different pieces of software. To enable valid comparisons, each silencer model was analysed over 10,000 frequencies and the analysis was processed on the same computer which had a Pentium 4 1.7 GHz processor.

Silencer 1 is a system of nested parallel paths, Figure 2. 13a. Each path has a single straight-through resonator as in Figure 2. 4a. This resonator sub-system is exchanged for the pipes connecting 'F_3' and 'F_4' on Figure 2. 3 and the bottom pipe connecting 'F_1' and 'F_2'. Small changes within triple pass silencer systems can often lead to expensive algorithm alterations. The triple pass silencer system, as shown in Figure 2. 13d, is exactly the same as Figure 2. 4c. Silencers 2 and 3 differ slightly from 4, but have significant effects on the algorithmic process and therefore the time required for analysis. Silencer 2 does not have any hole arrays on the inlet and outlet of the system, this means that loop-back paths can be exchanged for sub two-port elements. Significant sequential transfer matrix multiplication can be achieved for this system. Hence before sub-system reduction, identification of loop-back paths reduces to a single effective two-port element all those elements, which are within the dotted lines in Figure 2. 10. Silencer 3 has hole arrays on the inlet, but not on the outlet, this reduces significantly the number of elements that can be reduced by sequential multiplication of transfer matrices. However, due to the generality of the hybrid algorithm, the loop-back path on the right hand side of the resonator is still identified and therefore subsequently reduced. The fifth silencer system represents a complete silencer system which consists of a catalytic converter box, followed by a front box, Figure 2. 4a, and a rear, box Figure 2. 13b, together with interconnecting pipes, downpipe and tailpipe.

The time required to analyse the five silencer designs is displayed in Figure 2. 14. An internal clock provided by a C++ library was used to time the length of each silencer analysis. In the interests of scientific validation each silencer was analyzed three times for each piece of software over 10,000 frequencies. The averages over the three runs are shown in Figure 2. 14. There were insignificant variations between the runs. The timed runs show fully the computational time saving of the new hybrid algorithm as opposed to the general approach.

The timed results of silencer models 3 and 4, compared to the other designs, clearly demonstrate the large computational consequences of small design variations. The current conventional code LAMPS [9,11] is unable to model silencers 3 and 4, nor is there any known code that can do this, other than the hybrid and general codes given here. For this reason, it is not possible to obtain conventional code results for models 3 and 4. The general approach results in excessive time required for the analysis of these models.

The effectiveness of the hybrid algorithm is shown with the comparison of the other two methods using silencer 1. The hybrid code only requires 18% of the time compared to the general code. Yet the hybrid code is only 2.6 times slower than the conventional code. Silencers 3 and 4 involve vastly more complexity in their linkage of acoustic elements. This results in larger sub-system reduction matrices, but the hybrid algorithm is able to do the analysis in 10% of the time required by the 'general approach'. Whereas the conventional approach ceases to become an option, since it has not got an infinite library of algorithms.

Unlike many improvements for saving computational time, this algorithm does not affect the accuracy of the results. The hybrid algorithm reduces the acoustical characteristics of any silencer with a single inlet and outlet to a two-by-two transfer matrix over a range of frequencies. These transfer matrices are used, along with given source and radiation impedances, to determine, where appropriate, various noise measures.

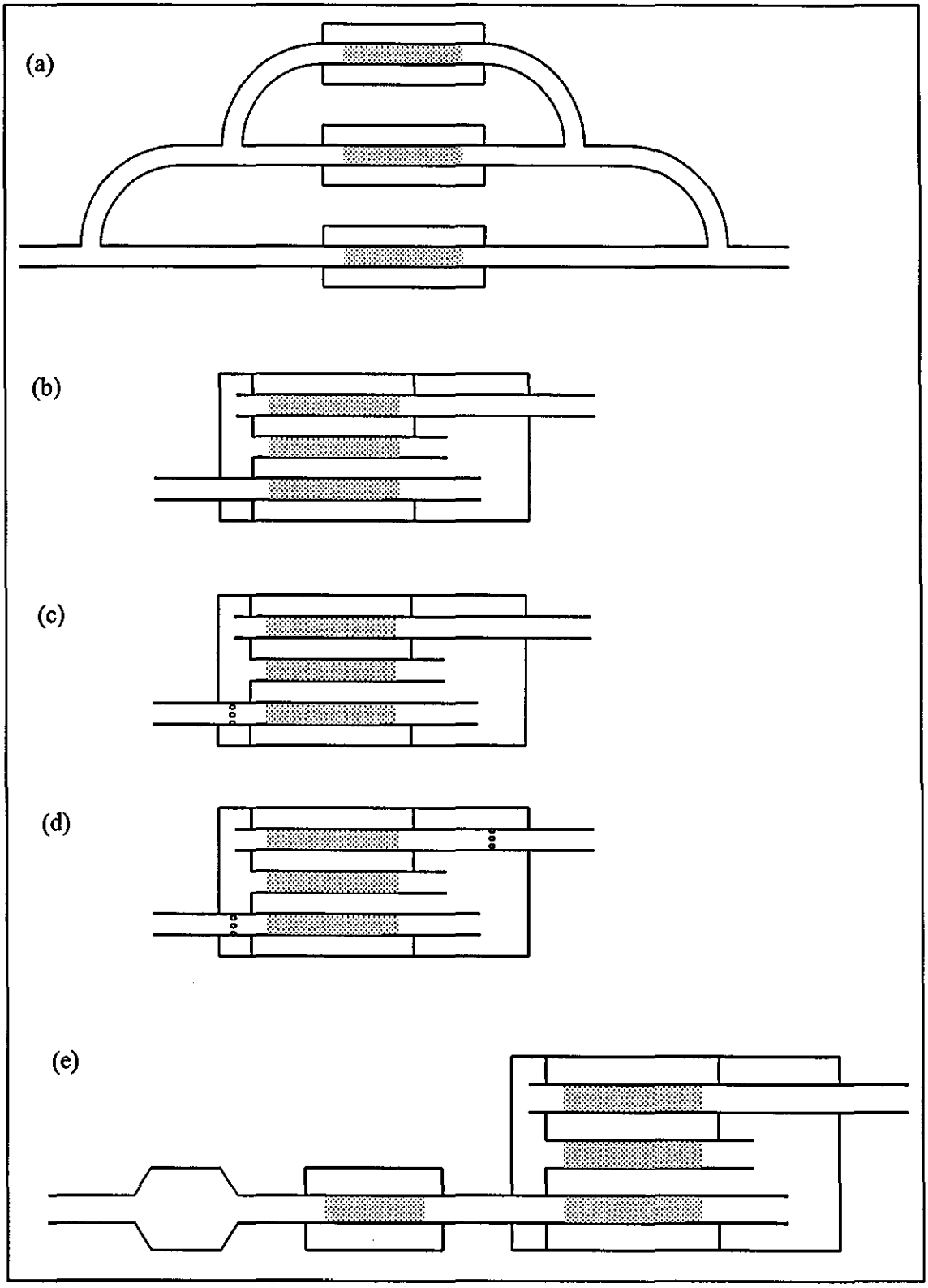

Figure 2. 13. Silencer systems used for time trials: (a)-(e) systems (1)-(5)

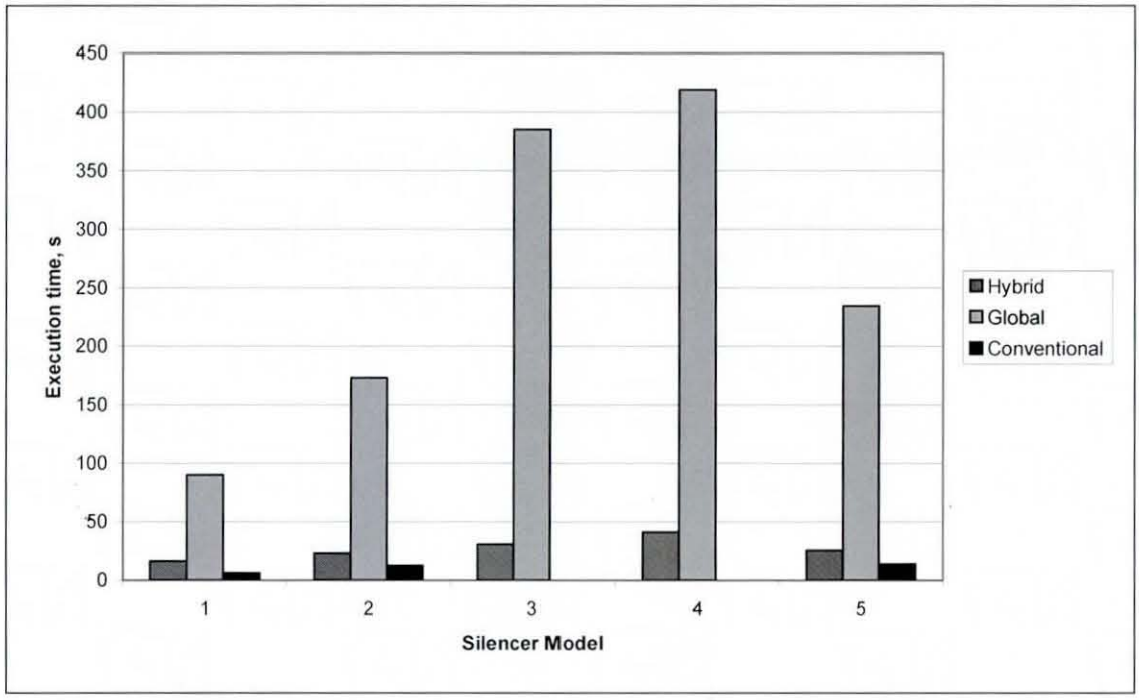

Figure 2. 14 Comparison of execution time for the different approaches

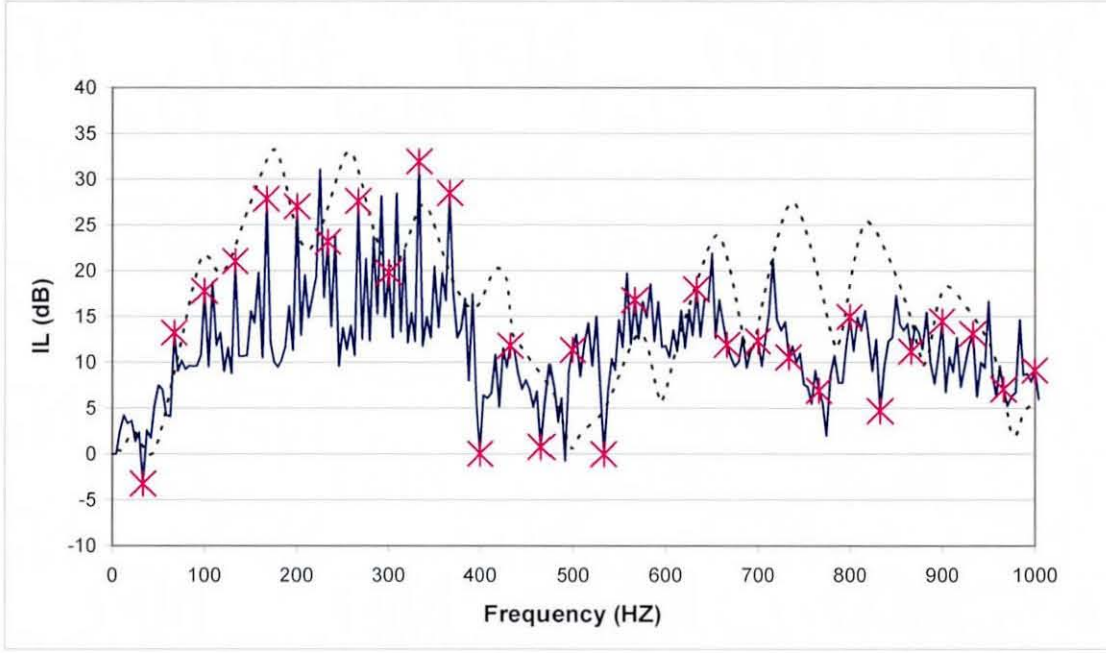

Figure 2. 15 Predicted and measured results of a silencer of the type shown in Figure 2. 13b with reference to a uniform pipe. ___ measured; X measurement at engine orders; --- predicted.

A practical example is shown Figure 2. 15, which compares the predicted and measured insertion loss results between a triple pass silencer system, as shown in Figure 2. 13b and a uniform pipe. In this case the source was a 2-litre 4-cylinder petrol engine running at 1000rpm. Signal-to-noise ratios are more trustworthy at the engine orders, which are highlighted in Figure 2. 15. The predicted results, in Figure 2. 15, relate closely to the measured results below the cut-off frequency [1], for plane-waves, as opposed to frequencies above. The cut-off frequency for the silencer shown by Figure 2. 13b is 700Hz. The distribution of mean flow is accounted for within the modelling of transfer matrices and therefore has no relevance to the type of algorithm used. Prediction accuracy is governed solely by the modelling of each transfer matrix associated with an individual acoustic element. Therefore, the predicted insertion loss as presented in Figure 2. 15 is exactly the same for the conventional, global or hybrid methods.

2.9 Conclusion

The hybrid algorithm incorporates successfully the advantages of the conventional and general codes whilst minimizing the disadvantages of both methods. The hybrid algorithm delivers a two-by-two transfer matrix relating the acoustic pressure and velocity at the sole inlet to the sole outlet. This provides many uses to which the transfer matrices can be applied. Identification of sub-systems within sub-systems/systems that can be reduced to an effective sub two-port element makes the hybrid algorithm general. The multiplication of consecutively sequenced transfer matrices associated with two-port elements, in combination with a strategically constructed internal log, maximises the computational efficiency. The hybrid code gains exceptional savings in computational time required to analyze a silencer compared to the general code, whilst only using twice as much time compared to the conventional code. The conventional code requires separate dedicated reduction routines for each variant of silencer, whereas the hybrid algorithm uses one general algorithm.

CHAPTER 3

Modelling Multiple Time-Variant Sources

3.1 Introduction

Linear, frequency-domain, plane wave modelling is an effective and exceptionally efficient method for predicting the low frequency, acoustic characteristics of silencer systems [1]. An overall transfer matrix for a complete silencer system, as given by the algorithm of Chapter 2, is sufficient to determine the transmission loss of a silencer system. However, the evaluation of insertion loss or engine noise reduction [5] requires in addition specific characteristics of the source. Therefore, source modelling is vitally important for the evaluation of the effectiveness of an exhaust system. The LAMPS software [15,69] model makes use of a source impedance at the sole inlet to the silencer system. This source impedance is assumed to be known, but is poorly characterised, see Section 1.4.3.

This chapter extends the capability of LAMPS to account for multi-cylinder source inputs to the silencer system and removes the requirement for a known source impedance. Thus, effects of phase difference between cylinders, manifold designs and wave cancellation in the manifold are all included. It is necessary that the source model is linear, if one is to avoid the complication of time-domain [6] or hybrid models [17-19]. Since exhaust silencers are modelled by a linear, frequency-domain, plane wave technique, it is appropriate to investigate the effects of modelling the exhaust manifold with the same technique [69,71]. The noise source of each cylinder can be characterized by a periodic, time-varying, linear valve model, thus ensuring that the complete source is properly modelled by a full admittance matrix that cross-couples all harmonics [71].

3.2 Modelling of a simple source

3.2.1 Idealized equation for valve flow

Let the in-cylinder source pressure be $P_s(t)$, where t is time. The gas in the cylinder discharges through a valve into an exhaust system, see Figure 3. 1. Let the pressure just downstream of the valve be $P(t)$ and the acoustic velocity through the valve be $U(t)$. Both pressures are measured relative to atmospheric pressure.

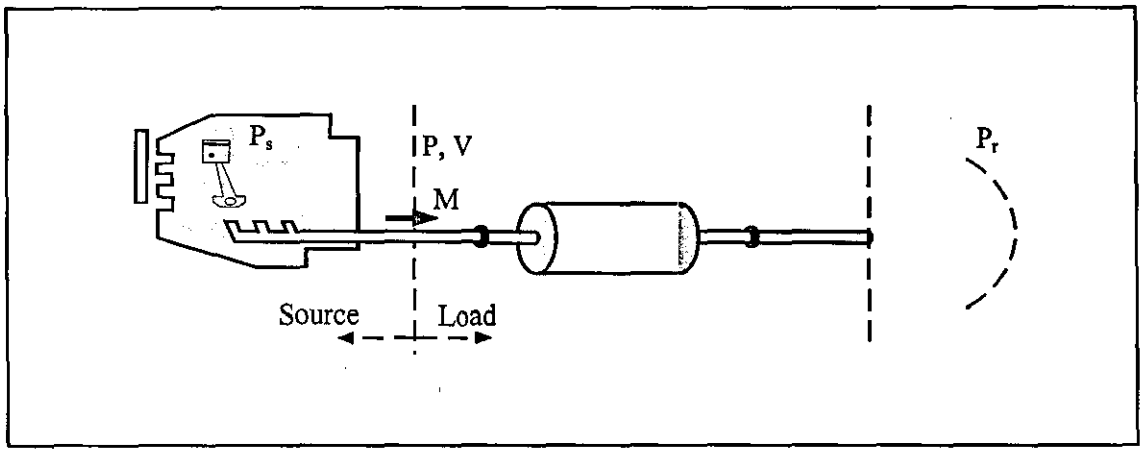

Figure 3. 1 Source-engine load model

An idealized time-variant linear equation for flow through a valve is [71]:

$$\overline{\rho}\overline{c}U(t) = C_d[P_s(t) - P(t)] \tag{3.1}$$

where C_d is a non-dimensional constant which is the discharge coefficient. Also $\overline{\rho}$, $\overline{c}$ are the mean density and speed of sound of the gas flow through the valve respectively. In reality the flow through the valve is nonlinear, indeed as the valve first opens, the flow is choked [23]. However, it is necessary to linearise the valve flow equation in order to incorporate it as the source in a linear exhaust system analysis.

For constant engine speed, a valve has a periodic cycle which is defined by the RPM of the crankshaft; during one cycle, two revolutions for a four-stroke engine, each valve will be fully closed for a proportion of the period. When a valve is closed, the discharge of flow through the valve will be zero. Let the open area of the valve be described by a function $\tilde{A}(t)$ which is periodic with a period T. Therefore, the revised equation of discharge over a period T is

$$\overline{\rho c}V(t) = C_d\tilde{A}(t)[P_s(t) - P(t)] \quad \tilde{A}(t)\begin{cases} \neq 0, 0 \le t \le \tau \\ = 0, \tau \le t \le T \end{cases}, \tag{3.2}$$

where $V(t)$ is the volume velocity through the valve.

Let $A(t) = \tilde{A}(t)/A_{max}$, where A_{max} is the maximum open area of the valve. If,

$$v(t) = \left(\frac{\overline{\rho c}}{A_p}\right)V(t), \tag{3.3}$$

where A_p is the area of the pipe into which the valve discharges, then it follows from equation (3.2) that

$$v(t) = C_v A(t)[P_s(t) - P(t)] \qquad \begin{cases} 0 < A(t) \le 1, 0 \le t \le \tau \\ A(t) = 0, \tau \le t \le T \end{cases}, \tag{3.4}$$

where

$$C_v = C_d\frac{A_{\max}}{A_p}. \tag{3.5}$$

Let the time-dependent variables be expanded using the complex Fourier series

$$v(t)=\sum_{j=-\infty}^{+\infty} v_j e^{i\omega_j t} \quad , \tag{3.6}$$

$$P_s(t)=\sum_{j=-\infty}^{+\infty} S_j e^{i\omega_j t} \quad , \tag{3.7}$$

$$P(t)=\sum_{j=-\infty}^{+\infty} P_j e^{i\omega_j t} \tag{3.8}$$

and

$$C_v A(t)=\sum_{j=-\infty}^{+\infty} A_j e^{i\omega_j t} \quad , \tag{3.9}$$

where $\omega_j=2\pi j/T$ is the frequency component and $i=\sqrt{-1}$. Using equation (3.4) in conjunction with equations (3.6) to (3.9), a matrix relationship in the frequency domain can characterize the time-variant source as

$$\begin{bmatrix} v_{-N} \\ \cdots \\ v_0 \\ \cdots \\ v_N \end{bmatrix} = \begin{bmatrix} A_0 & \cdots & A_{-N} & \cdots & A_{-2N} \\ \cdots & A_0 & \cdots & \cdots & \cdots \\ A_N & \cdots & A_0 & \cdots & A_{-N} \\ \cdots & \cdots & \cdots & A_0 & \cdots \\ A_{2N} & \cdots & A_N & \cdots & A_0 \end{bmatrix} \begin{bmatrix} S_{-N}-P_{-N} \\ \cdots \\ S_0-P_0 \\ \cdots \\ S_N-P_N \end{bmatrix}, \tag{3.10}$$

where the equations have been truncated to N harmonics. It is assumed that higher harmonics are negligible. The relationship in equation (3.10) can be characterized alternatively as

$$\{\mathbf{v}\}=[\mathbf{A}]\{\mathbf{S}-\mathbf{P}\}, \tag{3.11}$$

where [**A**] is the admittance matrix.

3.2.2 Valve model

An exhaust system with a time-variant source can be modelled in the frequency domain if the open area of the valve, $A(t)$, is known, see equation (3.2). However, for an internal combustion engine source, generally only the valve lift is known as a function of the crank angle. From relevant valve/valve seat geometry, such as the valve seat angle, thickness of valve seat and the radius of the valve, together with information on the valve lift with respect to the crank angle, then the valve open area can be calculated. This is likely to lead to a complicated function, or at least a function that cannot be integrated analytically. However, if a numerical integration technique, such as the Trapezium Rule [90], is used in conjunction with the complex Fourier series, the complex Fourier coefficients can be evaluated.

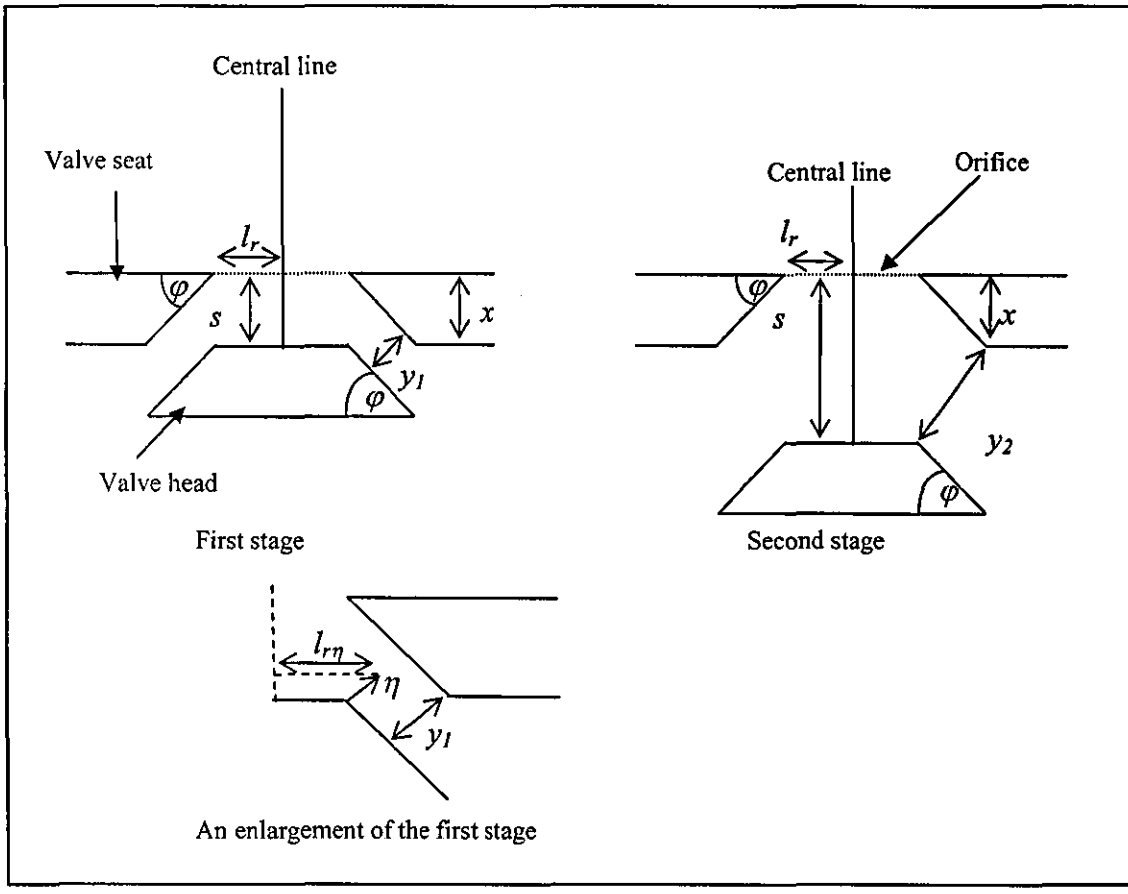

Figure 3. 2 The first and second stage of valve open area calculation

1
The relationship between valve lift and valve open area is explained in three stages. The first stage, see Figure 3. 2, occurs when the valve head is close to the valve seat. Here s relates to the valve lift, let x be the thickness of the valve seat and φ be the angle of the valve seat. Let the valve radius be l_r. The open area of flow in this stage is calculated by finding the open area perpendicular to the faces of the valve head and valve seat. Let η_d be the distance from the top corner of the valve head to the point η, which is measured in a direction perpendicular to the valve, see Figure 3. 2. The radial distance to point η is

$$l_{r\eta} = l_r + \eta_d \cdot \sin(\varphi). \tag{3.12}$$

The total flow area of an element of length $d\eta_d$ and radius $l_{r\eta}$ is thus

$$dA_{\eta_d} = 2\pi l_{r\eta}\, d\eta_d . \tag{3.13}$$

Hence the total open area of the valve is

$$A_v = 2\pi \int_0^{y_1} (l_r + \eta_d \cdot \sin(\varphi))\, d\eta_d , \tag{3.14}$$

or

$$A_v = 2\pi \cdot y_1 \left(l_{r\eta} + \frac{1}{2} \cdot y_1 \cdot \sin(\varphi) \right), \tag{3.15}$$

where y_1 is the perpendicular distance between the valve head and seat, see Figure 3. 2. However, the equation ceases to be valid when the perpendicular to the valve head from the top corner of the valve head no longer intersects with the valve seat. This occurs when

$$s - x > y_1 \cdot \cos(\phi). \tag{3.16}$$

However

$$y_1 = s \cdot \cos(\varphi), \tag{3.17}$$

thus, substituting equation (3.17) into equation (3.16) and rearranging, it follows that

$$s > \frac{x}{1-\cos^2(\varphi)}. \tag{3.18}$$

When equation (3.18) is first satisfied, the second stage commences. In this stage the open area is calculated by using y_2 to calculate the open area of flow, where y_2 is the direct distance between the top corner of the valve head and the bottom corner of the valve seat, see Figure 3. 2. The horizontal and vertical components of y_2 are

$$y_{2h} = x \cdot \cot(\varphi) \tag{3.19}$$

and

$$y_{2v} = s - x, \tag{3.20}$$

respectively, thus

$$y_2 = \sqrt{(s-x)^2 + (x \cdot \cot(\varphi))^2}. \tag{3.21}$$

Let y be measured in the direction of y_2 from the valve head. Thus the total open area of the valve, in this stage, can be calculated by

$$A_v = 2\pi \int_0^{y_2} \left(l_r + y \cdot \frac{y_{2h}}{y_2} \right) dy, \tag{3.22}$$

or

$$A_v = 2\pi \cdot y_2\left(l_r + \frac{1}{2}\cdot x \cdot \cot(\varphi)\right). \tag{3.23}$$

However, there is an upper limit of open area of flow through the valve seat. It is capped due to the area of the valve orifice, see Figure 3. 2. The third stage occurs when $A_v = \pi l_r^2$ and if this happens, then the open valve area remains at πl_r^2. Therefore, to summarise,

$$A_v = \begin{Bmatrix} 2\pi \cdot s \cdot \cos(\varphi)\cdot\left(l_r + \frac{1}{2}\cdot\cos(\varphi)\cdot\sin(\varphi)\right) & 0 < s \le \frac{x}{1-\cos^2(\varphi)} \\ 2\pi \cdot \sqrt{(s-x)^2 + (x\cdot\cot(\varphi))^2}\cdot\left(l_r + \frac{1}{2}\cdot x\cdot\cot(\varphi)\right) & \frac{x}{1-\cos^2(\varphi)} < s \text{ and } A_v < \pi l_r^2 \\ \pi l_r^2 & \textit{otherwise} \end{Bmatrix}, \tag{3.24}$$

3.2.3 A single cylinder engine

As explained in Chapter 2, if any part of an exhaust system has a sole inlet and outlet, then a two-by-two transfer matrix can be evaluated to relate the convective acoustic pressure and velocity between the inlet and outlet at any specified frequency. In a general case, let X represent the inlet of a two-port element, or a reduced silencer system with a sole inlet and outlet, and similarly, let Y represent the outlet. Let the two-by-two transfer matrix for a given frequency ω_j be

$$\begin{bmatrix} P_{\omega_j} \\ V_{\omega_j} \end{bmatrix}_X = \begin{bmatrix} a_{\omega_j} & b_{\omega_j} \\ c_{\omega_j} & d_{\omega_j} \end{bmatrix}_{XY} \begin{bmatrix} P_{\omega_j} \\ V_{\omega_j} \end{bmatrix}_Y \tag{3.25}$$

and let $[\mathbf{a}]_{XY}$ be the diagonal matrix of coefficients a_{ω_j} for harmonics $-N$ to N, namely

$$[\mathbf{a}]_{XY} = \begin{bmatrix} a_{-N} & \cdots & 0 & \cdots & 0 \\ \cdots & \cdots & \cdots & \cdots & \cdots \\ 0 & \cdots & a_0 & \cdots & 0 \\ \cdots & \cdots & \cdots & \cdots & \cdots \\ 0 & \cdots & 0 & \cdots & a_N \end{bmatrix}_{XY} . \tag{3.26}$$

The other coefficients of the transfer matrix in equation (3.25) can be inserted into similar matrices and referenced by $[b]_{XY}$, $[c]_{XY}$ and $[d]_{XY}$. Thus the pressure and velocity vectors at X and Y for the same harmonics, $\{\mathbf{P}\}_X$, $\{\mathbf{v}\}_X$, $\{\mathbf{P}\}_Y$ and $\{\mathbf{v}\}_Y$ can be related by

$$\{\mathbf{P}\}_X = [\mathbf{a}]_{XY}\{\mathbf{P}\}_Y + [\mathbf{b}]_{XY}\{\mathbf{v}\}_Y \tag{3.27}$$

and

$$\{\mathbf{v}\}_X = [\mathbf{c}]_{XY}\{\mathbf{P}\}_Y + [\mathbf{d}]_{XY}\{\mathbf{v}\}_Y . \tag{3.28}$$

Suppose it is possible to relate the pressure and velocity vectors at some general point X through the equation

$$\{\mathbf{v}\}_X = [\mathbf{G}]_X\{\mathbf{S}\}_X + [\mathbf{H}]_X\{\mathbf{P}\}_X \tag{3.29}$$

where matrices [G] and [H] and vector {S} are known. Thus from equations (3.27) and (3.28)

$$\{\mathbf{v}\}_Y = ([\mathbf{d}]_{XY} - [\mathbf{H}]_X[\mathbf{b}]_{XY})^{-1}[\mathbf{G}]_X\{\mathbf{S}\}_X + ([\mathbf{d}]_{XY} - [\mathbf{H}]_X[\mathbf{b}]_{XY})^{-1}([\mathbf{H}]_X[\mathbf{a}]_{XY} - [\mathbf{c}]_{XY})\{\mathbf{P}\}_Y . \tag{3.30}$$

This can be re-written as

$$\{\mathbf{v}\}_Y = [\mathbf{G}]_Y \{\mathbf{S}\}_Y + [\mathbf{H}]_Y \{\mathbf{P}\}_Y, \tag{3.31}$$

where

$$[\mathbf{G}]_Y = ([\mathbf{d}]_{XY} - [\mathbf{H}]_X [\mathbf{b}]_{XY})^{-1} [\mathbf{G}]_X, \tag{3.32}$$

$$[\mathbf{H}]_Y = ([\mathbf{d}]_{XY} - [\mathbf{H}]_X [\mathbf{b}]_{XY})^{-1} ([\mathbf{H}]_X [\mathbf{a}]_{XY} - [\mathbf{c}]_{XY}) \tag{3.33}$$

and

$$\{\mathbf{S}\}_Y = \{\mathbf{S}\}_X. \tag{3.34}$$

Hence, if matrices [**G**] and [**H**] and vector {**S**} are known at point *X*, they can be evaluated at point *Y*.

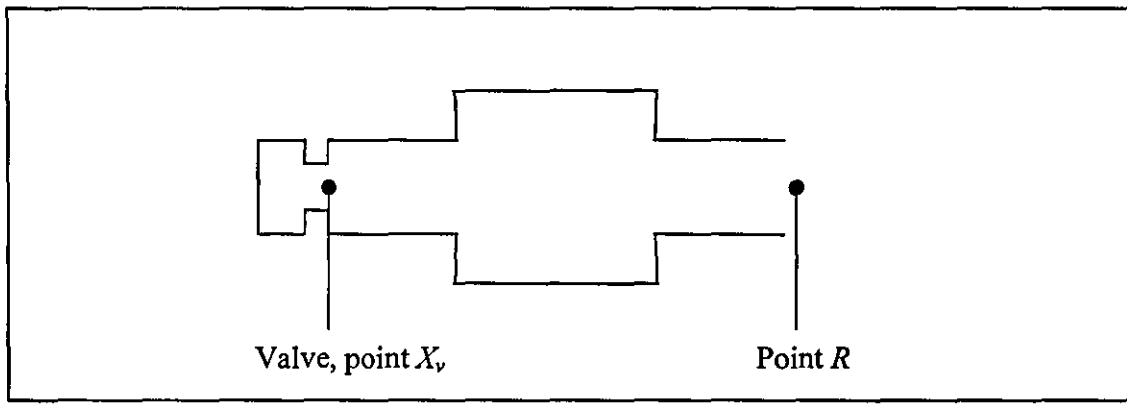

Figure 3.3 Schematic diagram of an exhaust system of a one cylinder engine

Consider a single cylinder engine as shown in Figure 3.3. Let point *R* denote the radiation point into the atmosphere and point X_v, upstream of point *R*, be the position of the outlet of the valve. The transfer matrix relating the pressure and velocity at point X_v to point *R* can be written as

$$\begin{bmatrix} P_{\omega_j} \\ V_{\omega_j} \end{bmatrix}_{X_v} = \begin{bmatrix} a_{\omega_j} & b_{\omega_j} \\ c_{\omega_j} & d_{\omega_j} \end{bmatrix}_{X_v R} \begin{bmatrix} P_{\omega_j} \\ V_{\omega_j} \end{bmatrix}_R . \tag{3.35}$$

Thus the set of equations (3.26) to (3.34) are valid with $X=X_v$ and $Y=R$. At the valve, $X=X_v$, the matrices $[\mathbf{G}]_X$ and $[\mathbf{H}]_X$ are known, as can be seen from the comparison of equations (3.11) and (3.29). Thus

$$[\mathbf{G}]_{X_v} = [\mathbf{A}] \tag{3.36}$$

and

$$[\mathbf{H}]_{X_v} = -[\mathbf{A}]. \tag{3.37}$$

Furthermore $\{\mathbf{S}\}_{X_v} = \{\mathbf{S}\}$, the in-cylinder pressure vector, is also assumed to be known. Thus equations (3.31) to (3.34), with $Y=R$, yield known matrices [**G**] and [**H**] and vector {**S**}, hence a relationship between pressure and velocity at point R can be evaluated.

The radiation impedance at the tailpipe exit, point R, can be calculated at any specific frequency [71], thus a known diagonal matrix can be formed, $[\mathbf{Z}]_R$, where

$$\{\mathbf{P}\}_R = [\mathbf{Z}]_R \{\mathbf{v}\}_R . \tag{3.38}$$

This equation is combined with equation (3.31) to give

$$\{\mathbf{v}\}_R = ([\mathbf{I}] - [\mathbf{H}]_R [\mathbf{Z}]_R)^{-1} [\mathbf{G}]_R \{\mathbf{S}\}_{X_v} . \tag{3.39}$$

Thus the velocity vector, $\{v\}_R$, at the radiation point of any single cylinder engine can be calculated. Together with the known radiation impedance matrix, this enables calculation of the sound radiation from the exhaust tailpipe.

3.3 Multi-cylinder engines

Complications occur when considering multi-cylinder engines as there are various manifold designs. Also the cylinders in this type of engine are out of phase, but phase-related. In the simplest case, all the pipes from the cylinders/valves meet at a single junction, as shown in Figure 3. 4. More complicated examples of manifold design are shown in Figure 3. 5a-b. An algorithm has to be sufficiently general to allow the analysis of any design of manifold from the simplest, as in Figure 3. 4, to the more complicated, such as those in Figure 3. 5.

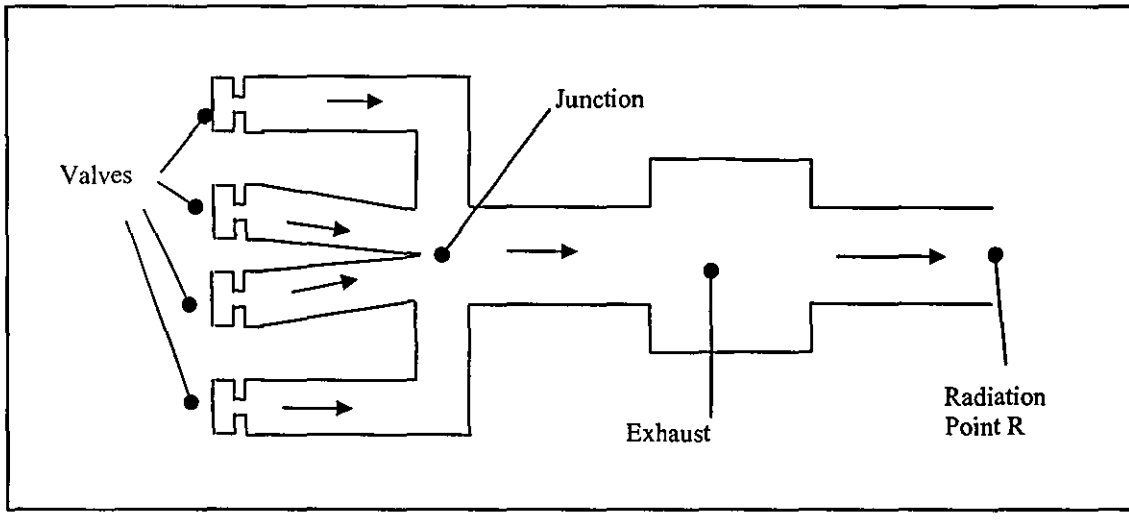

Figure 3. 4 A simple four cylinder manifold with an exhaust attached

Consider a simple progression from a single cylinder engine, as in Figure 3.3, to a twin cylinder engine, shown in Figure 3. 6. Let a point X_e be immediately downstream of a given valve e. At each valve e, the application of the general equation as in equation (3.29) with the valve matrix admittance equation (3.11) gives

$$\{\mathbf{v}\}_{X_e} = [\mathbf{G}]_{X_e}\{\mathbf{S}\}_{X_e} + [\mathbf{H}]_{X_e}\{\mathbf{P}\}_{X_e} \tag{3.40}$$

where

$$[\mathbf{G}]_{X_e} = [\mathbf{A}]_e, \tag{3.41}$$

$$[\mathbf{H}]_{X_e} = -[\mathbf{A}]_e \tag{3.42}$$

and

$$\{\mathbf{S}\}_{X_e} = \{\mathbf{S}\}_e. \tag{3.43}$$

Let I_e represent the input point to a junction J from the manifold branch to a valve e, as in Figure 3. 6. Thus by setting X=X_e and Y=I_e in equations (3.31) to (3.34) and applying it to the matrix equation at each valve, the relationship between pressure and velocity vectors at each inlet to the junction is known. This is characterised mathematically as

$$\{\mathbf{v}\}_{I_e} = [\mathbf{G}]_{I_e}\{\mathbf{S}\}_e + [\mathbf{H}]_{I_e}\{\mathbf{P}\}_{I_e}. \tag{3.44}$$

Let point J be the outlet of the manifold junction, see Figure 3. 6. As a first approximation, at a junction the convective acoustic pressure is constant and the sum of convective acoustic mass velocities into a junction equals their sum out [1]. Thus

$$\{\mathbf{P}\}_{I_e} = \{\mathbf{P}\}_J \text{ for all inputs } I_e \tag{3.45}$$

and

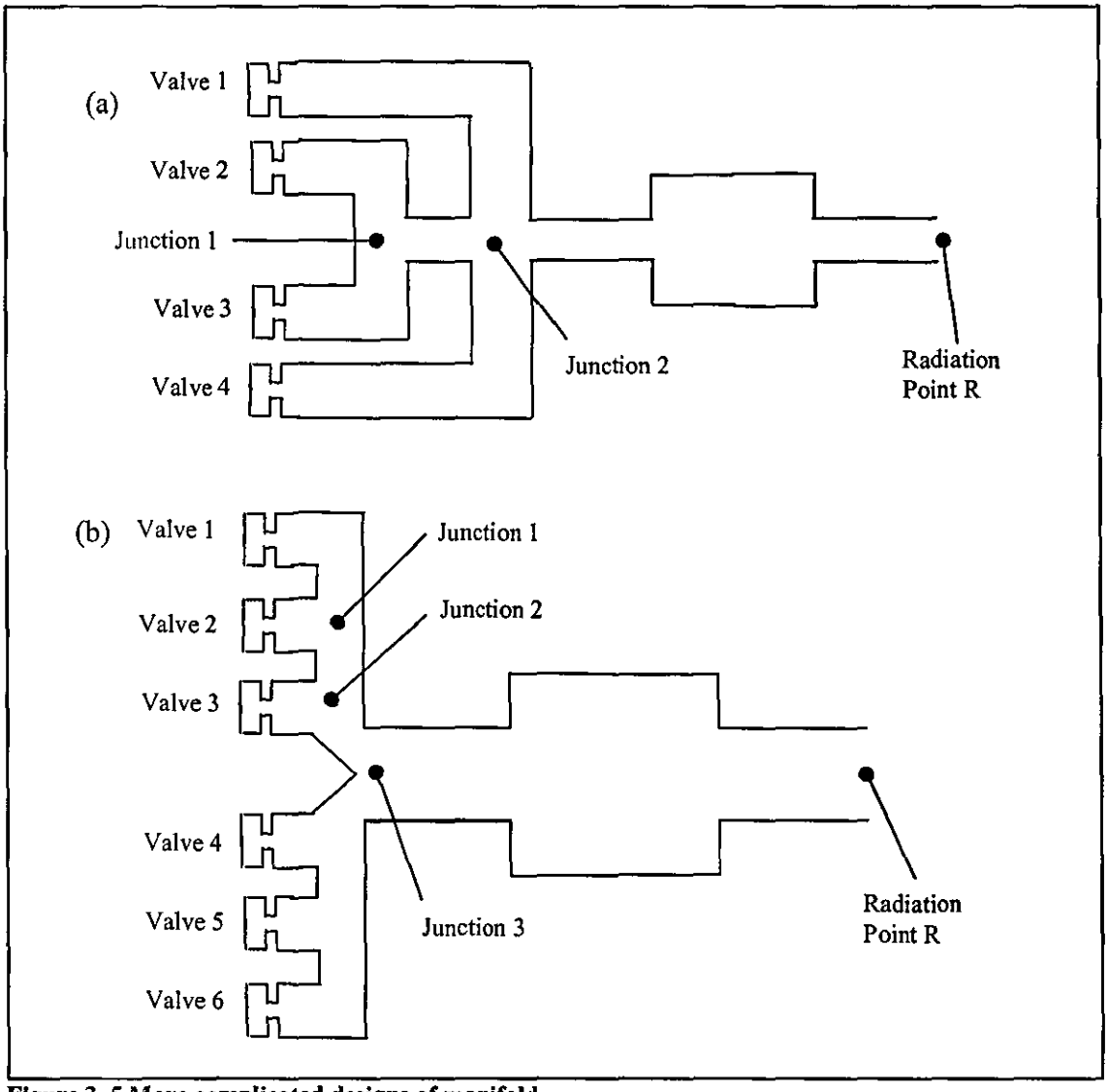

Figure 3. 5 More complicated designs of manifold

$$\sum_e \{\mathbf{v}\}_{I_e} = \{\mathbf{v}\}_J . \tag{3.46}$$

Therefore, from equations (3.44) to (3.46),

$$\{\mathbf{v}\}_J = \sum_e \left([\mathbf{G}]_{I_e}\{\mathbf{S}\}_{I_e}\right) + \left(\sum_e [\mathbf{H}]_{I_e}\right)\{\mathbf{P}\}_J . \tag{3.47}$$

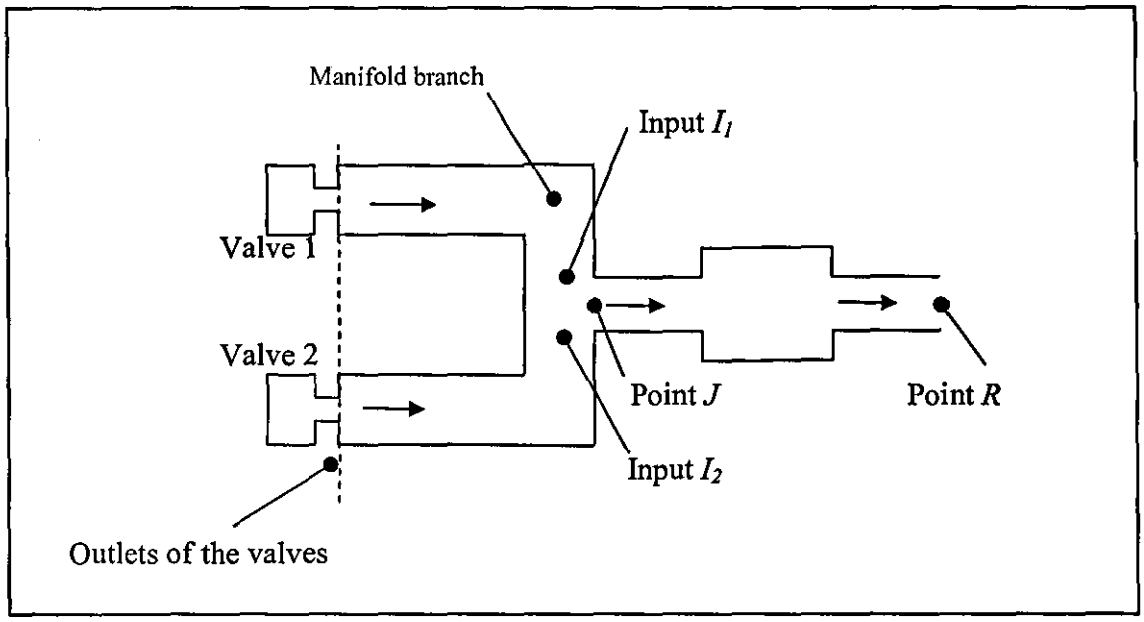

Figure 3. 6 Simple twin source system

This is in the general format of equation (3.29), namely

$$\{\mathbf{v}\}_J = [\mathbf{G}]_J \{\mathbf{S}\}_J + [\mathbf{H}]_J \{\mathbf{P}\}_J \tag{3.48}$$

where

$$\{\mathbf{S}\}_J = \sum_1^2 \left([\mathbf{G}]_{I_e} \{\mathbf{S}\}_{I_e}\right), \tag{3.49}$$

$$[\mathbf{G}]_J = [\mathbf{I}] \tag{3.50}$$

and

$$[\mathbf{H}]_J = \sum_1^2 [\mathbf{H}]_{I_e} . \tag{3.51}$$

Again it should be noted that matrices [**G**] and [**H**] and vector {**S**} are all known at point *J*, thus equation (3.48) models fully all sources and is now in exactly the same, matrix equation format as for the single-cylinder system. The analysis between point *J* and point *R* progresses with the application of equations (3.31) to (3.34), where *X*=*J* and *Y*=*R*. Then, since the relationship between pressure and velocity at the radiation point is known, as with the single cylinder engine, the velocity vector, $\{\mathbf{v}\}_R$, can be evaluated by using equation (3.39), as $[\mathbf{Z}]_R$ is known.

Internal combustion engines generally have several cylinders with time-variant valves, each of which essentially have the same valve behaviour and cylinder pressure. These can be modelled as time-dependent functions. However, they are distinguished between each other by a phase shift. A method to integrate this phase relationship into the frequency domain model is achieved through a phase shift constant τ. This affects equations (3.6) to (3.9) and is shown by the equations

$$v(t+\tau)=\sum_{j=-\infty}^{+\infty}\left(v_j e^{i\omega_j\tau}\right)e^{i\omega_j t}\ , \tag{3.52}$$

$$P_s(t+\tau)=\sum_{j=-\infty}^{+\infty}\left(S_j e^{i\omega_j\tau}\right)e^{i\omega_j t}\ , \tag{3.53}$$

$$P(t+\tau)=\sum_{j=-\infty}^{+\infty}\left(P_j e^{i\omega_j\tau}\right)e^{i\omega_j t} \tag{3.54}$$

and

$$CA(t+\tau)=\sum_{j=-\infty}^{+\infty}\left(A_j e^{i\omega_j\tau}\right)e^{i\omega_j t}\ . \tag{3.55}$$

This enables the admittance matrix and a source pressure vector at the valve to be adjusted prior to any matrix manipulation. Therefore, these equations do not need to be adjusted

further to account for phase shifting. At each cylinder there are two matrices, **[G]** and **[H]**, and one source vector **{S}**, which are different for each cylinder as a result of the phase relationship.

3.3.1 Simple four cylinder manifold

Consider the four cylinder engine and manifold of Figure 3. 4. The acoustic behaviour at the inlets to the junction can be evaluated by firstly calculating the admittance matrix, see equation (3.11), at each of the valves. The equations (3.52) to (3.55) can be applied to the admittance matrix to phase relate the sources for each cylinder. Subsequently, equations (3.31) to (3.34) can be applied to each of the matrix equations associated with each valve, to acquire the relationship between pressure and velocity at each of the inlets to the junction.

The application of equations (3.48) to (3.51) over the four inlets to the junction results in a generalised equation format, as in equation (3.29), at the outlet of the junction, point *J*. Thus, the relationship between the unknown pressure and velocity vectors at the outlet of the junction can be evaluated to a single matrix equation.

This matrix equation is in the same general format as equation (3.29), hence by applying equations (3.31) to (3.34), a pressure and velocity relationship at the radiation, point *R*, can be gained, see Section 3.2.3. As the radiation impedance, $[\mathbf{Z}]_R$, is known, $\{\mathbf{v}\}_R$ can be calculated by using equation (3.39).

3.3.2 Complicated four cylinder manifold

This general method and analysis is found to apply to any general manifold configuration. By way of example, the systems of Figure 3. 5 are considered.

With reference to Figure 3. 5a, the relationship at the inlets of 'Junction 1' can be expressed as a single matrix equation through the application of equation (3.47) for each inlet. This is achieved by the application of the general matrix equations (3.31) to (3.34) at valves two and three to characterise the acoustic behaviour of the inlets to 'Junction 1', as the behaviour at the valve is always calculable. Through another application of equations (3.31) to (3.34), the relationship between the unknown pressure and velocity vectors at the outlet of 'Junction 1' can be used to evaluate the relationship at an inlet of 'Junction 2'.

At 'Junction 2' the relationship between pressure and velocity at one inlet is already known, whereas the relationship at the other two inlets are so far unknown. However, each of these inlets is connected to a valve via a single two-port sub-system. These relationships at the inlets can be evaluated through further application of equations (3.31) to (3.34), as only a two-port sub-system connects 'Valve 1' to an inlet of the 'Junction 2' and 'Valve 4' to an inlet of the same junction. Thus equation (3.47) gives a single matrix equation that models effectively all four noise sources as a single equivalent source.

Now there is only a single two-port sub-system between the single outlet of 'Junction 2', and the radiation point. Thus the velocity vector, {v}, at the radiation point can be evaluated, see Section 3.2.3.

3.3.3 Complicated six cylinder manifold

'Valve 1' and 'Valve 2', in Figure 3. 5b, form the same modelling characteristics as 'Valve 2' and 'Valve 3' of Figure 3. 5a. Hence, given that each of the two valves are connected to 'Junction 1' via single two-port sub-systems, they can be modelled using the same technique, as given in Section 3.3.1. Thus, the outlet of 'Junction 1' can be modelled as a single equivalent source.

The sole outlet of 'Junction 1' and 'Valve 3' combined with the two-port sub-systems that connect them to 'Junction 2', form the same sort of sub-system as valves one, two and 'Junction 1'. Therefore, the acoustic behaviour at the outlet of 'Junction 2' can be modelled as a single equivalent source. Equations (3.31) to (3.34) allow the relationship between the pressure and velocity vectors at the inlet of 'Junction 3' to be gained, given that the relationship between the vectors at the outlet of 'Junction 2' and the acoustic properties of the connecting two-port sub-system are known.

In the example of Figure 3. 5b, valves four to six constitute the same form of sub-system as valves one to three and can be reduced in the same manner. Hence, at 'Junction 3' there are two inlets and one outlet; therefore, as explained in Section 3.3.1, this can be modelled as a single equivalent source with a single matrix equation. Now there is only a single two-port sub-system between the single outlet of 'Junction 3' and the radiation point. Thus the velocity vector, $\{\mathbf{v}\}$, at the radiation point can be evaluated, see Section 3.2.3.

3.4 Multiple time-variant source algorithms

The hybrid algorithm presented in Chapter 2 can be extended to ensure that all the elements are analysed in the correct order. The introduction of time-variant sources as an additional type of element initially causes problems. These elements comprise of a sole outlet which immediately affects the path fraction technique, if there is more than one time-variant source. It affects the path fraction as the hybrid algorithm was classified initially as a reduction algorithm that assumes an exhaust has only a sole inlet and outlet, see Chapter 2. This problem can be overcome by assigning a source path fraction to each time-variant source element, with a value

$$\phi_c = \frac{1}{n_c}, \tag{3.56}$$

where n_c is the number of cylinders. Thus, all sources have been included when this path fraction reaches unity.

To increase computational efficiency, all two-port sub-systems are reduced prior to manipulation. This applies to any sub-system with a sole inlet and outlet and is equally applicable within the manifold section as within complex silencer geometries.

3.4.1 Changes to the hybrid algorithm

(All flowcharts relevant to this chapter can be found at the end of the chapter)

The addition of a new element, a time-variant source, and the reclassification of the nature of the hybrid algorithm causes problems with the 'Search for an element' algorithm, with reference to Section 2.6.8. The new algorithm, as shown in Flowchart 3.1, replaces Flowchart 2.8 and is solely requested by the 'Locating an element' algorithm, as shown on Flowchart 2.7.

A major new objective of this improved 'Search for an element' algorithm is to record the last time-variant source element that the hybrid algorithm has encountered. This is achieved primarily by using the new integer variable *SID*, in the 'Search for an element' algorithm, to record the ID number when a time-variant source element is found. A Boolean variable is also introduced to the new algorithm, which changes from false to true, when a time-variant source element which has already been logged is found.

As in Flowchart 2.8, Flowchart 3.1 starts by setting initially the parameters *SID*, *L* and *r*, see Section 2.6.8. It then searches through the 'general' log for an element with an unmarked outlet, whilst logging the ID of the first time-variant source element, if present, in *SID*.

If the 'general' log does not contain an element with an unmarked outlet, nor a time-variant source element, then r would equal 1 and L would remain false, and then the algorithm will proceed to search the 'problem' log, as with Flowchart 2.8. However, if L is true, the algorithm will automatically return a different time-variant source element to Flowchart 2.7. All the time-variant source elements are linked to the next associated time-variant source element by a pointer. Therefore, Flowchart 3.1 will return the time-variant source element pointed to by the most recent time-variant source element which is logged in the 'general' log.

The adaptations to Flowchart 2.8 enable time-variant source elements to be viewed as a 'problem element'. However, engine source elements are not viewed as problematic as resonator elements, therefore they are not stored within the 'problem' log, see Section 2.6.8.

3.4.2 Multiple time-variant source reduction

Replacing Flowchart 2.8 with 3.1 allows all consecutive two-port elements and sub-systems that have a sole inlet and outlet to be reduced. However, due to the time-varying source elements, further system reduction has to occur once the frequency analysis of all two-port sub-systems has been calculated. When time-variant source analysis is evaluated within the frequency domain, the mathematical system requires a set of two-by-two transfer matrices to be calculated for each reduced two-port system over a frequency range $-\omega N$ to ωN in steps of ω. This enables coefficient matrices such as those in equation (3.26) to be evaluated.

The 'Time-variant source reduction' algorithm starts initially by setting the parameters to their default value and the element inlet/outlet flags, see Chapter 2. It then proceeds to create the admittance matrix for each valve and time shifts the complex Fourier coefficients accordingly, see equations (3.10) and (3.52) to (3.55). At this point, the

algorithm creates a general matrix equation, see equation (3.29), that relates the pressure and velocity immediately downstream of the valve. Hence, it can relate the vectors downstream of the two-port sub-system which is attached to the valve. The algorithm does this procedure for all of the valves.

Now the 'Time-variant source reduction' algorithm reverts back to the first source that it has encountered and proceeds to locate a fork element by using the 'Locating an element' algorithm, see Flowchart 2.7. The acoustic variables at each inlet to this fork are by now each characterised by a form of the general matrix equation (3.29). Thus equation (3.47) can be applied to the inlet equations to find an equation at the sole outlet. Hence, equations (3.31) to (3.34) can be used to find the pressure and velocity vector relationship downstream of the outlet. If that outlet is not a radiation point, then the 'Time-variant source reduction' algorithm loops back to locate another element. The looping back within this algorithm will eventually locate a radiation point. Thus, equation (3.38) and (3.39) can be applied, if required, to evaluate the radiation velocity vector, $\{\mathbf{v}\}_R$.

3.5 Validation tests

The theory presented in Section 3.2, combined with the improved hybrid algorithm, as in Section 3.4, can model mathematically any exhaust manifold and silencer. A demonstration of the generality and accuracy of the theory and algorithmic capability can be illustrated by modelling the acoustic behaviour of a known exhaust manifold and silencer.

In the first instance, for basic verification, the theory is applied to evaluate the characteristics of simplistic systems to ensure that the predictions replicate the known behaviour.

Simple validation tests can be used to verify the model used to characterise multi-cylinder engines in Section 3.3. Consider a four cylinder engine, see Figure 3. 7, where each valve

is connected to a fork by a single pipe or branch. The pipe connecting 'Valve 1' has a length L_1, likewise for the other valves, and the exhaust system is a simple pipe of length L_e, where L_e is 1000mm. The non-dimensional open area of the valve, with respect to A_{max}, is given by

$$A(t)=\begin{cases}\frac{1}{2}\left[1+\cos\left(\frac{6\pi t}{T}-\pi\right)\right], & 0\le t\le\frac{T}{3}\\ 0, & \frac{T}{3}<t<T\end{cases}, \qquad A(t+T)=A(t) \tag{3.57}$$

where T is the period of one valve cycle.

This model of the valve open area is the same one used for single cylinder investigations [71]. The maximum open area of the valve, A_{max}, is 100mm^2 and the radii of the branches is 20mm, so A_p=400π mm^2. The cross-sectional area of the exhaust pipe is set at four times that of a single branch. Let the pressure within the cylinder, when the valve is open, be a constant 10Pa. Also, let the temperature throughout the system be a constant, 600K. The coefficient of discharge, C_d, in the validation tests was evaluated assuming pseudo-steady state velocity from the linear model as stated in equation (3.1) using a constant pressure difference level across the valve of 10Pa. Thus C_v in equation (3.4) can be evaluated.

Although simplistic, this models correctly the general behaviour of a valve in a four-stroke engine, since the exhaust valve is timed to open before BDC and close after TDC, extending the valve open period beyond $T/4$. Furthermore, the actual cylinder pressure throughout the exhaust cycle is nearly constant, albeit much higher than the value assumed here to ensure linearity. The results for the validation tests are obtained using 30 acoustic harmonics, N=30. The speed of the engine is set to 1000RPM, therefore the valve frequency is 8.33Hz and firing frequency is 33.33Hz.

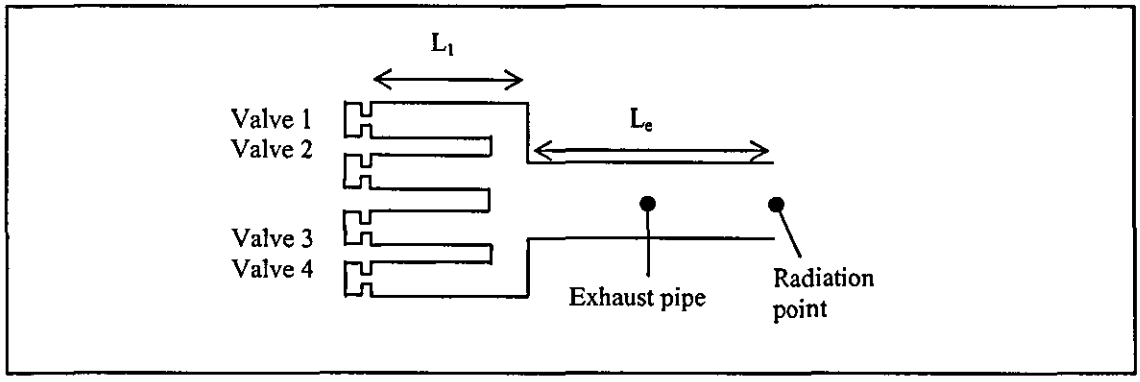

Figure 3. 7 Simplistic manifold geometry used for validation

The pressure at the radiation point, see Figure 3. 7, for each harmonic mode will be calculated for a selection of branch lengths, thus illustrating the firing sequences and wave cancellations.

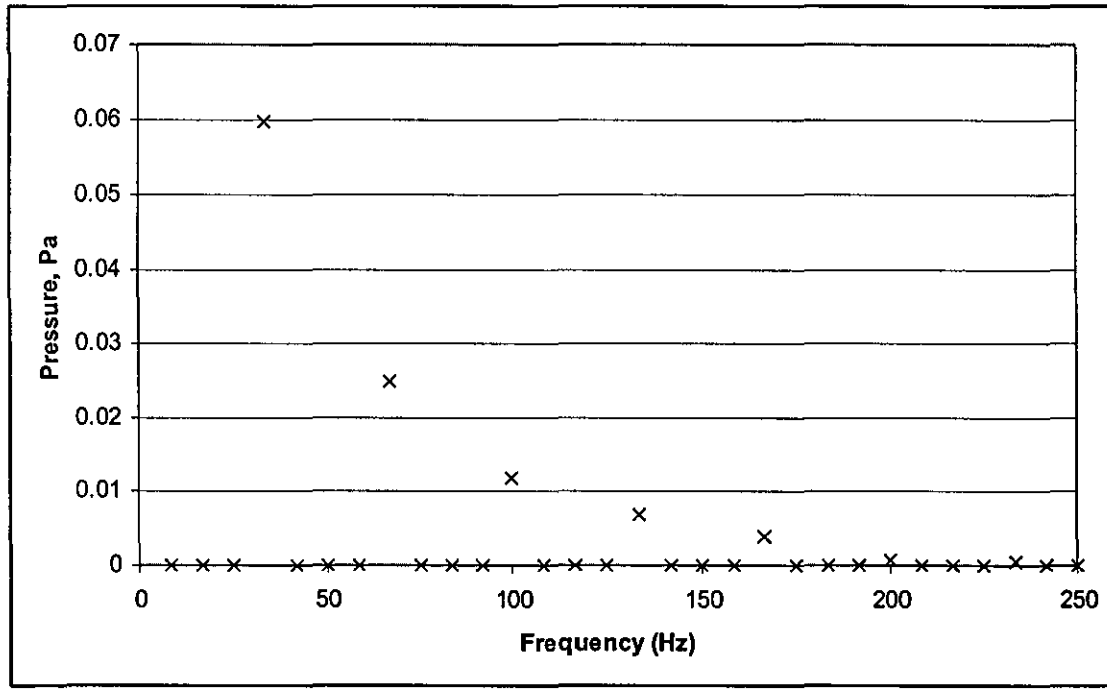

Figure 3. 8 Pressure at the radiation point for validation test 1

The first validation test considers the harmonic pressure modes when all the pipes between the valves and the fork are of length 100mm. Also the cylinder associated with 'Valve 1' fires first, followed by 'Valve 3', then 'Valve 4' and lastly 'Valve 2'. Each cylinder fires with a quarter of a period separating them. Figure 3. 8 illustrates the results

for the first validation test and clearly indicates that the wave cancels at all valve frequencies except multiples of the firing frequency.

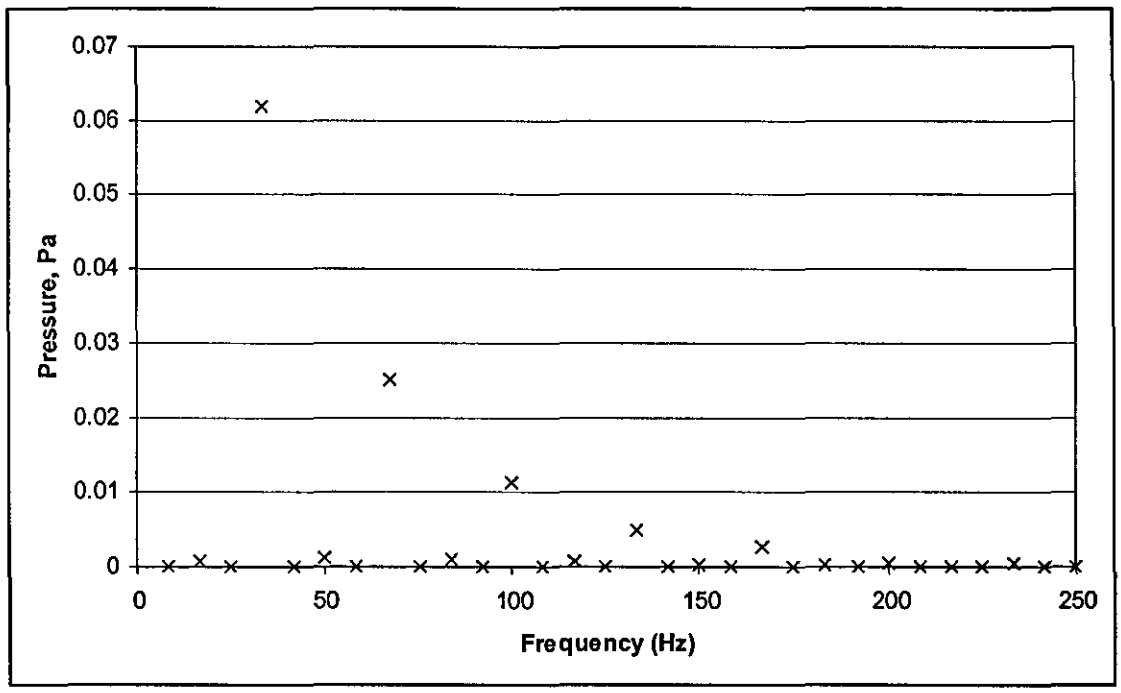

Figure 3. 9 Pressure at the radiation point for validation test 2

The second validation test uses exactly the same system as in the first test, except the length of each pipe connecting 'Valve 2' to the fork and likewise 'Valve 3' to the fork, is set to 70mm. Note that the other pipes remain at 100mm. The firing order in this test case starts with 'Valve 1' that fires, first followed by 'Valve 3', then 'Valve 4' and lastly 'Valve 2'. Thus, the wave cancels at every odd harmonic and the pressure magnitude should be higher at every fourth harmonic, coinciding with the firing frequency. Figure 3. 9 shows the wave behaviour as predicted and thus validates the source model. This validates that pipes that have the same length are modelled differently as a result of phase changes.

3.6 Application

The theoretical model is now used to compare theoretical results against experimental results for various exhaust systems. Arvin Meritor [93] produce and develop commercially exhaust manifolds and silencers and have made available a set of experimental results for this validation process.

3.6.1 Modelling the valve data values

Valve data acquired from Arvin Meritor allows the valve open area to be evaluated, thus the related coefficients of the complex Fourier series can be calculated. Since the valve lift in relation to the crank angle, see Figure 3. 10, and the geometry of the valve seat are known, then the open area of the valve can be calculated, see Figure 3. 11.

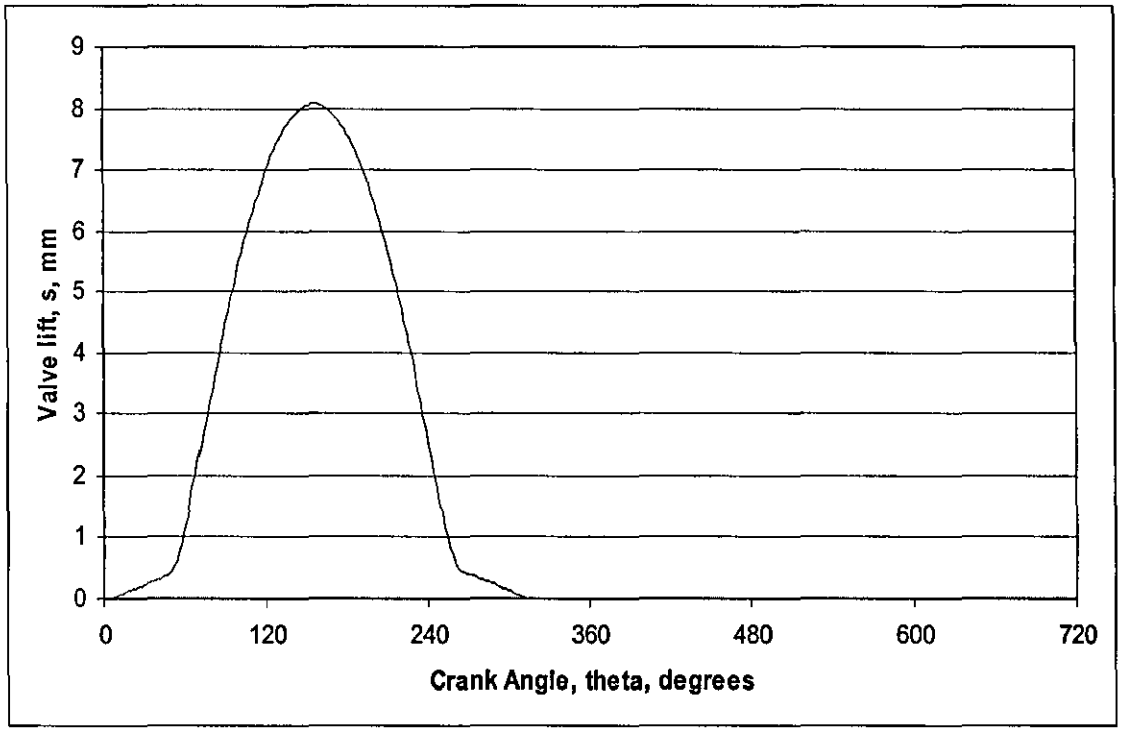

Figure 3. 10 Valve lift curve

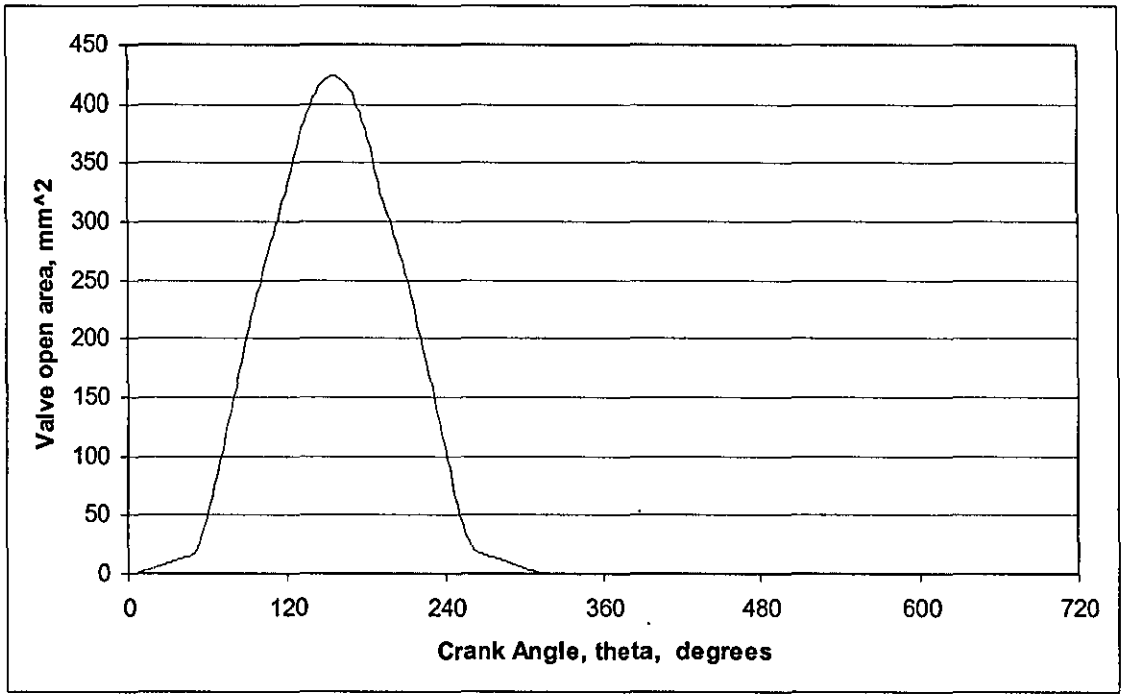

Figure 3. 11 Valve open area curve

The complex Fourier series coefficients, as in equation (3.10), can be acquired by integrating numerically the evaluated function for the open area of flow. This is achieved by using the Trapezium Rule [90]. Since the corresponding values of the crank angle and valve lift are known, then the coefficients of the complex Fourier series associated with the valve open area curve are always calculable.

The valve open area curve is periodic, therefore only the complex Fourier coefficients for one cycle need to be calculated. Recorded non-zero valve lift values are known for every crank angle, θ, from θ=0° to θ=324° in steps of 2°, and maximum value of valve lift, s, occurs at θ=162°. Equation (3.24) enables the valve open area to be calculated from a given valve lift and corresponding crank angle. Since the period of a valve cycle is determined by the RPM of the engine, the valve angular frequency is

$$\omega = \frac{RPM}{60\beta} 4\pi, \tag{3.58}$$

Let there be another variable σ, where

$$\sigma = \frac{\theta - 162}{720} \cdot \frac{2\pi}{\omega}, \tag{3.59}$$

such that σ=0 corresponds to the maximum valve lift and $-\pi < \sigma \leq \pi$ for one cycle. The variable, σ, expresses the same valve open area curve, except the period of one valve cycle is between -π and π radians. Therefore, the curve has the correct angular units for integration. Complex Fourier coefficients can be evaluated by

$$c_n = \frac{1}{T} \int_{-\frac{T}{2}}^{\frac{T}{2}} f(t) e^{\frac{i2\pi nt}{T}} dt. \tag{3.60}$$

where T is the period of one valve cycle; therefore the complex Fourier coefficients of the normalized valve open area curve are calculated by combining equations (3.24) and (3.58) to (3.60), resulting in

$$A_n = \frac{1}{A_{\max}} \frac{\omega}{2\pi} \int_{-\frac{\pi}{\omega}}^{\frac{\pi}{\omega}} A_v(s_\sigma) \cdot e^{i\omega n\sigma} \, d\sigma. \tag{3.61}$$

The variable s_σ is the valve lift at σ given the crank angle θ. Equation (3.61) can be integrated numerically using the Trapezium Rule.

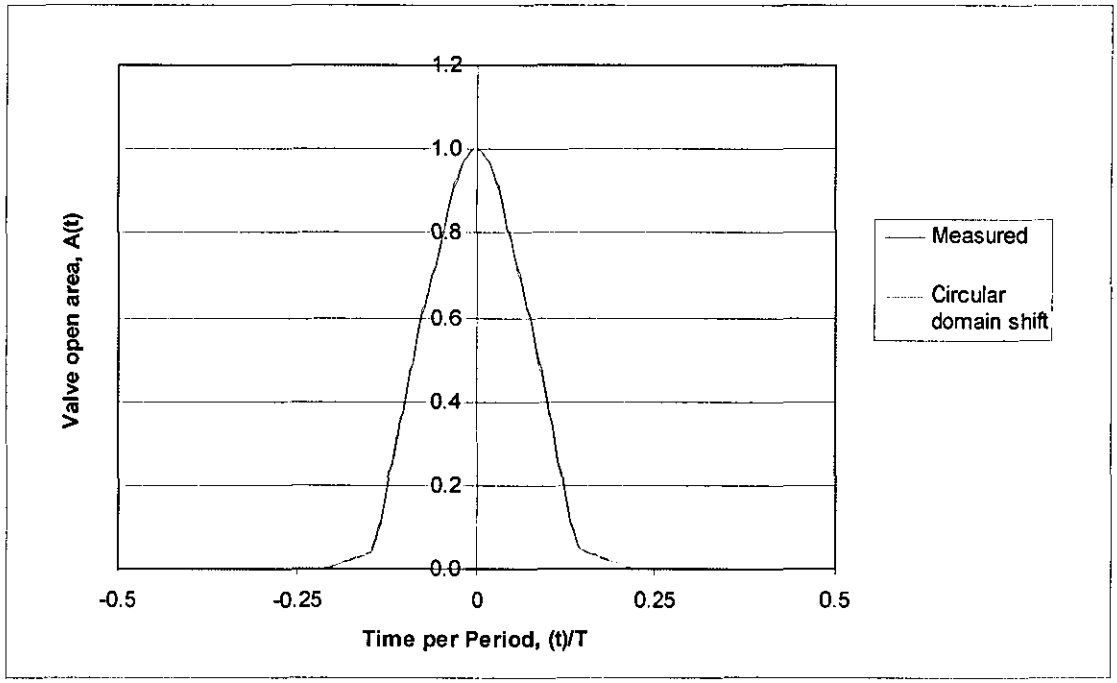

Figure 3. 12 Arvin 'non-dimensional valve open area curve'

Figure 3. 12 shows the non-dimensional valve open area curve over a complete valve cycle. Once the associated Fourier coefficients of the non-dimensional curve are found, resizing of the amplitude and period are easily calculable, for A_{-2N} to A_{2N} in steps of N. The resized and phase shifted Fourier coefficients are used to form an admittance matrix see equation (3.10). The accuracy of the admittance matrix is determined by the number of harmonics used in complex Fourier series, see equations (3.6) to (3.9).

The 'Measured' curve, with respect to Figure 3. 12, shows the valve open area curve in relation to one complete valve period. The measured valve open area values are multiplied by a factor to create a non-dimensional curve. On the same figure the 'Circular domain shift' curve illustrates the same relationship, however, the complex Fourier coefficients have been calculated for the first 30 modes and from these coefficients, the time domain relationship has been re-acquired by the inverse Fourier transform. These two curves, shown on the same graph, indicate that accuracy has not been lost when truncating the Fourier series at N=30.

3.6.2 Modelling a manifold

A manifold usually consists of two-port elements, such as pipes and area changes, which are joined together by fork elements. A typical example of this is the Arvin Meritor manifold shown in Figure 3. 13.

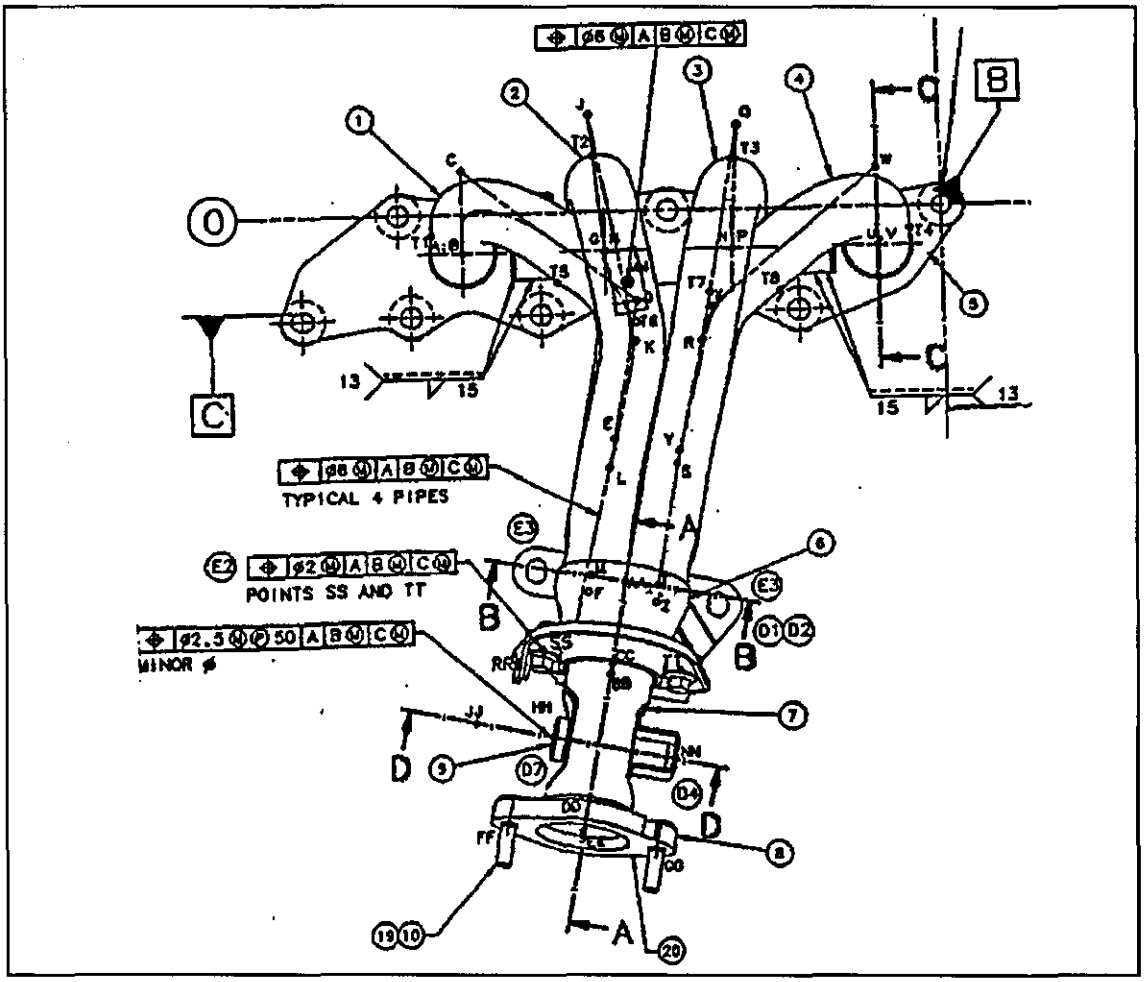

Figure 3. 13 A diagram of the Arvin manifold

(Figure 3. 13 is taken from an Arvin Meritor diagram)

This manifold can be represented in an acoustic element format, see Figure 3. 14. 'Pipe 1' and 'Area Change 2' represent the two exhaust runners that exit each piston cylinder immediately downstream of the valve. Since each cylinder/valve always has a pair of

runners, they can be modelled as a single pipe with twice the cross-sectional area of the pipe. The exhaust runners are located inside the cylinder head and are not shown on Figure 3. 13. 'Pipe 3' in Figure 3. 14 represents the four separate branches of the manifold from the cylinder head, all of which are of the same length and meet at one point represented by the fork element.

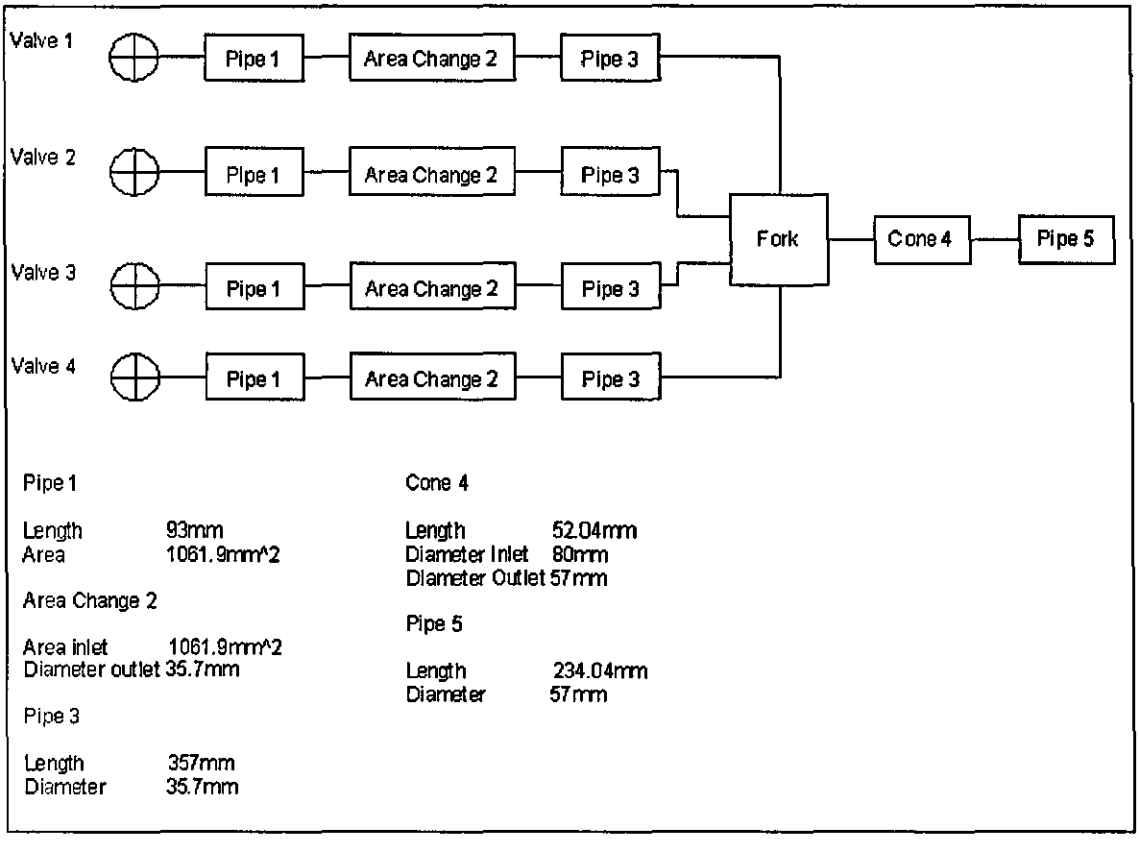

Figure 3. 14 Acoustic element representation of the Arvin manifold

Since each path between the valve and fork has exactly the same geometry, including temperature and flow settings, the firing sequence is irrelevant. However, modelling the time phase relationship between the four valves is crucial. The maximum area value (MAV) on the open valve area curve associated with the second valve has to lead the MAV of the first valve by a quarter of a period. Likewise, the MAV of the third valve open area of flow has to lead the MAV on the second valve by a quarter of a period, similarly with the fourth valve. The valve open area curves are the same for each cylinder/valve except for a phase shift; therefore, to phase shift the time dependent curve

in the frequency domain, complex harmonic dependent coefficients are used, these are shown in equations (3.52) to (3.55).

3.6.3 Modelling silencers

The experimental and theoretical results compare six silencers against a control. This control is a uniform straight pipe of length 551mm and a diameter of 54mm. The six silencers are used in both the theoretical and experimental analyses. These silencers have similar geometries with different perforate porosities and other special configurations. Figure 3. 15 illustrates the complex silencer geometry involved in the Arvin Meritor Silencer IA00085, upon which the other five silencers are based.

The changes to silencer model 'IA00085' for the other five silencers, as illustrated in Figure 2. 10, are explained in the table below:

Silencer	Perf A	Perf B	Perf C	Note
IA00085	34%	34%	34%	
IA00087	6%	6%	6%	Welded Baffles
IA00088	6%	100%	6%	No Return Pipe
IA00089	34%	34%	34%	Holes on inlet, 10 holes, diameter 5.0, evenly spaced around inlet pipe, 66mm from the end wall.
IA00090	6%	34%	0%	No holes in Perf C, solid-walled pipe
IA00092	34%	34%	34%	Holes on inlet (10 holes, diameter 5.0, 66mm from end wall) and outlet (5 holes, diameter 5.0, 52mm from end wall), evenly spaced around inlet /outlet pipe.

Table 3. 1 Properties of different silencer models

A schematic diagram of silencer model 'IA00092' is shown in Figure 2. 4c.

These special configuration changes, although small, introduce large algorithmic complications; hence the hybrid algorithm has to be used to calculate a set of transfer

matrices of each silencer. The time-variant method requires calculations at a set of frequencies that have to be calculated for every multiple of the valve frequency. The number of frequencies required in the set is determined by the number of harmonics required for the Fourier series.

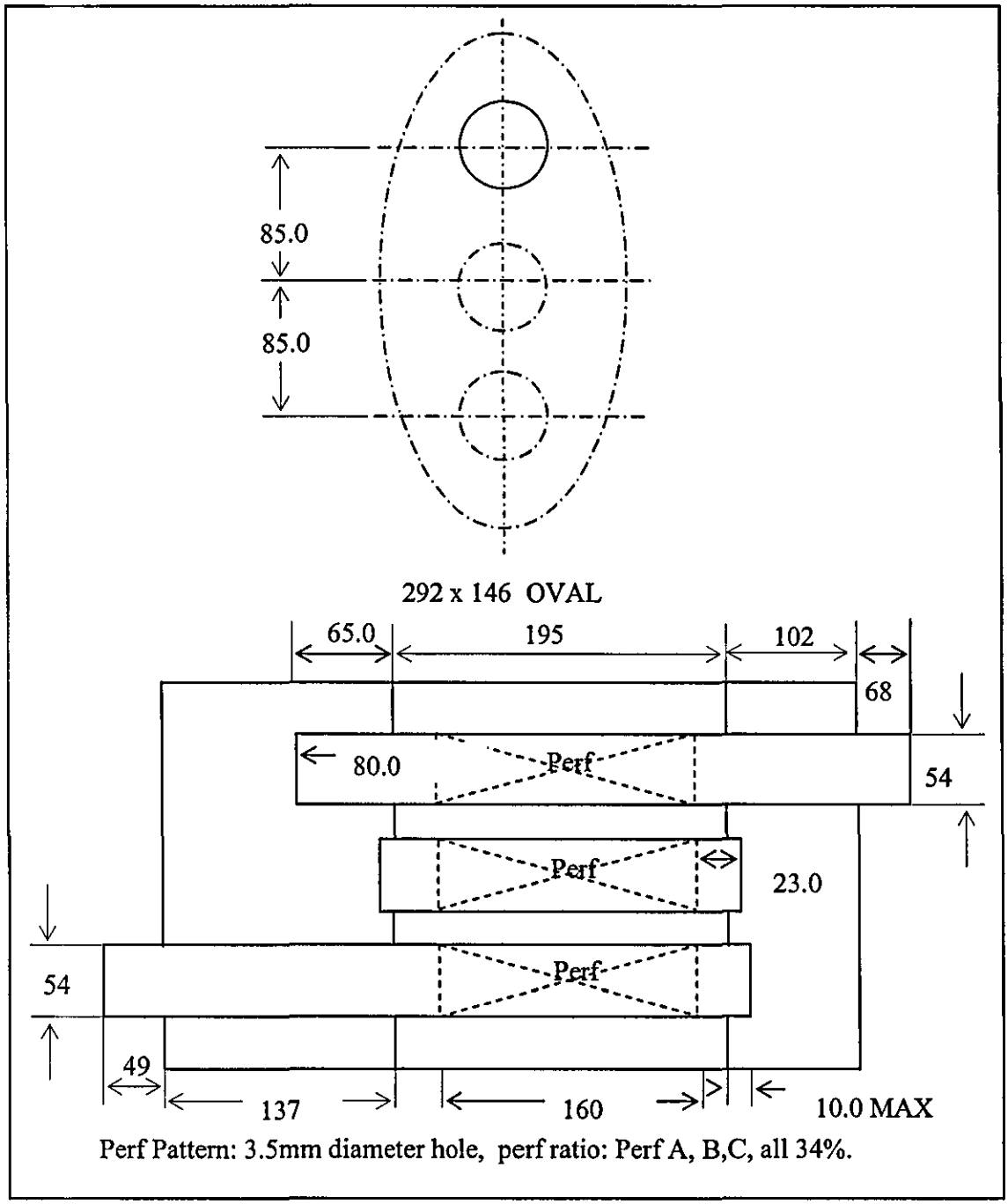

Figure 3. 15 Silencer IA00085

A complete exhaust system consists of a manifold, as shown in Figure 3. 14, the exhaust silencer system, as shown in Figure 3. 15, and the 'connecting pipe' system. The connecting pipe system often contains secondary silencers, catalytic converters, etc. The systems here used a connecting pipe system as shown in Figure 3. 16.

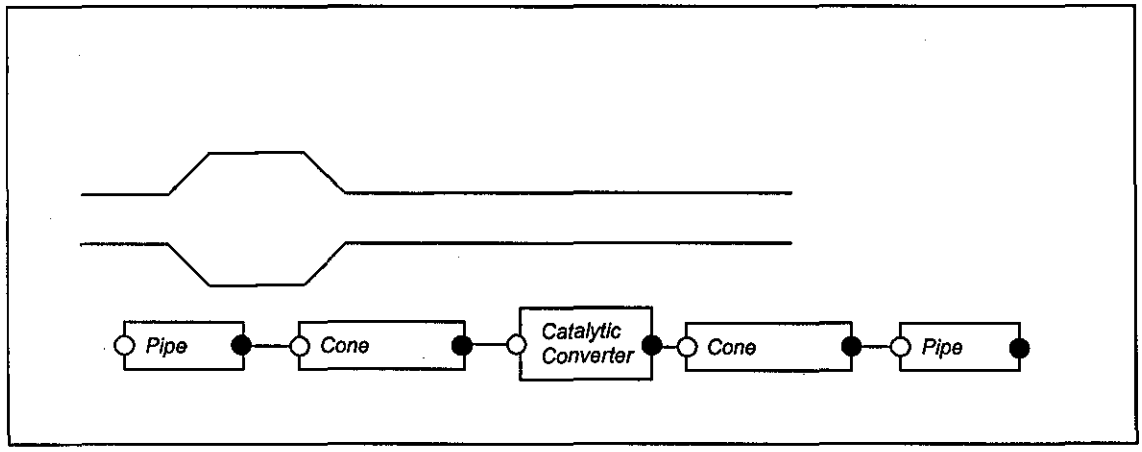

Figure 3. 16 Interconnecting pipe between the manifold and exhaust

3.7 Evaluation of insertion loss

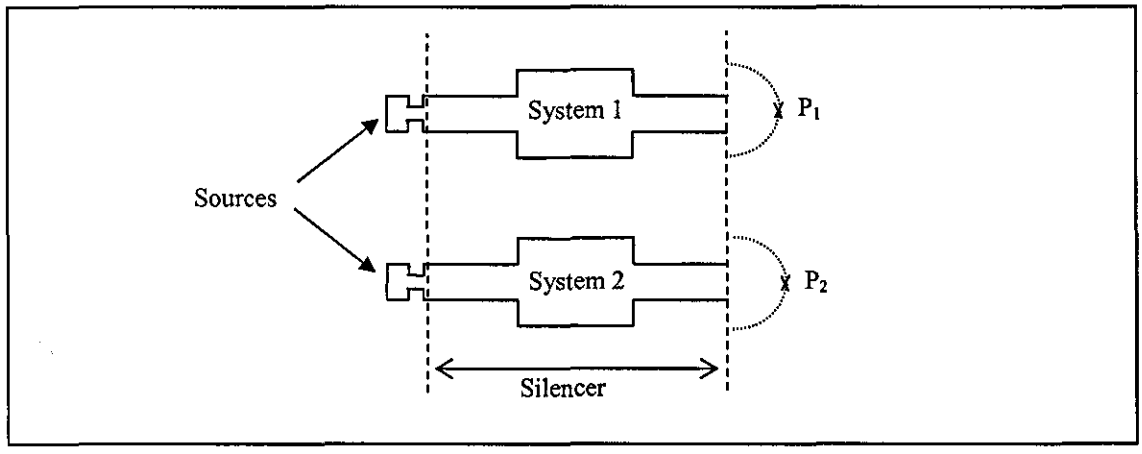

Figure 3. 17 Two exhaust system with identical sources

Insertion loss compares the radiated sound power into the free field from the outlets of two exhaust systems, assuming that they are each attached to an identical source. Let W_k be the radiated sound power from system k, then the insertion loss is [1].

$$IL = 10\log_{10}\left(\frac{W_1}{W_2}\right). \tag{3.62}$$

3.7.1 Experimental measurement of insertion loss

In order to calculate the insertion loss from exhaust measurements, the sound pressure is measured in the free field at the same relative location to the tailpipe orifice in each case. Then, insertion loss is evaluated using

$$IL = 20\log_{10}\left(\frac{P_1}{P_2}\right). \tag{3.63}$$

3.7.2 Prediction of insertion loss using source model

Section 3.2 has shown a method for modelling the source and exhaust systems with the option of acquiring the acoustic velocity at the radiation point. Since the radiation impedance is known, insertion loss can be calculated without the need of a source impedance.

The velocity vector, $\{\mathbf{v}\}_R$, at the radiation of the exhaust system is always calculable, see equation (3.39). Therefore, insertion loss can be evaluated at velocity modes, v_n see equation (3.10) by

$$W_n = v_n P_n, \tag{3.64}$$

$$Z_n = \frac{P_n}{v_n} \tag{3.65}$$

and

$$IL = 10\log_{10}\left|\frac{v_{1n}^2 Z_{1rn}}{v_{2n}^2 Z_{2rn}}\right|, \tag{3.66}$$

where Z_r is the radiation impedance, n is the mode and numerical subscripts denote different systems.

3.7.3 Conventional prediction of insertion loss

Conventionally, a source impedance is assumed to be known, such that the source can be represented by the equation

$$P_S - P_I = Z_S V_I . \tag{3.67}$$

Here P_I represents the pressure at the outlet of the source, where P_S and Z_S are the pressure and impedance of the source. The pressure and velocity at the outlet of the source can be related to those at the radiation point by

$$\begin{bmatrix} P_I \\ V_I \end{bmatrix} = \begin{bmatrix} a & b \\ c & d \end{bmatrix} \begin{bmatrix} P_R \\ V_R \end{bmatrix}, \tag{3.68}$$

where P_R and V_R are the pressure and velocity located at the radiation/outlet of the silencer, respectively. Substituting P_I and V_I into equation (3.67) to express source pressure in terms of source impedance, radiation pressure and velocity via equation (3.68), gives

$$P_S = aP_R + bV_R + Z_S(cP_R + dV_R). \tag{3.69}$$

Given a known radiation impedance, Z_R, such that

$$Z_R = \frac{P_R}{V_R}, \tag{3.70}$$

equation (3.69) can be re-written as

$$\frac{P_S}{P_R} = a + \frac{b}{Z_R} + Z_S\left(c + \frac{d}{Z_R}\right). \tag{3.71}$$

Since

$$W_R = P_R V_R, \tag{3.72}$$

insertion loss in equation (3.62) can be written as

$$IL = 10\log_{10}\left|\frac{P_{R2}^2 Z_{R2}}{P_{R1}^2 Z_{R1}}\right|. \tag{3.73}$$

Assuming constant source pressure, P_s, for the two systems, it follows from equation (3.70) that

$$IL = 20\log_{10}\left|\sqrt{\frac{Z_{R2}}{Z_{R1}}}\,\frac{a_2 Z_{R2} + b_2 + c_2 Z_S Z_{R2} + d_2 Z_S}{a_1 Z_{R1} + b_1 + c_1 Z_S Z_{R1} + d_1 Z_S}\right|. \tag{3.74}$$

This characterisation of insertion loss is heavily dependent on the source impedance, assumed as a known single value at every frequency. Not only is source impedance poorly characterised, but the concept of a single source impedance value, at a given frequency, becomes invalid if the source is time-variant.

However, the source model given here is capable of calculating the insertion loss with time-varying sources and does not require a source impedance value. This represents a major improvement, in addition to that of fully accounting for valve timing and manifold design.

3.8 Results

3.8.1 Results using constant pressure

The experimental data received from Arvin Meritor was in the form of insertion loss against frequency for a constant speed and load of the engine. The LAMPS3 [15] software was used to produce similarly predicted results, given a source impedance. Therefore, the results from the theoretical source model can be compared against both sets of results.

In the experimental measurements, a 2-litre 4-cylinder engine was attached to the whole exhaust system and ran at 1000 RPM. The 'Experimental' data indicated on Figures 3.19 to 3.30 display these experimental results for different silencers. However, results which correspond to firing frequencies have the greatest degree of accuracy. At these frequencies, predominant noise originates from the in-cylinder pressure, as opposed to flow generated noise (FGN) caused by the valve [15]. The 'Experimental' data are insertion loss results from experimental measurements and were recorded at every 4.17 Hz, which is an eighth of the firing frequency.

A valve has a periodic motion, therefore the period defines a valve frequency that is called the fundamental frequency; the gas exchange through the valve should only produce a sound wave at multiples or harmonics of the valve frequency. The 'Theoretical with constant pressure' data, see Figure 3. 19, display the insertion loss results using components of the velocity vector that correspond to multiples of firing frequency. This is

achieved by setting the valve frequency to 8.33Hz and calculating insertion loss using every fourth component, v_4, v_8, etc. and the corresponding radiation impedance. The components that do not correspond to integer multiples of firing frequency are zero, due to the symmetry of the manifold and are not shown on the figures. The theoretical models displayed in Figures 3.19 to 3.30 were calculated with 30 harmonics using a constant source pressure of 10Pa.

The 'Source Model with constant pressure' curve only displays the insertion loss that is calculated using the fourth velocity component, v_4, i.e. the first non-zero velocity component corresponding to firing frequency. This is achieved using the theory presented in Section 3.2.3 and ensuring that fundamental frequency was calculated for a frequency range from 0.25Hz to 250Hz increasing by 0.25Hz, whilst maintaining the same mass flow rate.

During the recording of the sound measurements, noise was observed between harmonic frequencies. This noise was not background noise and it was exiting through the outlet of the exhaust, which indicated that there was flow generated noise (FGN) being produced in the exhaust system. Figures 3.19 to 3.30 show the recorded experimental results as indicated by the 'Experimental' data on the graphs and this data indicates that there is FGN present. These results were obtained from Arvin Meritor.

Within an exhaust system, FGN is considered a secondary source, as compared with the obvious source of the high pressure gas release from the cylinders through the exhaust valves of the internal combustion engine [15]. These secondary sources occur primarily at pipe junctions, area expansions and contractions, or any areas of discontinuities in duct systems that disturb the gas flow propagating through the system [82]. As the RPM of the engine increases, FGN is more noticeable.

Consider the case that all of the FGN is being produced in the silencer; see FGN_1 with respect to Figure 3. 18. If this was true, then all the recorded experimental insertion loss results between the harmonic frequencies would be below 0dB, see the 'Experimental' curves in Figures 3.20, 3.22, 3.24 etc. The assumption is based on the fact that the control

system would not have any FGN. Since this contradicts the observation, FGN is not produced solely within the silencer. Furthermore, if the FGN were produced at the tailpipe exit, the insertion loss would be zero, since the mass flow rate through both systems is the same. Therefore, FGN is being produced at the valves, as one might have expected, see FGN_2 in Figure 3. 18. Since the mass flow rate through the valves of both systems is the same, then so should be the level of FGN and hence the insertion loss values, as measured across the entire frequency spectrum, would remain valid if this were the dominant secondary noise source.

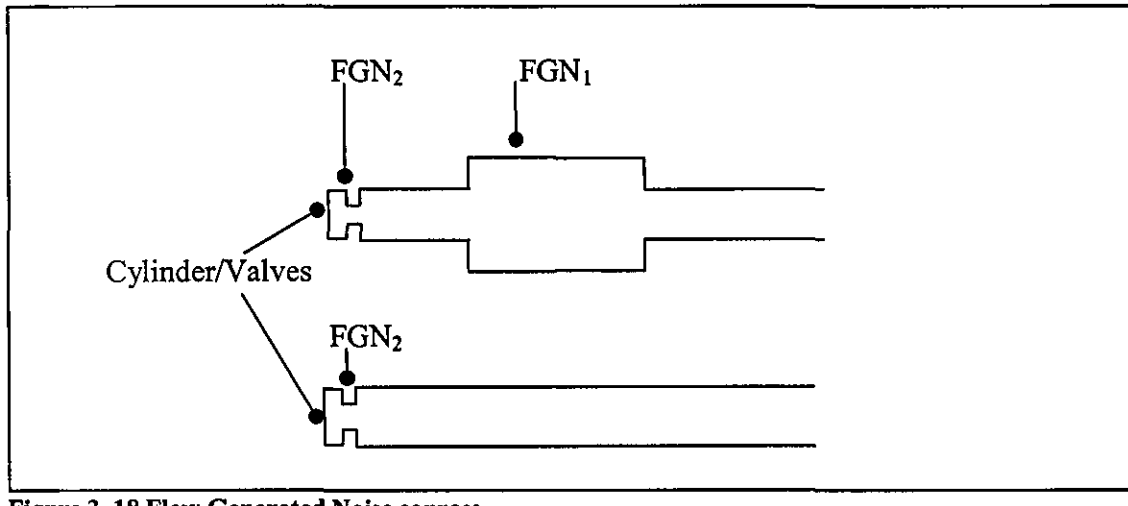

Figure 3. 18 Flow Generated Noise sources

The 'Source Model with constant pressure' curve in Figure 3. 20 is a theoretical attempt to model the insertion loss at all frequencies, although the effective source impedance can be expected to be different at the firing frequencies to that of the other frequencies. Section 3.2 explains the theoretical process to obtain a relationship between pressure and velocity at the outlet of a given exhaust system with multiple time-variant valves. Given one fundamental frequency, a relationship between pressure and velocity can be acquired. Therefore, insertion loss at the outlet of the exhaust is known for frequencies ω to $N\omega$ in steps of ω. The insertion loss result which corresponds to firing frequency should have the greatest prediction accuracy, but this no longer extends to integer multiples of firing frequency.

The 'Lamps Eng Imp' curves, with respect to Figures 3.20, 3.22, 3.24 etc., illustrate the insertion loss between two exhaust systems using an approximation of constant engine source impedance $Z_s = \rho c(1+i)/\sqrt{2}$. This empirical value has been obtained from a best-fit analysis of measured and predicted results over a wide range of exhaust systems and engine source combinations. The experimental results Figures 3.19 to 3.30 were obtained by Arvin Meritor.

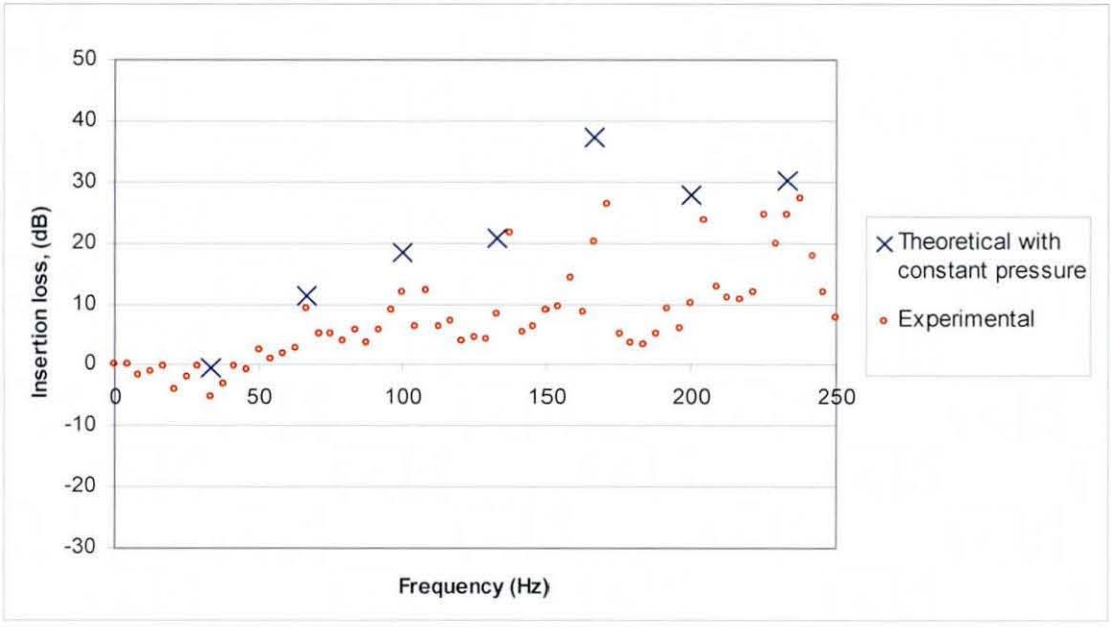

Figure 3. 20 Insertion loss of silencer IA00085 with reference to the control system: order analysis

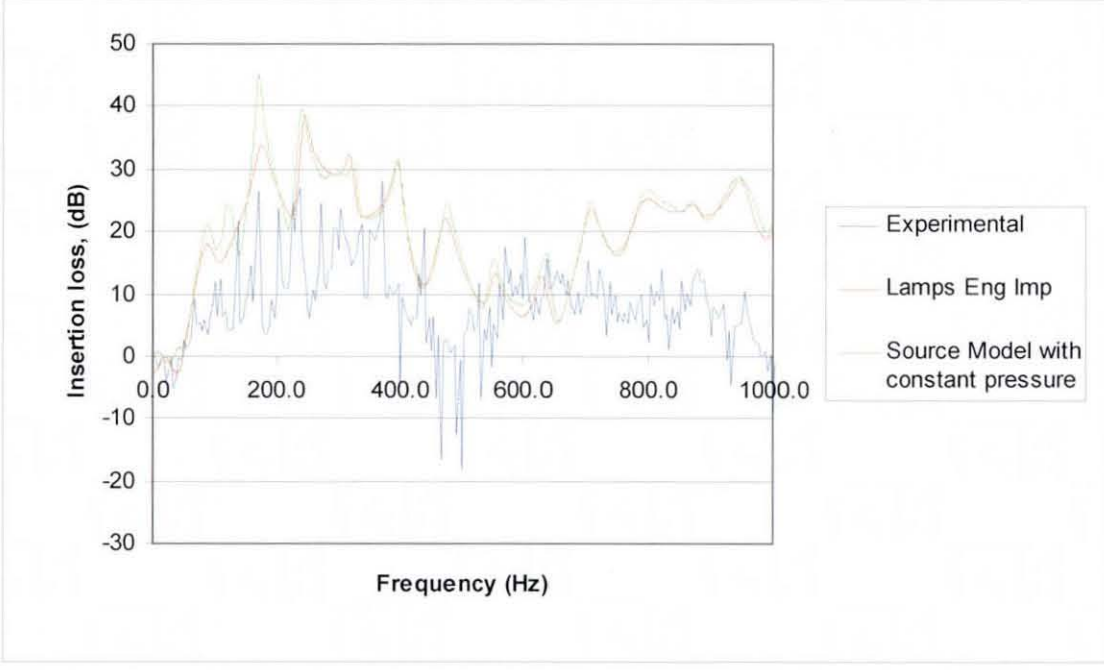

Figure 3. 21 Insertion loss of silencer IA00085 with reference to the control system: frequency analysis

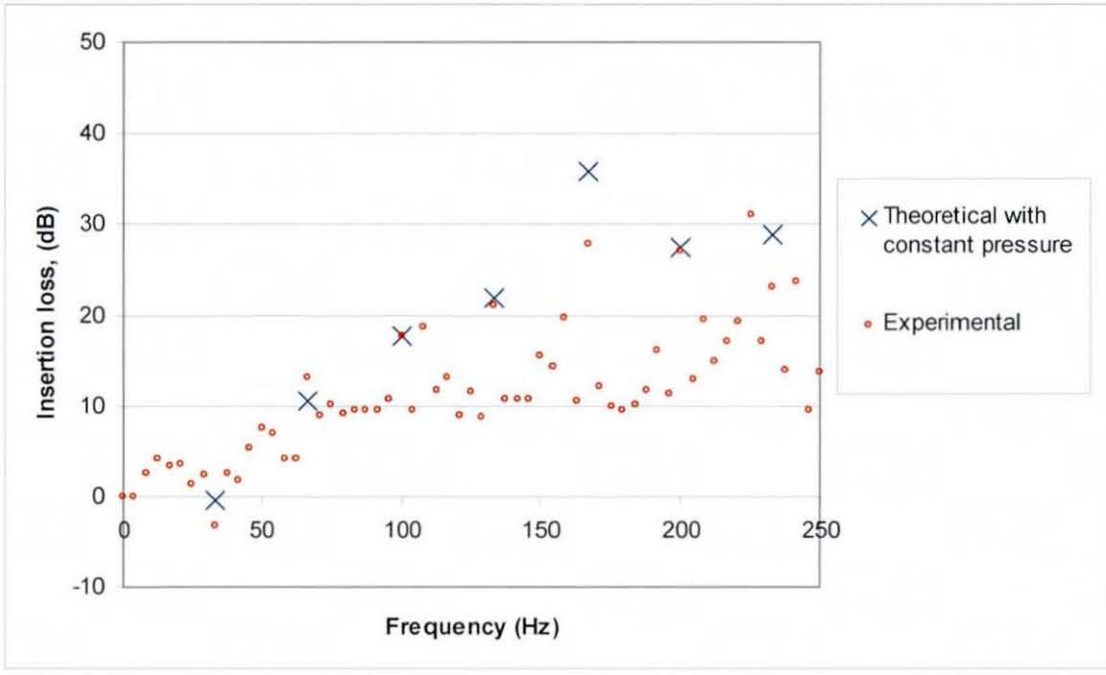

Figure 3. 22 Insertion loss of silencer IA00087 with reference to the control system: order analysis

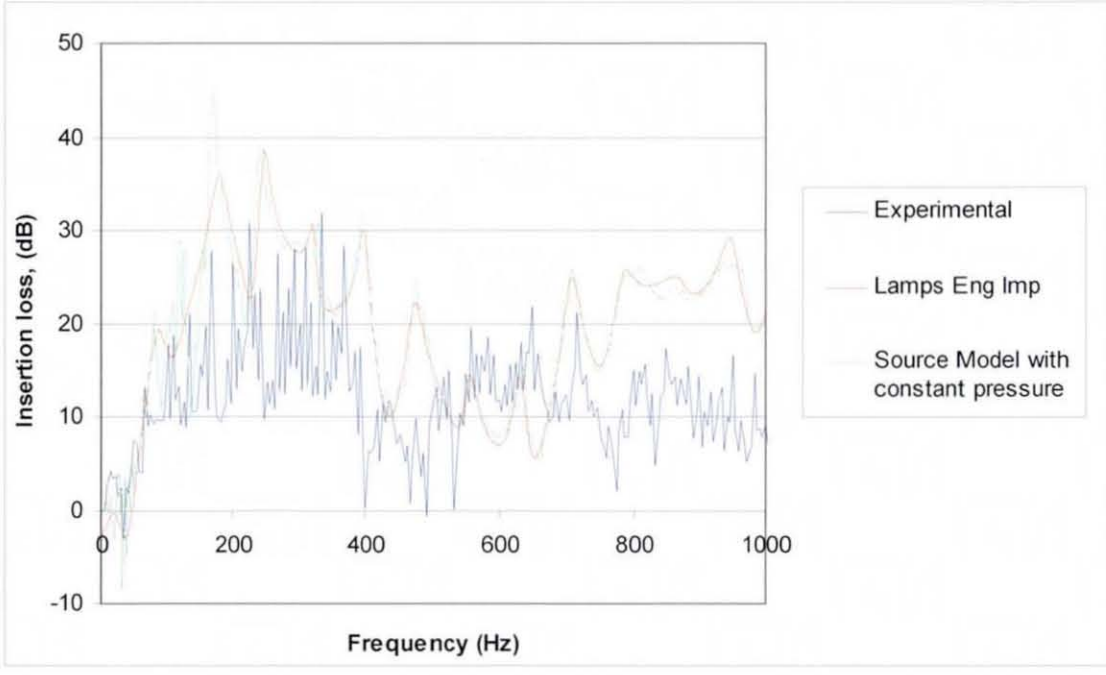

Figure 3. 23 Insertion loss of silencer IA00087 with reference to the control system: frequency analysis

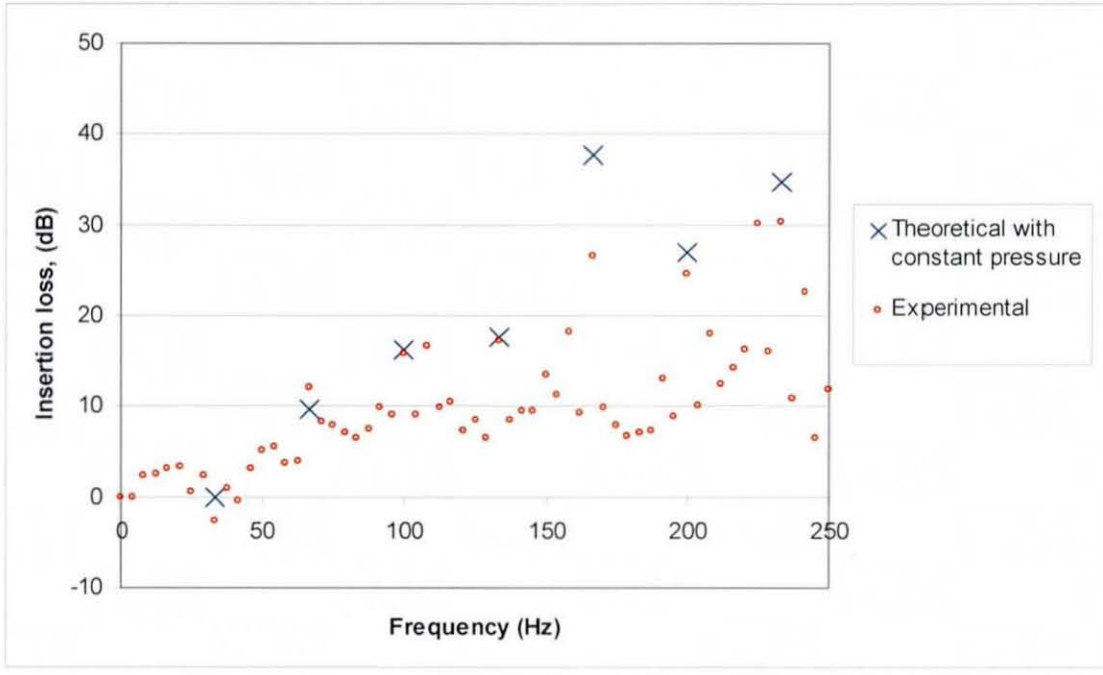

Figure 3. 24 Insertion loss of silencer IA00088 with reference to the control system: order analysis

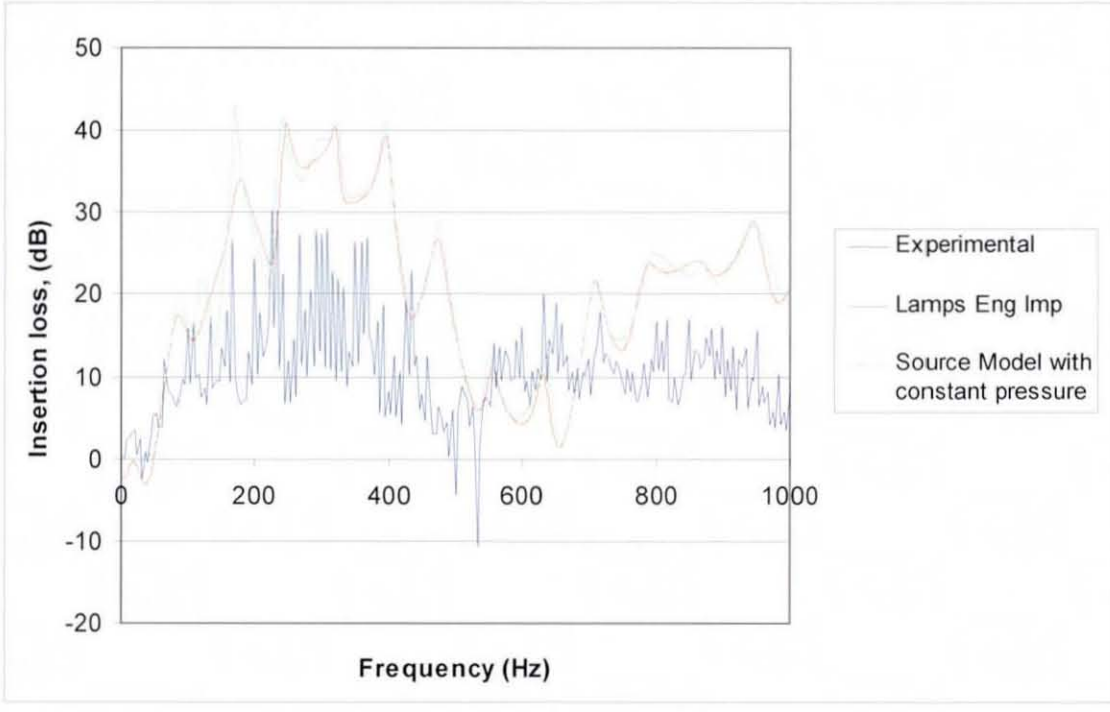

Figure 3. 25 Insertion loss of silencer IA00088 with reference to the control system: frequency analysis

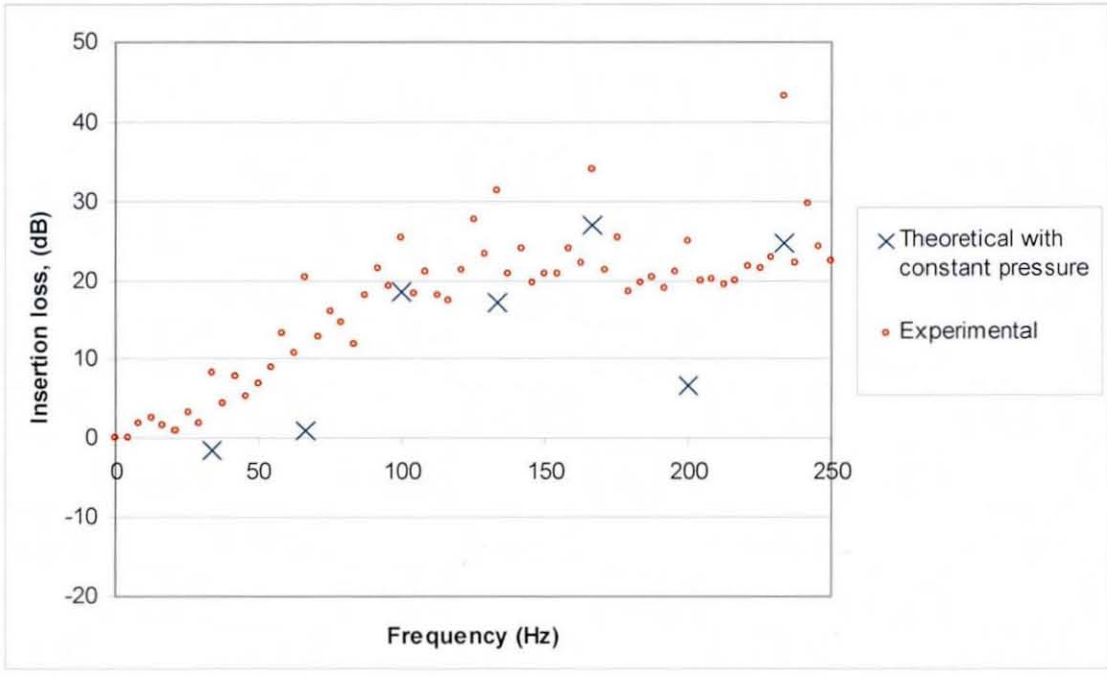

Figure 3. 26 Insertion loss of silencer IA00089 with reference to the control system: order analysis

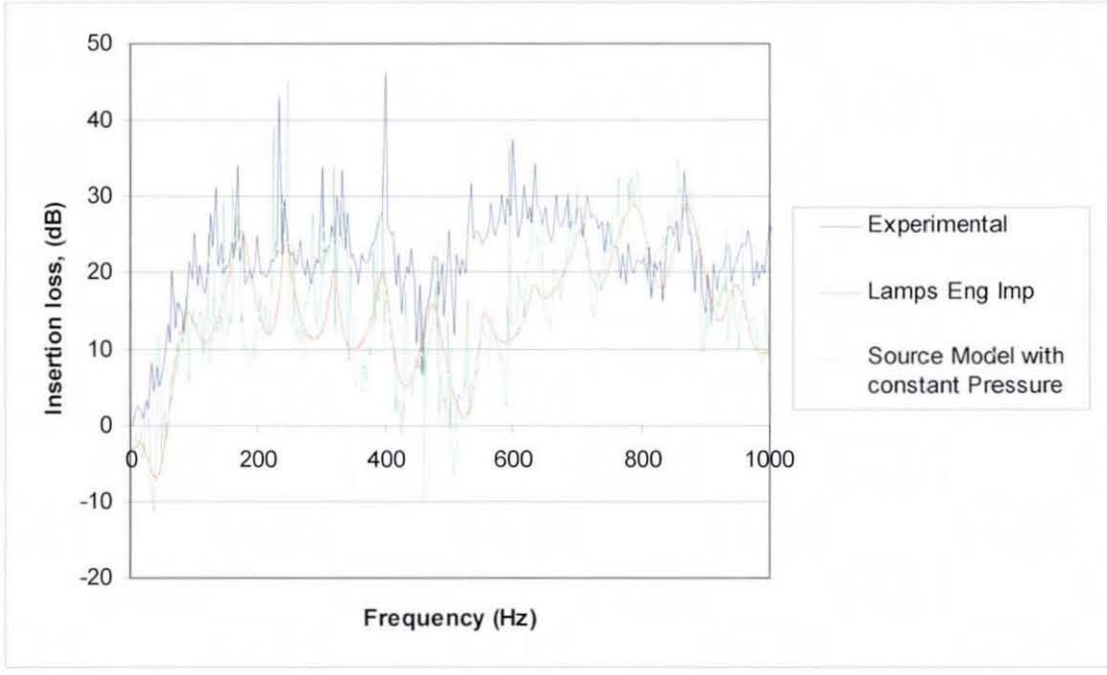

Figure 3. 27 Insertion loss of silencer IA00089 with reference to the control system: frequency analysis

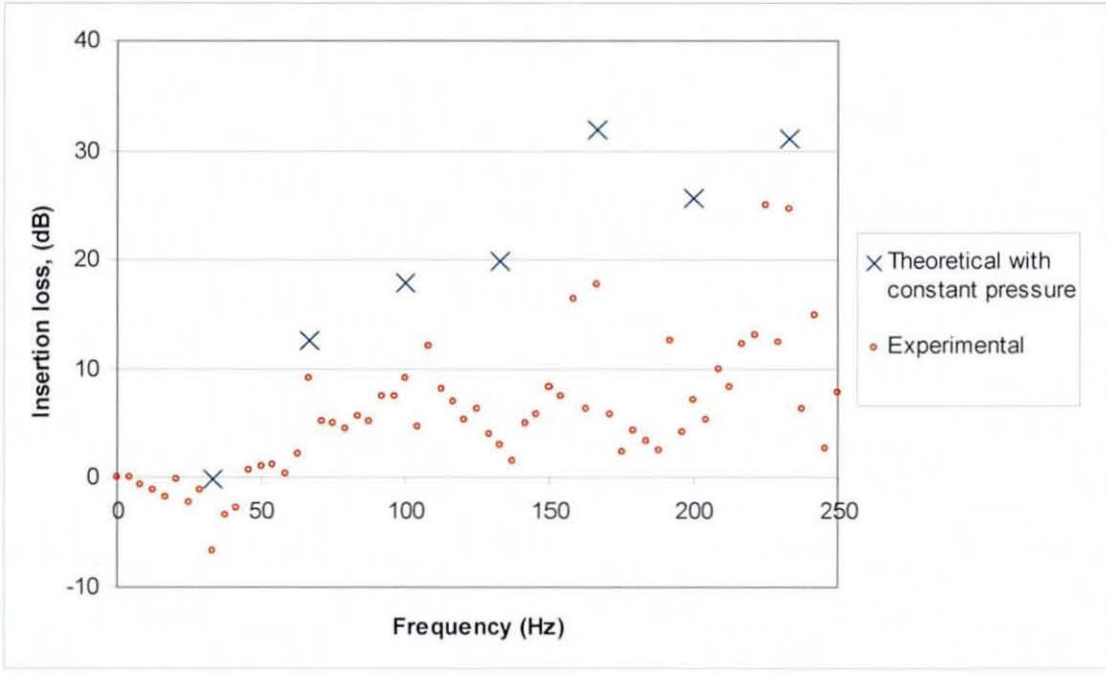

Figure 3. 28 Insertion loss of silencer IA00090 with reference to the control system: order analysis

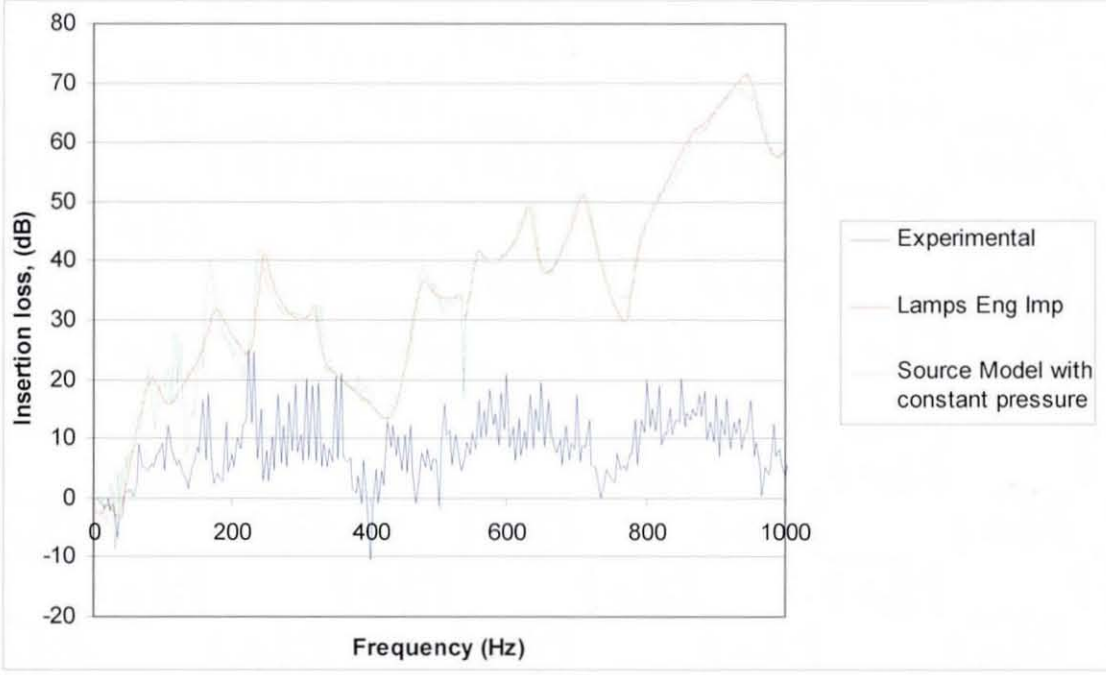

Figure 3. 29 Insertion loss of silencer IA00090 with reference to the control system: frequency analysis

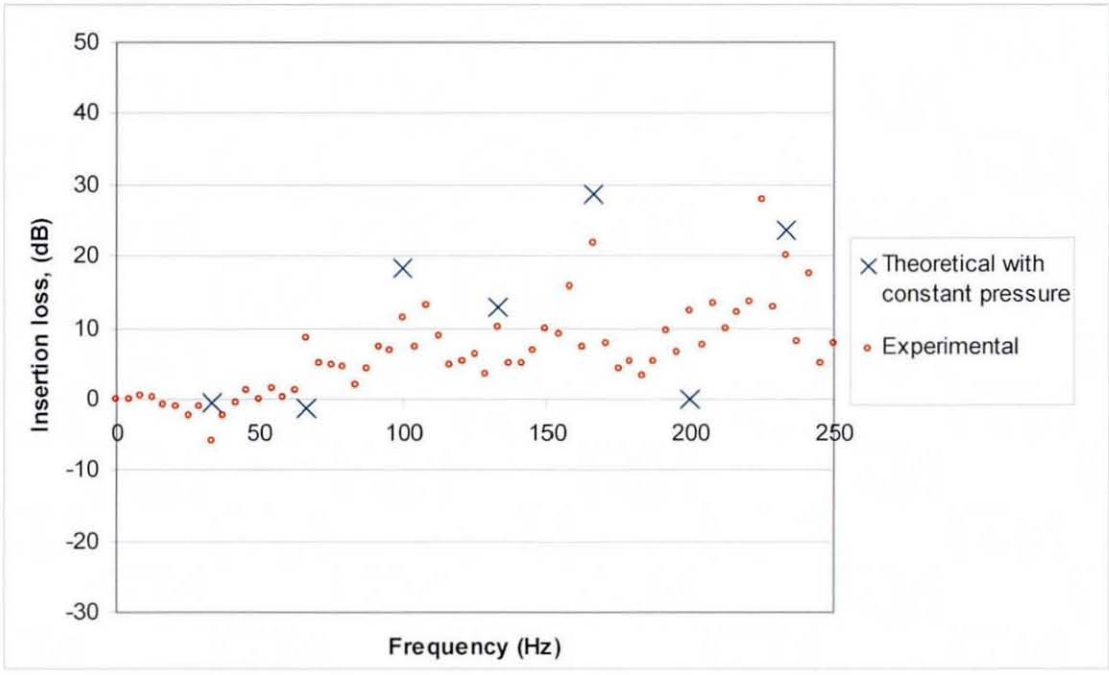

Figure 3. 30 Insertion loss of silencer IA00092 with reference to the control system: order analysis

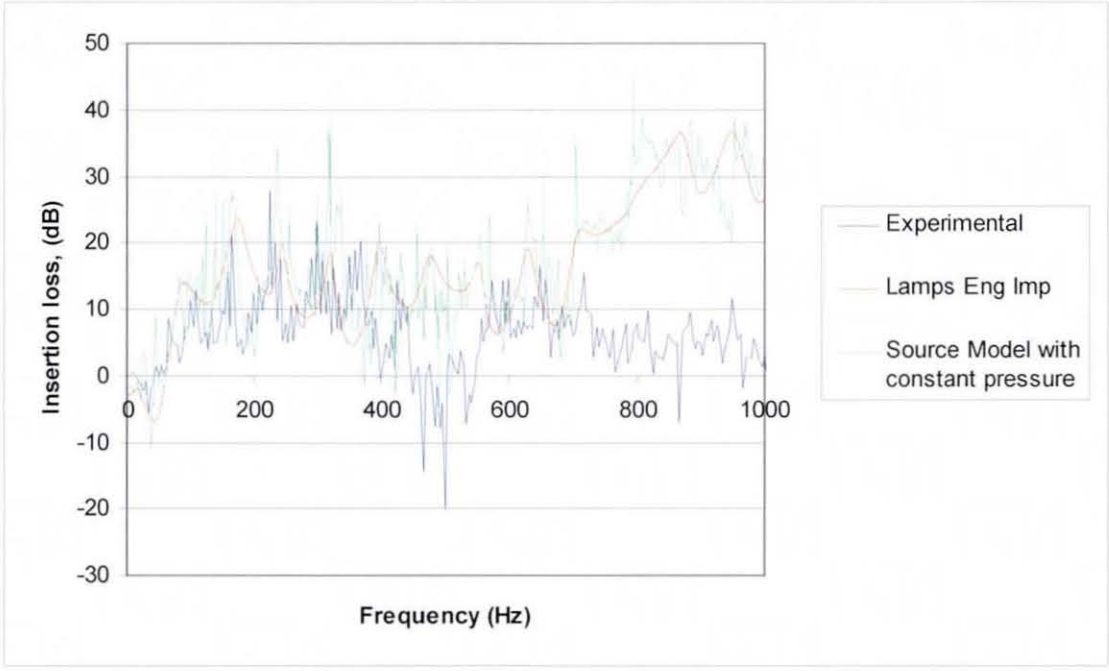

Figure 3. 31 Insertion loss of silencer IA00092 with reference to the control system: frequency analysis

As Figures 3.19 to 3.30 illustrate, the source model tends to give similar results to LAMPS3, where the source impedance is engine impedance. There is a much greater discrepancy between the measured results and the theoretical results than between the two sets of theoretical results, particularly at high frequencies. The cut-on frequency [1] of non-planar waves for these silencers is approximately 700 Hz, such that the theoretical results are invalid above this frequency and can be expected to deteriorate in accuracy as the cut-on frequency is approached from below. Furthermore, the experimental results can be expected to decrease in accuracy with increasing frequency as the signal-to-noise ratio decreases. The signal-to-noise ratio is greatest at firing frequency, diminishes with higher multiples of firing frequency and is worse still at all other frequencies. Greatest attention should therefore focus on the low frequency results at integer multiples of firing frequency, as shown in Figures 3.19, 3.21, 3.23, etc.

The quality of fit at these data points is clearly greater than the general accuracy apparent from Figures 3.20, 3.22, 3.24, etc. even when attention is restricted to the 0-250 Hz region. However, careful comparison reveals that the integer multiples of firing frequency tend to correspond to the high points of the measured curves, which indicates that the accuracy of the measured values is severely compromised by low signal-to-noise ratios at other frequencies. When comparison is made only at low integer multiples of firing frequency, reasonably good comparison between measured and predicted results for all three sets of predictions can be found. In particular, the full analysis of the 'Theoretical with constant pressure' data is not consistently better than the 'Lamps Eng Imp' data. The 'Theoretical with constant pressure' data requires the use of 30 harmonics. This necessitated inverting square matrices of size 61 by 61, which required excessive computational time as compared with using a constant source impedance. Thus, pragmatically, there seems little practical value in the source model approach, although a purist would much prefer a theoretical source model to an empirical source impedance. Furthermore, the source model does include the effects of manifold geometry, valve lift curve and valve timing, which are not appreciated in insertion loss results that simply show the difference between two exhaust systems on the same engine/manifold source. Unfortunately, experimental results of insertion loss or noise reduction that include

variations of the source or manifold are not currently available. There are large differences in insertion loss predictions at 190Hz between 'Source model with constant pressure' and 'Lamp Eng Imp' series, see Figures 3.20, 3.22, 3.24 and 3.28. A reasonable explanation is currently unattainable at this stage.

As a first attempt to improve the quality of the results from the source model, the effect of an increase of cylinder pressure upon the predicted insertion loss has been investigated. Assuming that there is pseudo-steady flow through the valve into a pipe of area, A_p, and that the valve can be regarded as a plate with an orifice, then the velocity of discharge through the valve [71] is

$$V \approx 0.61\sqrt{\frac{2A_p^{\,2}\tilde{A}_v^{\,2}\Delta P}{\bar{\rho}\left(A_p^{\,2}-\tilde{A}_v^{\,2}\right)}}, \tag{3.75}$$

where ΔP is the change in pressure across the valve, P_s-P. If the area of the pipe is significantly greater than the open area of the valve,

$$V \approx 0.61\tilde{A}_v\sqrt{\frac{2\Delta P}{\bar{\rho}}}. \tag{3.76}$$

This implies that the difference in pressure is proportional to the square of the velocity and hence is actually non-linear. Comparing equations (3.1) and (3.76), it follows that

$$C_d = \frac{\bar{\rho}\bar{c}V}{\tilde{A}_v\Delta P} = \frac{\bar{\rho}\bar{c}0.61}{\Delta P}\sqrt{\frac{2\Delta P}{\bar{\rho}}}, \tag{3.77}$$

therefore

$$C_d = 0.61\bar{c}\sqrt{\frac{2\bar{\rho}}{\Delta P}}. \tag{3.78}$$

The theoretical 'Source Model with constant pressure' and 'Theoretical with constant pressure' series results, displayed in Figure 3. 20 to 3. 30, show the predicted insertion loss between two specific exhaust systems where the pressure difference across the valve is 10Pa. This ensures linear acoustic behaviour within the manifold, but is unrealistic as the actual pressure drop across the valve is generally much higher. Thus, the effects on the insertion loss results when cylinder pressure is increased should be investigated.

Equation (3.78) shows the coefficient of discharge is inversely proportional to the square root of the pressure difference. Therefore, as the pressure difference across the valve increases, the coefficient of discharge tends towards zero. Physically, this relationship is plausible, because as the pressure difference increases, the admittance matrix, [**A**], tends to zero, therefore the impedance matrix $[\mathbf{A}]^{-1}$ tends to infinity [71].

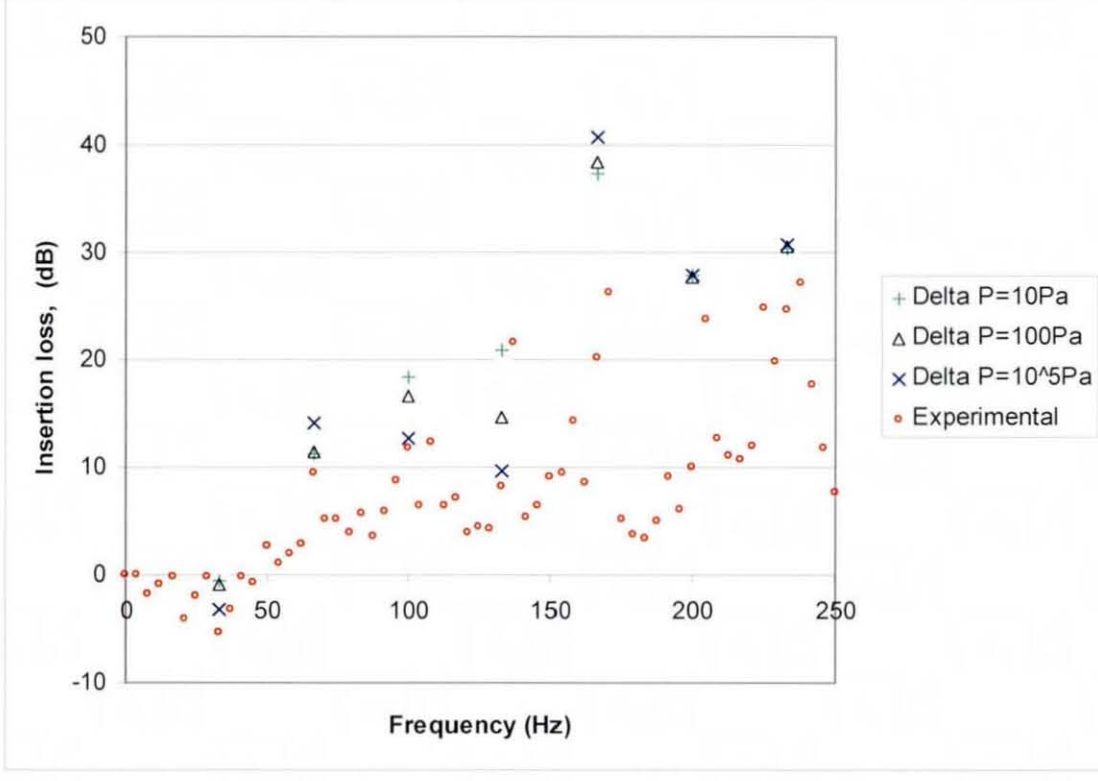

Figure 3. 32 The effect on insertion loss of silencer IA00085 when the constant pressure across the valve is changed

Figure 3. 31 shows theoretical insertion loss results as compared to the experimental results, for the silencer IA00085 versus the control system. The theoretical results are from the time-variant source model and are non-zero only at integer multiples of firing frequency, where the firing frequency is 33.33Hz. Exactly the same manifold and silencer geometries were used for the three theoretical series, 'Delta P=10Pa', 'Delta P=100Pa' and 'Delta P=10^5Pa'. The corresponding non-dimensional discharge coefficients for each pressure value across the valves are 102.7, 32.48 and 1.027, given a mean density and sound speed of 0.588kg/m^3 and 491m/s respectively, see equation (3.78). There is no general trend to imply that a particular value of pressure difference tends to produce a markedly better insertion loss prediction. The variation between insertion loss predictions for different discharge coefficients is generally small, which suggests that the non-linearity is not the major cause for the disparity between the measured and predicted results. Although, of course the full effects of non-linearity are not apparent for any given constant value of discharge coefficient.

Validation of the conclusion for the effects of the discharge coefficient on insertion loss results can be seen on Figure 3. 32 and Figure 3. 33, where different constant pressure vectors were used to generate insertion loss predictions. Again, it can be concluded that the discharge coefficient has a small effect on the predictions, which re-iterates that non-linearity is probably not the major cause of disagreement for disparity between measured and predicted results.

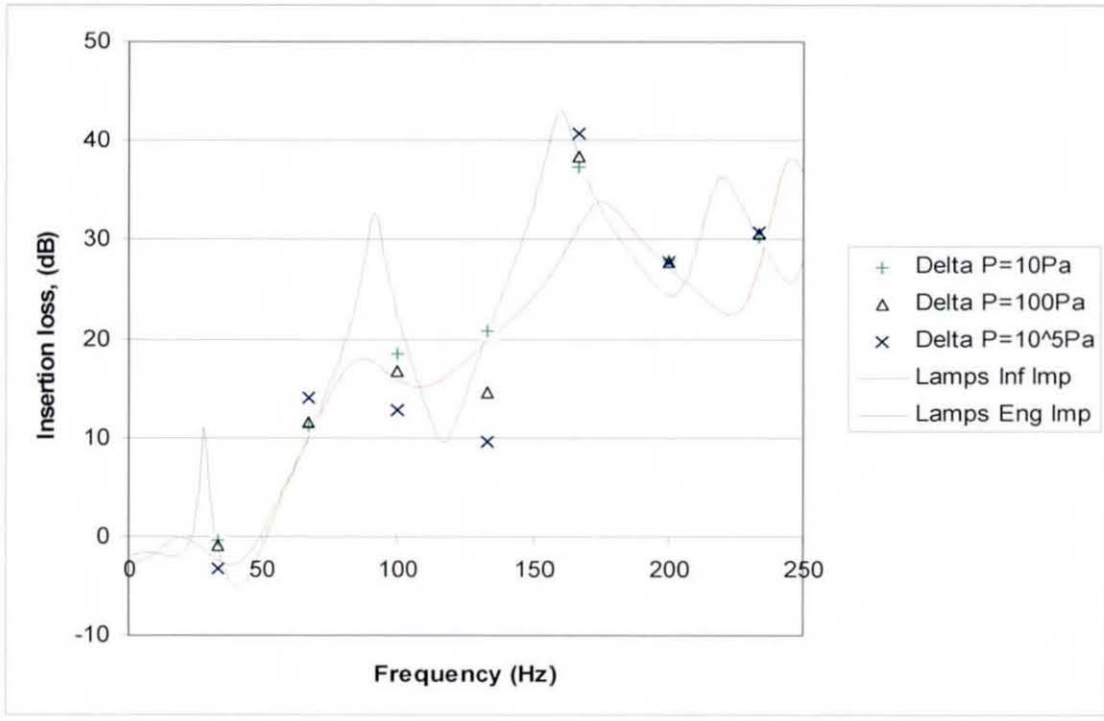

Figure 3. 33 The effect on insertion loss on silencer IA00085, when the constant pressure across the valve is changed, compared with Lamps insertion loss predictions Source Model and Lamps Engine and Infinite Impedance series.

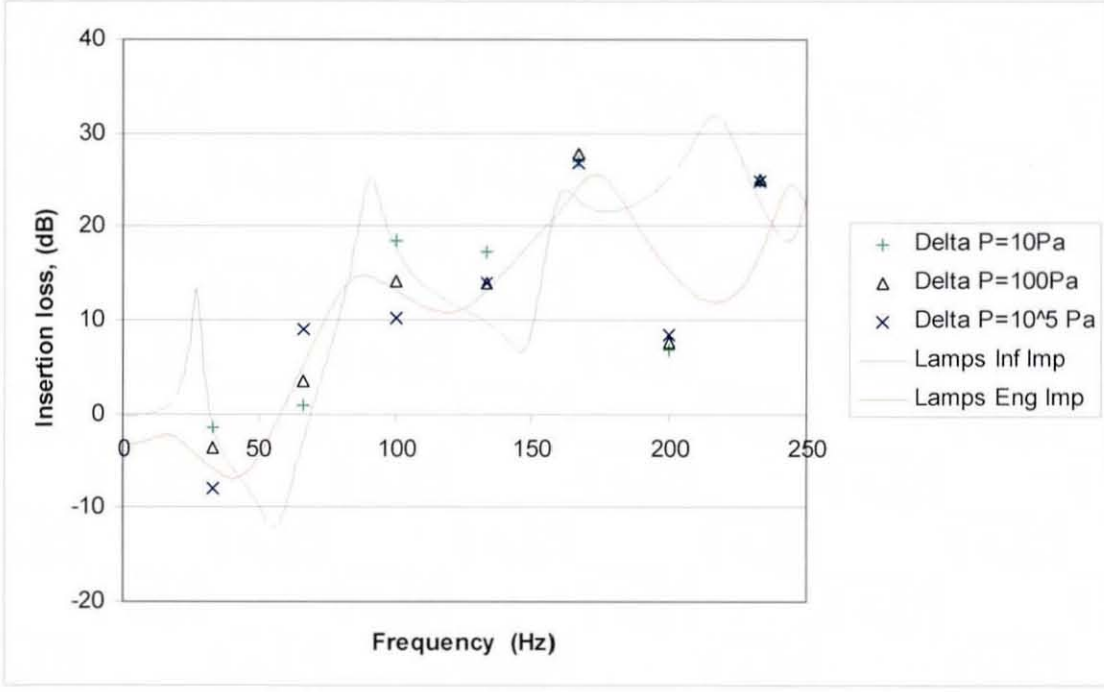

Figure 3. 34 The effect on insertion loss on silencer IA00089, when the constant pressure across the valve is changed, compared with Lamps insertion loss predictions Source Model and Lamps Engine and Infinite Impedance series.

3.8.2 Results using time-varying cylinder pressure

An alternative attempt to improve the results generated by the source model is to include a time-variant cylinder pressure curve, or a cylinder pressure which varies with the angle of the crankshaft. Arvin Meritor recorded the pressure level within a cylinder over a complete period, this is shown by the 'Measured' curve in Figure 3. 35. When moving to the frequency domain from the time-domain, 30 harmonics are used. In order to verify that this number was sufficient, a conversion back into the time-domain was undertaken and is shown as the 'Circular domain shift' curve of Figure 3. 35.

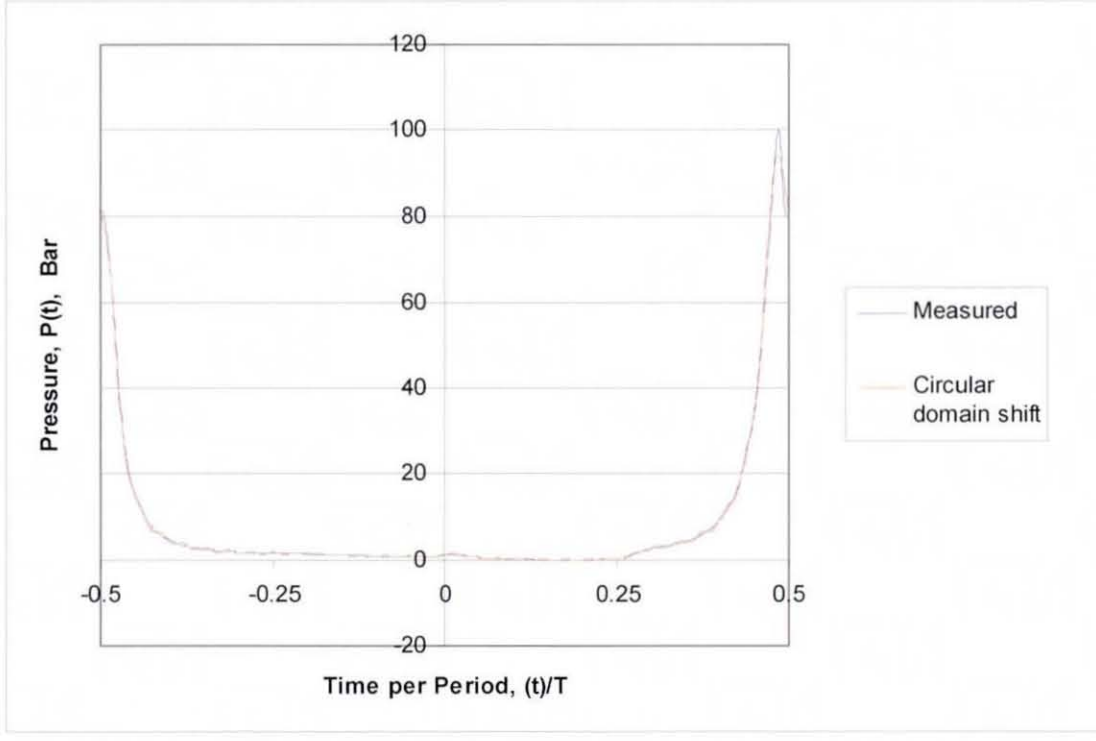

Figure 3. 35 Pressure level within a cylinder over a complete period T

The valve is closed between -0.5t/T to -0.225t/T and 0.225t/T to 0.5t/T. When the valve is open, it can be seen that the complex Fourier series models the time varying pressure difference level sufficiently accurately using 30 harmonics. When including a time-variant cylinder pressure curve, it is vitally important to phase the curve correctly with the valve open area curve, as shown in Figure 3. 36.

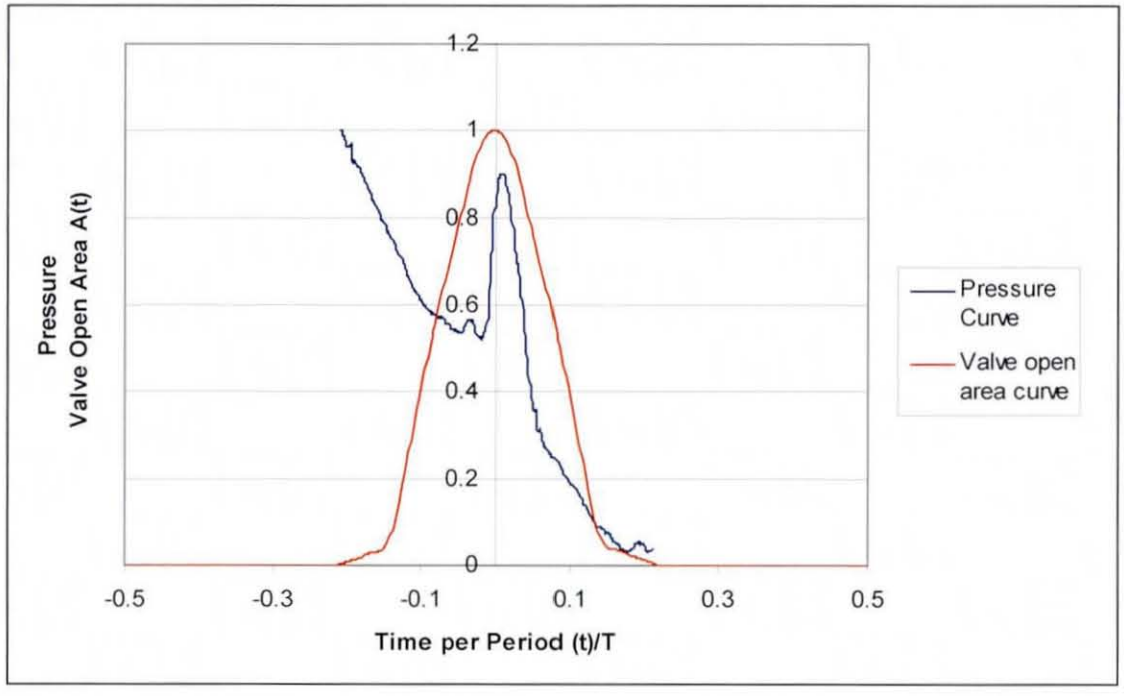

Figure 3. 36 Non-dimensional pressure difference and valve open area curve

Inclusion of a time-variant pressure curve only requires the adaptation of the source pressure vector, $\{\mathbf{S}\}$, that appears in the source model. Since the pressure level is known for a given crank angle and the period is also known

$$S_n = \frac{1}{P_{\max}} \frac{\pi}{2\omega} \int_{\sigma_1}^{\sigma_2} P_{s_\sigma} e^{i\omega n\sigma} \, d\sigma \tag{3.79}$$

where S_n represents the complex Fourier coefficient of the pressure curve for harmonic n. Let P_{max} be the maximum pressure found in the cylinder when the valve is open, ω is the angular frequency of the valve. Also σ_1 and σ_2 correspond to the angle at which the valve opens and closes respectively. This can be integrated numerically using the trapezium rule.

Since the pressure difference level and valve open area are time-variant, the validity of using ΔP and C_d in equations (3.9) and (3.78) to calculate A_{max} and C_v respectively is questionable. A more realistic evaluation of C_d, say $C_{\bar{d}}$ is

$$C_{\bar{d}} = 0.61\bar{c}\sqrt{\frac{2\overline{\rho}}{\overline{\Delta P_v}}}, \tag{3.80}$$

where $\overline{\Delta P_v}$ is the average pressure difference level across the valve when the valve is open. The more realistic evaluation of C_v, say $C_{\bar{v}}$,is

$$C_{\bar{v}} = C_{\bar{d}}\frac{\overline{A_v}}{A_p}, \tag{3.81}$$

where $\overline{A_v}$ is the average open area of the valve.

Once the Fourier coefficients of the non-dimensional pressure curve have been calculated, the amplitude of the varying pressure curves can be changed. Figure 3. 36 to 3.47 displays results calculated with a varying pressure curve, where the maximum pressure value across the valve, when it is open, is 10Pa.

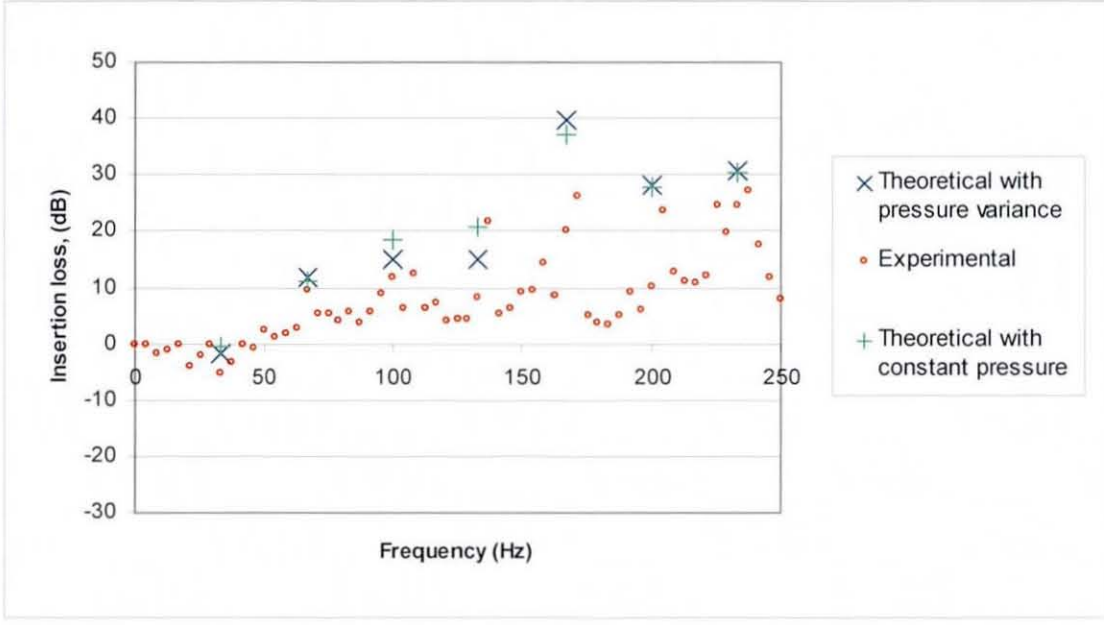

Figure 3. 37 Insertion loss of silencer IA00085 with reference to the control system, with time-varying cylinder pressure: order analysis

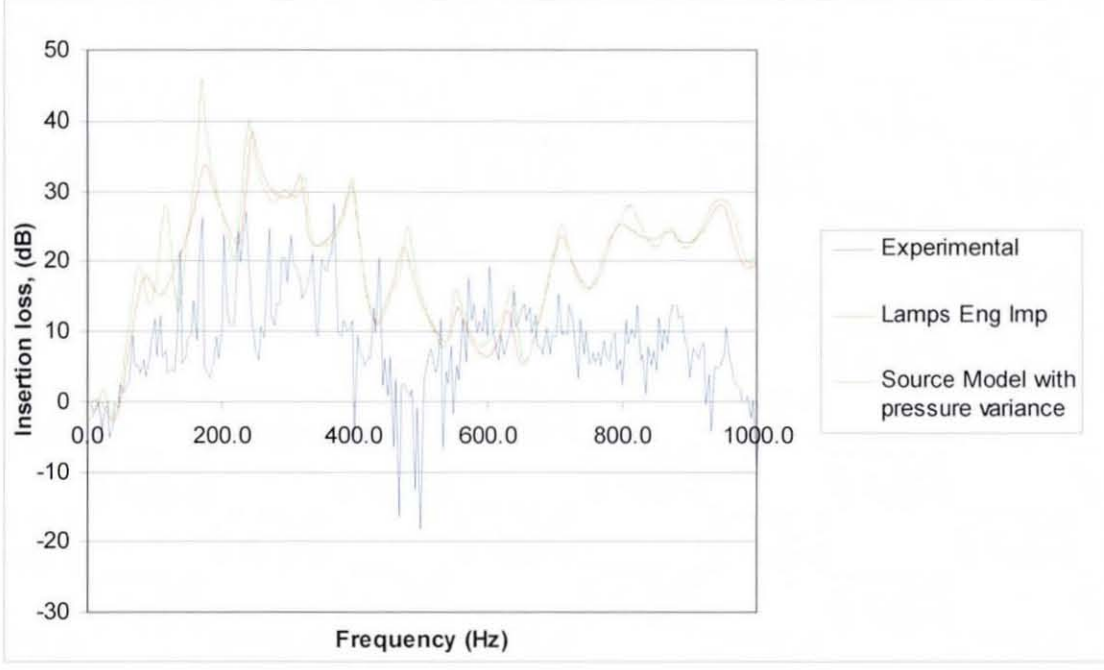

Figure 3. 38 Insertion loss of silencer IA00085 with reference to the control system, with time-varying cylinder pressure: frequency analysis

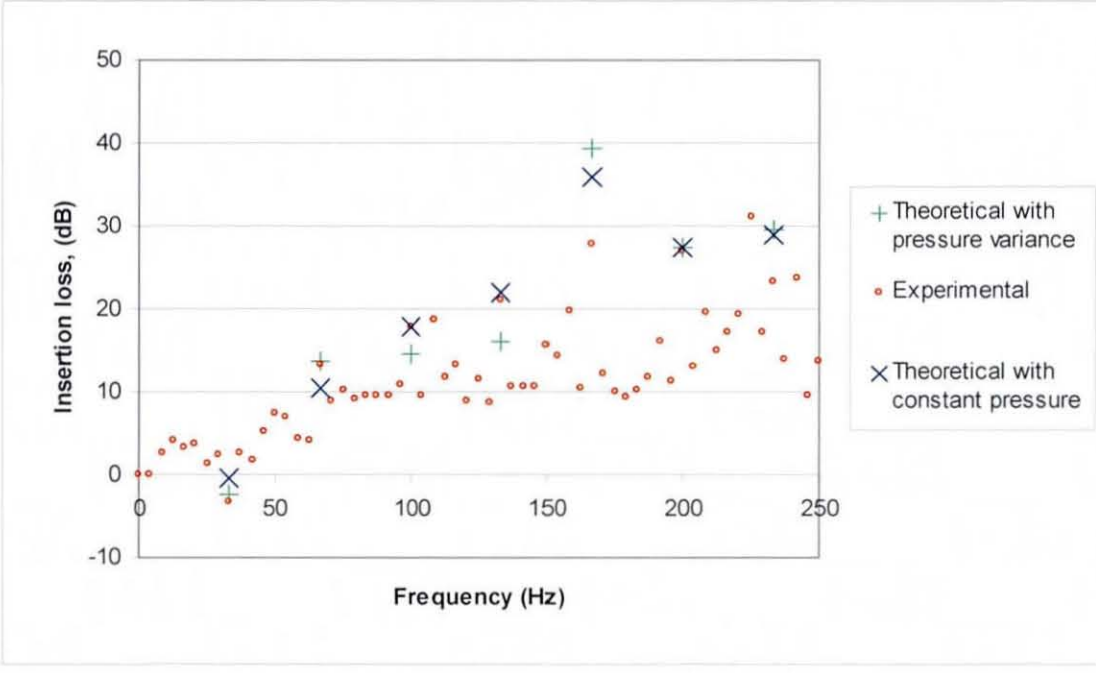

Figure 3. 39 Insertion loss of silencer IA00087 with reference to the control system, with time-varying cylinder pressure: order analysis

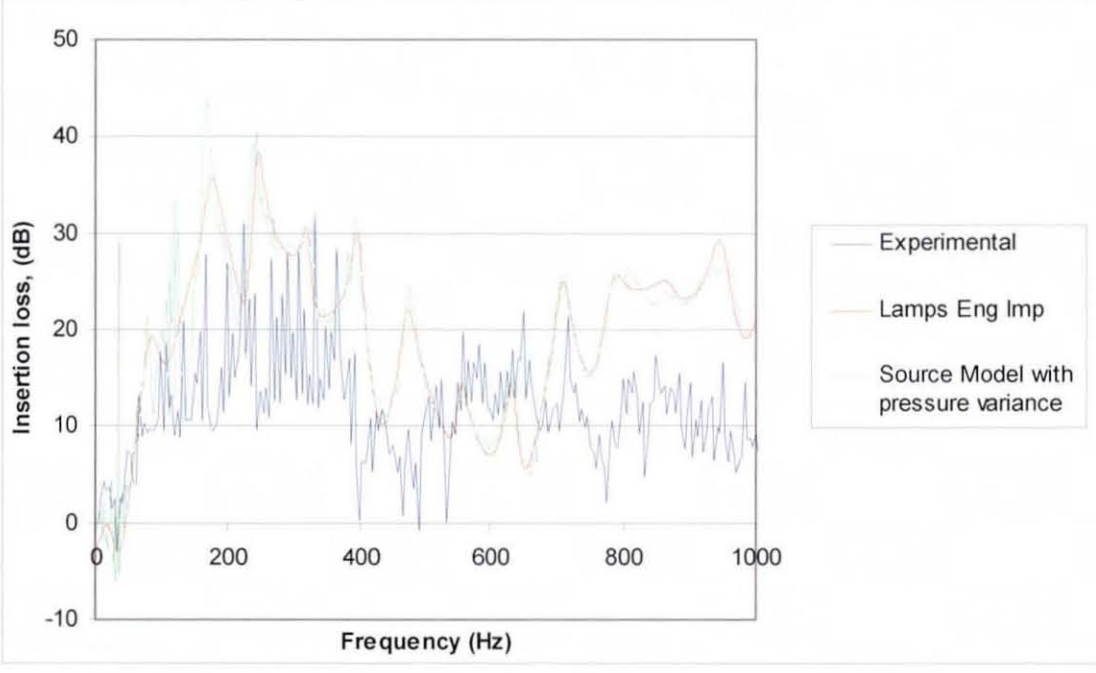

Figure 3. 40 Insertion loss of silencer IA00087 with reference to the control system, with time-varying cylinder pressure: frequency analysis

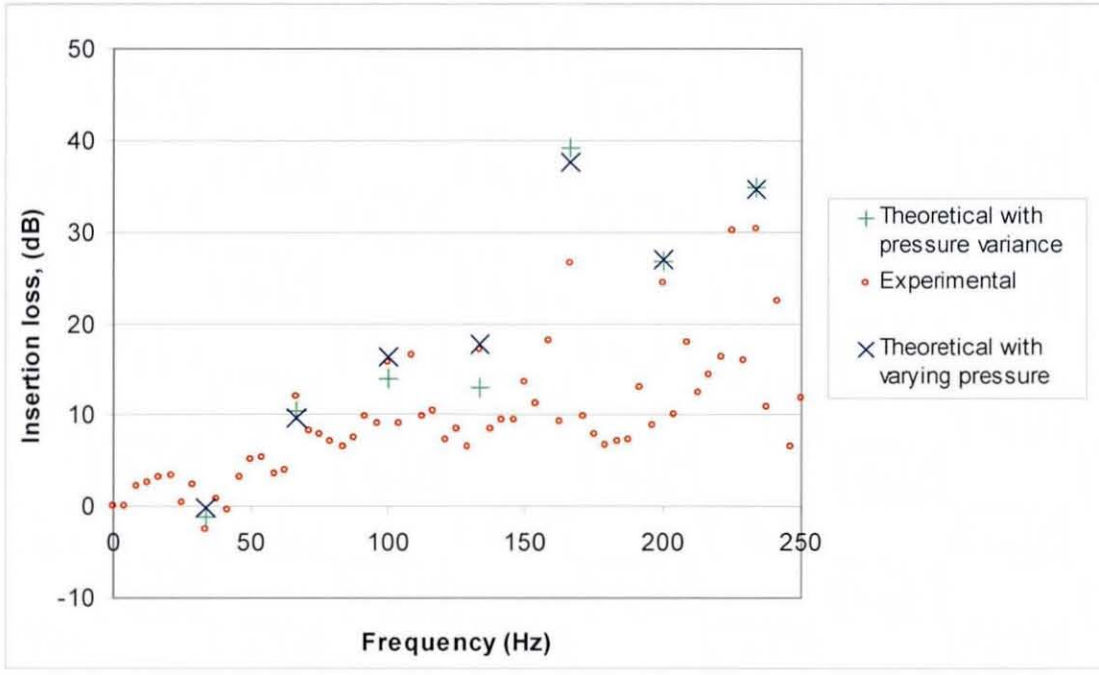

Figure 3. 41 Insertion loss of silencer IA00088 with reference to the control system, with time-varying cylinder pressure: order analysis

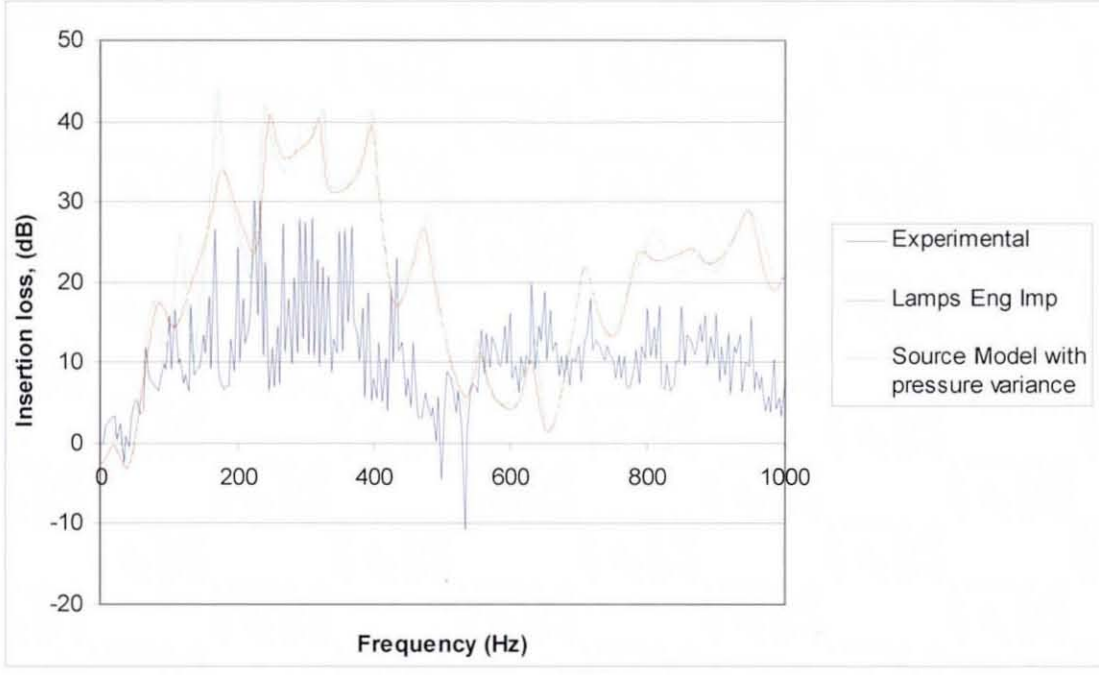

Figure 3. 42 Insertion loss of silencer IA00088 with reference to the control system, with time-varying cylinder pressure: frequency analysis

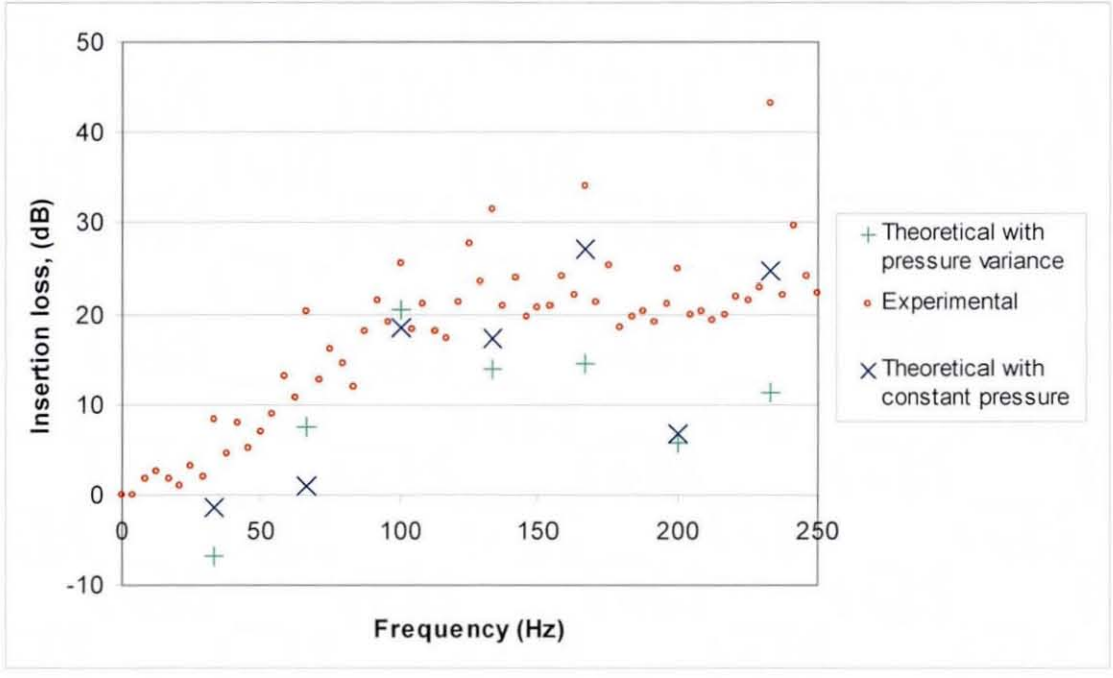

Figure 3. 43 Insertion loss of silencer IA00089 with reference to the control system, with time-varying cylinder pressure: order analysis

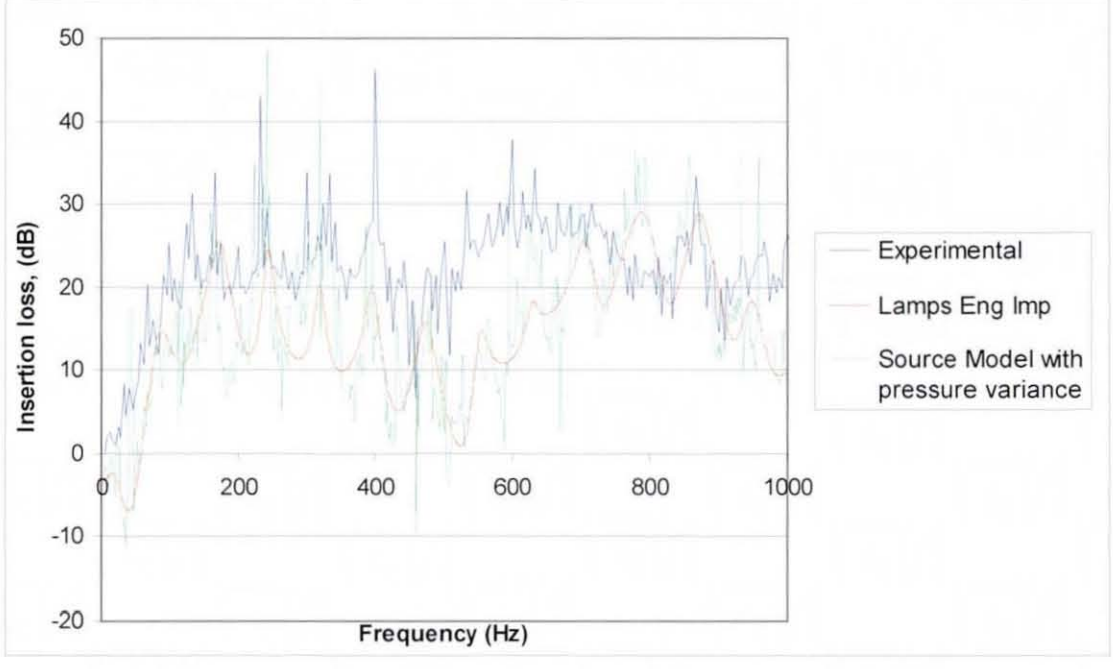

Figure 3. 44 Insertion loss of silencer IA00089 with reference to the control system, with time-varying cylinder pressure: frequency analysis

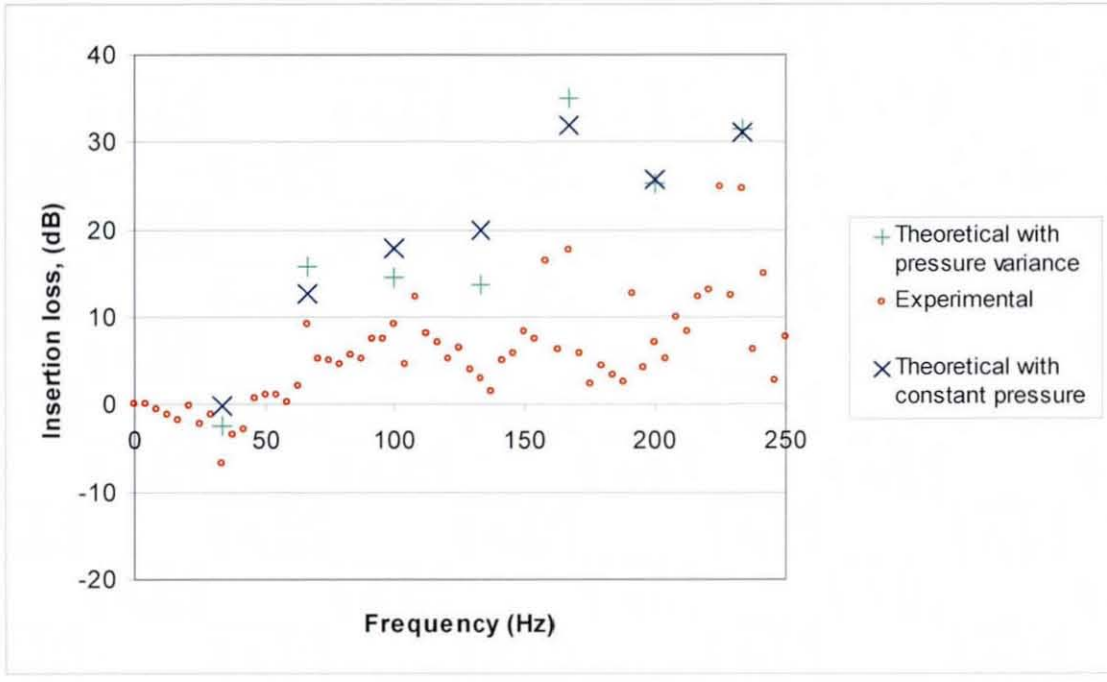

Figure 3. 45 Insertion loss of silencer IA00090 with reference to the control system, with time-varying cylinder pressure: order analysis

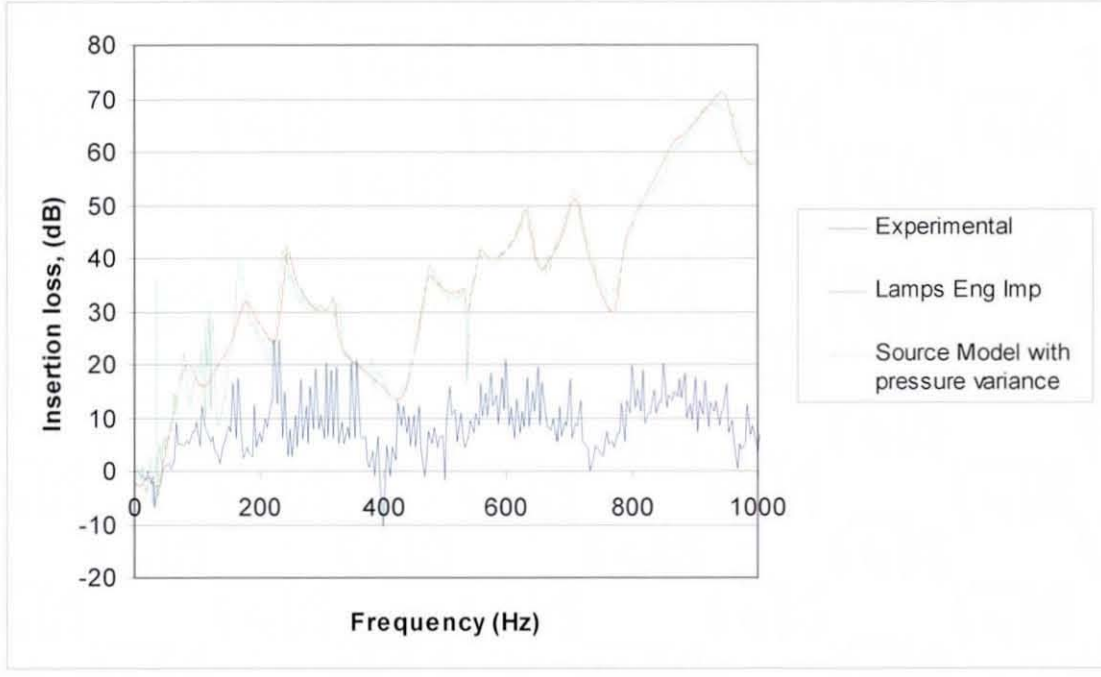

Figure 3. 46 Insertion loss of silencer IA00090 with reference to the control system, with time-varying cylinder pressure: frequency analysis

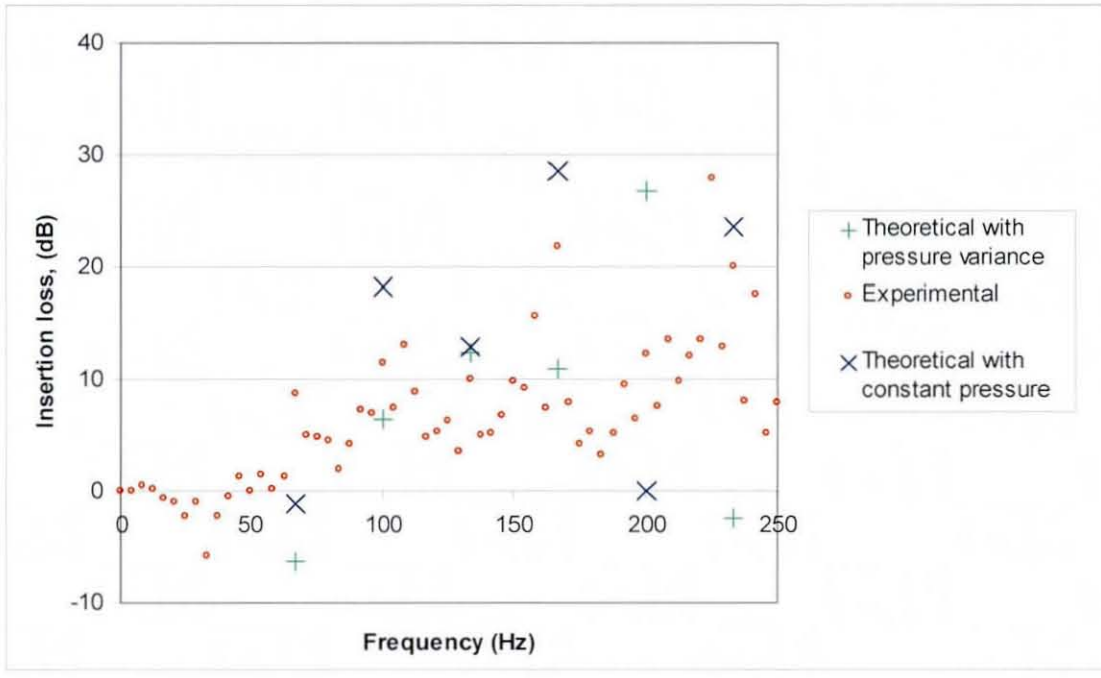

Figure 3. 47 Insertion loss of silencer IA00092 with reference to the control system, with time-varying cylinder pressure: order analysis

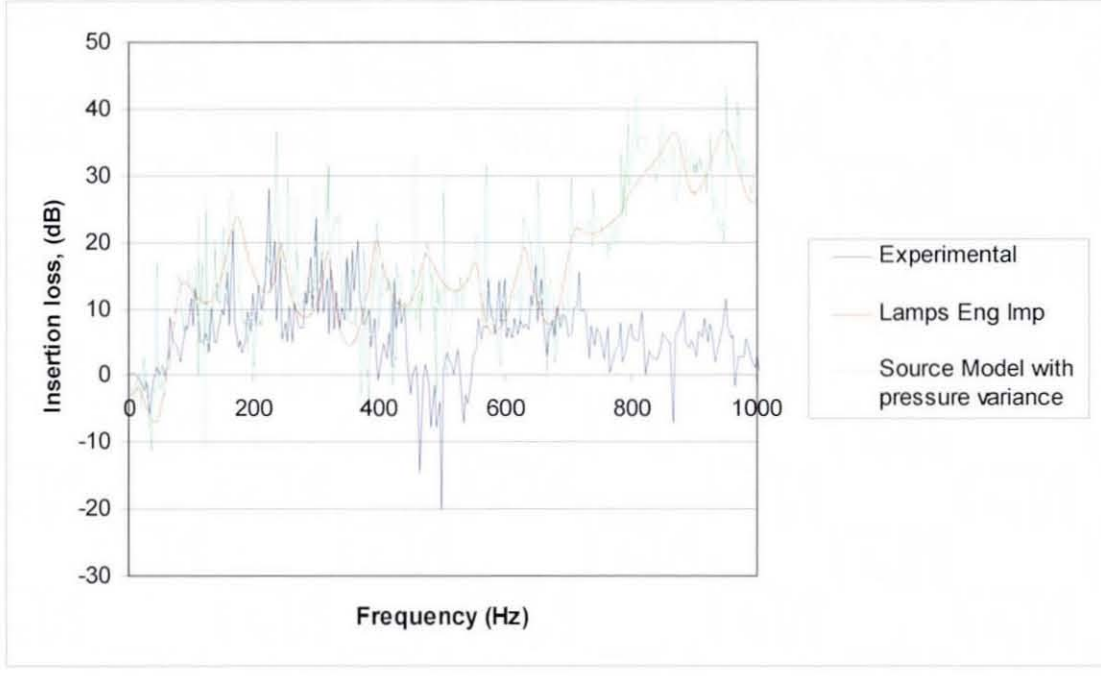

Figure 3. 48 Insertion loss of silencer IA00092 with reference to the control system, with time-varying cylinder pressure: frequency analysis

Figure 3. 36 to 3. 47 show the calculated insertion loss predictions using a varying pressure curve instead of a constant pressure. As before and for similar reasons, the most reliable results for validation are those at low integer multiples of firing frequency. It is seen that there is no consistent general trend to judge whether or not this model predicts insertion loss more accurately with a varying cylinder pressure, as compared to a constant cylinder pressure. As in Section 3.8.1, there are also large differences insertion loss predictions at 190Hz, see Figure 3.37, 3.39, 3.41 and 3.45.

When the 'Source Model with pressure variance' and 'Theoretical with pressure variance' series are overlaid on the same graph, the insertion loss is seen to be virtually identical, see Figure 3. 48 and Figure 3. 49. These observations lend credence to the 'Source Method with pressure variance' results shown in earlier figures.

In a final attempt to improve the accuracy of validation of the source model, a time-varying cylinder pressure is combined with a high pressure difference level across the valve. Figure 3. 50 demonstrates the difference between measured insertion loss and theoretical predictions using a constant pressure difference, 10Pa, and predictions using varying pressure curves. These curves have a maximum pressure difference of 10Pa and 100Pa. The pressure factor increases within the cylinder are indicated in the legends of the graphs by 'Amp x10' for a factor increase of 10.

The difference between 'Theoretical with pressure variance' and 'Theoretical with pressure variance, Amp x10' series is similar compared to the same calculations undertaken with constant pressure, see Figure 3. 31. Thus, it can be concluded again that variations in insertion loss results due to the discharge coefficient are small.

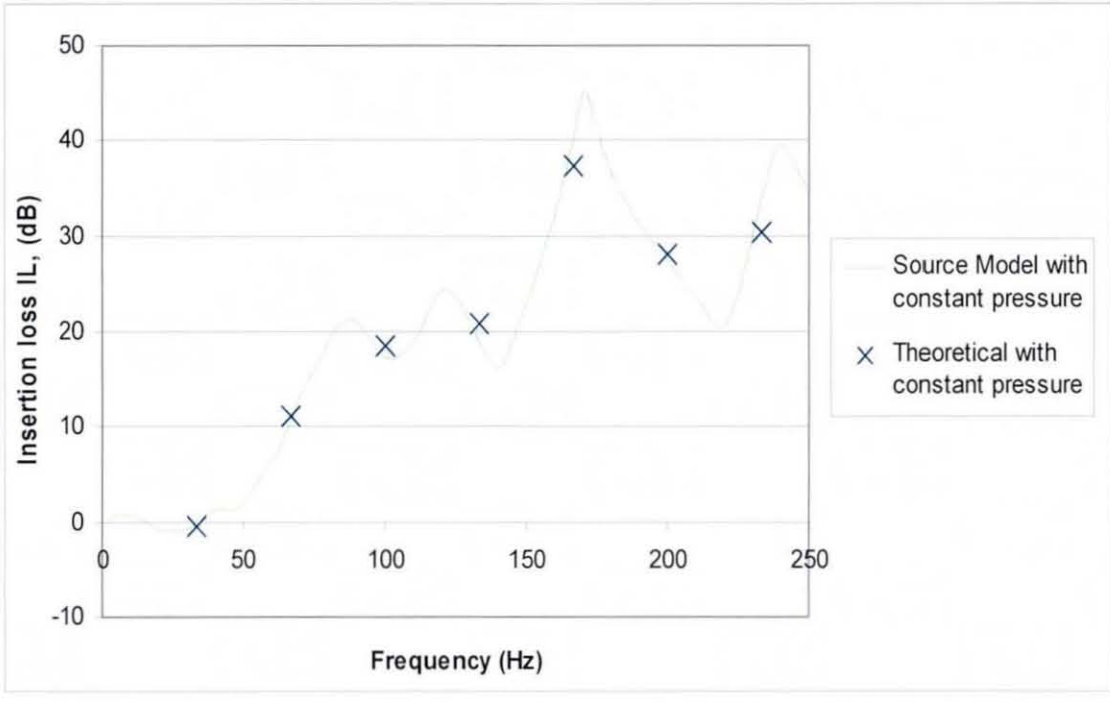

Figure 3. 49 Insertion loss of silencer IA00085 with reference to the control system, with constant cylinder pressure, comparing fundamental frequencies with harmonic frequencies

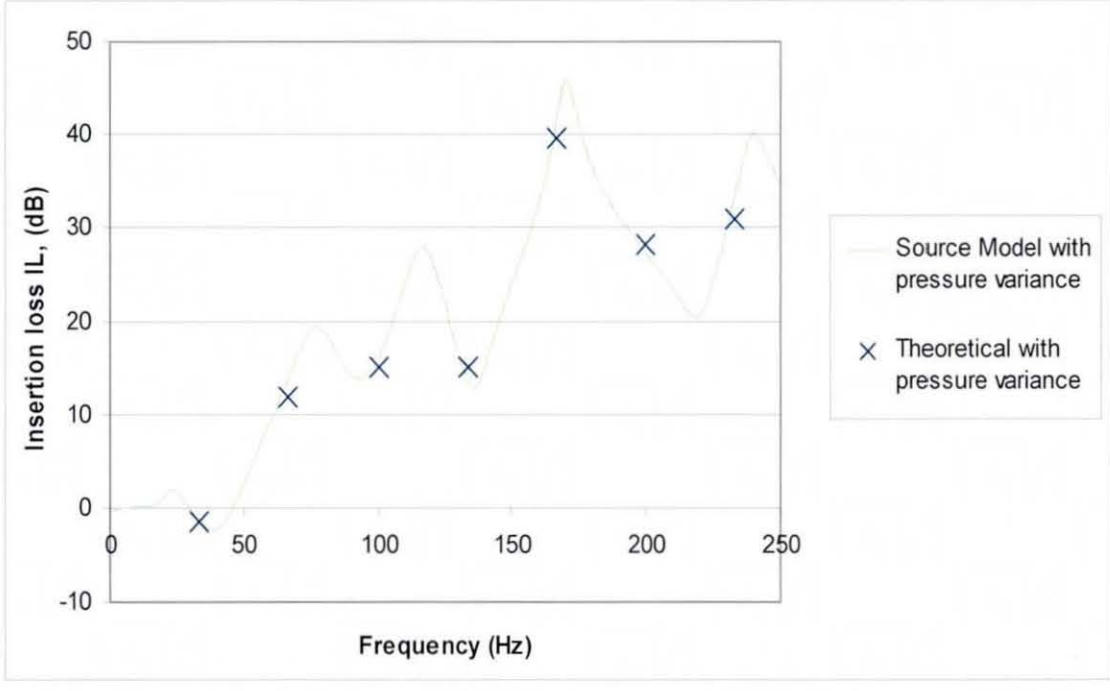

Figure 3. 50 Insertion loss of silencer IA00085 with reference to the control system, with varying cylinder pressure, comparing fundamental frequencies with harmonic frequencies

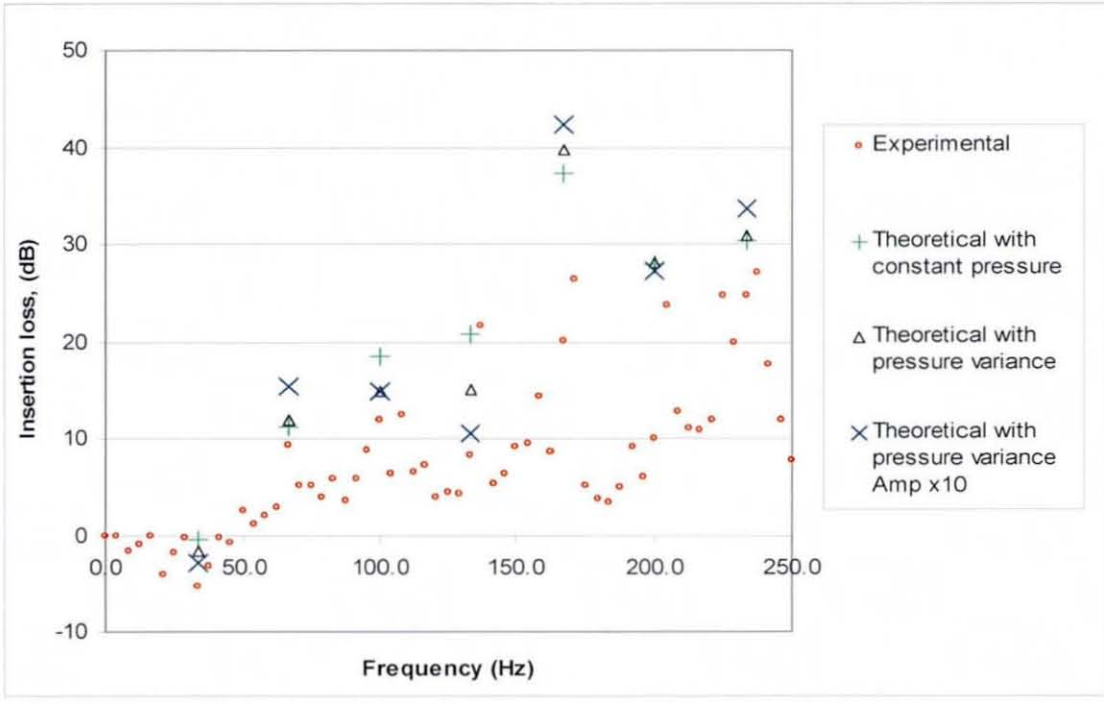

Figure 3. 51 Insertion loss of silencer IA00085 with reference to the control system, comparing constant pressure of 10Pa with varying pressure at harmonic frequencies

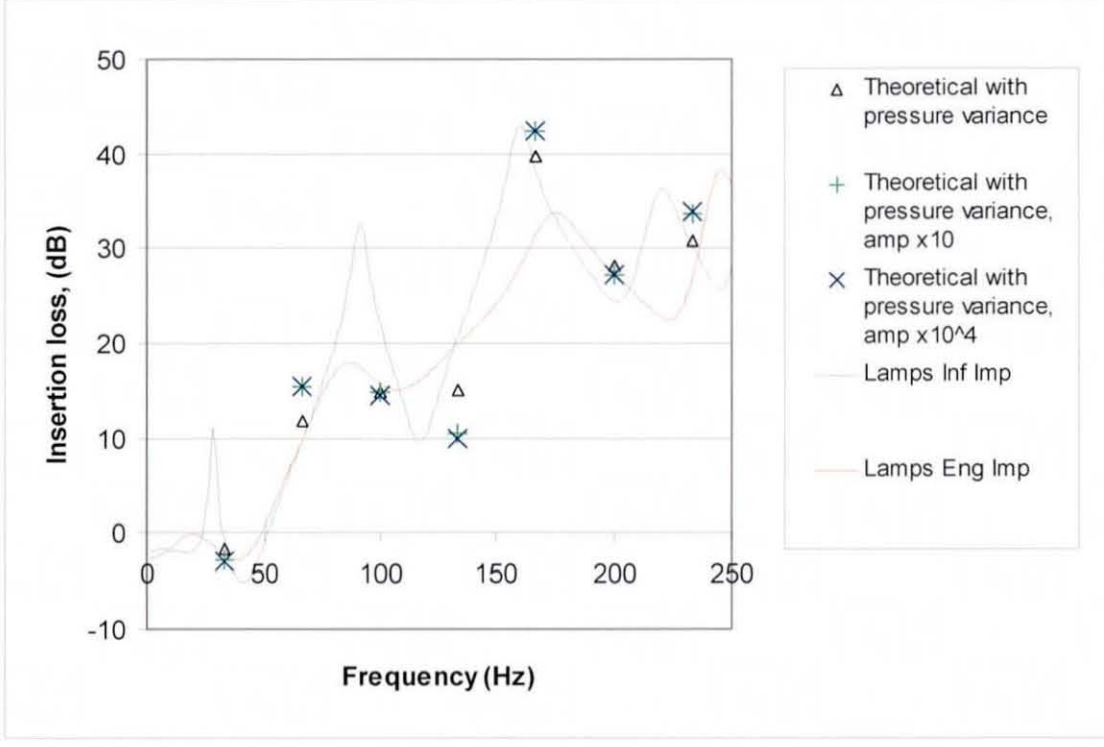

Figure 3. 52 Insertion loss of silencer IA00085 with reference to the control system, comparing varying pressure curves with difference at harmonic frequencies with Lamps Engine and Infinite Impedance series.

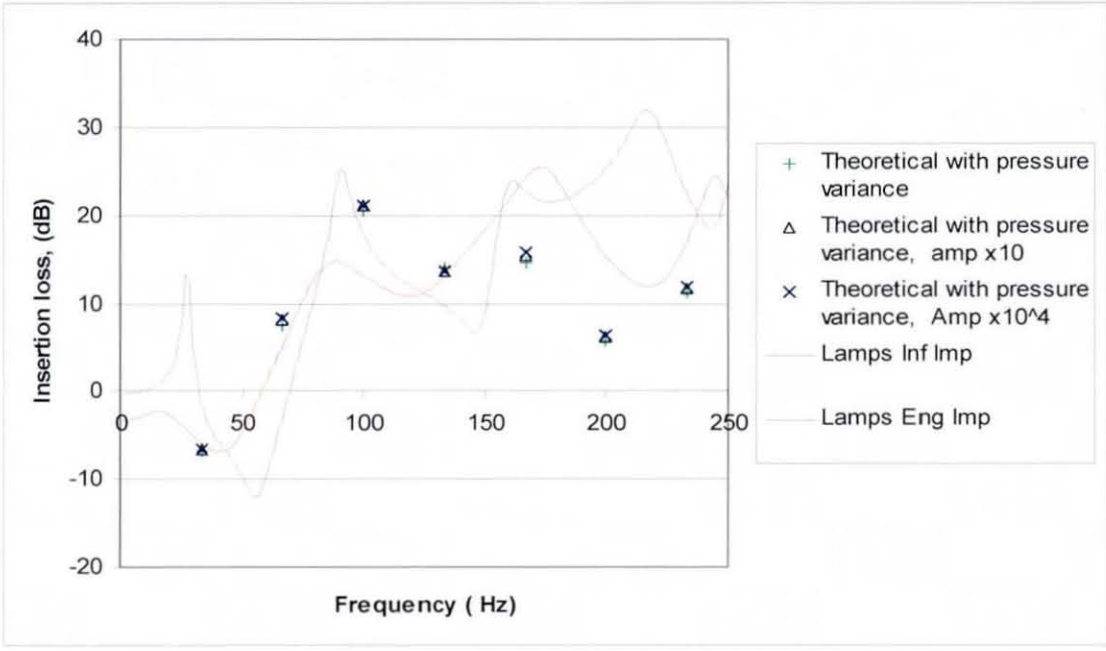

Figure 3. 53 Insertion loss of silencer IA00089 with reference to the control system, comparing varying pressure curves with difference at harmonic frequencies with Lamps Engine and Infinite Impedance series.

Figure 3. 52 and Figure 3. 53 show insertion loss prediction with time-varying pressure plots for two different silencers. The different series show the predictions when the maximum pressure inside the cylinder is 10Pa, 100Pa and 10^5Pa as compared against LAMPS results. This is a further indication that non-linearity is not the major cause of the disparity between measured and predicted results.

3.9 Conclusion

The derivation of the general equations to characterize the general, time-variant, acoustic behaviour between the inlet and outlet of a two-port element has enabled manifolds with time-variant sources to be analysed, with slight modifications for multiple one-port sources and multi-port junctions. This has created a valuable analysis and software tool. The validity of the general equations has been demonstrated and the software has been

used to predict insertion loss results of the Arvin Meritor manifold and silencer configurations.

Through the investigation of time-variant source modelling of internal combustion engines, the research has led to the reconfirmation of the empirical estimate of engine impedance, $Z_s = \rho c(1+i)/\sqrt{2}$, as a good approximation on the exhaust side of an IC-engine. When the pressure difference across the valve entered the non-linear domain of wave propagation, the linearized version of the discharge coefficient still gave sensible results.

The manifold which this chapter considered was a simple geometric design; however, the general equations and software that have been developed as a result of this work can be applied to more complicated geometric designs of manifold. The generality of work within this chapter is easily adaptable to calculate other exhaust measurements, for example, noise reduction or even radiated sound level, if the source model was extended to predict source amplitude. Although the source model has not led to a more demonstrable accurate insertion loss prediction, in comparison to experimental measurement, it is possible that this is only due to limitations on the experimental accuracy. It has been shown that changes to the source model only give rise to small changes in insertion loss, thus experimental results of very high accuracy are required in order to validate changes to the model.

Flowchart 3.1, Searching for an element algorithm

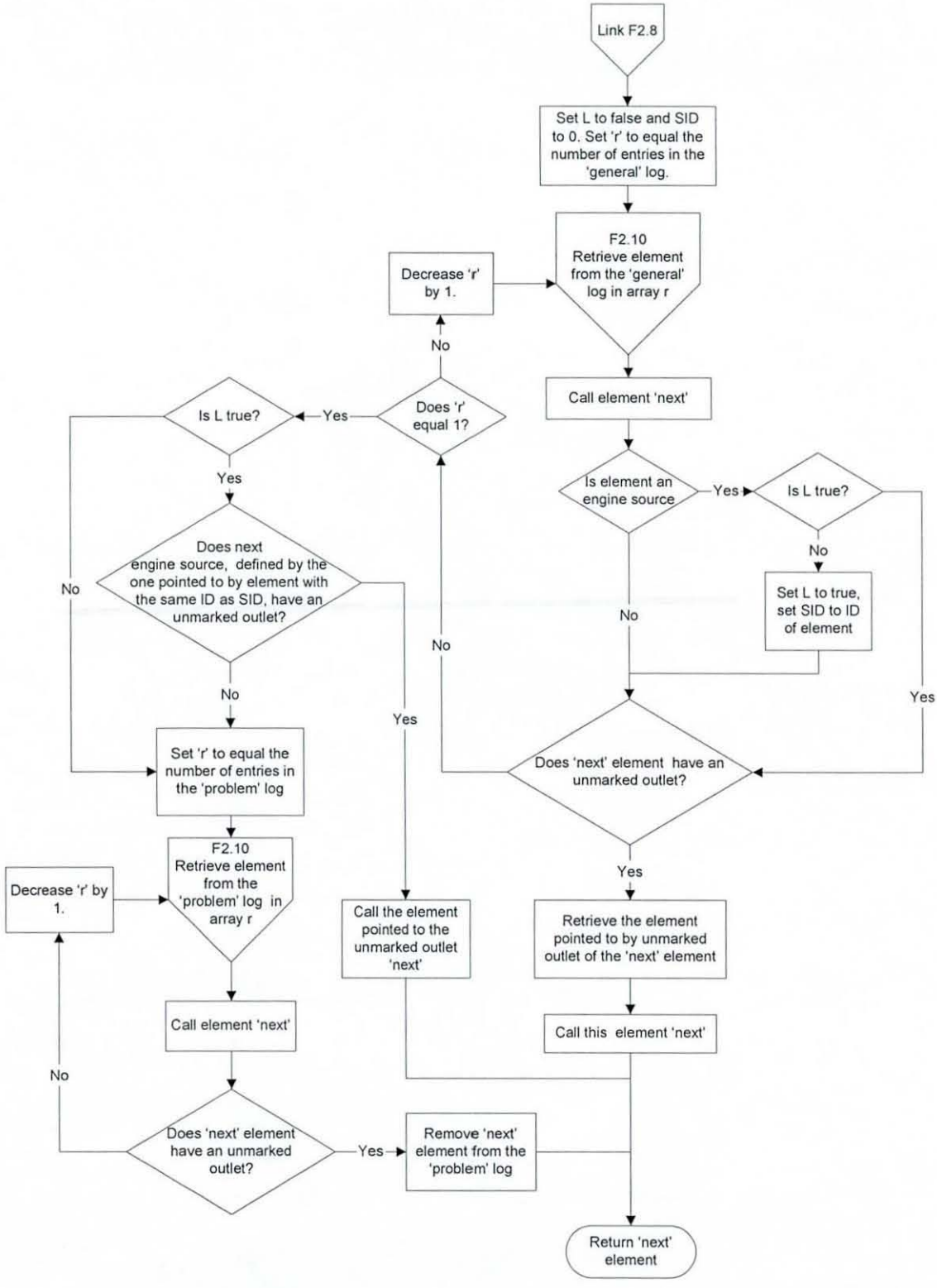

Flowchart 3.2, Time-variant source reduction algorithm

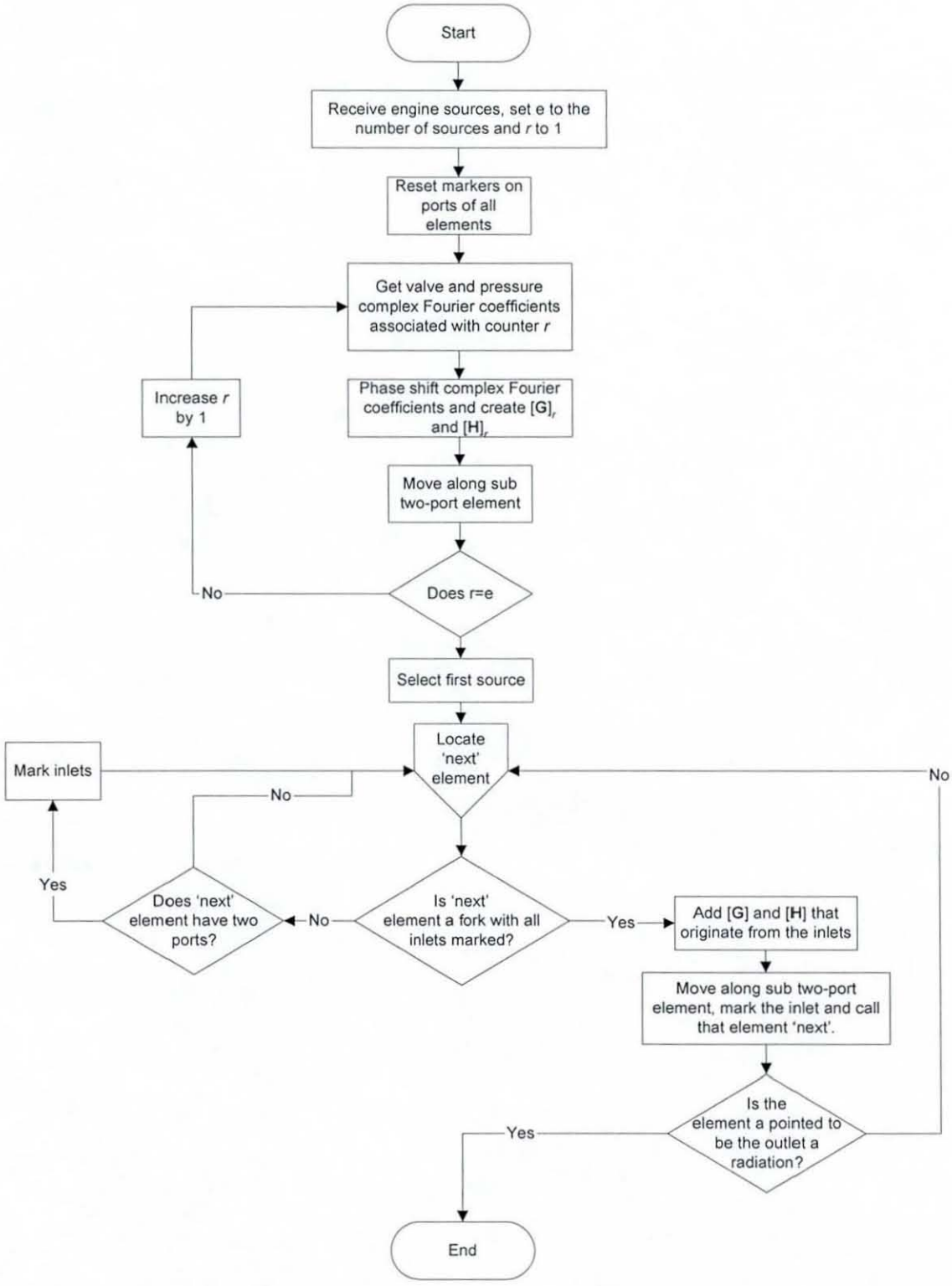

CHAPTER 4

Modelling of Source Impedance Measurement Methods

4.1 Introduction

Ideally, a silencer prediction program would evaluate the absolute level of noise radiated from the tailpipe orifice of a given silencer system at a specific engine operating condition. In order to model this, using linear frequency domain analysis, it is necessary to know the value of the source strength and impedance in addition to the overall transfer matrix and radiation impedance at each frequency. In contrast, transmission loss of an exhaust system performance [1,5] is a relatively simple performance criteria to model, as it only requires knowledge of the overall transfer matrix of the system. However, it is difficult to measure for validation purposes, since it requires multiple in-duct pressure measurements, nor does it yield a full indication of silencer effectiveness. Insertion loss and external noise reduction, from the source to the free field, both require knowledge of source and radiation impedance in addition to the overall transfer matrix. Insertion loss is particularly easy to measure as it requires only free-field measurements and is therefore a favourite for validation purposes.

Conventional, linear, acoustic codes such as LAMPS [11] can evaluate a range of noise measures including insertion loss and external noise reduction. In these cases, a single, effective source location is assumed with a given source impedance. Whereas radiation impedance is well modelled, the estimation of source impedance is relatively very crude, usually either an empirical constant, or even an infinite value.

There are two main methods of measuring source impedance, the indirect [71] and direct [72] methods. Both methods assume that the single effective source at the given location can be characterised by a single, frequency-dependent source impedance value, that is also assumed to be independent of the load impedance. The indirect method also assumes that the source strength can be characterised similarly. The two-load indirect method of measuring source impedance requires measurements of complex pressure to be taken, generally in the free field [75]. The three and four load indirect measurement methods do not require the phase of the pressure to be measured [76].

All these different techniques of measuring source impedance with the indirect method yield results with negative resistances at some frequencies when used on IC-engine sources [71]. Negative resistance is physically implausible, as it suggests that the pressure wave travelling towards the source gains energy when it is reflected away from the source [94]. Negative resistance results were attributed to measurement error [71]. Therefore, multiple load techniques were developed to minimise the errors, by virtue of having an over-determined system for the post-measurement calculations. However, negative resistance values still remained after the post-measurement calculations. Measurement error and the accumulative effect that it has on the calculation could contribute to the presence of measured negative resistance values, but the magnitudes of the errors are not large enough for this to be the dominant cause. Another possible source of negative resistance could be attributed to time-variance of the source [94]. The steady flow within a duct could also cause an effect on the reflection coefficient at the valve, in the same way that it has been shown that steady flow can cause the reflection coefficient to be greater than one [94]. Yet another possible cause is non-linearity of the source [94]. Through studies of experimental results, enhanced measuring and calculation techniques were developed; despite extensive studies, a cohesive explanation for negative resistance could not be formulated [94]. The variants of the indirect measurement method all assume that the effective source impedance obtained is independent of the acoustic load [75-81]. This assumption was shown to be flawed in the case of a linear, time-variant source through an analytical investigation of the indirect measurement method [71]. Thus, every load pair will give rise to a different value for the effective source impedance [77,79,81].

In reality, both the entire concept of a single source impedance value, as well as the indirect experimental technique for its measurement, are flawed when the source is time-variant, as is the case for all IC engines. In reality, a source impedance matrix is required to characterise a linear, time-variant source [71].

The direct method [72] uses a secondary source in the load section of the manifold/silencer system. The secondary source has to be significantly louder than the primary source, so as to make the effect of the primary source negligible on pressure measurements within the exhaust system. This is difficult to obtain, as the primary source from an internal combustion engine has very high magnitude. Even if the secondary source could be made significantly louder than the primary source, its magnitude would be so great as to render all the sound waves to be non-linear, which would in turn invalidate the measurement of the 'linear' source impedance. Another problem with the direct measurement method is that the microphones have to be placed within the exhaust duct and are therefore easily damaged by the high pressure waves and the hot, corrosive exhaust gases [72]. Furthermore, the direct method cannot measure the source strength, as opposed to the indirect method, which can evaluate both source strength and impedance. Hence, for practical reasons, the indirect method is usually used to evaluate source data for an IC-engine. However, for time-variant sources of small amplitude, the direct measurement method tends to produce results for resistance that are fully positive [72]. Therefore, the direct method of measuring source impedance has some advantage over the indirect method. The disadvantages are mostly practical, so it is possible to model the direct measurement technique to study whether it is better than the indirect method in principle.

Analytical models of the direct and indirect measurement methods as applied to an idealised, linear, time-variant source have been studied. These studies were centred on a single-cylinder, time-variant, internal combustion engine with a simplistic, linear valve model. The model of the indirect measurement method yielded negative resistance components of source impedance [71], whereas the direct method yielded solely positive resistance values [72]. Both methods are extended here to study the effective source

impedance of multiple-cylinder engines, to determine whether or not these characteristics change. Furthermore, it is possible from these models to investigate the degree to which dependence upon the acoustic load influences the calculated values for source impedance. Comparisons of predicted results with a large set of measured data from a truck engine source [95] are given to study these criteria.

In principle, it is best to evaluate insertion loss or external noise reduction using the source model of Chapter 3, which makes the source impedance redundant. However, despite the flaws within the indirect and direct measurement methods of source impedance, the insertion loss predictions that result from measured source impedance values are sometimes in good agreement with experimental results [71]. Since it is much simpler to use an effective source impedance, as opposed to a full model of the source, it is of interest to study whether or not there is any correlation between predicted and measured values.

4.2 Indirect measurement method for source impedance

The indirect measurement method is used to determine a frequency dependent source impedance at a chosen effective source location, say point 'E' see Figure 4. 1. The acoustic variables at points 'E' and 'R', with respect to Figure 4. 1, can be related by a two-by-two transfer matrix, see Chapter 2; therefore, given the radiation impedance at 'R', a load impedance can be evaluated at point 'E'.

The acoustic coupling of an engine source and exhaust system has an electro-acoustic analogy [1,71], see Figure 4. 2. Thus an equation for the source characteristics can be written as

$$P_E - P = VZ_E, \tag{4.1}$$

where Z_E is the source impedance. Thus, if the load impedance, Z_L, is known where

$$P = Z_L V, \tag{4.2}$$

then equations (4.1) and (4.2) combine to give

$$P_E = P\left(1+\frac{Z_E}{Z_L}\right). \tag{4.3}$$

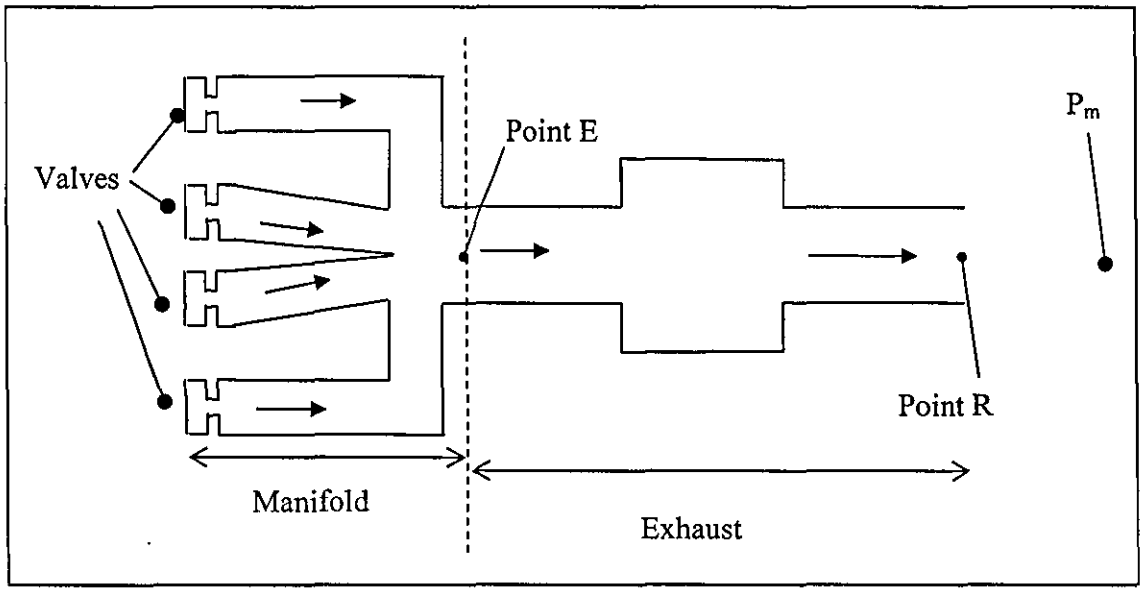

Figure 4. 1 Schematic diagram of manifold and silencer system

Given the assumption that the source pressure remains the same for any two different acoustic loads, then it can be concluded from equation (4.3) that

$$P_1\left(1+\frac{Z_E}{Z_{L_1}}\right) = P_2\left(1+\frac{Z_E}{Z_{L_2}}\right), \tag{4.4}$$

where the different loads/exhaust systems are denoted by numerical subscripts.

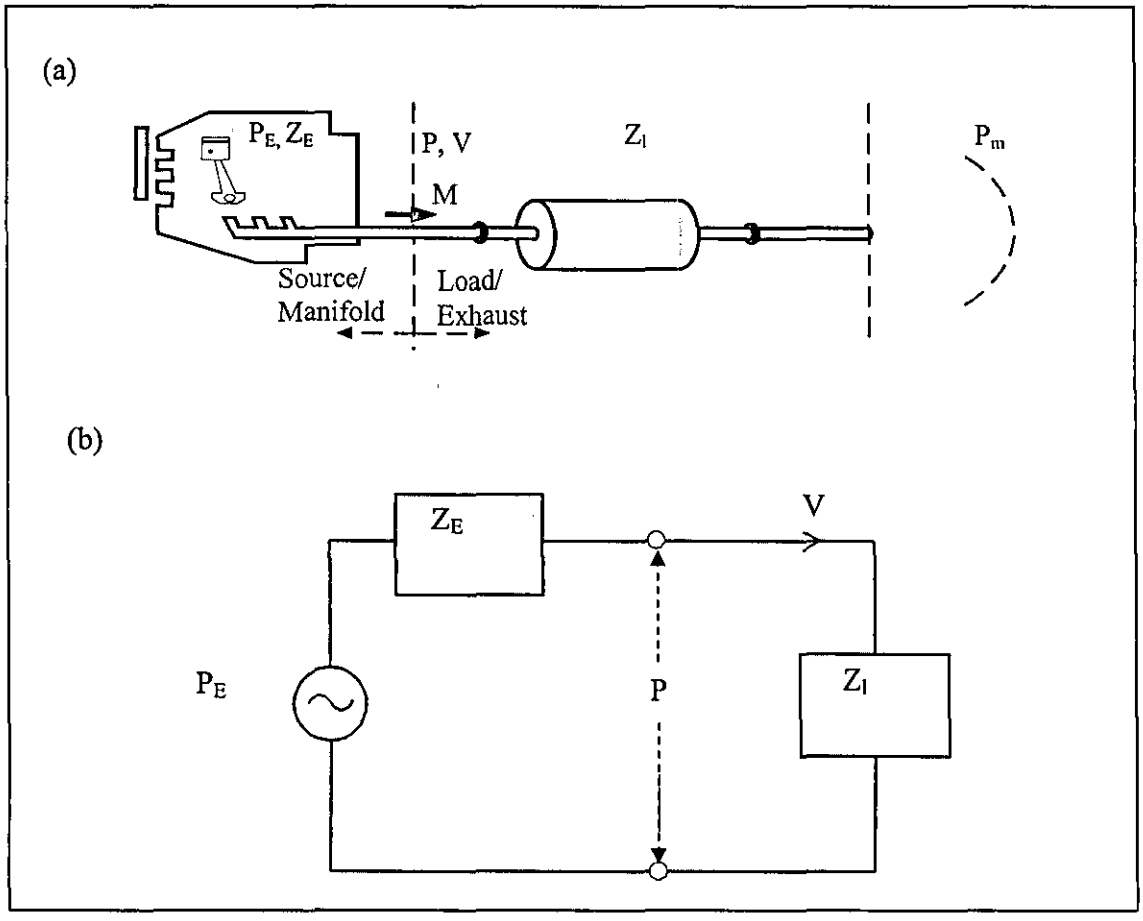

Figure 4. 2 Electro-acoustic analogy

Alternatively, this equation can be rearranged to give [75],

$$Z_E = \frac{Z_{L_1} Z_{L_2} (P_1 - P_2)}{Z_{L_1} P_2 - Z_{L_2} P_1}. \tag{4.5}$$

Thus, if the pressure is measured at the source outlet for two different loads of known impedance, the source impedance can be inferred. In practice, the measurements are at some distance from the source, or even in the free field, and then the pressure at the outlet is calculated from the measurement using the load impedance and transfer matrix between the source outlet and measurement positions [75].

4.3 Modelling the indirect measurement method

It is known from Chapter 3 that a time-variant source can be characterized acoustically by a system of matrices and vectors, see equation (3.11), that can be expressed in a general format as shown in equation (3.29). The acoustic behaviour of a silencer system is calculated solely within the frequency domain, where the behaviour at a specific frequency does not depend on another frequency [1], unlike the time-variant source [71,75]. The model of the time-variant source, when expressed in the frequency domain, has a square source impedance matrix [71], $[A]^{-1}$,see Section 3.2.1. In contrast, the load impedance of the silencer system matrix can be described using a diagonal matrix, since the acoustic silencer load is frequency dependent and time-invariant. The mathematical notation is exactly the same as in Section 3.2, see equation (3.26). Thus, a general matrix equation can be acquired at an evaluation point, say point 'E' see Figure 4. 1. Therefore, given two acoustic load impedance matrices from two different exhaust systems, whilst keeping the cylinder source pressures constant, the pressure vector at point 'E' can be calculated for each system. Since the load impedance Z_L and the pressure at the source outlet P are now known at each frequency component of the engine source, an effective source impedance at each of these frequency values can be calculated from equation (4.5). The single cylinder example of evaluating indirect source impedance at a valve outlet is extended here to incorporate multiple time-variant sources, based on the theory in Chapter 3.

A whole exhaust system, from the time-variant multiple sources to the radiation point, can be modelled as two different sections, a manifold and silencer, with respect to Figure 4. 1. Chapter 3 explains how any general, geometric manifold design that has multiple time-variant sources and a single outlet can be characterized by a matrix equation. Any manifold section, which has a single outlet, can be characterized at the last junction, say point J, or somewhere along the downpipe, say 'Point E' with respect to Figure 4. 1, see Section 3.3. The relationship between pressure and velocity can be acquired by using the general equations (3.29) and (3.31) to (3.34) which enables progression of the general

relationship from the last junction, point *J*, to any effective source location, 'Point E', along a two-port sub-system; hence in this case *X=J* and *Y=E*.

4.4 Direct measurement method for source impedance

The direct measurement method for source impedance requires an injection of noise, at a specified frequency, somewhere in the acoustic load section. This injected noise has to be significantly greater than that which originates from the exhaust valves. The simplest example of the direct measurement method of source impedance is to consider a source connected to a uniform duct, as shown in Figure 4. 3, which has an injected noise signal located somewhere along the duct system [72].

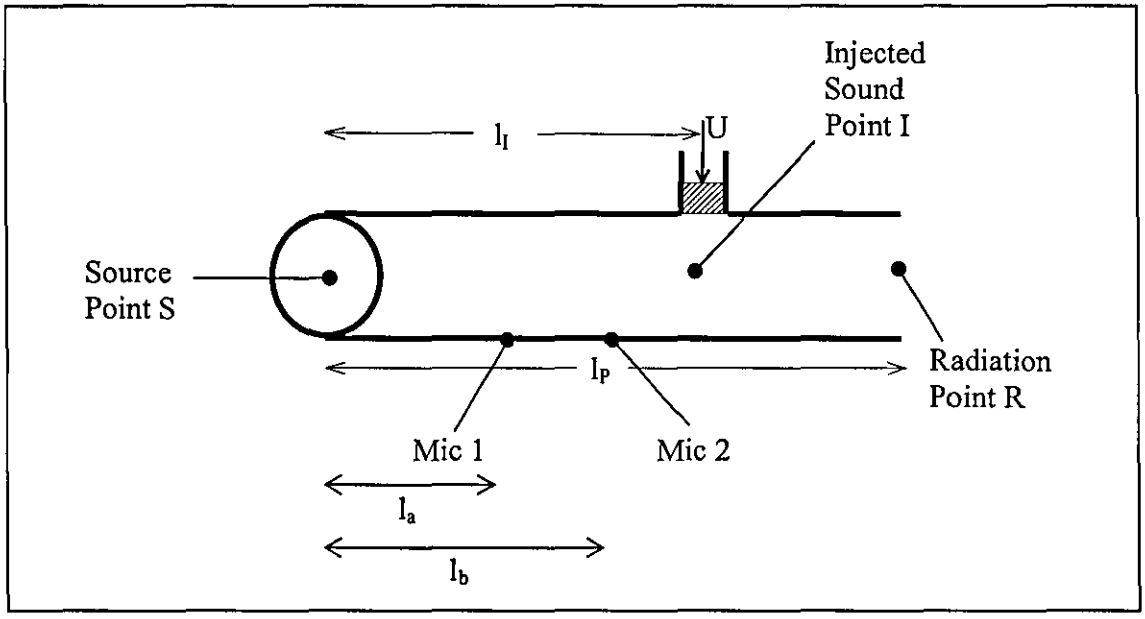

Figure 4. 3 Experimental setup of the direct measurement method of source impedance

The direct method of measuring source impedance relies heavily on the hypothesis that 'sufficiently strong' acoustic waves can be directed towards the source, in this case a running internal combustion engine. The pressure field generated from the injected noise

has to have an amplitude large enough for the pressure waves radiating from the original source to be relatively insignificant.

Let there be two microphones placed between the injected source and the engine source, see Figure 4. 3. The distances between the noise sources, the radiation position and the microphones need to be known. The measured pressures at distances l_a and l_b from the initial source can be used to evaluate a pressure value at their midpoint, $0.5(l_a+l_b)$ away from the source. The calculated pressure gradient at the midpoint, between the two microphones, allows an average velocity to be acquired. This is achievable since the change of pressure divided by the separation of distance, between the two microphones, is proportional to the velocity. Thus, the impedance in the direction towards the source can be evaluated at this position. Since the dimensions of the uniform pipe between this point and the source are known, a two-by-two transfer matrix can be constructed to relate the acoustic pressure and mass velocity variables at this point to those at the source location. Hence, the source impedance can be calculated. Lengths l_a and l_b are changed in order to acquire source impedance values in different frequency intervals to minimise the effects of experimental error.

4.5 Modelling the direct measurement method

4.5.1 Refined valve model

Let the pressures, relative to atmospheric pressure, be $P_S(t)$ and $P(t)$ upstream and downstream of the valve respectively. Let the velocity of flow through the valve be $u(t)$, see Figure 4. 4. Let the linearized relationship between pressure and velocity across the valve [72] be

$$[P_s(t)-P(t)]=\frac{\overline{\rho c}u(t)}{C_d}+\overline{\rho l}\frac{du(t)}{dt}\,, \tag{4.6}$$

where l is the thickness of the orifice which includes the mass end corrections [1,72].

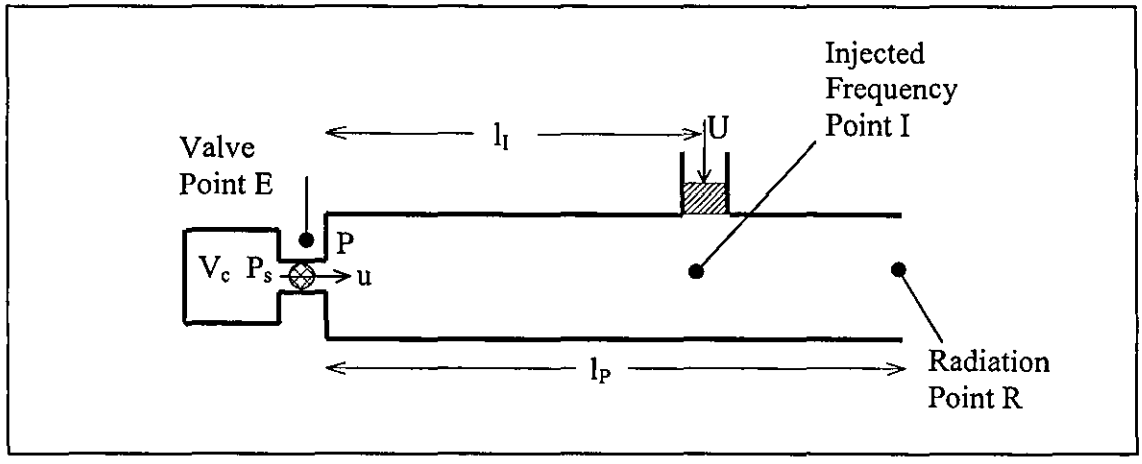

Figure 4. 4 Simple single source connected to a straight pipe with an injected noise signal somewhere in the engine load

Equation (4.6) characterises an idealized, inertial, linear time-variant equation for flow through a valve. It is a refinement of equation (3.1) to incorporate inertial effects. The work given here is an extension of earlier work on the analytical modelling of the direct measurement method for a single cylinder engine [72] to the multi-cylinder case. The valve model of equation (4.6) was used within the earlier work [72], but algebraic manipulation given there has been found to be incorrect. Therefore, full details of the analysis are given here. Let the valve have a periodic open area function $\tilde{A}(t)$, as in Section 3.2. Thus equation (4.6) can be re-written to express the discharge through the valve as

$$\overline{\rho c}\left[1+\frac{lC_d}{\bar{c}}\frac{d}{dt}\right]\frac{V(t)}{\tilde{A}(t)} = C_d\left[P_s(t)-P(t)\right], \quad \tilde{A}(t)\begin{cases}\neq 0, 0\le t\le \tau,\\ = 0, \tau\le t\le T,\end{cases} \tag{4.7}$$

where $V(t)$ is the volume velocity through the valve. As in Section 3.2.1, let $A(t)=\tilde{A}(t)/A_{max}$ and $v(t)=\left(\overline{\rho c}/A_p\right)V(t)$. Now equation (4.7) can be re-written as

$$\left[\frac{v(t)}{A(t)}+\frac{lC_d}{\bar{c}A(t)}\frac{dv(t)}{dt}-\frac{v(t)}{(A(t))^2}\frac{lC_d}{\bar{c}}\frac{dA(t)}{dt}\right]=C_1C_d[P_s(t)-P(t)],\quad \begin{Bmatrix}0<A(t)\le 1, 0\le t\le \tau,\\ A(t)=0, \tau\le t\le T,\end{Bmatrix}, \tag{4.8}$$

or

$$\left[\frac{A(t)}{C_d}+\frac{lA(t)}{\bar{c}}\frac{d}{dt}-\frac{l}{\bar{c}}\frac{dA(t)}{dt}\right]v(t)=C_1A(t)^2[P_s(t)-P(t)],\ \begin{Bmatrix}0<A(t)\le 1, 0\le t\le \tau,\\ A(t)=0, \tau\le t\le T,\end{Bmatrix}. \tag{4.9}$$

where $C_1 = A_{max} / A_p$.

4.5.2 Modelling injected noise

The periodic behaviour of the valve can be modelled in the time domain as a sum of Fourier components of angular frequencies $\omega_j=2\pi/T$. Let Ω_f represent the injected angular frequency component; therefore, the Fourier components which describe the time-variant relationship between pressure and velocity must be redefined [72]. Thus, the time dependent variables concerned with the direct method can be expanded as complex Fourier series,

$$v(t)=\sum_{j=-\infty}^{+\infty}v_j e^{i(\Omega_f+\omega_j)t}\ , \tag{4.10}$$

$$P_s(t)=\sum_{j=-\infty}^{+\infty}S_j e^{i(\Omega_f+\omega_j)t}\ , \tag{4.11}$$

$$P(t)=\sum_{j=-\infty}^{+\infty}P_j e^{i(\Omega_f+\omega_j)t} \tag{4.12}$$

and

$$A(t)=\sum_{j=-\infty}^{+\infty}A_j e^{i\omega_j t} \tag{4.13}$$

Note that j=0 corresponds to the frequency of the injected signal and not to steady-state conditions. Inserting these expansions into equation (4.9) gives

$$\begin{aligned}&C_1\left(\sum_{z=-\infty}^{z=\infty}A_z e^{i\omega_z t}\right)\left(\sum_{g=-\infty}^{g=\infty}A_g e^{i\omega_g t}\right)\left(\sum_{r=-\infty}^{r=\infty}\left(S_r e^{i(\Omega_f+\omega_r)t}-P_r e^{i(\Omega+\omega_r)t}\right)\right)=\\&\frac{1}{C_d}\left(\sum_{u=-\infty}^{u=\infty}A_u e^{i\omega_u t}\right)\left(\sum_{h=-\infty}^{h=\infty}v_h e^{i(\Omega_f+\omega_h)t}\right)-\frac{l}{c}\left(\sum_{n=-\infty}^{n=\infty}A_n i\omega_n e^{i\omega_n t}\right)\left(\sum_{m=-\infty}^{m=\infty}v_m e^{i(\Omega_f+\omega_m)t}\right)+\\&\frac{l}{c}\left(\sum_{w=-\infty}^{w=\infty}A_w e^{i\omega_w t}\right)\left(\sum_{q=-\infty}^{q=\infty}i(\Omega_f+\omega_q)v_q e^{i(\Omega_f+\omega_q)t}\right)\end{aligned} \tag{4.14}$$

Now consider within equation (4.14) a single frequency component, say $\Omega_f+\omega_k$, such that $h+u=k$, $q+w=k$, $z+r+g=k$ and $n+m=k$. Hence

$$\begin{aligned}&C_1\sum_{r=-\infty}^{r=\infty}\sum_{g=-\infty}^{g=\infty}\left(A_{k-r-g}A_g e^{i\omega_{k-r}t}\left(S_r e^{i(\Omega_f+\omega_r)t}-P_r e^{i(\Omega_f+\omega_r)t}\right)\right)=\\&\sum_{h=-\infty}^{h=\infty}\left(\left(\frac{1}{C_d}+i\frac{l}{c}\left((\Omega_f+\omega_h)-\omega_{k-h}\right)\right)\left(A_{k-h}e^{i\omega_{k-h}t}\right)\left(v_h e^{i(\Omega_f+\omega_h)t}\right)\right)\end{aligned} \tag{4.15}$$

Thus

$$C_1 \sum_{r=-\infty}^{\infty}\sum_{g=-\infty}^{\infty}\left(A_{k-r-g}A_g\left(S_r - P_r\right)\right) = \sum_{h=-\infty}^{\infty}\left(\left(\frac{1}{C_d} + \frac{il}{c}\left(\left(\Omega_f + \omega_h\right) - \omega_{k-h}\right)\right)A_{k-h}v_h\right). \tag{4.16}$$

Again it is assumed that only the first N harmonics of the acoustic pressure and velocity are non-negligible, such that a finite matrix equation can be derived from equation (4.16), namely

$$[\mathbf{D}](\{\mathbf{S}\} - \{\mathbf{P}\}) = [\mathbf{F}]\{\mathbf{v}\}, \tag{4.17}$$

where

$$[\mathbf{D}] = C_1\begin{bmatrix} \sum_{g=-N}^{g=N} A_{-g}A_g & \cdots & \sum_{g=-N}^{g=N} A_{-N-g}A_g & \cdots & \sum_{g=-N}^{g=N} A_{-2N-g}A_g \\ \cdots & \sum_{g=-N}^{g=N} A_{-g}A_g & \cdots & \cdots & \cdots \\ \sum_{g=-N}^{g=N} A_{N-g}A_g & \cdots & \sum_{g=-N}^{g=N} A_{-g}A_g & \cdots & \sum_{g=-N}^{g=N} A_{-N-g}A_g \\ \cdots & \cdots & \cdots & \sum_{g=-n}^{g=n} A_{-g}A_g & \cdots \\ \sum_{g=-N}^{g=N} A_{2N-g}A_g & \cdots & \sum_{g=-N}^{g=N} A_{N-g}A_g & \cdots & \sum_{g=-N}^{g=N} A_{-g}A_g \end{bmatrix} \tag{4.18}$$

and

$$[\mathbf{F}] = \begin{bmatrix} f(N,0)A_0 & \cdots & f(0,-N)A_{-N} & \cdots & f(-N,-2N)A_{-2N} \\ \cdots & f\left(\frac{N}{2},0\right)A_0 & \cdots & \cdots & \cdots \\ f(N,N)A_N & \cdots & f(0,0)A_0 & \cdots & f(-N,-N)A_{-N} \\ \cdots & \cdots & \cdots & f\left(\frac{-N}{2},0\right)A_0 & \cdots \\ f(N,-2N)A_{2N} & \cdots & f(0,-N)A_N & \cdots & f(-N,0)A_0 \end{bmatrix} \tag{4.19}$$

where

$$f(n_1,n_2)=\frac{1}{C_d}+i\frac{l}{c}\left(\left(\Omega_f+\omega_{n_1}\right)-\omega_{n_2}\right). \tag{4.20}$$

Hence the matrix expression for velocity is

$$\{\mathbf{v}\}=[\mathbf{F}]^{-1}[\mathbf{D}]\left(\{\mathbf{S}\}-\{\mathbf{P}\}\right). \tag{4.21}$$

Therefore, the admittance matrix at the outlet of the time-variant valve is $[\mathbf{F}]^{-1}[\mathbf{D}]$ and the impedance matrix is $[\mathbf{D}]^{-1}[\mathbf{F}]$.

A simple, single time-invariant source model, as in Figure 4. 2b, has an electrical circuit analogy [1] which gives rise to

$$P_E(\Omega_f)-P(\Omega_f)=Z_E(\Omega_f)V(\Omega_f)=\zeta_E(\Omega_f)v(\Omega_f), \tag{4.22}$$

see equation (4.1) and Section 4.2, or

$$v(\Omega_f)=\alpha_E(\Omega_f)\left[P_E(\Omega_f)-P(\Omega_f)\right] \tag{4.23}$$

where ζ_E is a non-dimensional source impedance for any given frequency component Ω_f and α_E is its inverse, admittance.

4.5.3 The source 'cavity' model

In the direct measurement method, the source impedance is measured at the entry to the source region as viewed from the exhaust side of the system at the frequency of the

injected signal, Ω_f. Thus, in the analysis technique, it is necessary to evaluate the admittance $\alpha(\Omega_f) = -v_o/P_o$, see equation (4.21). Hence the admittance is

$$\alpha\left(\Omega_f\right) = \sum_{j=-N}^{j=N} \Gamma_{0j} \frac{\left(P_j - S_j\right)}{P_0}, \tag{4.24}$$

where Γ_{0j} refers to the cells in the central row of the matrix ($[\mathbf{F}]^{-1}[\mathbf{D}]$), given that j denotes the column number, see equation (3.10).

Thus, the evaluated admittance is dependent on the source geometry, valve motion and the relative magnitude of the components of acoustic pressure within the system. This implies that the measurements of the source impedance are load dependent. When the open area of the valve is constant, thus time-invariant, the previous statement does not apply, since then A_j=0, $j\neq0$. When the valve is closed, which also implies it is time-invariant, the velocity of flow through the valve is zero, hence the admittance is also zero. However, if the valve is open and time-invariant, then the admittance as determined by the direct method is $\alpha(\Omega_f)=-v_0/P_0$, whereas the required source admittance of the active source region is $\alpha_E(\Omega_f)=-v_0/(P_0-S_0)$. Hence, in general the admittance, $\alpha(\Omega_f)$, of a time-invariant source is equivalent to the required admittance, $\alpha_E(\Omega_f)$, provided that $P_E(\Omega_f)=S_0=0$; therefore $\alpha=\alpha_E=\Gamma_{00}$. Thus the pressure, P_0, has to be large enough so that the cylinder source pressure is insignificant, i.e. S_0=0. The magnitude of the injected signal required to achieve this, in practical measurements on an IC-engine source, will be such that it is highly non-linear, even if it is achievable. However, analytical modelling is capable of assuming negligible source pressure whilst maintaining a linear injected signal.

The cylinder source region, with a time-invariant valve, can be modelled as a Helmholtz resonator with a fixed 'cavity' and 'neck', which can be modelled by the volume of the cylinder and the valve constriction respectively. When the valve is time-variant, then the cross-sectional area of the 'neck' of the Helmholtz resonator is time-variant.

As just noted, the direct method only gives the required source admittance when the valve is closed, or when it is open, but time-invariant and $S_0 = 0$, i.e. there is insignificant pressure fluctuation within the source region. Thus, the valve must have an insignificantly small admittance, i.e. the valve is effectively closed, or else the source 'cavity' must have an infinite admittance, i.e. it is extremely large such that the mass influx/efflux from the injected signal does not alter the pressure in the source region. This is in addition to the requirement in the latter case that the pressure variations which arise from the in-cylinder explosions and subsequent piston motion are negligible, as compared to pressure fluctuations in the system caused by the injected signal [72].

Thus, the model of the direct method for source evaluation of time-variant internal combustion engines is constrained in that the velocity of flow caused by the piston motion, $u(t)$ see Figure 4. 4, has to be negligible in comparison to the acoustic velocity associated with the injected signal. This denotes that the source must be modelled effectively with a constant 'cavity' volume, V_c. This model considers only a low frequency range, such that the 'cavity' associated with a cylinder can be modelled as a lumped-compliance [1]. Thus, a diagonal matrix [**C**] can be created that produces a relationship between the source pressure vector, {**S**}, and the acoustic mass velocity, {**v**}, through the valve,

$$\{\mathbf{S}\} = [\mathbf{C}]\{\mathbf{v}\}\,, \tag{4.25}$$

where the coefficients of [**C**] are

$$\chi_j = \frac{\mathrm{i}A_p}{k_j V_c}\,, \tag{4.26}$$

where $k_j = (\Omega_j + \omega_j)/c_o$. Coefficients χ_j tend to zero as the volume increases; hence, the pressure fluctuations within the cylinder tend to zero as well, but the volume of a cylinder belonging to an internal combustion engine is not large enough for the requirement of

S_j=0 to be met, even if the piston motion produced negligible pressure fluctuations in comparison to the injected signal.

4.5.4 Evaluation of source impedance

The behaviour of the valve can be characterised by equation (4.21) and the source vector, {S}, by equation (4.25); thus at the outlet of the valve the acoustic velocity vector is

$$\{\mathbf{v}\}_E = [\mathbf{F}]_E^{-1}[\mathbf{D}]_E[\mathbf{C}]_E\{\mathbf{v}\}_E - [\mathbf{F}]_E^{-1}[\mathbf{D}]_E\{\mathbf{P}\}_E, \tag{4.27}$$

or

$$\{\mathbf{v}\}_E = -([\mathbf{F}]_E - [\mathbf{D}]_E[\mathbf{C}]_E)^{-1}[\mathbf{D}]_E\{\mathbf{P}\}_E. \tag{4.28}$$

Two-by-two transfer matrices relate the pressure and velocity at point 'E' to point 'I' of the injected signal and to the radiation point 'R', where

$$\begin{bmatrix} P_E \\ V_E \end{bmatrix} = \begin{bmatrix} \cos k_j l_P & \mathrm{i}\sin k_j l_P \\ \mathrm{i}\sin k_j l_P & \cos k_j l_P \end{bmatrix} \begin{bmatrix} P_R \\ V_R \end{bmatrix} \quad \mathrm{j} \neq 0 \tag{4.29}$$

and

$$\begin{bmatrix} P_E \\ V_E \end{bmatrix} = \begin{bmatrix} \cos k_j l_I & \mathrm{i}\sin k_j l_I \\ \mathrm{i}\sin k_j l_I & \cos k_j l_I \end{bmatrix} \begin{bmatrix} P_I \\ V_I \end{bmatrix} \quad , \tag{4.30}$$

see Figure 4. 4. Given that the radiation impedance at point 'R' is known, then

$$P_E = \left(\frac{Z_R \cos k_j l_P + i \sin k_j l_P}{i Z_R \sin k_j l_P + \cos k_j l_P} \right) V_E \quad j \neq 0 \quad . \tag{4.31}$$

The pressure and velocity relationship between points 'I' and 'R' is simply

$$\begin{bmatrix} P_I \\ V_{IR} \end{bmatrix} = \begin{bmatrix} \cos k_j(l_P - l_I) & \mathrm{i}\sin k_j(l_P - l_I) \\ \mathrm{i}\sin k_j(l_P - l_I) & \cos k_j(l_P - l_I) \end{bmatrix} \begin{bmatrix} P_R \\ V_R \end{bmatrix}, \tag{4.32}$$

where V_{IR} is the velocity out of the junction, labelled by 'Point I' with respect to Figure **4. 4**, towards the radiation. Since all the pressures at a junction are equal [1], let P_I represent those pressures. Mass conservation at point 'I' states that the net sum of the acoustic mass velocities equates to zero, whilst the pressure at the point is constant, which enables an expression that encompasses all j components, thus at point 'E'

$$\{\mathbf{P}\}_E = [\mathbf{B}]\{\mathbf{v}\}_E + v_{IN}\{\mathbf{d}\}, \tag{4.33}$$

where matrix [**B**] is a diagonal matrix and v_{IN} is the mass velocity associated with the injected frequency. The coefficients for the matrix, [**B**], and vector {**d**} are described through ψ and γ respectively

$$\psi_j = \frac{Z_R \cos k_j l_P + \mathrm{i}\sin k_j l_P}{\mathrm{i}Z_R \sin k_j l_P + \cos k_j l_P} \tag{4.34}$$

and

$$\gamma_j = \begin{cases} \psi_0 \cos k_0 l_I - \mathrm{i}\sin k_0 l_I, & j = 0 \\ 0, & j \neq 0 \end{cases}. \tag{4.35}$$

Substitution of the pressure vector using equation (4.28) and (4.33) at point 'E', gives

$$([\mathbf{D}]_E([\mathbf{C}]_E - [\mathbf{B}]) - [\mathbf{F}]_E)\{\mathbf{v}\}_E = [\mathbf{D}]_E v_{IN}\{\mathbf{d}\}. \tag{4.36}$$

Thus $\{\mathbf{v}\}_s/v_{IN}$ can be evaluated and $\{\mathbf{P}\}/v_{IN}$ can be gained from equation (4.33); hence the acquired source impedance can be calculated simply by

$$Z(\Omega_f) = -\frac{P_0}{V_0}. \tag{4.37}$$

4.5.5 General equation format for effective single source engines

The assumed source location, point 'E', for the direct measurement of a single cylinder engine is at the outlet of the valve. Sections 4.5.1 to 4.5.3 have shown the modelling techniques for the valve and source. Let the general matrix equation, that relates acoustic mass velocity and pressure vectors, at the outlet of the valve be

$$\{\mathbf{v}\}_E = [\mathbf{H}]_E \{\mathbf{P}\}_E, \tag{4.38}$$

where

$$[\mathbf{H}]_E = -([\mathbf{F}]_E - [\mathbf{D}]_E [\mathbf{C}]_E)^{-1} [\mathbf{D}]_E. \tag{4.39}$$

Since all the equations from (4.27) to (4.37) are general, $\{\mathbf{P}\}_E$ in equation (4.38) can be substituted with equation (4.33), hence

$$\{\mathbf{v}\}_E = [\mathbf{H}]_E ([\mathbf{B}]\{\mathbf{v}\}_E + v_{IN}\{\mathbf{d}\}), \tag{4.40}$$

thus

$$\{\mathbf{v}\}_E \frac{1}{v_{IN}} = ([\mathbf{I}] - [\mathbf{H}]_E [\mathbf{B}])^{-1} [\mathbf{H}]_E \{\mathbf{d}\}. \tag{4.41}$$

Therefore, the source impedance at the injected frequency Ω_f corresponding to the harmonic equation at j=0, can be evaluated using equations (4.41), (4.33) and (4.37).

4.6 Modelling direct measurement method for multi-cylinder engines

Multi-cylinder engines have an assumed single source location, point 'E', somewhere between the outlet of the manifold and the inlet of the first silencer box, see Figure 4. 5. The behaviour at each valve, which is part of the source, can be expressed by Fourier coefficients of $\tilde{A}(t)$. The valves within a manifold have the same valve open area curve, but are phase related. The Fourier coefficients can be adapted to model the phase relationship, see equation (3.55). Once the coefficients for each valve are phase related, then equations (4.18) to (4.20) and (4.26) can be used to calculate the matrix relationship at the outlet of each valve. These matrices are used to characterise the behaviour between acoustic velocity and pressure vectors at the outlet of the valves, see equations (4.38) and (4.39).

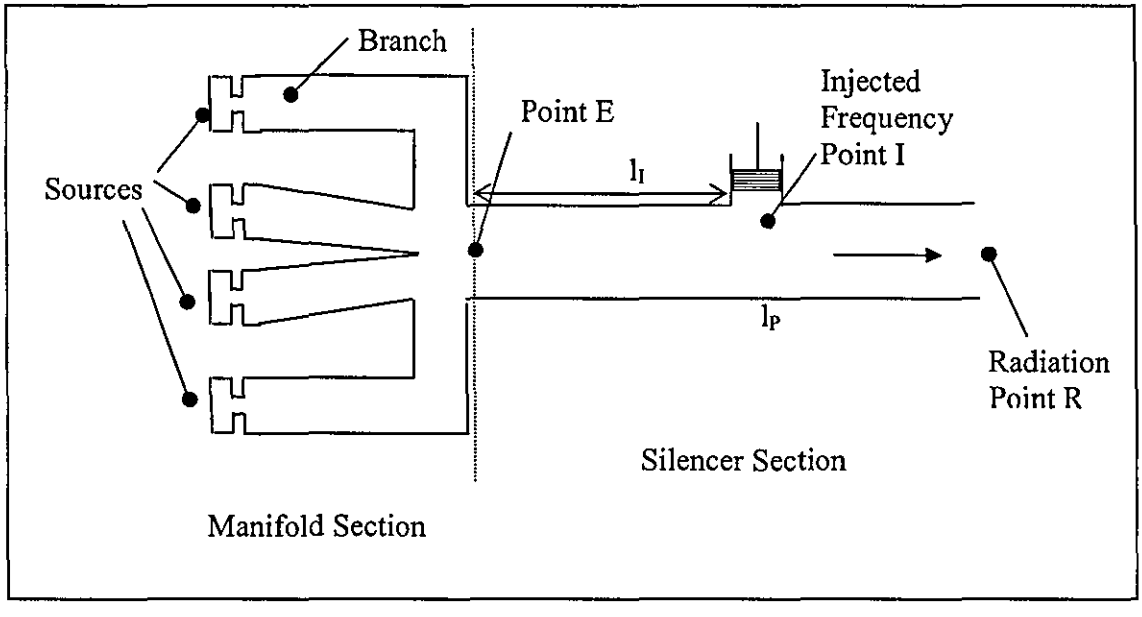

Figure 4. 5 Direct method applied to multi-sources

The acoustic relationship at the outlet of each valve is known and has the form of a general equation, see equation (3.29). However, the source term is modelled via a diagonal matrix, see equations (4.26), (4.38) and (3.31) to (3.34). Thus, the pressure and velocity vectors at any general points X and Y, where Y is closer to the radiation point than X, can be related by

$$\{\mathbf{v}\}_Y = [\mathbf{H}]_Y \{\mathbf{P}\}_Y, \tag{4.42}$$

where

$$[\mathbf{H}]_Y = ([\mathbf{d}]_{XY} - [\mathbf{H}]_X [\mathbf{b}]_{XY})^{-1} ([\mathbf{a}]_{XY} - [\mathbf{H}]_X [\mathbf{c}]_{XY}), \tag{4.43}$$

see Section 3.2.3. This section also refers to the sum of velocity vectors into a junction equalling those out; with the direct measurement method there is no known source vector, $\{\mathbf{S}\}$. Therefore, this summation is achieved by

$$\{\mathbf{v}\}_J = \left(\sum_e [\mathbf{H}]_{I_e} \right) \{\mathbf{P}\}_J, \tag{4.44}$$

where J is the point at a junction, I_e is an inlet of that junction and e is the number of inlets. Equations (4.42) and (4.43) replace the general equations (3.31) to (3.34), also equation (4.44) replaces (3.47). Thus the matrix relationship between the pressure and velocity vectors at 'E', see Figure 4. 5, can be acquired, refer to Sections 3.3. This is not only true for the manifold in Figure 4. 5, but for all manifolds.

At point 'E' a general matrix equation format is known, see equation (4.38), thus equations (4.40) and (4.41) can be applied to evaluate a measured source impedance, $Z_m(\Omega_f)$, see Section 4.5.4 to 4.5.5.

4.7 Results for the indirect measurement method

Extensive, experimental characterization of the source impedance of a Volvo truck engine was investigated by Sabry Allam, Hans Boden and associates as part of the European project ARTEMIS [95].

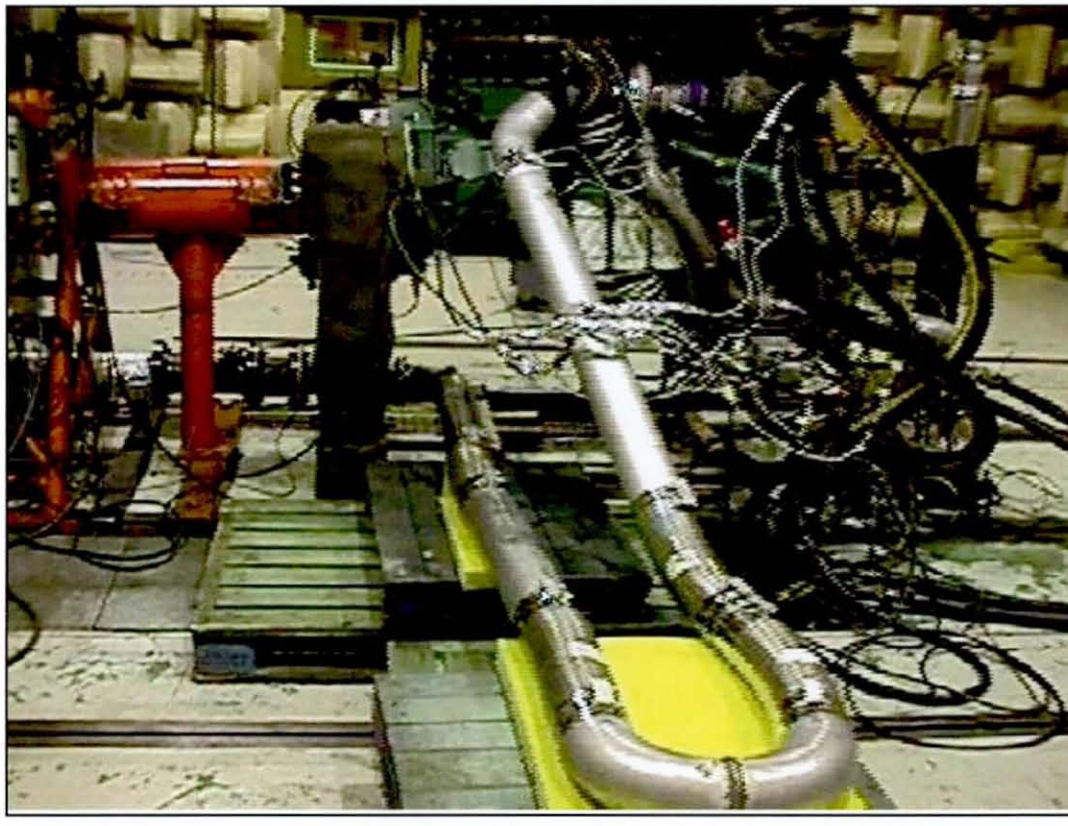

Figure 4. 6 The Volvo engine on a test rig, where there silver pipe is the exhaust section, photo taken from [95]

The experimental measurements were undertaken in a Swedish Volvo truck laboratory where 12 different engine operating conditions, each with 9 acoustic loads, were used to evaluate the impedance of the Volvo internal combustion engine. The speed and load on the engine was varied to obtain the different operating conditions, with engine speeds of 1200RPM, 1400RPM, 1600RPM and 1800RPM and engine loads of 25%, 50% and 100%

of full load. Only a representative selection of the results at different engine speeds and loads is shown in this section as the volume of experimental results is very large.

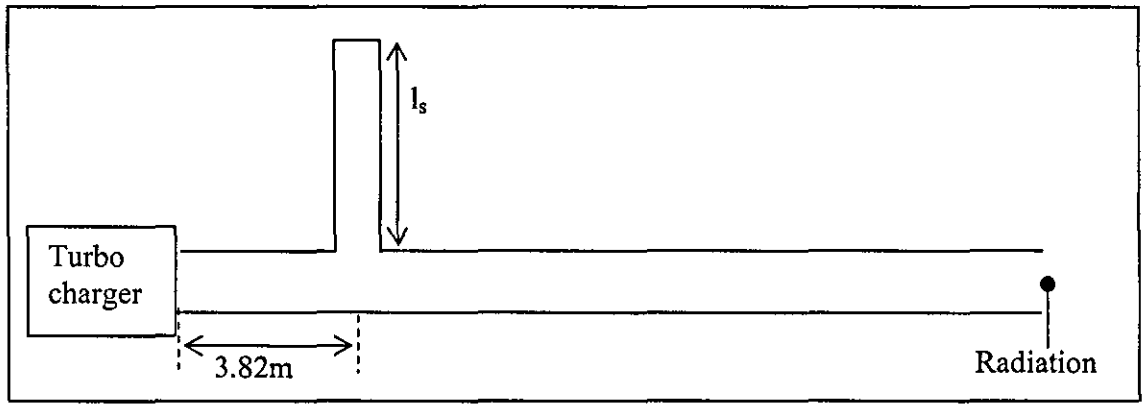

Figure 4. 7 Schematic diagram of the exhaust section of the test rig

The exhaust section of the test rig, as shown in Figure 4. 7, consisted of a main exhaust pipe with a side branch pipe. The side branch was placed 3.82m downstream of the outlet of the turbo-charger. The 9 acoustic loads differed only in the length l_s, of the side branch. Side branches of lengths 0mm, 350mm, 743mm, 1343mm, 1737mm, 1940mm, 2430mm, 2735mm and 3130mm were used.

Basic specifications			
Bore	[mm]	&131	
Stroke	[mm]	150	
Conrod length	[mm]	260	
Total displacement	[L]	12.13	
Displacement per cylinder	[L]	2.01	
Number of cylinders	[-]	6	
Firing order	[-]	1-5-3-6-2-4	
Compression ratio (current)	[-]	≈ 17.5:1	
Peak firing pressure limit	[bar]	185	
Fuel		Diesel	
Lower heating value	[kJ/kg]	42890	
Stoichiometric A/F ratio	[kg/kg]	14.57	
Fuel injection equipment		EUI (p_{max} = 1800 bar)	
Swirl number (acc. to AVL definition)	[-]	0.035	
Inner valve seat diameter intake	[mm]	2x36.3	
Inner valve seat diameter exhaust	[mm]	2x37.12	
Valve timing at mm clear. (Exh. / Int.)	[mm]	1.3 / 0.2	1 / 1
EVO (deg. CRA BBDC)		66	(80)
EVC (deg. CRA ATDC)		7	(17)
IVO (deg. CRA BTDC)		44	1
IVC (deg. CRA ABDC)		56	13
Turbocharger - Holset (US98):		HX55 - E9861B / HX55 – E9861B	

Table 4. 1 Main Engine Data, acquired from [97]

The key characteristics of the engine are given in Table 4.1. A one-dimensional model of the geometric configuration of the manifold and turbocharger, sufficient for a LAMPS model of the system, is given in Figure 4. 8. A simplistic volume model of the turbocharger is used here, as this has been shown [96] to be accurate at the low frequencies of evaluation considered in the following results. Information on the valve lift curve was also supplied by Volvo and was used to generate Figure 4. 9.

The mathematics and algorithms within Chapter 3 are used to acquire a matrix relationship between pressure and acoustic mass velocity immediately downstream of the turbo charger, see Figure 4. 7 and Figure 4. 8. Then, an acoustic load impedance is calculated for each harmonic frequency for a specific load. Hence, given a pair of acoustic loads for a single engine operating condition, the source impedance at multiples of the valve frequency can be calculated, see Section 4.2. For each engine operating condition, experimental measurements of pressure were recorded at engine orders [3, 6, 9, 12, 15, 18, 21, 24, 27, 30, 33, 36] and hence the effective source impedance was evaluated at the same engine orders. Note that since it is a six-cylinder engine, the third engine order equates to the firing frequency. Due to the symmetry in the manifold and the firing order, as given in Figure 4.8 and Table 4.1 respectively, there is destructive interference at the manifold exit between output from different cylinders at frequencies that are not multiples of the firing frequency. Thus, in order to minimise experimental error, measurements were only made for the engine orders given above, which equate to high sound levels in the exhaust system and hence high signal-to-noise ratio. Since the valve frequency is half the crankshaft frequency, 72 harmonics of valve frequency are needed in the theoretical results to model the full range of frequencies captured by the measurements. Theoretical results for effective source impedance can then, in principle, be evaluated at every valve harmonic, since signal-to-noise is not an issue. However, again due to the symmetry in the manifold and the firing order, as given in Figure 4.8 and Table 4.1 respectively, there is complete wave cancellation at the manifold exit, but the wave amplitudes are noticeably greatest at multiples of firing frequency. To simplify comparison with experimental

results, theoretical results are only given at the same engine orders for which experiment measurements were recorded.

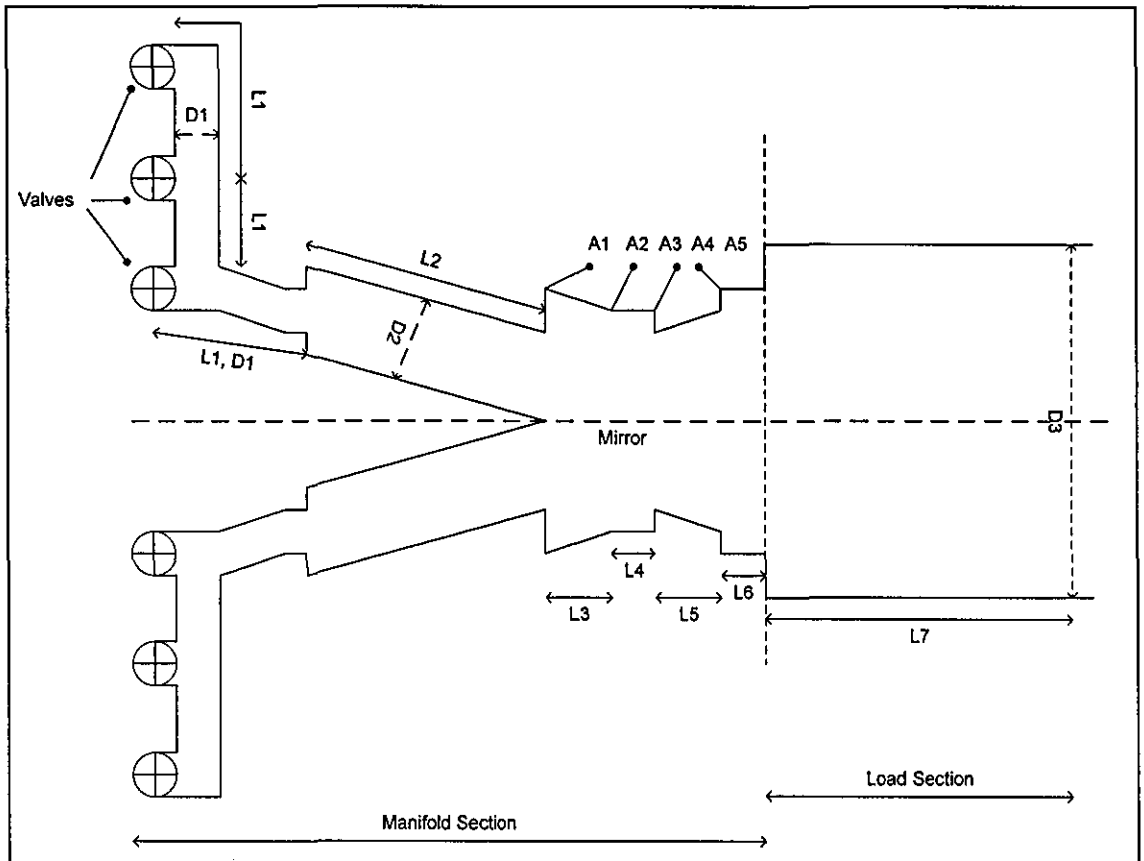

Diameter of elements	Lengths of Elements
D1 = 46mm	L1 = 395.8mm
D2 = 54mm	L2 = 70mm
D3 = 123mm	L3 = 330mm
	L4 = 335mm
Area of elements	L5 = 46mm
	L6 = 48mm
A1 = 6221mm^2	L7 = 15000mm
A2 = 4788mm^2	
A3 = 3300mm^2	
A4 = 4152mm^2	
A5 = 6221mm^2	

Figure 4. 8 One dimensional model of the Volvo truck manifold

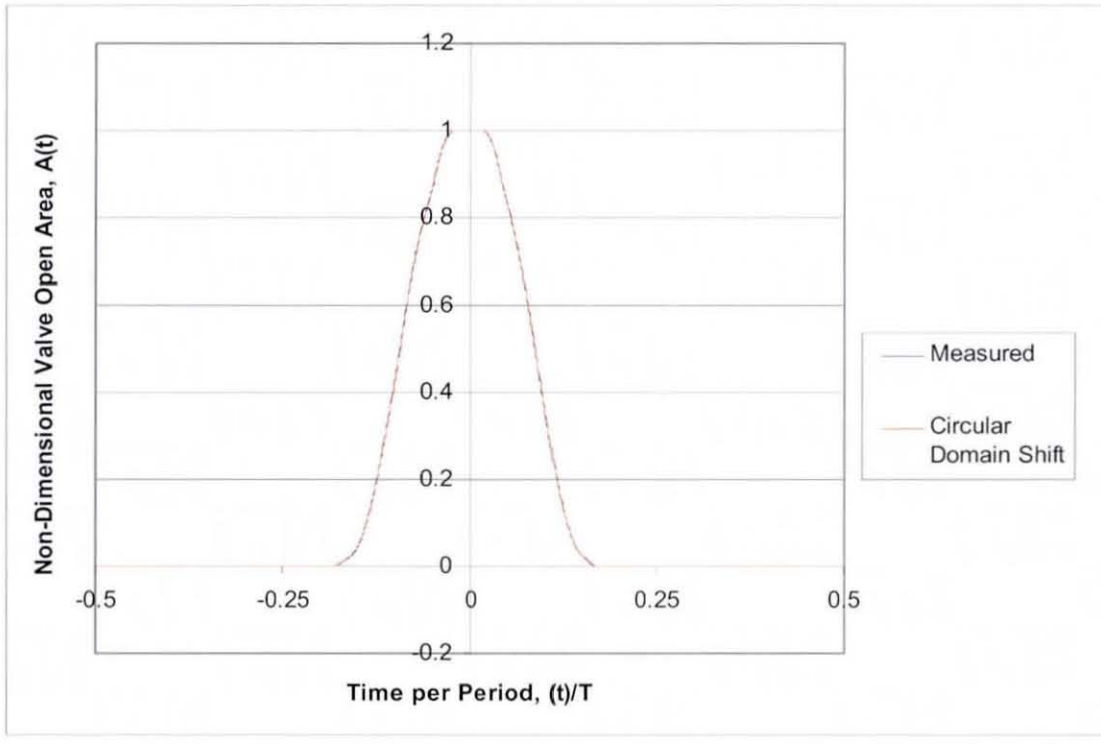

Figure 4. 9 Volvo 'non-dimensional valve open area curve

The 'Measured' series in Figure 4. 9 illustrates the given non-dimensional valve open area curve of the valve over a complete valve time period, *T*. The 'Circular Domain Shift' series illustrates the same curve, once the complex Fourier series has been used to express the time-dependent, periodic function in the frequency domain and transferred back to the time domain. This illustrates the accuracy of using 72 harmonics.

The geometry of the manifold and acoustic load is known, as is the open area curve of the valve, therefore the Normalized Effective Source Impedance (NESI) can be calculated as shown in Sections 4.2 and 4.3. The achieved results will be displayed in two parts, resistance and reactance.

There are 9 acoustic loads; however, only 2 loads are needed to calculate the effective source impedance [75]. Consequently, there are 36 possible estimates of the source impedance. Each engine speed and percentage engine load condition has 2 figures associated with it, each of which displays separately the resistance and reactance. The first

figure displays all the 36 estimates of NESI, for example Figure 4. 10. Simple averages of each NESI at individual frequencies are evaluated and the four estimated NESI values that are furthest from the averages are highlighted by the 'Outlier Paired Loads'. The second figure for each engine operating condition shows various estimates of the average calculated and measured effective source impedance, see for example Figure 4.11. This second figure shows 3 different sets of theoretical results given by different methods of averaging, as compared to one set of averaged experimental results acquired from the ARTEMIS Report [95]. The 'Average' series on a given figure relates to a straight average of all NESI values from every acoustic load pair at individual frequencies. The 'Doctored Average' is a similar straight average of NESI values for all pairs, but omitting the 'Outlier Paired Loads', thus eliminating rogue values.

The 'Experimental' series as acquired from the ARTEMIS Report are obtained via the singular value decomposition method [95], where the 36 separate estimates of source impedance are regarded as an over-determined set of equations for the single effective source impedance value. Briefly, suppose

$$[\mathbf{L}]\{\mathbf{x}\} = \{\mathbf{Q}\}, \tag{4.45}$$

where [**L**] is an m by n matrix which represents a general set of linear equations in conjunction with vector {**Q**} of size m by 1, where {**x**} of size n by 1 represents the unknowns that need to be solved. Hence n is the number of unknowns and m is the number of equations. The single value decomposition routine finds two orthonormal matrices [**U**] and [**V**] of sizes m by n and n by n respectively such that

$$\{\mathbf{x}\} = [\mathbf{V}][\mathbf{J}][\mathbf{U}]^T\{\mathbf{Q}\}, \tag{4.46}$$

where [**J**] is a square, diagonal matrix which has positive diagonal components, the inverse of the singular values. This method aims to reduce the residual vector {**r**} in

$$\{\mathbf{r}\} \equiv |[\mathbf{L}]\{\mathbf{x}\} - \{\mathbf{Q}\}|. \tag{4.47}$$

The third set of averaged theoretical results shown on the second of the figures for each engine condition are also obtained via single value decomposition to allow for direct comparison with the experimental results.

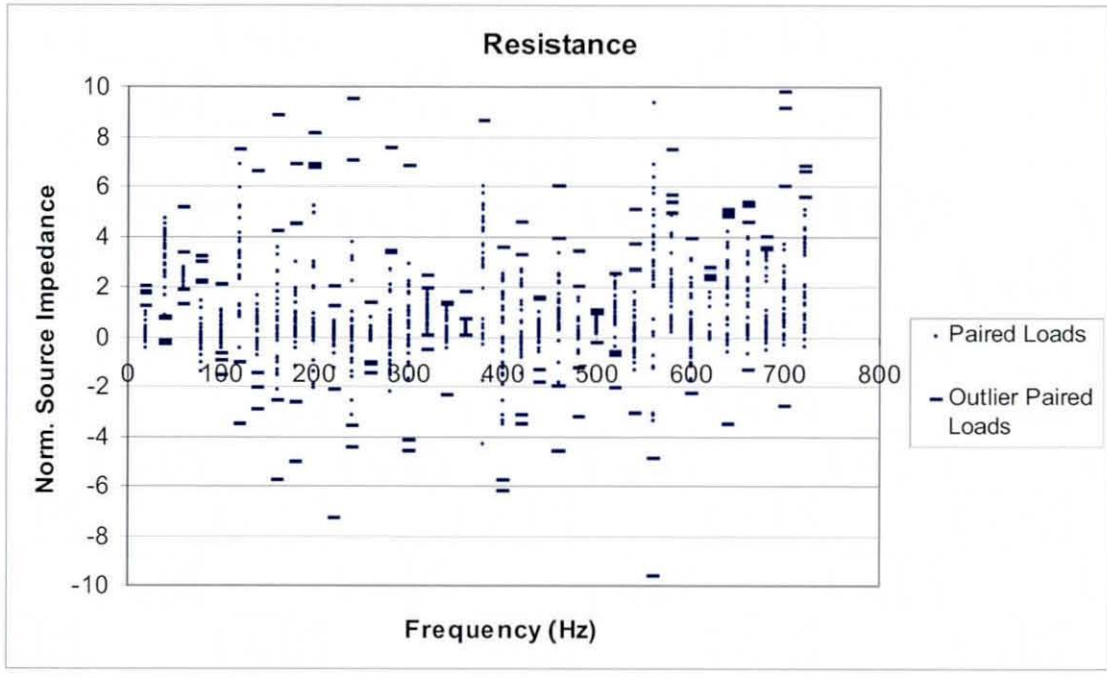

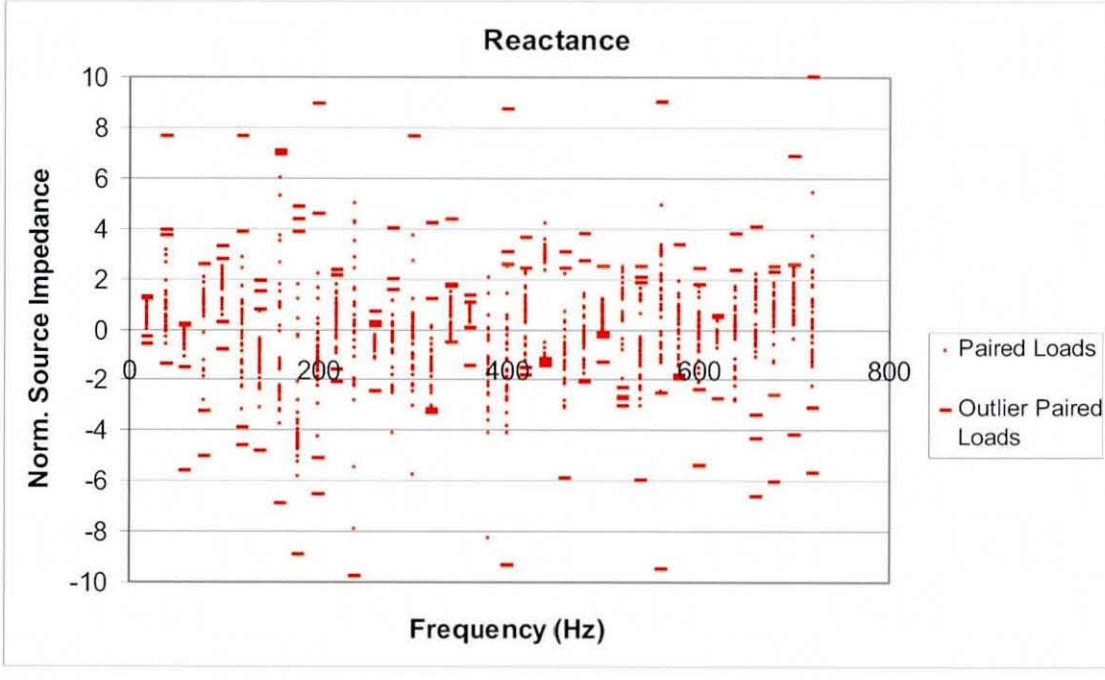

Figure 4. 10 Measured source impedance of the Volvo manifold at 1200RPM calculated with 9 acoustic loads, 50% engine load

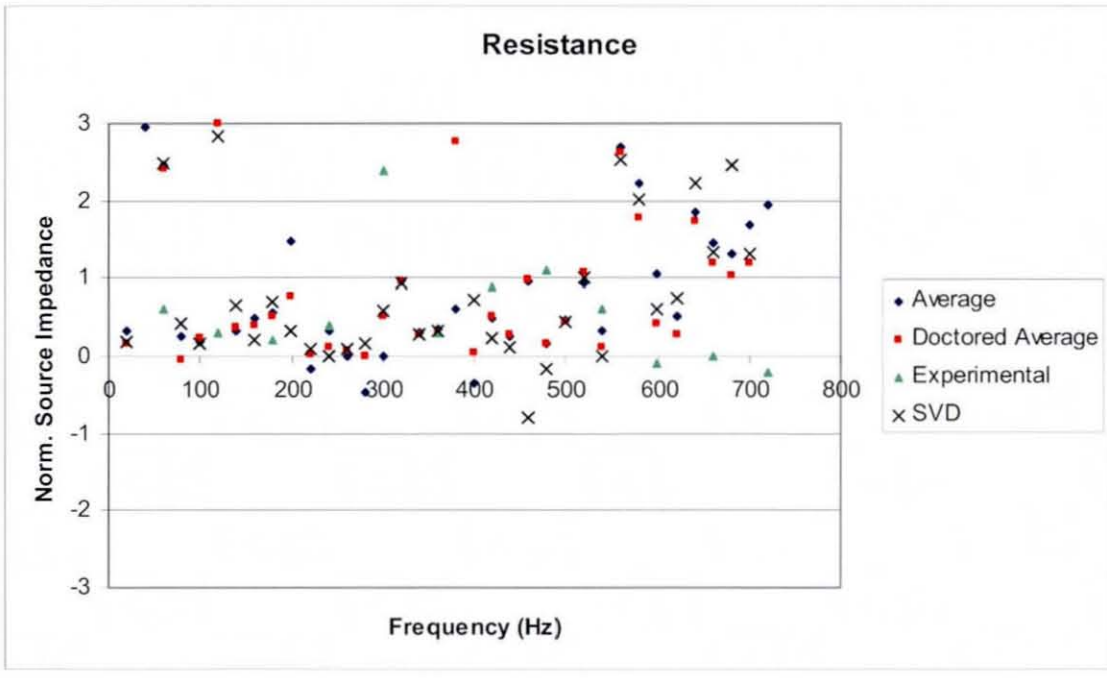

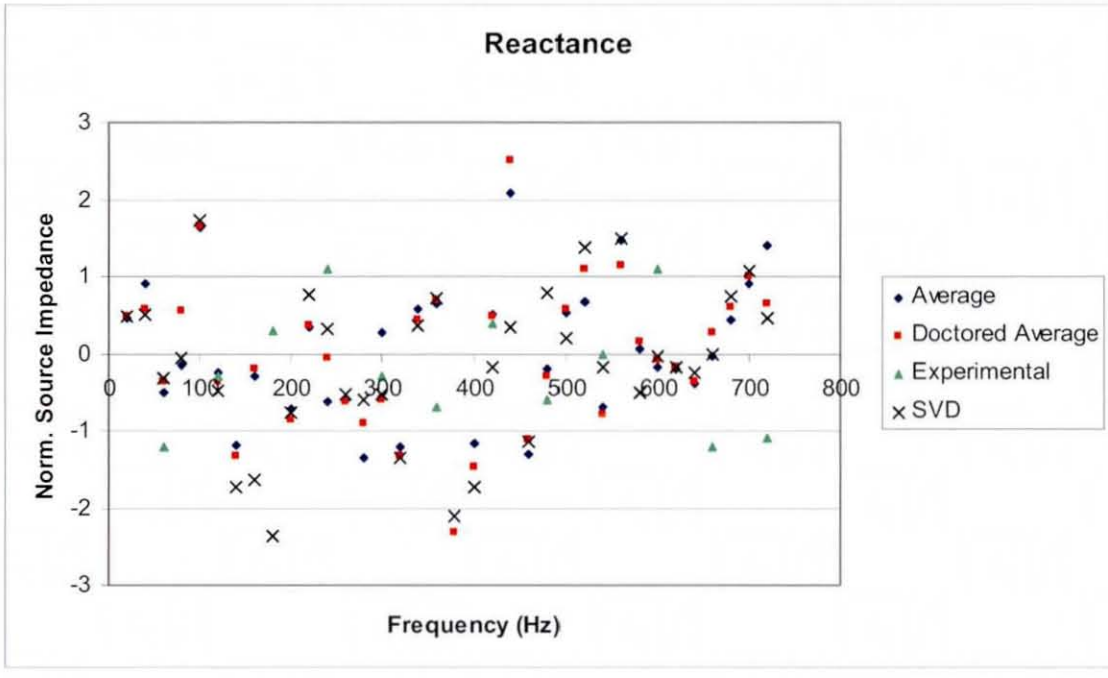

Figure 4. 11 Measured source impedance reactance of the Volvo manifold at 1200RPM calculated with 9 acoustic loads, 50% engine load, using averaging techniques

The results gained from calculating the source impedance of the Volvo manifold, when the engine is running at 1200RPM, at 50% engine load, are shown in Figure 4. 10. The results suggest that the evaluation of NESI, determined by a single frequency and not a matrix, are heavily load dependent. Although Figure 4. 10 displays possible rogue values separately, see 'Outlier Paired Loads' series, the range and spread of all of the 'Paired Load' series is still large.

The Artemis project evaluated measured NESI at an individual frequency using averaging techniques, on the assumption that differences were due to experimental error rather than load dependence. Single value decomposition was used to average the experimental results and is expressed through the 'Experimental' series on Figure 4. 11. On this figure the experimental results are compared against theoretical predictions of evaluating measured NESI by using averaging, doctored averaging and single value decomposition. The theoretical points are plotted at engine orders. There is no distinct correlation between theoretical and experimental averaging. At an engine speed of 1200RPM and 50% load, there does not appear to be any advantage in using doctored averaging, as opposed to the straight averaging technique. Strangely, the theoretical averaging and doctored averaging techniques seem to correlate more closely with the experimental results as opposed to the theoretical single value decomposition results. However, the use of single value decomposition with this type of data spread and range is problematic.

The majority of the theoretical and measured NESI resistance results are at least positive, which concurs with the physical meaning of source resistance. This is in marked contrast to theoretical and measured NESI results for a single-cylinder engine [71]. Furthermore, Figure 4. 11 does show that the three different averaging techniques provide results within a plausible range for both resistance and reactance components of NESI.

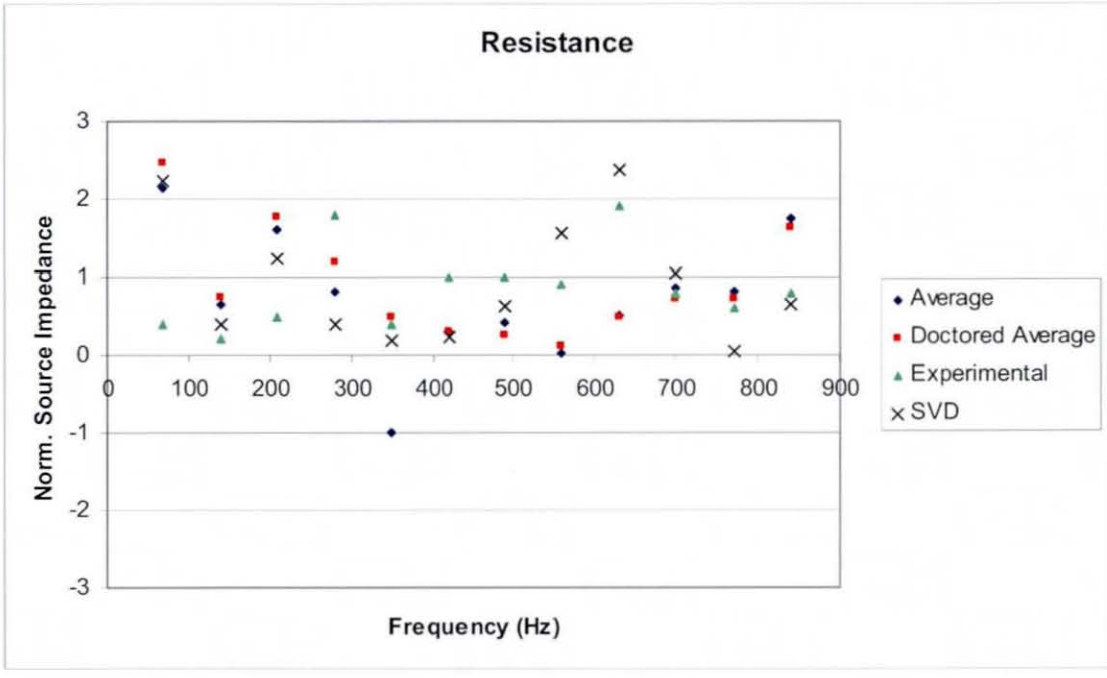

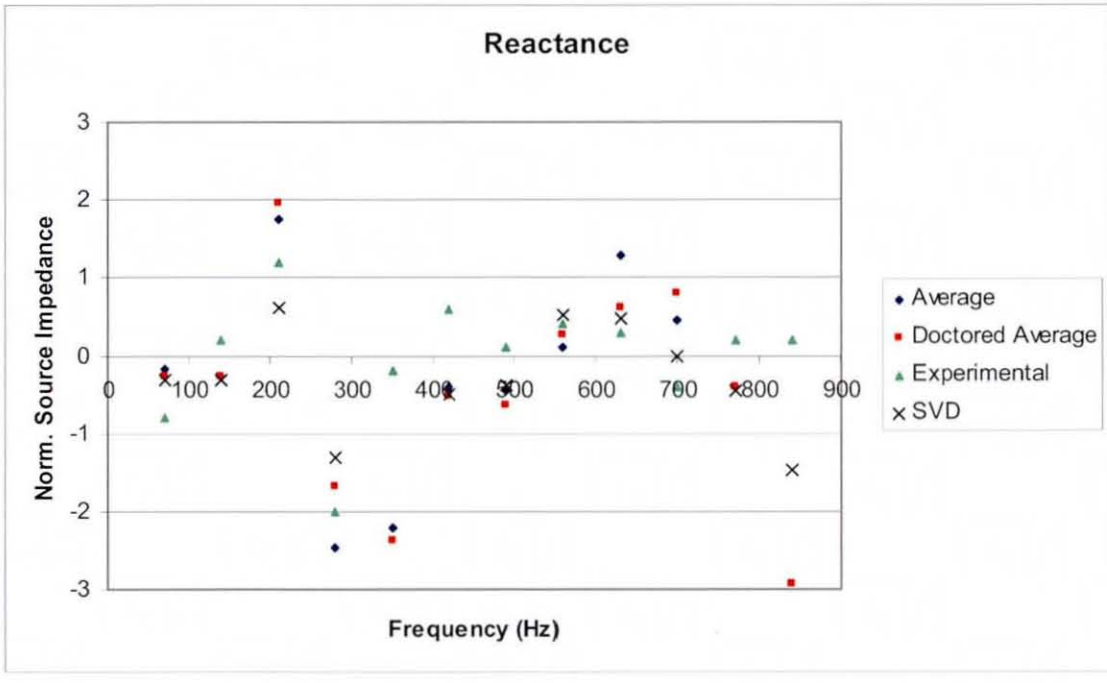

Figure 4. 12 Measured source impedance of the Volvo manifold at 1400RPM calculated with 9 acoustic loads, 25% engine load, using averaging techniques

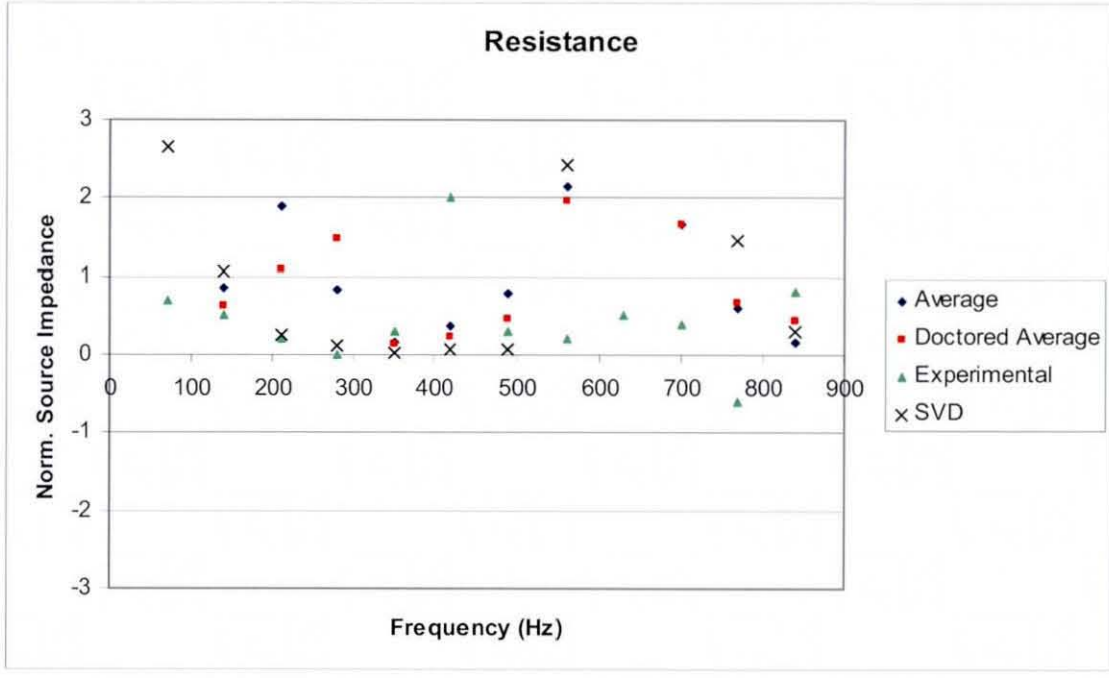

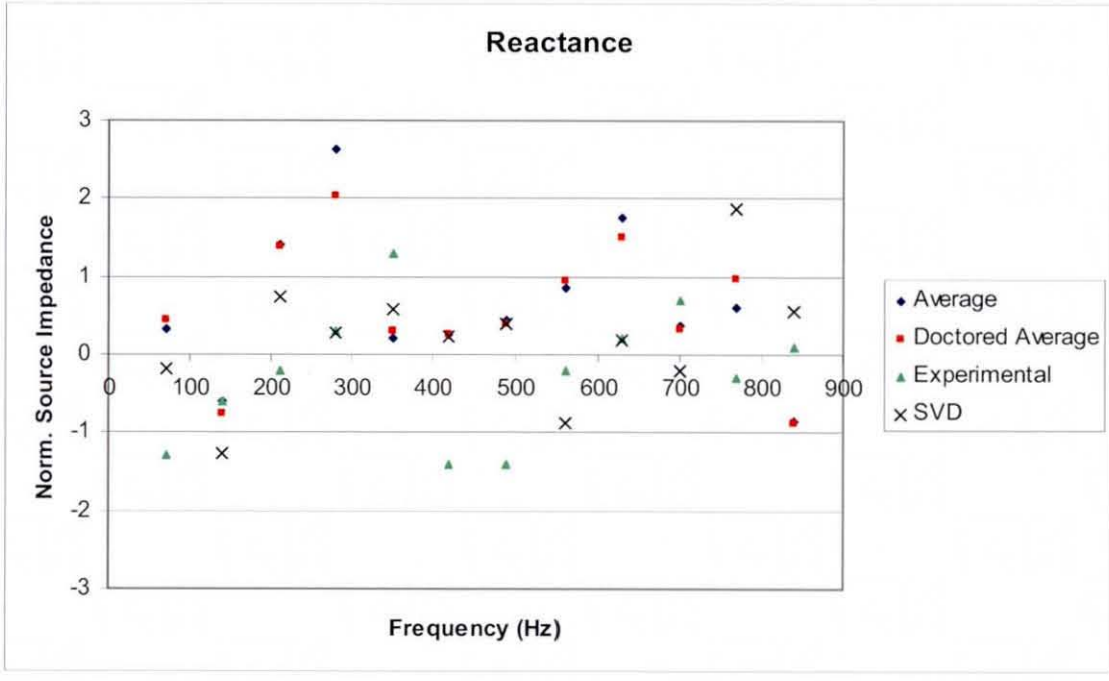

Figure 4. 13 Measured source impedance of the Volvo manifold at 1400RPM calculated with 9 acoustic loads, 50% engine load, using averaging techniques

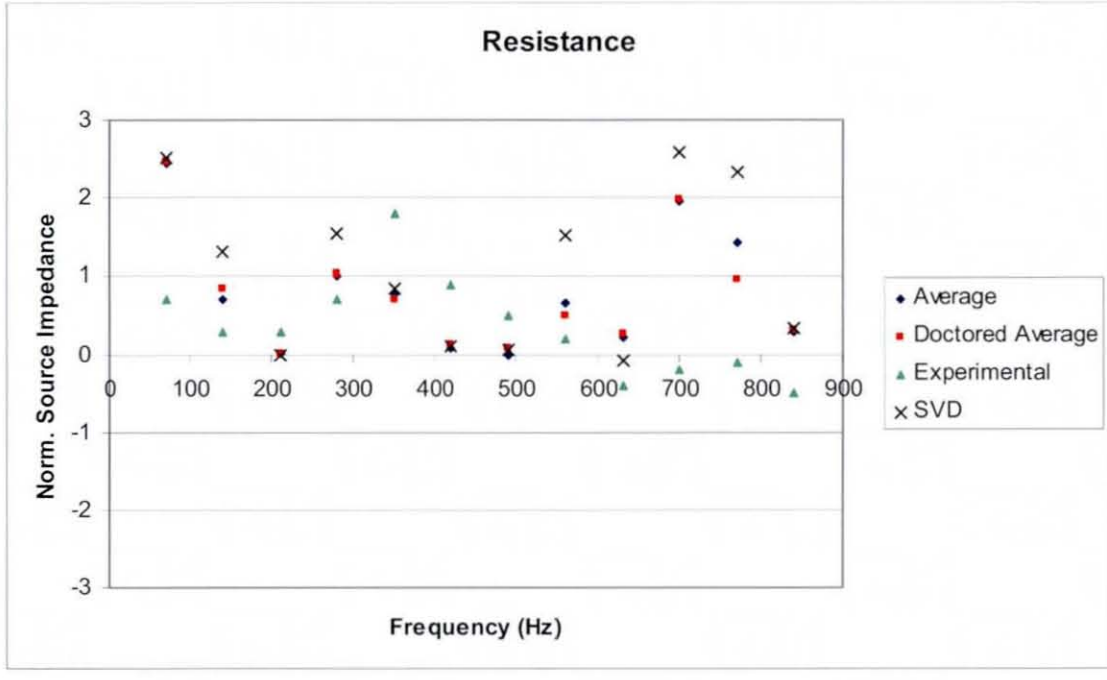

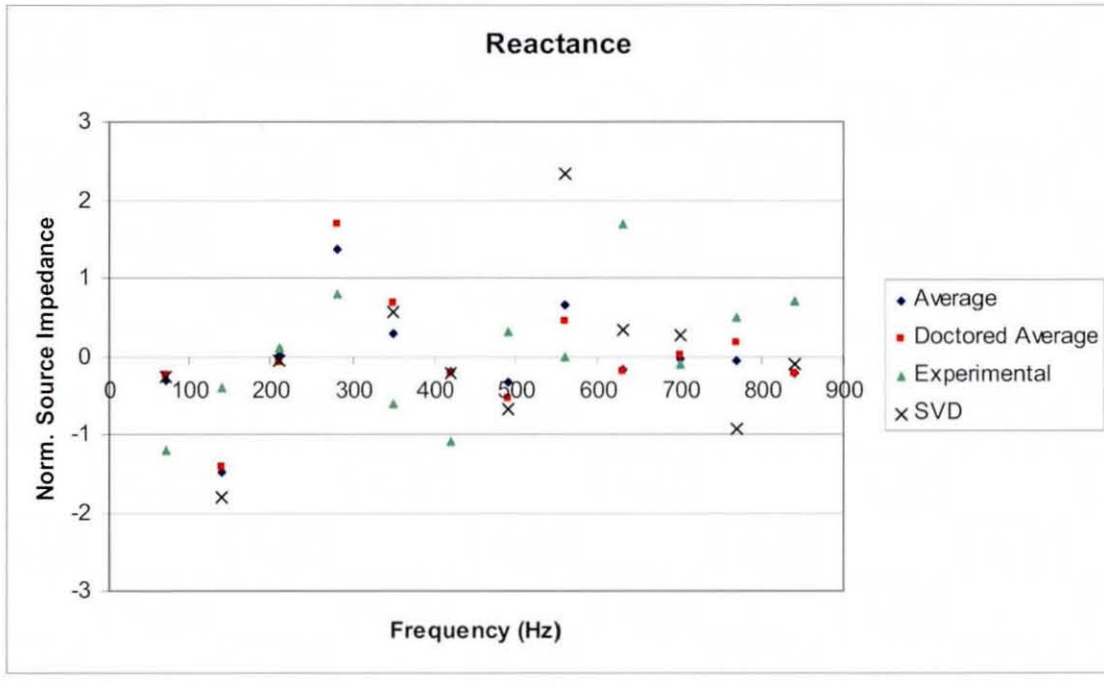

Figure 4. 14 Measured source impedance of the Volvo manifold at 1400RPM calculated with 9 acoustic loads, 100% engine load, using averaging techniques

Figure 4. 12 to 4. 14 show predicted and measured NESI results at an engine speed of 1400RPM and for 25%, 50% and 100% of full engine load. Again, the theoretical results do not correlate significantly with the experimental results; therefore, no specific conclusions can be drawn. However, general observations can be made.

Firstly, the dependence of the effective source impedance values upon the acoustic loads used in their evaluation is found to be very significant. Secondly, the use of straight averaging and doctored averaging gives theoretical results that correlate better than with the experimental values, as opposed to the theoretical results using singular value decomposition. There are no significant advantages to using doctored averaging as opposed to the straight averaging technique; they both have the same qualitative correlation with experimental results. Figure 4. 12 to 4. 14 show that the range of both the theoretical and experimental averaged results, at any given frequency, decreases as the percentage load increases. Theoretical modelling of different engine loads is achieved by using differing mass flow rates and temperatures throughout the manifold/exhaust system to represent the particular loads. Figure 4. 10 to 4.14 indicate on a general level that the majority of NESI resistance components are positive. This complies with the concept of source impedance, since negative source resistance is physically implausible.

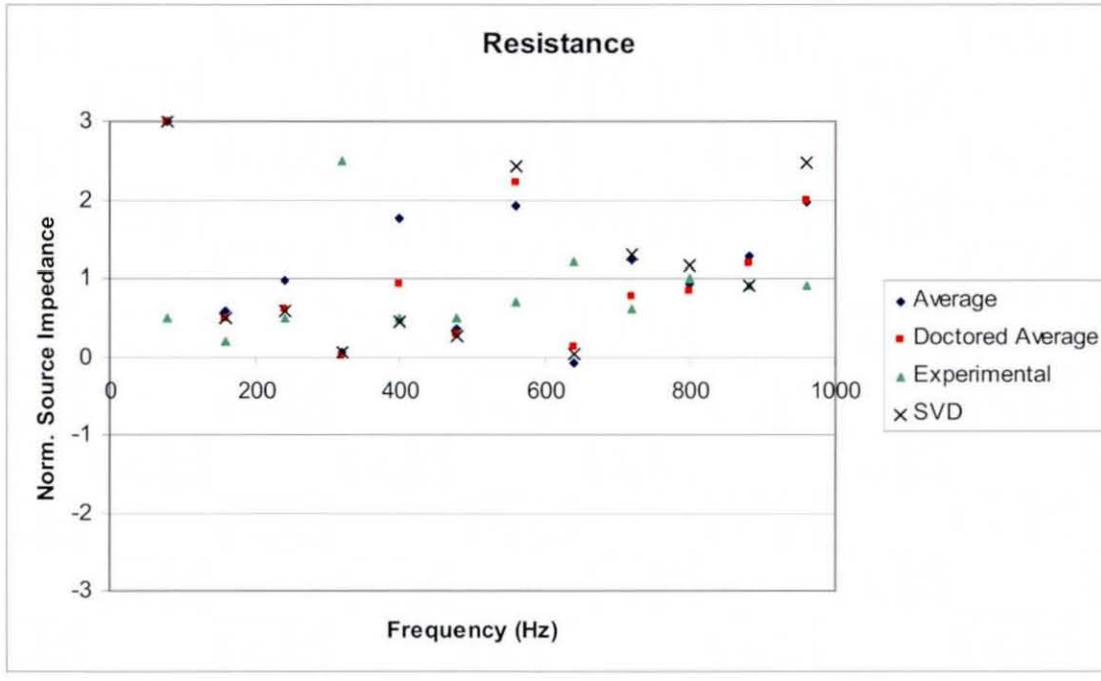

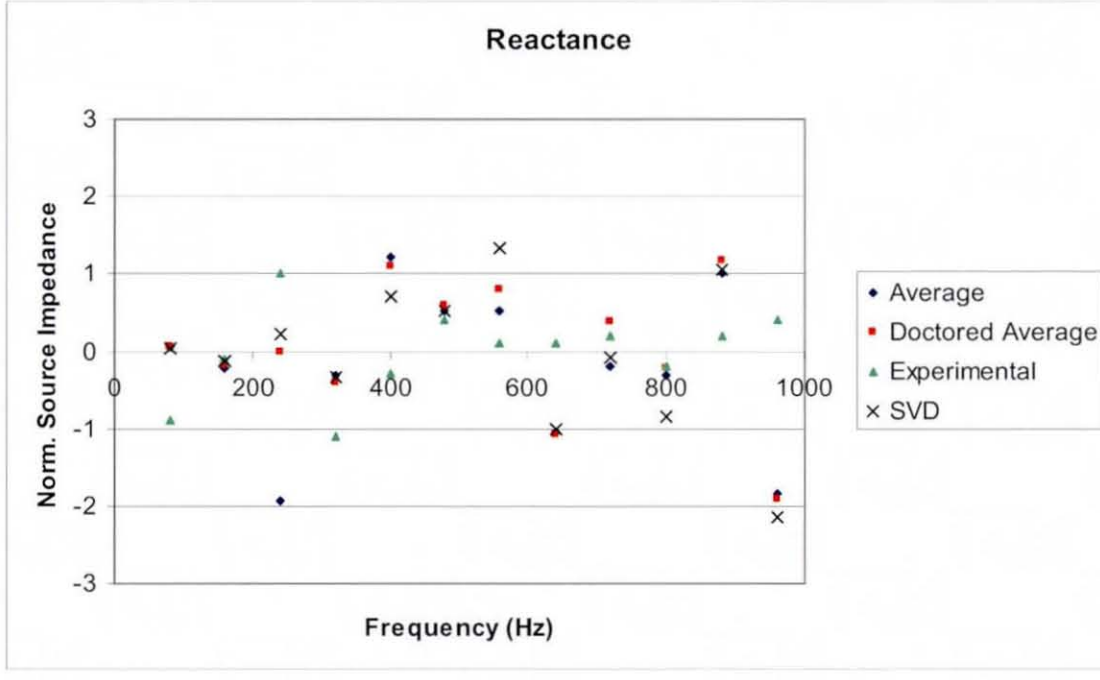

Figure 4. 15 Measured source impedance of the Volvo manifold at 1600RPM calculated with 9 acoustic loads, 50% engine load, using averaging techniques

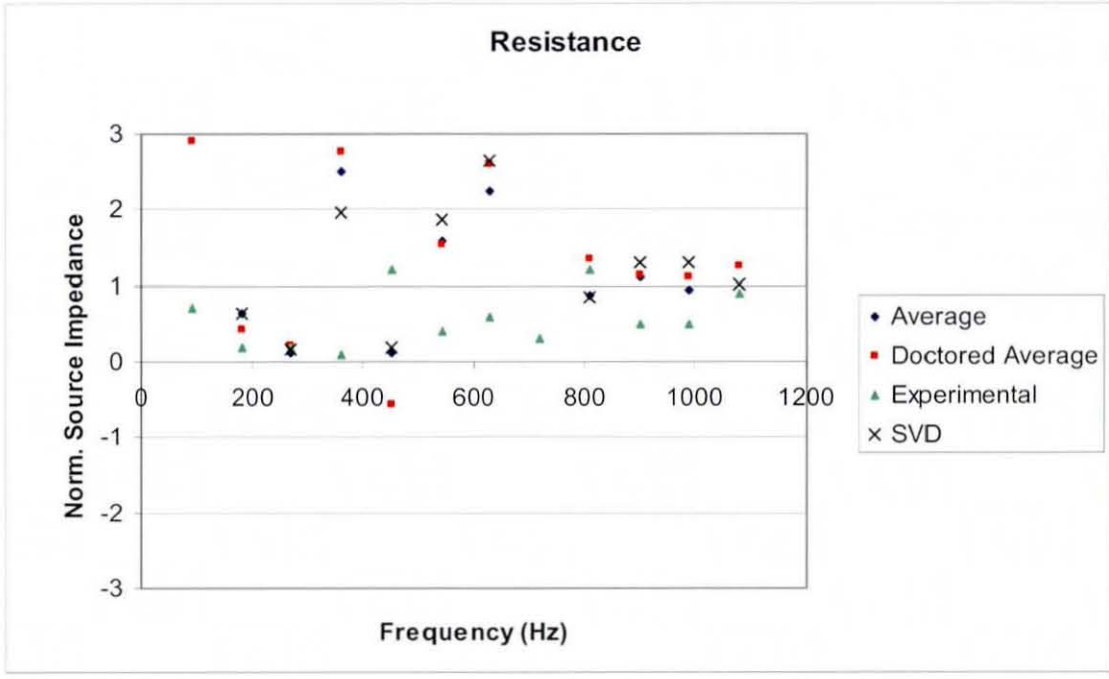

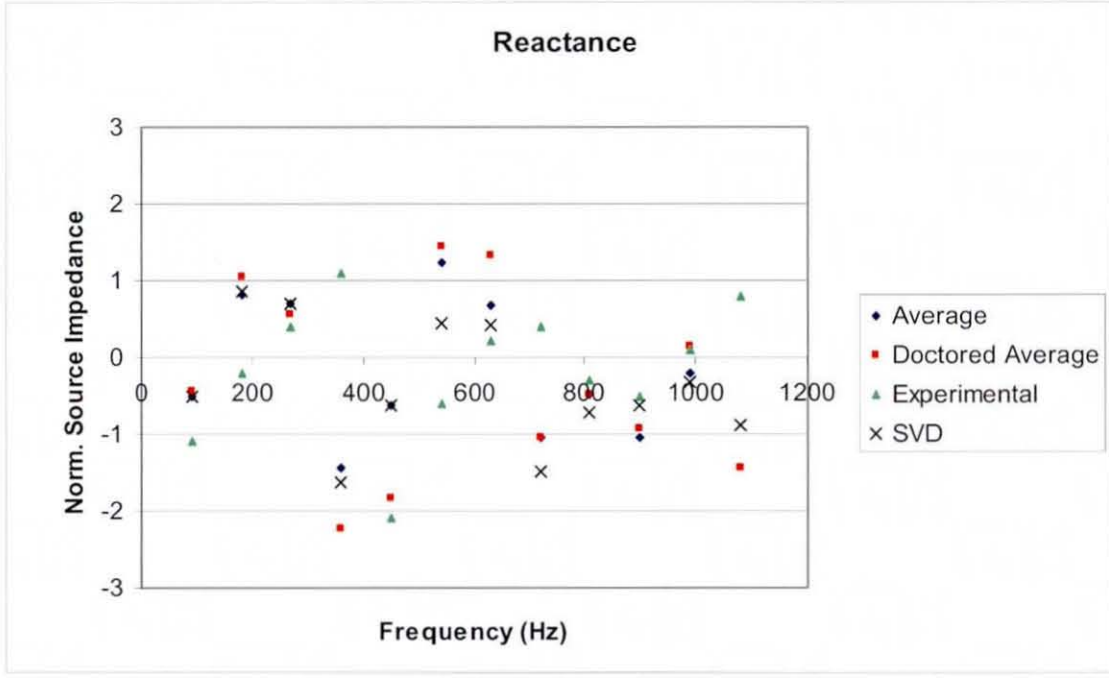

Figure 4. 16 Measured source impedance of the Volvo manifold at 1800RPM calculated with 9 acoustic loads, 50% engine load, using averaging techniques

Experimental results for 1200RPM, 1400RPM, 1600RPM and 1800RPM, all running at 50% engine loads, were all available from the Artemis project; these are shown with theoretical results in Figure 4. 11, Figure 4. 13, Figure 4. 15 and Figure 4. 16. These results re-iterate the conclusions gained from Figure 4. 10 to 4.14 and previous work for a single-cylinder engine [71], in particular that the measurement of source impedance is heavily load dependent. Also, the measured effective source impedance results bear no resemblance to the real source characteristics [71]. Even the concept that the source can be represented by a single frequency-dependent impedance value is flawed.

4.8 Results for the direct measurement method

There are no experimental results that can be used for a comparison against theoretical results for direct measurement method for multi-cylinder, internal combustion engines. Since a modelling method was developed for multiple, idealized, linear, time-variant sources, which enabled source impedance to be evaluated via a model of the indirect measurement method, it was appropriate to extend the capability to incorporate a model of the direct measurement method.

Although fictitious, the manifold used in the calculations for analysis of the direct measurement method is representative of real systems for a four cylinder internal combustion engine. The manifold chosen for the results has a simple, symmetrical design with four time-variant sources, each characterised by a non-dimensional valve open area curve,

$$A(t)=\begin{cases}\dfrac{1}{2}\left[1+\cos\left(\dfrac{6\pi t}{T}-\pi\right)\right], & 0\le t\le\dfrac{T}{3}\\ 0, & \dfrac{T}{3}\le t\le T\end{cases}\Bigg\}, \quad A(t+T)=A(t), \tag{4.48}$$

where t is time and T is the period. This time domain function is chosen to represent a real valve open area function. The valves, with respect to Figure 4. 5, are phase related and each are timed to open before bottom dead centre and close after top dead centre. Therefore, the total open period of each valve is beyond $T/4$. The results for multiple, idealized, linear, time-variant sources use a four cylinder four-stroke engine, as shown in Figure 4. 5. Each source has constant pressure and a time-variant valve which is characterised by equation (4.48) and has a quarter of a phase time lag in relation to the valve associated with the previously fired cylinder. The silencer section of the pipe network is exactly the same as the original pipe configuration in similar previous work for a single-cylinder engine [72]. Thus l_I=1500mm and l_P=900mm. The temperature within the manifold and silencer is kept constant at 350°C, such that the speed of sound is 500m/s.

With respect to Figure 4. 5, the cross-sectional area of each manifold branch from the source to the exhaust pipe is a quarter of that area. Hence, the diameter of each branch is 20mm and therefore, if the maximum valve open area, A_{max}, is 25mm^2, the coefficient C_1 remains the same, namely C_1=0.01984, see Section 4.5.2. The speed of sound through each of the valves is also taken to be 500m/s and the coefficient of discharge is evaluated in the same way as in Chapter 3. The results are evaluated with 30 harmonics of the valve, which is sufficient to ensure accurate evaluation of the valve open area. The Helmholtz resonance that arises from the assumed constant volume of the cylinder and the valve 'neck' is characterised acoustically by matrix [**C**], where V_c=0.25 litres, see Section 4.5.3.

The general equation immediately downstream at each valve can be evaluated, see equations (4.38), (4.39), Section 3.2.3 and Figure 4. 5. Then the pressure and velocity vectors at the inlet to the manifold branch fork can be acquired by equations (4.42) and (4.43) and subsequently summed by equation (4.44). At this point, the matrix relationship describes the behaviour between pressure and velocity at the source location point 'E', see Figure 4. 5. Thus, it can be modelled as an 'effective' single source such that equations (4.38) to (4.41) can be used to evaluate the modelled source impedance via the direct measurement modelling method, see Section 4.5. The two-by-two transfer matrices which

characterise the behaviour between the source location, injected signal and the radiation point are calculated via the hybrid algorithm, see Chapter 2.

Figure 4. 17 shows the resistive and reactive components of source impedance at point 'E', with respect to Figure 4. 5. It indicates clearly where resonant frequencies occur. These resonances are strongly associated with the length of the load pipe, l_p. A rigid closed-open pipe resonates when the acoustic length of the pipe, l is an odd number of quarter multiples of the wavelength, λ [1], also the speed of sound is known, c_o. Thus

$$l = \lambda\left(\frac{2n+1}{4}\right), \quad \text{n} = 0, 1, 2, 3, \ldots\ldots \tag{4.49}$$

and the resonant frequencies are then

$$f_r = \frac{c_o}{l}\left(\frac{2n+1}{4}\right), \tag{4.50}$$

where c_o is the speed of sound. If the load pipe is taken to be a closed-open pipe, the predicted resonances including end correction effects [1] are at 81.4Hz, 244Hz, 407.4Hz, 570.4Hz, 733.4Hz and 896.3Hz. These relate closely, although not precisely, to the observed resonances of the source impedance in Figure 4.17, namely 81Hz, 244Hz, 406Hz, 568Hz, 731Hz and 893Hz. It should be noted that the point at which the effective source impedance is calculated is not a valve, but a junction, which remains fully open. However, the resonant frequencies in the source impedance results resemble very closely the predicted acoustic resonances of the load pipe from the assumed position of the source to the tailpipe exit, if this is taken to be a closed-open pipe. A reason for this behaviour is not apparent immediately from the analysis, but it does illustrate clearly that the effective source impedance evaluated by the direct method is strongly load dependent.

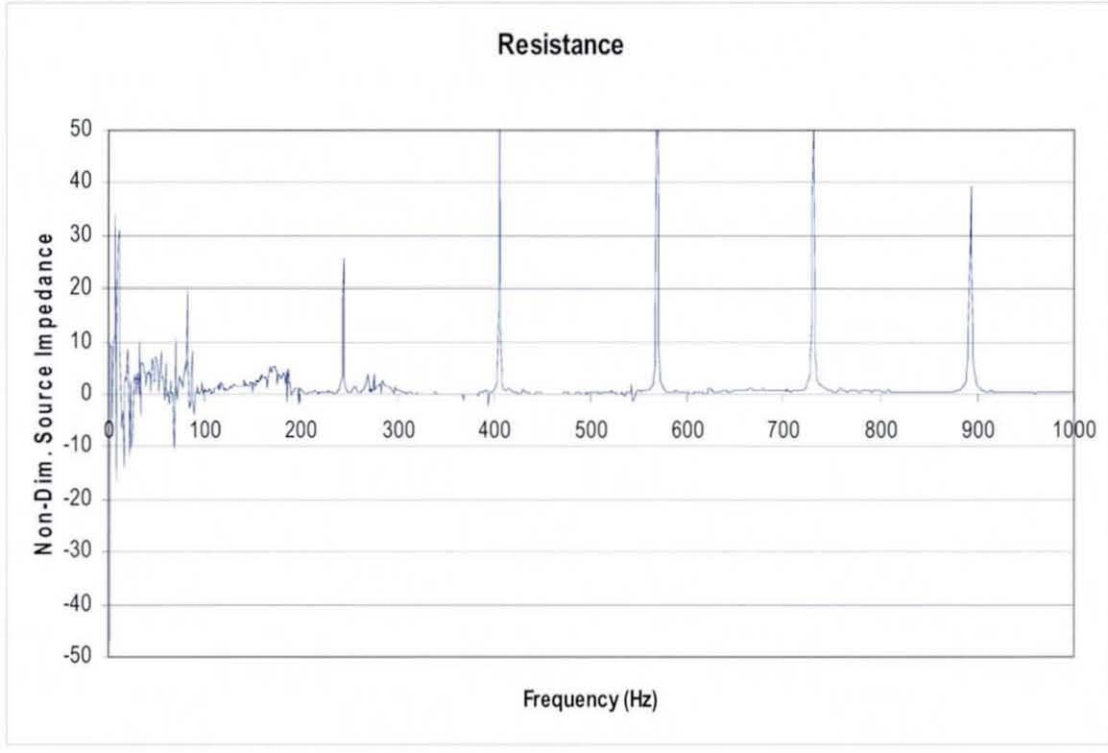

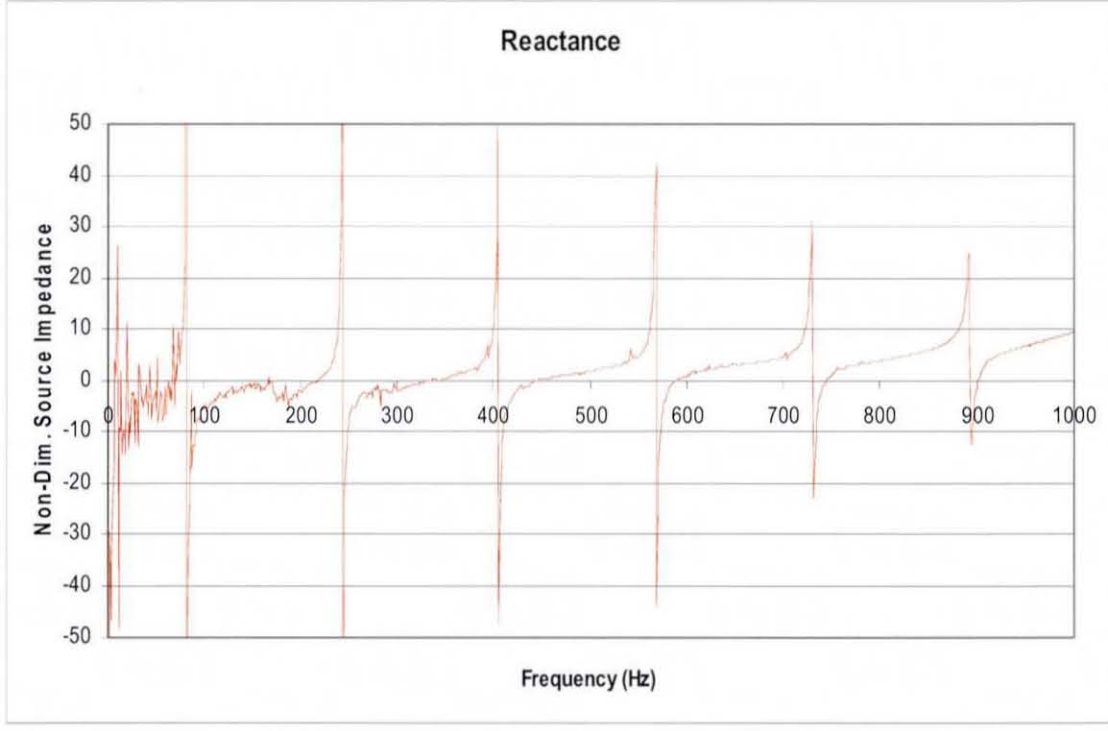

Figure 4. 17 Source impedance, l_P=1500mm and l_I=900mm, all manifold branch lengths 100mm, engine speed 1400RPM

Note that the lowest quarter wave resonance of the manifold branch, 100mm, is 1250Hz, therefore, it does not affect the frequency range as observed in Figure 4. 17. Nor should the manifold pipe length be added to the load pipe length, to give resonances in a closed-open pipe from valves to tailpipe orifice. Addition of the manifold branch length makes the comparison between the predicted and calculated resonant frequencies worse and the following results lend further weight to this assertion.

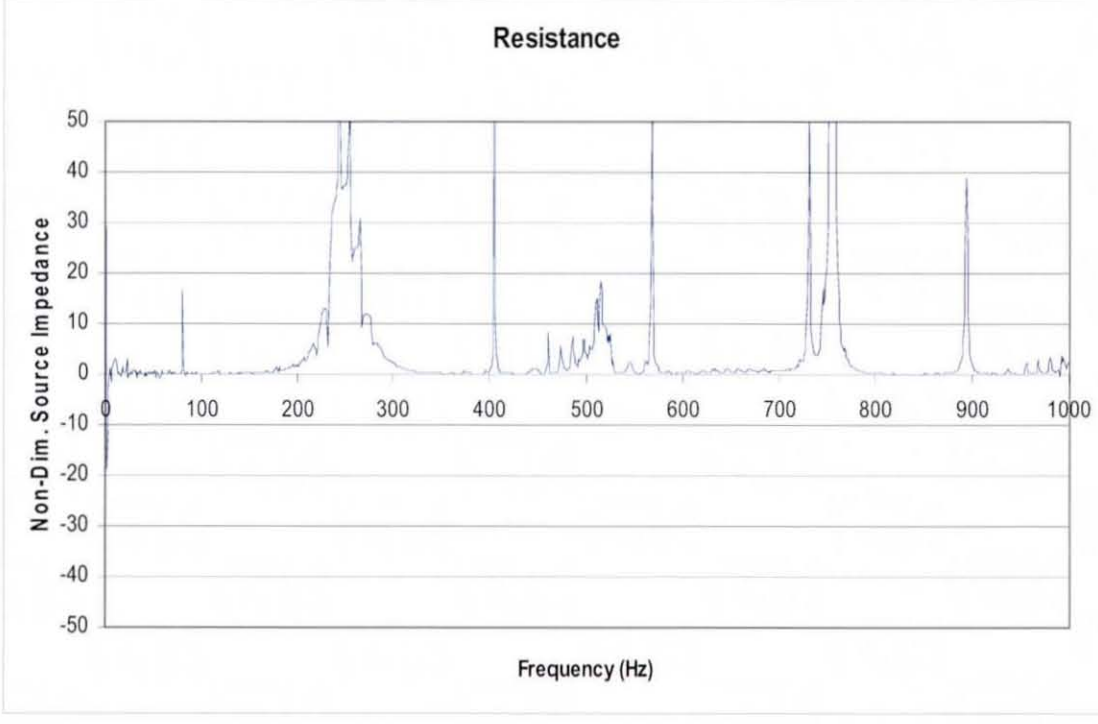

Figure 4. 18 Source impedance, l_p=1500mm and l_l=900mm, all manifold branch lengths 500mm, engine speed 1400RPM

Exactly the same analysis was repeated, but the manifold branch lengths were increased to 500mm, see Figure 4. 18. The resonances at 83.3Hz, 250.2Hz, 416Hz, etc, remain unchanged and as noted can be related closely to resonances in a closed-open pipe of physical length l_p=1500mm. There are now a further set of distinct resonances at 250Hz, 500Hz and 750Hz which are due to the length of the manifold branches. These resonances occur when the length of the branches are at quarter and half integer multiples of the wavelength. There is a strong resonance at the quarter-wave condition relative to that at

the half-wave. In principle, the manifold branches resonate at odd multiples of quarter wavelength when the valve is closed, giving a closed-open pipe and multiples of half wavelength when the valve is open, giving an open-open pipe. The presence of both sets of resonances and the relative dominance of the quarter-wave ones is accounted for possibly by the fact that the valve is closed for a greater proportion of the cycle than it is open, but both conditions do occur.

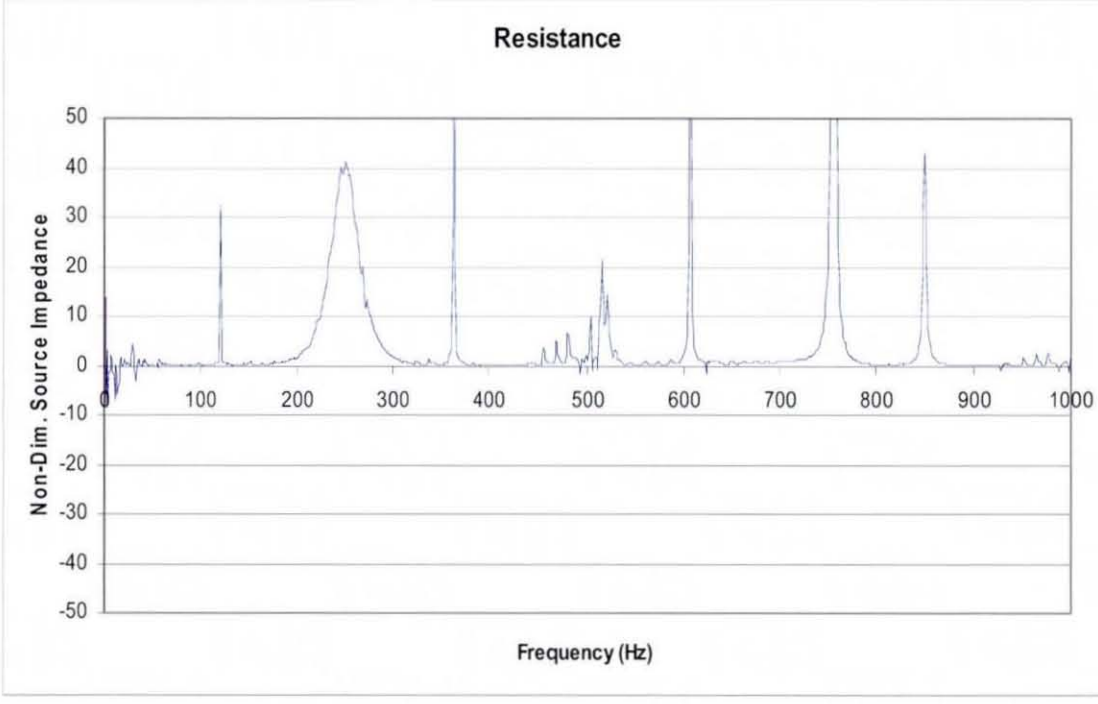

Figure 4. 19 Source impedance, l_p=1000mm and l_l=400mm, all manifold branch lengths 500mm, engine speed 1400RPM

The resonant frequencies of the branches and silencer system are totally independent of each other, as shown in Figure 4. 19 compared to Figure 4. 18. On Figure 4. 19 there are resonances at 125Hz, 375Hz, 625Hz and 875Hz, which are a result of the change of length of the load pipe, to l_P=1000mm. However, there is no shift in the resonant frequencies due to the manifold branch lengths, at 250Hz, 500Hz, 750Hz.

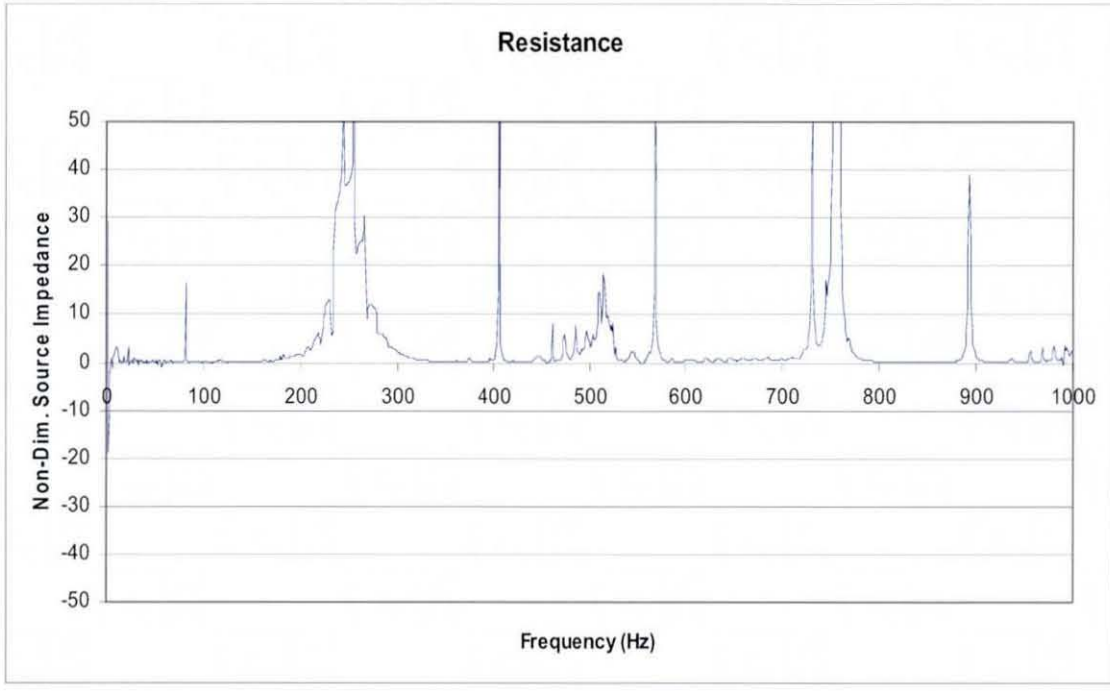

Figure 4. 20 Source impedance, l_P=1500mm and l_I=400mm, all manifold branch lengths 500mm, engine speed 1400RPM

The positioning of the injected signal, l_I, with respect to Figure 4. 5 does not have an effect on the analytical measurement of source impedance via the direct method. This is due to $\{\mathbf{d}\}$ being a sparse vector, see equations (4.33) and (4.35),

$$\{\mathbf{d}\} = \begin{Bmatrix} 0 \\ \vdots \\ 0 \\ \gamma_0 \\ 0 \\ \vdots \\ 0 \end{Bmatrix}, \tag{4.51}$$

which means that the vector $\{\mathbf{v}\}_E$, gained from equation (4.41), is the sum of the central column of

$$[\mathbf{M}] = \left([\mathbf{I}] - [\mathbf{H}]_E [\mathbf{B}]_E\right)^{-1} [\mathbf{H}]_E, \tag{4.52}$$

multiplied by γ_0. In order to obtain either the impedance or admittance at the injected frequency, P_0 needs to be evaluated. Now

$$\{\mathbf{v}\}_E = \begin{Bmatrix} v_{-N} \\ \vdots \\ v_0 \\ \vdots \\ v_N \end{Bmatrix} \tag{4.53}$$

and from equations (4.33) to (4.35)

$$P_0 = \psi_0 v_0 + \gamma_0 v_{IN} . \tag{4.54}$$

Let

$$[\mathbf{M}] = \begin{bmatrix} M_{-N,-N} & \cdots & M_{-N,0} & \cdots & M_{-N,N} \\ \cdots & M_{\frac{-N}{2},\frac{-N}{2}} & \cdots & \cdots & \cdots \\ M_{0,-N} & \cdots & M_{0,0} & \cdots & M_{0,-N} \\ \cdots & \cdots & \cdots & M_{\frac{N}{2},\frac{N}{2}} & \cdots \\ M_{N,-N} & \cdots & M_{N,0} & \cdots & M_{N,N} \end{bmatrix}, \tag{4.55}$$

using equation (4.41), equation (4.55) can be rearranged to give

$$P_0 = \left(\psi_0 M_{0,0} + 1\right)\gamma_0 v_{IN}, \tag{4.56}$$

therefore

$$Z\left(\Omega_f\right) = -\frac{\psi_0 M_{0,0} + 1}{\psi_0 M_{0,0}}. \tag{4.57}$$

Equations (4.51) to (4.57) have shown analytically that the positioning of the injected signal has no effect on the measurement of source impedance via the direct method, since neither ψ_0 nor $M_{0,0}$ involves the length l_1. Figure 4. 18 in comparison with Figure 4. 20 illustrates that if the length of l_1 is altered, the measurement of source impedance remains the same; hence, supporting the analytical proof in equations (4.51) to (4.57).

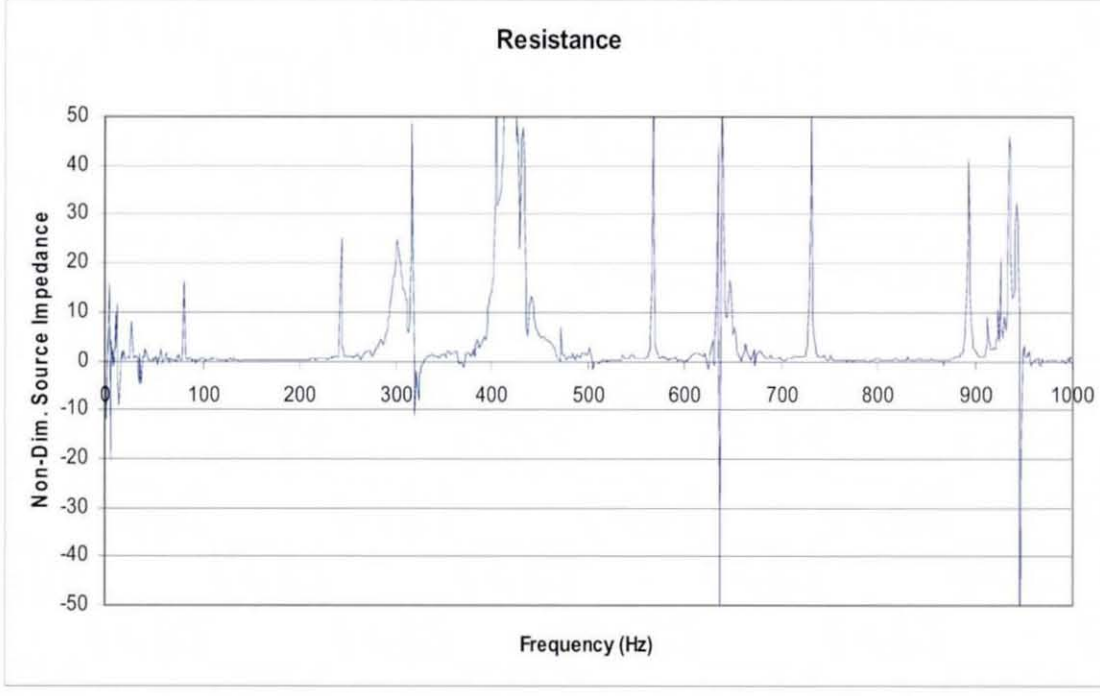

Figure 4. 21 Source resistance, l_P=1500mm and l_1=900mm, branch lengths 500mm 300mm 300mm 500mm, firing piston sequence 1342, engine speed 1400RPM

Figure 4. 21 illustrates the calculated source resistance, where the manifold branches of the system have differing lengths. Figure 4. 18 illustrates the measured source resistance of a similar system with equal manifold branches. There are still resonant spikes at 83.3Hz, 250Hz, 416Hz etc., as a result of the length of the silencer pipe. The manifold branches of length 300mm resonate initially at 416Hz when the corresponding valves are closed, then at 833Hz when they are open. Likewise with 500mm branches, the first resonant frequency is at 250Hz when the valves are closed. When all four branches are not the same length, then the resonance is not as pronounced.

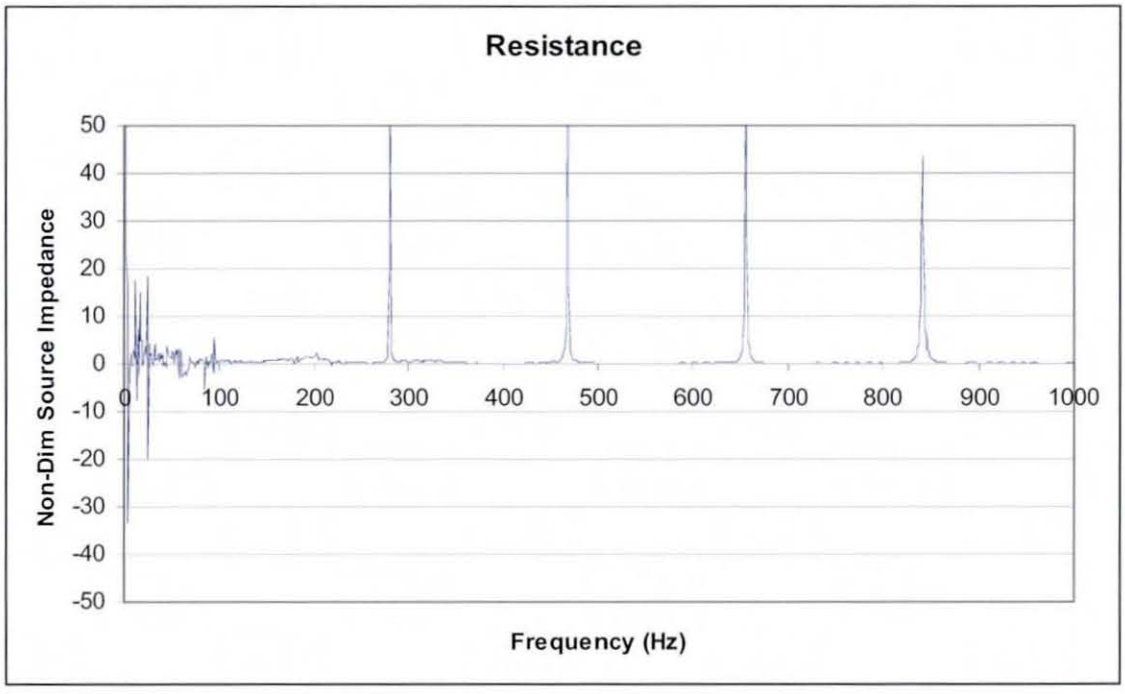

Figure 4. 22 Source impedance, l_P=1300mm and l_I=700mm, all manifold branch lengths 100mm and a 200mm between the junction in the manifold and the evaluation point engine speed, 1400RPM

Figure 4. 22 describes the resistive component of source impedance given that all the manifold branches are 100mm, l_P=1300mm, l_I=700mm and the distance between the junction where the manifold branches are joined and the evaluation point is 200mm. This analysed system illustrates the change in source impedance when only the evaluation point is moved downstream of the source. Thus, Figure 4. 22 can be compared to Figure 4. 17; the only difference between the systems that these two figures are illustrating respectively is that the evaluation point of source impedance has been moved downstream by 200mm. Figure 4. 22 illustrates resonant frequencies at 94Hz, 281Hz, 468Hz, 655Hz and 843Hz. These frequencies are close to the predicted resonant frequencies of the pipe with length l_P, i.e. 95Hz, 285Hz, 665Hz and 885Hz. The results shown in Figure 4. 22 confirm that the direct measurement method for modelling source impedance is heavily load dependent.

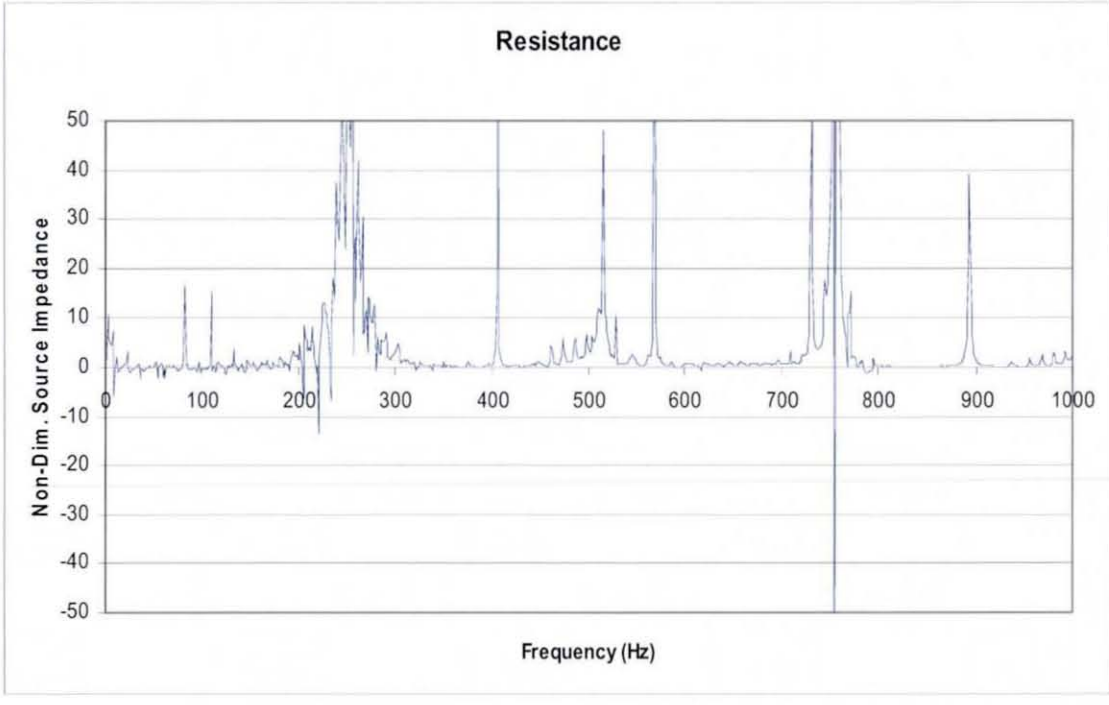

Figure 4. 23 Source impedance, l_p=1500mm and l_t=900mm, all manifold branch lengths 500mm, engine speed 1400RPM, without Fourier coefficients larger than N

The valve open area curve Fourier coefficients $A_{\pm j}$, with respect to equations (4.18) and (4.19), tend towards zero as j increases, but they are certainly not negligible. This procedure of modelling source impedance via the direct method requires Fourier coefficients that describe the valve motion in equation (4.16), from -3N to 3N, if N harmonics are required to gain significant accuracy for calculating source impedance, Z. In order to test whether the Fourier coefficients are negligible for $j>N$, these coefficients have been set to zero. Figure 4. 23 represents the resistive component of the source impedance calculated for the same system which was used in the results for Figure 4. 18. However, the Fourier coefficients $A_{\pm j}$, $j>N$, are set to zero. Figure 4. 18 and 4. 22 illustrate that these coefficients provide more numerical stability. Also, when coefficients $A_{\pm j}$, where $j>N$, are set to zero, a few rogue resonances appear that produce negative resistances, which are physically implausible.

4.9 Conclusion

As might be expected, the concept of a single frequency-dependent source impedance value to characterise a linear, time-variant source is as flawed for a multi-cylinder source, as for a single-cylinder source. In both cases, a source impedance matrix is actually required. However, from a practical consideration, use of a single frequency-dependent source impedance value is helpful when analysing the performance of exhaust systems, because it is so much simpler and quicker than using a full source model or equivalent source impedance matrix. This is particularly true in optimisation studies, when many thousands of exhaust system designs are evaluated during this process at hundreds or thousands of frequencies. In principle, both the indirect and direct methods can be used to determine experimentally an effective single frequency-dependent source impedance value for an IC-engine. In practice, only the indirect method is suitable for this application. However, models of both techniques have been extended successfully from single-cylinder to multi-cylinder engines, using an idealised, linear, time-variant representation for each source.

With respect to the indirect method, the large range and spread of results for a specific valve frequency, or engine order, highlight that the source impedance is heavily dependent on the acoustic load. Alternatively, the results are an acknowledgement that the source impedance is time-variant and should be modelled within the frequency domain through an admittance matrix. Thus, the development of the experimental technique to use an ever-increasing number of loads, in an attempt to reduce perceived experimental errors, was itself totally erroneous. Every load pair will produce a different value of effective source impedance, even in the absence of any error. It is the actual concept of a single source impedance value that is flawed, for a time-variant source. Given the use of multiple loads and hence a requirement for some form of averaging, it was found that there are no advantages or disadvantages over using a simple or doctored averaging technique. However, a single value decomposition (SVD) technique should not be used, as rogue values can change significantly the acquired average. In this regard it should be

noted that the experimental results used for comparison here were averaged via the SVD method.

The initial concerns about the indirect measurement method arose from the fact that it frequently produced negative source resistance values, which are physically implausible, when used on an IC-engine. The earlier model of the indirect method, as applied to an idealised, linear, single-cylinder, time-variant source, confirmed the tendency for the method to yield negative resistance values. The results from the model of the indirect method as applied to an idealised, multi-cylinder, time-variant source, as given here, show much less tendency for the resistance values to be negative. This trend is confirmed in the experimental results using the Volvo engine. It is not possible to conclude whether or not this effect is purely due to the use of a multi-cylinder source, or has something to do with the specific source used, such as the degree of symmetry in the manifold.

Consider next the direct method. The valve model for an idealized, inertial, linear, time-variant source, as used in the analysis of this method, for a single-cylinder engine was discovered to be modelled incorrectly. This error has been discovered and corrected. The development of the correct expressions for the admittance matrix at the valve leads to an increase in the complexity of the analysis, as compared to that published previously [72]. The results for effective source impedance from the model of the direct method with a multi-cylinder, time-variant source exhibit a variety of resonances. It was possible, through use of the model, to attribute these resonances to various aspects of the geometry of the system, in particular the lengths of the manifold branches and the load pipe. The significance of a manifold branch resonating when the time-variant valve is closed or open could be seen. Also, the resonance of the exhaust pipe could be observed. The latter point indicates that the direct method, like the indirect method, yields an effective source impedance value that is highly load dependent. The placement of the injected noise signal does not have an effect on the evaluation of the source impedance and this is explained by simple algebraic and matrix manipulation.

The observation of the numerical stability when $A_{\pm j}$ $j>N$ are set to zero, highlights the need to include all the calculated, complex Fourier coefficients when dealing with intricate designs and the critical factor of choosing the correct number of harmonics. Finally, it is observed that the resistance values are generally positive. This conforms with the findings from analytical results on a single-cylinder source and from experimental measurements on various sources. Since there are practical problems in using the direct measurement method on an IC-engine source, there are unfortunately no experimental results available for direct comparison.

CHAPTER 5

Modelling Multiple Radiation Points, Monopole and Dipole Sources

5.1 Introduction

Engineering of automotive exhaust systems is evolving as the knowledge and creativity of designers and engineers expand. Subsequently, the capability of predictive software has to encompass more features. Substantial research has been undertaken on modelling any complexity of silencer which consists of a single inlet and outlet; however, current software does not have the capability to analyse systems with multiple inlets and outlets, or multiple sources and tailpipes.

Within the current modelling of linear, plane wave, frequency domain analysis, an exhaust system with a single inlet and outlet can be characterized fully by an overall two-by-two transfer matrix. This relates the acoustic pressure and mass velocity variables at the single inlet to similar quantities at the single outlet, see Chapter 2. This overall transfer matrix is sufficient to determine the transmission loss of the exhaust system. Alternatively, when combined with information about the radiation impedance at the single outlet and source properties at the single inlet, more general noise measures such as radiated noise, external noise reduction, or insertion loss can be calculated.

Many automotive vehicles now have exhaust systems with twin tailpipes. In some cases a sprung flap valve is incorporated in one of the tailpipes such that it is forced open at high

mean flow rates, thereby reducing back pressure, but remains closed at low mean flow rates to reduce the level of radiated sound. There are even vehicles with V-engines that have a separate exhaust system for each bank of cylinders, each with a twin tailpipe, and where the two systems are interconnected, by a balance pipe. Thus, even if a bank of cylinders and its manifold is modelled as a single source, this still represents a two source, four tailpipe system.

Therefore, it is desirable that plane wave, linear, frequency domain code has the capability to analyse silencers with multiple sources and multiple radiation positions. This chapter adapts the hybrid code, developed in Chapter 2, to include the capability of analysing multiple radiation points. It progresses further to include analysis of multiple radiation points with multiple, time-variant sources. When there is more than one inlet and/or outlet to the exhaust system, an overall two-by-two transfer matrix is no longer sufficient to allow for subsequent evaluation of the various noise measures. It will be shown that the addition of each extra radiation point requires one extra equation and variable to be added to the overall transfer matrix. The chapter also encompasses the capability of including monopole and dipole sources within the exhaust system, as discussed in Section 1.4.4. In principle, these would allow for loudspeaker inputs, such as those used in active noise control, or for flow generated noise sources, respectively.

5.2 Multiple radiation algorithm

5.2.1 Illustrated use of the algorithm

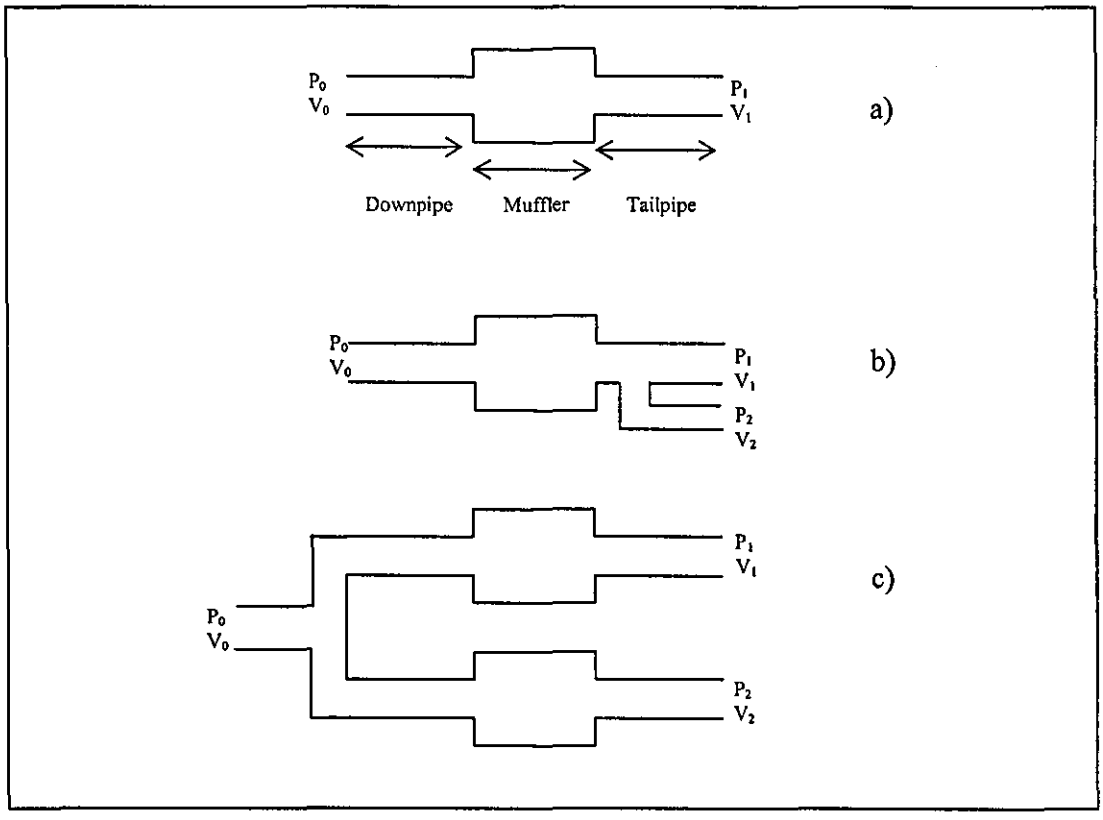

Figure 5. 1 Evolution from single to multiple radiations

As Figure 5. 1 shows, the simple extension from an exhaust system with a single inlet and outlet, to a system which has a single inlet and two outlets, encounters a permutation problem. This problem occurs because the secondary radiation point could be placed anywhere within the system. In more general cases, this is complicated further by the fact that a number of radiation points can be placed anywhere within the system. Therefore, there needs to be a general algorithm to encompass the infinite number of permutations that arise with multiple radiation points.

5.2.2 Radiation attached to a side-branch

Consider the simplest of cases, where there is a straight pipe with a secondary radiation branching off somewhere along the pipe, see Figure 5. 2. A primary radiation is the final radiation which the hybrid algorithm encounters, whereas the other radiations are named secondary radiations.

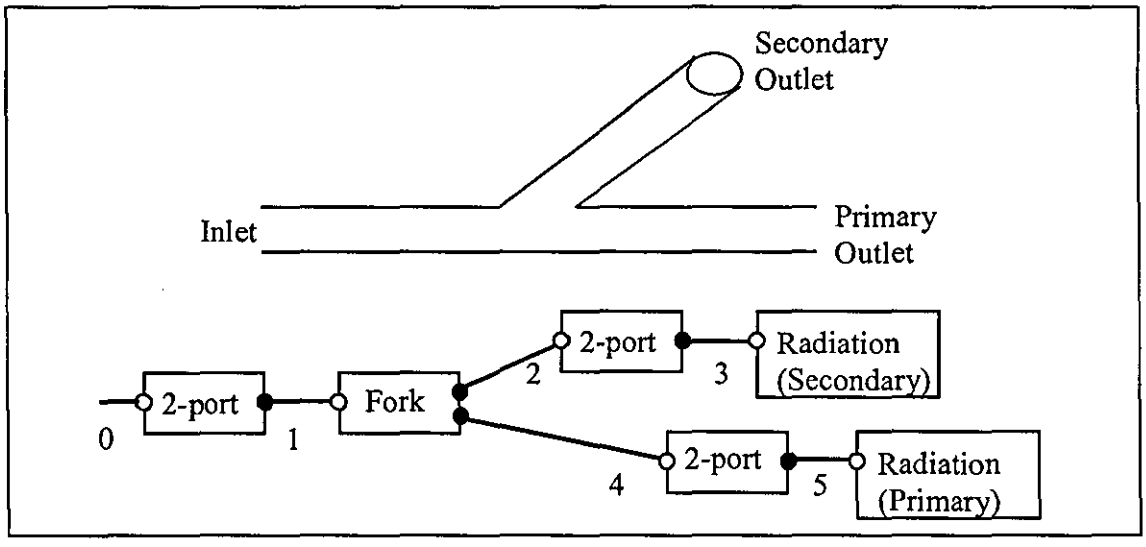

Figure 5. 2 The simplest case of multiple radiations

The radiation impedance of a given outlet can be calculated for every frequency, therefore, given the transfer matrix of the intermediate two-port system, the relationship between pressure and velocity at position *2*, with respect to Figure 5. 2, is known. Hence, the secondary radiation position can be modelled as a termination/closed end with a known impedance. However, the acoustic pressure and velocity at this position, as well as at the primary radiation position, need to be known after the overall reduction/analysis of the exhaust system, in order to evaluate the various noise calculations. Therefore, as the hybrid algorithm progresses through the silencer, the change between the pressure and velocity at the secondary radiation point, in relation to the pressure and velocity at inlet and primary outlet, needs to be recorded.

The path fraction analysis is exactly the same as for the closed end example in Section 2.5.4. Similarly, the analysis of any sub-system that has a single inlet and outlet, for example between positions 2 and 3, with respect to Figure 5. 2 can be reduced to a single equivalent two-by-two transfer matrix

$$\begin{bmatrix} P_2 \\ V_2 \end{bmatrix} = \begin{bmatrix} a_{23} & b_{23} \\ c_{23} & d_{23} \end{bmatrix} \begin{bmatrix} P_3 \\ V_3 \end{bmatrix}. \tag{5.1}$$

Now

$$Z_{r2} = \frac{a_{23} Z_{r3} + b_{23}}{c_{23} Z_{r3} + d_{23}}, \tag{5.2}$$

where Z_{r3} represents the radiation impedance at the secondary outlet and Z_{r2} is the impedance of the side branch. A three-by-three transfer matrix can now be evaluated to characterise the relationship between positions 1, 2 and 4, since

$$\begin{bmatrix} P_1 \\ V_1 \\ 0 \end{bmatrix} = \begin{bmatrix} 1 & 0 & 0 \\ 0 & 1 & 1 \\ 1 & 0 & -Z_{r2} \end{bmatrix} \begin{bmatrix} P_4 \\ V_4 \\ V_2 \end{bmatrix}, \tag{5.3}$$

assuming that the acoustic pressure at a fork is constant, namely

$$P_1 = P_2 = P_4. \tag{5.4}$$

The normal two-by-two transfer matrix equation can be applied to relate P_1 and V_1 to P_0 and V_0, via

$$\begin{bmatrix} P_0 \\ V_0 \end{bmatrix} = \begin{bmatrix} a_{01} & b_{01} \\ c_{01} & d_{01} \end{bmatrix} \begin{bmatrix} P_1 \\ V_1 \end{bmatrix}, \tag{5.5}$$

and hence from equation (5.3)

$$\begin{bmatrix} P_0 \\ V_0 \\ 0 \end{bmatrix} = \begin{bmatrix} a_{01} & b_{01} & b_{01} \\ c_{01} & d_{01} & d_{01} \\ 1 & 0 & -Z_{r2} \end{bmatrix} \begin{bmatrix} P_4 \\ V_4 \\ V_2 \end{bmatrix}. \tag{5.6}$$

The last row in equation (5.6) is now multiplied by $-1/Z_{r2}$, and the cells in the last column which are above the last row are set to zero using appropriate row operations with the last row, hence

$$\begin{bmatrix} P_0 \\ V_0 \\ 0 \end{bmatrix} = \begin{bmatrix} a'_{01} & b'_{01} & 0 \\ c'_{01} & d'_{01} & 0 \\ e'_{01} & f'_{01} & 1 \end{bmatrix} \begin{bmatrix} P_4 \\ V_4 \\ V_2 \end{bmatrix}. \tag{5.7}$$

Likewise

$$\begin{bmatrix} P_4 \\ V_4 \end{bmatrix} = \begin{bmatrix} a_{45} & b_{45} \\ c_{45} & d_{45} \end{bmatrix} \begin{bmatrix} P_5 \\ V_5 \end{bmatrix}, \tag{5.8}$$

which can be enlarged to

$$\begin{bmatrix} P_4 \\ V_4 \\ V_2 \end{bmatrix} = \begin{bmatrix} a_{45} & b_{45} & 0 \\ c_{45} & d_{45} & 0 \\ 0 & 0 & 1 \end{bmatrix} \begin{bmatrix} P_5 \\ V_5 \\ V_2 \end{bmatrix}, \tag{5.9}$$

such that equations (5.7) and (5.10) give

$$\begin{bmatrix} P_0 \\ V_0 \\ 0 \end{bmatrix} = \begin{bmatrix} a'_{01}a_{45} + b'_{01}c_{45} & a'_{01}b_{45} + b'_{01}d_{45} & 0 \\ c'_{01}a_{45} + d'_{01}c_{45} & c'_{01}b_{45} + d'_{01}d_{45} & 0 \\ e'_{01}a_{45} + f'_{01}c_{45} & e'_{01}b_{45} + f'_{01}d_{45} & 1 \end{bmatrix} \begin{bmatrix} P_5 \\ V_5 \\ V_2 \end{bmatrix}. \tag{5.10}$$

Therefore, equation (5.10) can be expressed in standardised format as

$$\begin{bmatrix} P_0 \\ V_0 \\ 0 \end{bmatrix} = \begin{bmatrix} a_{025} & b_{025} & 0 \\ d_{025} & e_{025} & 0 \\ g_{025} & h_{025} & 1 \end{bmatrix} \begin{bmatrix} P_5 \\ V_5 \\ V_2 \end{bmatrix}. \tag{5.11}$$

The additional equation will be termed a link equation, since it links the velocity associated with the non-primary radiation to the pressure and velocity at either the primary radiation point or at some intermediate point of the non-reduced network. The addition of a secondary radiation point creates an extra variable and equation within the overall transfer matrix. Similarly, if another radiation point is added, a further link equation and variable will be added to the transfer matrix equation.

5.2.3 General radiation attached to a side-branch (GRASB) algorithm

The hybrid algorithm needs very little adjustment to include the capability to analyse multiple radiation points. As the analysis of a non-primary radiation is similar to a closed end, the hybrid algorithm only needs to include the mathematical capability of analyzing the varying size of square transfer matrices.

The GRASB algorithm occurs when a radiation point, which is not the final radiation point is found by the hybrid algorithm, i.e. the path fraction is not unity. It first evaluates the impedance of the side-branch as shown in equations (5.1) and (5.2). Secondly, the GRASB algorithm locates the element attached to the inlet of the fork; this two-port element has a matrix associated with it which could be of any size, say n+2 by n+2, where n>0 implies previous secondary radiation points. However, the associated coefficients in the matrix can be adjusted to produce an intermediate standardised format, namely

$$\begin{bmatrix} P_0 \\ V_0 \\ 0 \\ \vdots \\ 0 \end{bmatrix} = \begin{bmatrix} a & b & 0 & \cdots & 0 \\ c & d & 0 & \cdots & 0 \\ e_{31} & e_{32} & 1 & \ddots & \vdots \\ \vdots & & \ddots & \ddots & 0 \\ e_{(n+2)1} & \cdots & \cdots & e_{(n+2)(n+1)} & 1 \end{bmatrix} \begin{bmatrix} P_1 \\ V_1 \\ V_{r1} \\ \vdots \\ V_{rn} \end{bmatrix}, \tag{5.12}$$

where V_{r1} to V_{rn} are velocities associated with the secondary radiation points. Equation (5.12) can be reduced further by using the third row to make the coefficients in the third column, below the third row, equate to zero. The same procedure is used for all the rows, below the third row, until and including row (n+2). Hence, equation (5.12) can be written as

$$\begin{bmatrix} P_0 \\ V_0 \\ 0 \\ \vdots \\ 0 \end{bmatrix} = \begin{bmatrix} f_{11} & f_{12} & 0 & \cdots & \cdots & 0 \\ f_{21} & f_{22} & 0 & \cdots & \cdots & 0 \\ \vdots & \vdots & 1 & \ddots & & \vdots \\ \vdots & \vdots & 0 & \ddots & \ddots & \vdots \\ \vdots & \vdots & \vdots & \ddots & \ddots & 0 \\ f_{(n+2)1} & f_{(n+2)2} & 0 & \cdots & 0 & 1 \end{bmatrix} \begin{bmatrix} P_1 \\ V_1 \\ V_{r1} \\ \vdots \\ V_{rn} \end{bmatrix}. \tag{5.13}$$

Thus, the addition of one more secondary radiation point will cause the transfer matrix in equation (5.13) to be enlarged to a (n+3) by (n+3) transfer matrix, namely

$$\begin{bmatrix} P_0 \\ V_0 \\ 0 \\ \vdots \\ \vdots \\ 0 \end{bmatrix} = \begin{bmatrix} f_{11} & f_{12} & 0 & \cdots & \cdots & 0 & f_{12} \\ f_{21} & f_{22} & 0 & \cdots & \cdots & 0 & f_{22} \\ \vdots & \vdots & 1 & \ddots & & \vdots & 0 \\ \vdots & \vdots & 0 & \ddots & \ddots & \vdots & \vdots \\ \vdots & \vdots & \vdots & \ddots & \ddots & 0 & 0 \\ f_{(n+2)1} & f_{(n+2)2} & 0 & \cdots & 0 & 1 & 0 \\ 1 & 0 & \cdots & \cdots & \cdots & 0 & -Z_{r(n+1)} \end{bmatrix} \begin{bmatrix} P_1 \\ V_1 \\ V_{r1} \\ \vdots \\ \vdots \\ V_{r(n+1)} \end{bmatrix}. \tag{5.14}$$

Now, the GRASB algorithm multiplies the last row in the enlarged matrix by $-1/Z_{r(n+1)}$ and uses that row to make the last cell values in the top two rows equate to zero. Thus, the enlarged matrix in equation (5.14) now has the same standardised format as (5.13).

5.2.4 General multiple radiation attached to a side-branch (GMRASB) algorithm

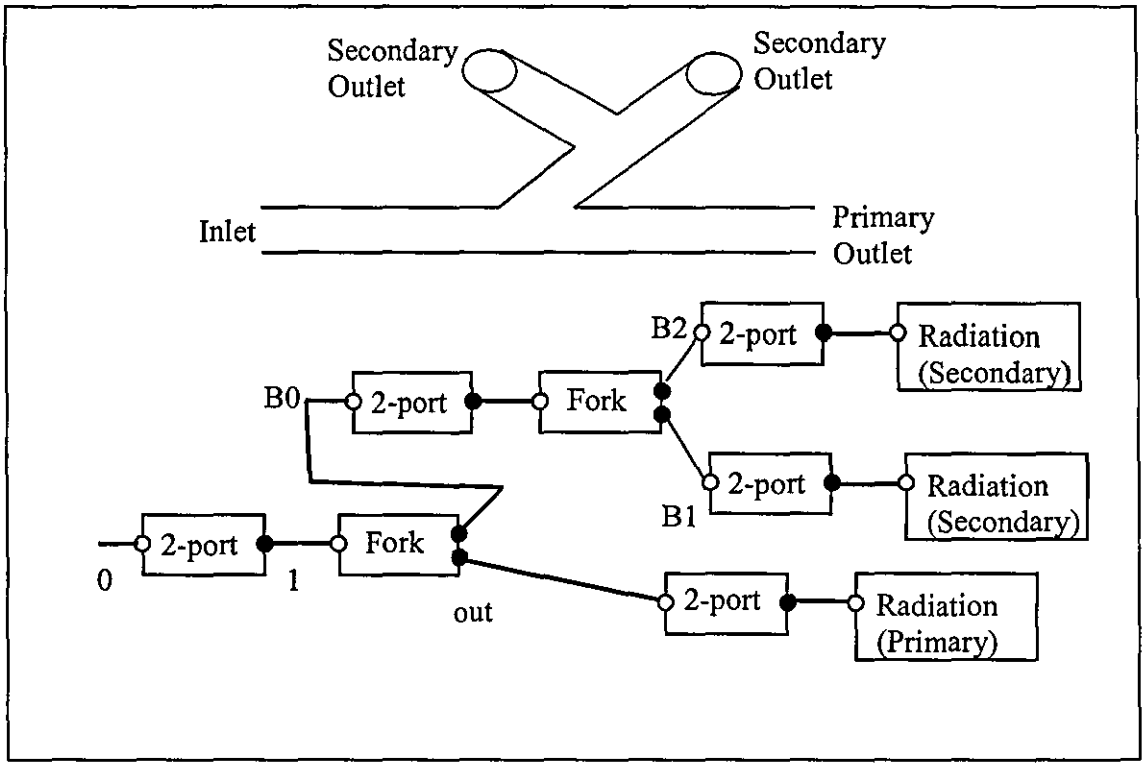

Figure 5. 3 Side-branch with multiple radiation points

The GRASB algorithm would not work if a side-branch had multiple, secondary radiation points, see Figure 5. 3. This could only occur following the GRASB algorithm. When a side-branch has multiple secondary radiation points, the impedance of the side-branch can always be obtained, provided that the radiation impedance at each point is known. Assume that such a side-branch exists with m number of secondary radiation points. Let point *B0* in this section represent the connection between a junction and the inlet of the

side-branch, where the junction has two outlets and one inlet. Let the first radiation point encountered along the side-branch be point *B1*. The whole side-branch can now be viewed as an effective two-port element from points *B0* to *B1* with m-1 secondary radiation points placed sequentially between the ports, such that an m+1 by m+1 transfer matrix can be written as

$$\begin{bmatrix} P_{B0} \\ V_{B0} \\ 0 \\ \vdots \\ 0 \end{bmatrix} = \begin{bmatrix} f_{11} & f_{12} & 0 & \cdots & \cdots & 0 \\ f_{21} & f_{22} & 0 & \cdots & \cdots & 0 \\ \vdots & \vdots & 1 & \ddots & & \vdots \\ \vdots & \vdots & 0 & \ddots & \ddots & \vdots \\ \vdots & \vdots & \vdots & \ddots & \ddots & 0 \\ f_{(m+1)1} & f_{(m+1)2} & 0 & \cdots & 0 & 1 \end{bmatrix} \begin{bmatrix} P_{B1} \\ V_{B1} \\ V_{B2} \\ \vdots \\ V_{Bm} \end{bmatrix}, \tag{5.15}$$

see Section 5.2.3. Now let point *B1* be a radiation point with known radiation impedance, $Z_{B1}=P_{B1}/V_{B1}$, such that equation (5.15) can be written as

$$\begin{bmatrix} P_{B0} \\ V_{B0} \\ 0 \\ \vdots \\ \vdots \\ 0 \end{bmatrix} = \begin{bmatrix} f_{11}Z_{B1}+f_{12} & 0 & \cdots & \cdots & 0 \\ \vdots & 0 & \cdots & \cdots & \vdots \\ \vdots & 1 & \ddots & & \vdots \\ \vdots & 0 & \ddots & \ddots & \vdots \\ \vdots & \vdots & \ddots & \ddots & 0 \\ f_{(m+1)1}Z_{B1}+f_{(m+1)2} & 0 & \cdots & 0 & 1 \end{bmatrix} \begin{bmatrix} V_{B1} \\ \vdots \\ \vdots \\ \vdots \\ V_{Bm} \end{bmatrix}. \tag{5.16}$$

Let the two-port element attached to the inlet of the junction, to which the side-branch is attached, have a transfer matrix of size (n+2) by (n+2), $n\geq 0$, where n represents the number of previous secondary radiation points, *A1* to *An*. Thus, the transfer matrix can be characterised by a standardised matrix, say

$$\begin{bmatrix} P_0 \\ V_0 \\ 0 \\ \vdots \\ 0 \end{bmatrix} = \begin{bmatrix} g_{11} & g_{12} & 0 & \cdots & \cdots & 0 \\ g_{21} & g_{22} & 0 & \cdots & \cdots & 0 \\ \vdots & \vdots & 1 & \ddots & & \vdots \\ \vdots & \vdots & 0 & \ddots & \ddots & \vdots \\ \vdots & \vdots & \vdots & \ddots & \ddots & 0 \\ g_{(n+2)1} & g_{(n+2)2} & 0 & \cdots & 0 & 1 \end{bmatrix} \begin{bmatrix} P_1 \\ V_1 \\ V_{A1} \\ \vdots \\ V_{An} \end{bmatrix}. \tag{5.17}$$

Points *0* and *1* represent the inlet and outlet of this two-port element respectively. All the pressures at a junction are constant, i.e. $P_1=P_{B0}=P_{out}$, where P_{out} is the pressure at the remaining outlet of the junction. Also, the sum of acoustic mass velocity into the junction is equal to the sum out, $V_1=V_{B0}+V_{out}$, thus, a matrix adaptation to the one in equation (5.17) using equation (5.16) can occur.

The GMRASB algorithm firstly enlarges the matrix in equation (5.17) by m columns and rows. Then, the algorithm sets the first cell value in rows n+3 to n+m+2 to 1. Finally it calculates the ratios between P_{B0} and V_{B1} to V_{BM}, see equation (5.16), and inserts them into the enlarged matrix

$$\begin{bmatrix} P_0 \\ V_0 \\ 0 \\ \vdots \\ \vdots \\ \vdots \\ \vdots \\ \vdots \\ 0 \end{bmatrix} = \begin{bmatrix} g_{11} & g_{12} & 0 & \cdots & \cdots & \cdots & \cdots & \cdots & \cdots & 0 & g_{12} \\ \vdots & g_{11} & 0 & \cdots & \cdots & \cdots & \cdots & \cdots & \cdots & 0 & g_{22} \\ \vdots & g_{12} & 1 & 0 & \cdots & \cdots & \cdots & \cdots & \cdots & 0 & 0 \\ \vdots & \vdots & 0 & \ddots & \ddots & & & & & 0 & \vdots \\ \vdots & \vdots & \vdots & \ddots & \ddots & \ddots & & & & & \vdots \\ g_{(n+2)1} & g_{(n+2)2} & 0 & \cdots & 0 & 1 & 0 & \cdots & \cdots & 0 & 0 \\ 1 & 0 & \cdots & & \cdots & 0 & -\dfrac{f_{11}Z_1+f_{12}}{f_{21}Z_1+f_{22}} & 0 & \cdots & \cdots & 0 \\ \vdots & \vdots & & & & & 0 & \dfrac{f_{11}Z_1+f_{12}}{f_{31}Z_1+f_{32}} & 0 & \cdots & 0 \\ \vdots & \vdots & & & & & \vdots & \ddots & \ddots & \ddots & \vdots \\ \vdots & \vdots & & & & & \vdots & & \ddots & \ddots & 0 \\ 1 & 0 & \cdots & \cdots & \cdots & \cdots & 0 & \cdots & \cdots & 0 & \dfrac{f_{11}Z_1+f_{12}}{f_{(m+2)1}Z_1+f_{(m+2)2}} \end{bmatrix} \begin{bmatrix} P_{out} \\ V_{out} \\ V_{A1} \\ \vdots \\ V_{An} \\ V_{B1} \\ \vdots \\ \vdots \\ V_{Bm} \end{bmatrix}. \tag{5.18}$$

Equation (5.2) and Section 5.2.2 describes how to obtain the impedance of a side-branch. The coefficients in the rows n+3 to n+m+2 are obtained through the same methodology. An example of this is as follows, the first row in equation (5.16) states

$$P_{B0} = (f_{11} Z_{B1} + f_{12}) V_{B1} \tag{5.19}$$

and the third row states that

$$0 = (f_{31} Z_{B1} + f_3) V_{B1} + V_{B3}. \tag{5.20}$$

Thus, since P_{out}=P_{B0},

$$P_{out} = -\frac{f_{11} Z_{B1} + f_{12}}{f_{31} Z_{B1} + f_{13}} V_{B3}. \tag{5.21}$$

Equation (5.21) constitutes row n+3 in the matrix equation (5.18). Now, as with the GRASB algorithm, the GMRASB algorithm rewrites the matrix in equation (5.18) in the standardised form. This is achieved by multiplying the last row by the inverse of the diagonal component, i.e. the last cell value, then using that row in row operations on rows 1 and 2 to make the last $(n+m+2)^{th}$ cells equate to zero. Lastly, the GMRASB algorithm multiplies rows n+3 to n+m+1 by the inverse of the respective diagonal cell values. Hence, equation (5.18) can be written as a (n+m+2) by (n+m+2) transfer matrix in standardised form.

Consider the entire network in Figure 5. 2 to be a side-branch, such that the primary radiation must now be considered as another secondary radiation. Thus, the GMRASB algorithm would be used to reduce the acoustic relationship of the side-branch into a matrix associated with the two-port element. This element would be connected to the inlet of a three port junction.

5.2.5 General matrix multiplication concerned with radiations (GMMR) algorithm

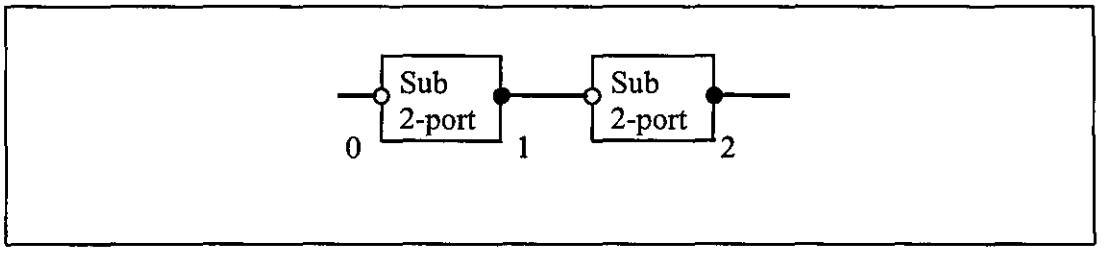

Figure 5. 4 Two consecutively sequenced sub-systems

GRASB and GMRASB algorithms have been concerned with adapting transfer matrices associated with a two-port element, which is immediately prior to a side-branch. In contrast the GMMR algorithm focuses on the reduction of transfer matrices associated with consecutively sequenced sub two-port elements, see Figure 5. 4, that have associated matrices of varying sizes due to the occurrence of radiation points. Consider any two sub-systems which have any number of secondary radiation elements, say m and n, that are connected together. Each sub-system can be represented in the general transfer matrix standardised form. The first is a m+2 by m+2 matrix

$$\begin{bmatrix} P_0 \\ V_0 \\ 0 \\ \vdots \\ \vdots \\ 0 \end{bmatrix} = \begin{bmatrix} e_{11} & e_{12} & 0 & \cdots & \cdots & 0 \\ \vdots & \vdots & 0 & \cdots & \cdots & 0 \\ \vdots & \vdots & 1 & \ddots & & \vdots \\ \vdots & \vdots & 0 & \ddots & \ddots & \vdots \\ \vdots & \vdots & \vdots & \ddots & \ddots & 0 \\ e_{(m+2)1} & e_{(m+2)2} & 0 & \cdots & 0 & 1 \end{bmatrix} \begin{bmatrix} P_1 \\ V_1 \\ V_{A1} \\ \vdots \\ \vdots \\ V_{Am} \end{bmatrix}, \tag{5.22}$$

where V_{A1} to V_{Am} are the velocities associated with secondary radiation points for this first sub-system. Likewise there will be a n+2 by n+2 matrix,

$$\begin{bmatrix} P_1 \\ V_1 \\ 0 \\ \vdots \\ \vdots \\ 0 \end{bmatrix} = \begin{bmatrix} g_{11} & g_{12} & 0 & \cdots & \cdots & 0 \\ \vdots & \vdots & 0 & \cdots & \cdots & 0 \\ \vdots & \vdots & 1 & \ddots & & \vdots \\ \vdots & \vdots & 0 & \ddots & \ddots & \vdots \\ \vdots & \vdots & \vdots & \ddots & \ddots & 0 \\ g_{(n+2)1} & g_{(n+2)2} & 0 & \cdots & 0 & 1 \end{bmatrix} \begin{bmatrix} P_2 \\ V_2 \\ V_{B1} \\ \vdots \\ \vdots \\ V_{Bn} \end{bmatrix}, \tag{5.23}$$

where V_{B1} to V_{Bn} are the velocities associated with secondary radiation points for the second sub-system.

Now, every pressure and acoustic mass velocity within the first sub-system is known in terms of P_1 and V_1. Equation (5.23) has a simple relationship for P_1 and V_1 in terms P_2 and V_2. The GMMR algorithm combines equations (5.22) and (5.23), thus eliminating variables P_1 and V_1. The algorithm first creates a null matrix of size $m+n+2$ by $m+n+2$. In the first $m+2$ rows, each row r is written with the first two columns as $e_{r1}g_{11}+e_{r2}g_{21}$ and $e_{r1}g_{21}+e_{r2}g_{22}$ respectively, to eliminate P_1 and V_1. The first two columns of the second matrix are copied straight into the last n rows of the enlarged matrix. Lastly, the GMMR algorithm inserts the value 1 into the diagonal components of the enlarged matrix, except for the top two rows. Hence

$$\begin{bmatrix} P_0 \\ V_0 \\ 0 \\ \vdots \\ \vdots \\ \vdots \\ \vdots \\ \vdots \\ \vdots \\ 0 \end{bmatrix} = \begin{bmatrix} e_{11}g_{11}+e_{12}g_{21} & e_{11}g_{12}+e_{12}g_{22} & 0 & \cdots & \cdots & \cdots & \cdots & \cdots & \cdots & 0 \\ e_{21}g_{11}+e_{22}g_{21} & e_{21}g_{12}+e_{22}g_{22} & 0 & \cdots & \cdots & \cdots & \cdots & \cdots & \cdots & 0 \\ \vdots & \vdots & 1 & \ddots & & & & & & \vdots \\ \vdots & \vdots & 0 & \ddots & \ddots & & & & & \vdots \\ \vdots & \vdots & \vdots & \ddots & \ddots & \ddots & & & & \vdots \\ e_{(m+2)1}g_{11}+e_{(m+2)2}g_{21} & e_{(m+2)1}g_{12}+e_{(m+2)2}g_{22} & \vdots & & \ddots & \ddots & \ddots & & & \vdots \\ g_{13} & g_{23} & \vdots & & & \ddots & \ddots & \ddots & & \vdots \\ \vdots & \vdots & \vdots & & & & \ddots & \ddots & \ddots & \vdots \\ \vdots & \vdots & \vdots & & & & & \ddots & \ddots & 0 \\ g_{1(n+2)} & g_{2(n+2)} & 0 & \cdots & \cdots & \cdots & \cdots & \cdots & 0 & 1 \end{bmatrix} \begin{bmatrix} P_2 \\ V_2 \\ V_{A1} \\ \vdots \\ \vdots \\ V_{Am} \\ V_{B1} \\ \vdots \\ \vdots \\ V_{Bn} \end{bmatrix}, \tag{5.24}$$

describes the relationship between all the points, i.e. inlet, outlet and secondary radiation, via a standardised transfer matrix.

The GMMR algorithm is also used immediately after the GRASB or GMRASB algorithm. An example of this occurs when a transfer matrix relationship between points *0* and *4* are known, see equations (5.6) and Figure 5. 2. Thus, a relationship between points *0* and *5* needs to be acquired. The resultant equation (5.11) is seen to be exactly as gained by the general GMMR algorithm.

5.2.6 A radiation point located in nested parallel paths

The procedures for analysis work well when secondary radiation elements, separated by two-port and fork elements, are in a consecutively sequenced order, see Sections 5.2.2 to 5.2.5. However, there is no guarantee that this will be so. Thus, the algorithm must have the capability to analyse any general silencer system that includes any number of non-primary radiation points placed anywhere within the system. An example of a non-primary radiation point which is not sequenced consecutively is illustrated in the two-pass, twin exhaust silencer box of Figure 5. 5.

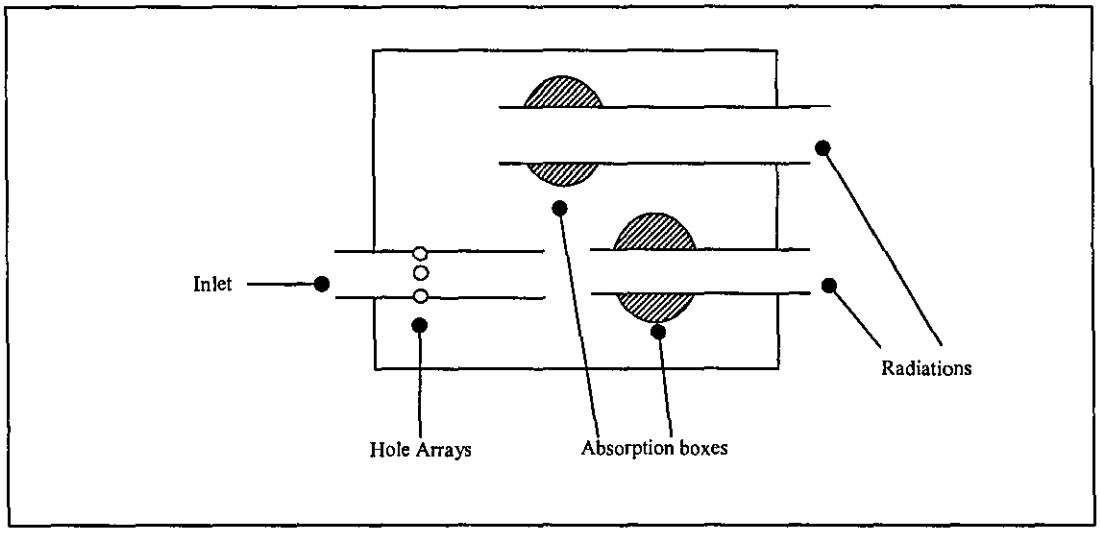

Figure 5. 5 Silencer with twin radiations

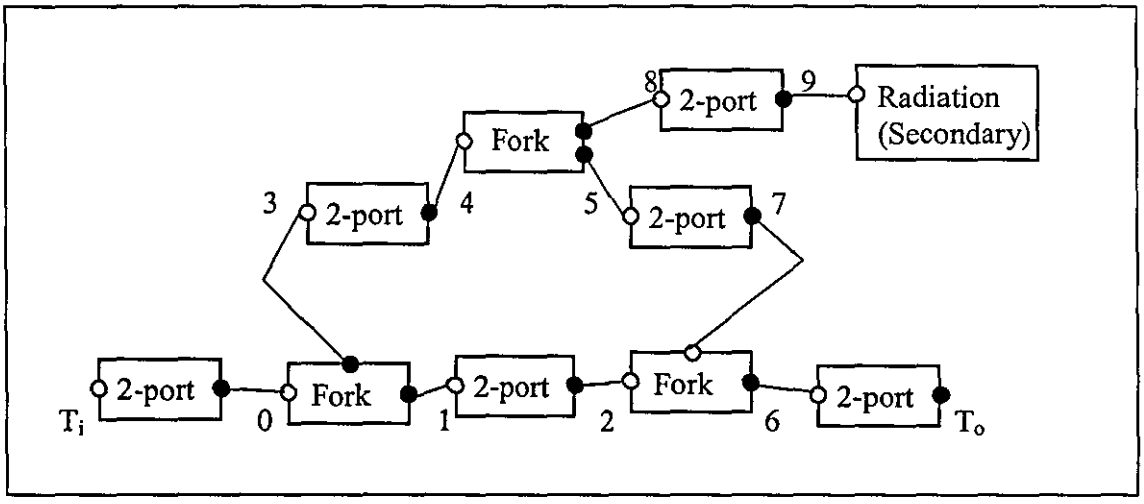

Figure 5. 6 A non-primary radiation located within a Quincke tube system

When all the initial sub-systems of this example have been reduced to equivalent two-port elements, see Chapter 2, then the system is similar to a Quincke tube one, as shown in Figure 5. 6.

5.2.7 General reduction concerned with radiations (GRR) algorithm

The path fraction analysis for such a system as in Figure 5. 6 is exactly the same as in Section 2.5.2, see Sections 2.5.4 and 5.2.2. Therefore, this section concentrates on creating a sub-system reduction matrix that can reduce any sub-system with any number of secondary radiation points, see Section 2.7. Consider the system in Figure 5. 6, but in order to add generality, let there be any number, *m*, of secondary radiation points between points *3* and *7*. Hence

$$\begin{bmatrix} P_3 \\ V_3 \\ 0 \\ \vdots \\ 0 \end{bmatrix} = \begin{bmatrix} g_{11} & g_{12} & 0 & \cdots & \cdots & 0 \\ g_{21} & g_{22} & 0 & \cdots & \cdots & 0 \\ \vdots & \vdots & 1 & \ddots & & \vdots \\ \vdots & \vdots & 0 & \ddots & \ddots & \vdots \\ \vdots & \vdots & \vdots & \ddots & \ddots & 0 \\ g_{(m+2)1} & g_{(m+2)2} & 0 & \cdots & 0 & 1 \end{bmatrix} \begin{bmatrix} P_7 \\ V_7 \\ V_{B1} \\ \vdots \\ V_{Bm} \end{bmatrix}, \tag{5.25}$$

where V_{B1} to V_{Bm} represent the velocities associated with the secondary radiation points.

The GRR algorithm re-writes the transfer matrices within the sub-system as in Section 2.2.2. An example of this re-writing of two-by-two transfer matrices is illustrated by the relationship between points *1* and *2*, with respect to Figure 5. 6. The pressures and acoustic mass velocities are ordinarily related as

$$\begin{bmatrix} P_1 \\ V_1 \end{bmatrix} = \begin{bmatrix} f_{11} & f_{12} \\ f_{12} & f_{22} \end{bmatrix} \begin{bmatrix} P_2 \\ V_2 \end{bmatrix}. \tag{5.26}$$

However, this can be re-written as

$$\begin{bmatrix} 0 \\ 0 \end{bmatrix} = \begin{bmatrix} -1 & 0 & f_{11} & f_{12} \\ 0 & -1 & f_{21} & f_{22} \end{bmatrix} \begin{bmatrix} P_1 \\ V_1 \\ P_2 \\ V_2 \end{bmatrix}. \tag{5.27}$$

Likewise the general, standardised transfer matrices as in equation (5.25) can be re-written as

$$\begin{bmatrix} 0 \\ \vdots \\ \vdots \\ \vdots \\ \vdots \\ 0 \end{bmatrix} = \begin{bmatrix} -1 & 0 & g_{11} & g_{12} & 0 & \cdots & \cdots & 0 \\ 0 & -1 & g_{21} & g_{22} & 0 & \cdots & \cdots & 0 \\ 0 & 0 & \vdots & \vdots & 1 & \ddots & & \vdots \\ \vdots & \vdots & \vdots & \vdots & 0 & \ddots & \ddots & \vdots \\ \vdots & \vdots & \vdots & \vdots & \vdots & \ddots & \ddots & 0 \\ 0 & 0 & g_{(m+2)1} & g_{(m+2)2} & 0 & \cdots & 0 & 1 \end{bmatrix} \begin{bmatrix} P_3 \\ V_3 \\ V_7 \\ V_{B1} \\ \vdots \\ \vdots \\ V_{Bm} \end{bmatrix}. \tag{5.28}$$

Thus, equations (5.27) and (5.28) can be placed into an enlarged matrix using the knowledge that the pressures at a junction are constant and the sum of acoustic mass velocities into the junction are equal to the sum of those out, such that

$$\begin{bmatrix} 0 \\ \vdots \\ \vdots \\ \vdots \\ \vdots \\ \vdots \\ \vdots \\ \vdots \\ \vdots \\ \vdots \\ \vdots \\ 0 \end{bmatrix} = \begin{bmatrix} -1 & 0 & f_{11} & f_{12} & 0 & 0 & 0 & 0 & 0 & 0 & \cdots & 0 & 0 & 0 & 0 & 0 \\ 0 & -1 & f_{21} & f_{22} & 0 & 0 & 0 & 0 & 0 & 0 & \cdots & 0 & 0 & 0 & 0 & 0 \\ 0 & 0 & 0 & 0 & -1 & 0 & g_{11} & g_{12} & 0 & 0 & \cdots & 0 & 0 & 0 & 0 & 0 \\ 0 & 0 & 0 & 0 & 0 & -1 & g_{21} & g_{22} & 0 & 0 & \cdots & 0 & 0 & 0 & 0 & 0 \\ \vdots & \vdots & \vdots & \vdots & \vdots & 0 & \vdots & g_{32} & 1 & \ddots & & \vdots & \vdots & \vdots & \vdots & \vdots \\ \vdots & \vdots & \vdots & \vdots & \vdots & \vdots & \vdots & \vdots & 0 & \ddots & \ddots & \vdots & \vdots & \vdots & \vdots & \vdots \\ \vdots & \vdots & \vdots & \vdots & \vdots & \vdots & \vdots & \vdots & \vdots & \ddots & \ddots & 0 & \vdots & \vdots & \vdots & \vdots \\ 0 & 0 & 0 & 0 & 0 & 0 & g_{(m+2)1} & g_{(m+2)2} & 0 & \cdots & 0 & 1 & 0 & 0 & 0 & 0 \\ -1 & 0 & 0 & 0 & 1 & 0 & 0 & 0 & 0 & \cdots & 0 & 0 & 0 & 0 & 0 & 0 \\ 0 & 0 & 0 & 0 & -1 & 0 & 0 & 0 & 0 & \cdots & 0 & 0 & 1 & 0 & 0 & 0 \\ 0 & 1 & 0 & 0 & 0 & 1 & 0 & 0 & 0 & \cdots & 0 & 0 & 0 & -1 & 0 & 0 \\ 0 & 0 & -1 & 0 & 0 & 0 & 1 & 0 & 0 & \cdots & 0 & 0 & 0 & 0 & 0 & 0 \\ 0 & 0 & 0 & 0 & 0 & 0 & -1 & 0 & 0 & \cdots & 0 & 0 & 0 & 0 & 1 & 0 \\ 0 & 0 & 0 & -1 & 0 & 0 & 0 & -1 & 0 & \cdots & 0 & 0 & 0 & 0 & 0 & 1 \end{bmatrix} \begin{bmatrix} P_1 \\ V_1 \\ P_2 \\ V_2 \\ P_3 \\ V_3 \\ P_7 \\ P_7 \\ V_{B1} \\ \vdots \\ V_{Bm} \\ P_0 \\ V_0 \\ P_6 \\ V_6 \end{bmatrix}. \tag{5.29}$$

The rows and columns are re-ordered such that the equations that relate the velocities associated with the secondary radiations, V_{B1} to V_{Bm}, are moved towards the bottom of the matrix and these variables occur at the bottom of the full vector of variables. Also, the P_0 and V_0 are expressed on the left hand side of the equals sign, with regards to equation (5.29). Thus,

$$\begin{bmatrix} 0 \\ \vdots \\ \vdots \\ \vdots \\ \vdots \\ \vdots \\ \vdots \\ \vdots \\ P_0 \\ V_0 \\ 0 \\ \vdots \\ \vdots \\ 0 \end{bmatrix} = \begin{bmatrix} -1 & 0 & f_{11} & f_{12} & 0 & 0 & 0 & 0 & 0 & 0 & 0 & \cdots & \cdots & 0 \\ 0 & -1 & f_{21} & f_{22} & 0 & 0 & 0 & 0 & 0 & 0 & 0 & \cdots & \cdots & 0 \\ 0 & 0 & 0 & 0 & -1 & 0 & g_{11} & g_{12} & 0 & 0 & 0 & \cdots & \cdots & 0 \\ 0 & 0 & 0 & 0 & 0 & -1 & g_{21} & g_{22} & 0 & 0 & 0 & \cdots & \cdots & 0 \\ 1 & 0 & 0 & 0 & -1 & 0 & 0 & 0 & 0 & 0 & 0 & \cdots & \cdots & 0 \\ 0 & 0 & 1 & 0 & 0 & 0 & -1 & 0 & 0 & 0 & 0 & \cdots & \cdots & 0 \\ 0 & 0 & 0 & 0 & 0 & 0 & 1 & 0 & 1 & 0 & 0 & \cdots & \cdots & 0 \\ 0 & 0 & 0 & -1 & 0 & 0 & 0 & -1 & 0 & 1 & 0 & \cdots & \cdots & 0 \\ 1 & 0 & 0 & 0 & 0 & 0 & 0 & 0 & 0 & 0 & 0 & \cdots & \cdots & 0 \\ 0 & 1 & 0 & 0 & 1 & 0 & 0 & 0 & 0 & 0 & 0 & \cdots & \cdots & 0 \\ 0 & 0 & 0 & 0 & 0 & 0 & g_{31} & g_{32} & 0 & 0 & 1 & \ddots & & \vdots \\ \vdots & \vdots & \vdots & \vdots & \vdots & \vdots & \vdots & \vdots & \vdots & \vdots & 0 & \ddots & \ddots & \vdots \\ \vdots & \vdots & \vdots & \vdots & \vdots & \vdots & \vdots & \vdots & \vdots & \vdots & \vdots & \ddots & \ddots & 0 \\ 0 & 0 & 0 & 0 & 0 & 0 & g_{(m+2)1} & g_{(m+2)2} & 0 & 0 & 0 & \cdots & 0 & 1 \end{bmatrix} \begin{bmatrix} P_1 \\ V_1 \\ P_2 \\ V_2 \\ P_3 \\ V_3 \\ P_7 \\ V_7 \\ P_6 \\ V_6 \\ V_{B1} \\ \vdots \\ V_{Bm} \end{bmatrix}$$

(5.30)

represents a reduction matrix that can be manipulated by row operations to produce a standardised transfer matrix relating P_0, V_0 to P_6, V_6 and V_{B1} to V_{Bm}. Hence, the GRR algorithm produces a reduction matrix similar to the one in equation (5.30) for any sub-system. If a sub-system has one sub two-port element, with an associated transfer matrix that has a size of m+2 by m+2, a reduction matrix can be formed. Thus, for any sub-system with any number of two-port elements with transfer matrices of varying sizes, one can create a reduction matrix. Consider a general reduction matrix with m secondary radiations that connects n+1 ports, where *0* is the inlet port and n is the outlet port. The matrix will have a size N=2n+m by N

$$\begin{bmatrix} 0 \\ \vdots \\ 0 \\ P_0 \\ V_0 \\ 0 \\ \vdots \\ 0 \end{bmatrix} = \begin{bmatrix} h_{11} & \cdots & \cdots & \cdots & \cdots & \cdots & \cdots & h_{N1} \\ \vdots & & & & & & & \vdots \\ \vdots & & & & & & & \vdots \\ h_{(N-m-1)1} & \cdots & \cdots & \cdots & \cdots & \cdots & \cdots & h_{N(N-m-1)} \\ h_{(N-m)1} & \cdots & \cdots & \cdots & \cdots & \cdots & \cdots & h_{N(N-m)} \\ h_{(N-m+1)1} & \cdots & \cdots & \cdots & \cdots & \cdots & \cdots & h_{N(N-m+1)} \\ \vdots & & & & & & & \vdots \\ h_{N1} & \cdots & \cdots & \cdots & \cdots & \cdots & \cdots & h_{NN} \end{bmatrix} \begin{bmatrix} P_1 \\ V_1 \\ \vdots \\ P_n \\ V_n \\ V_{B1} \\ \vdots \\ V_{Bm} \end{bmatrix}. \qquad (5.31)$$

Therefore, the final step is to find an m+2 by m+2 transfer matrix relationship between P_0, V_0 and P_n, V_n, V_{B1} to V_{Bm} by row operations. This can always be achieved since the variables of each inlet and outlet of the sub-system only appear once, each in a separate equation. This final step of matrix manipulation starts with finding the maximum value within the first N-m-2 rows in the first column. Let the largest value be in row 4, say $h_{4,1}$; now interchange rows 4 and 1. This partial pivoting is vitally important as many of the coefficients are zero. The last 2+m rows in equation (5.31) cannot be interchanged. The factors within row 1 are now subtracted from rows 2 to N to force the coefficients in the first column of these row to have the value zero. This is the Gauss-Jordan method with partial pivoting. The method is repeated in column 2 to force the coefficients in rows 3 to N to equal zero, this is repeated until column N-m-2 is reached. The method is general and will work on any square matrix which describes a sub-system with a single inlet and multiple outlets.

$$\begin{bmatrix} 0 \\ \vdots \\ 0 \\ P_0 \\ V_0 \\ 0 \\ \vdots \\ 0 \end{bmatrix} = \begin{bmatrix} h'_{11} & \cdots & \cdots & & \cdots & & \cdots & \cdots & h'_{1N} \\ 0 & \ddots & & & & & & & \vdots \\ \vdots & \ddots & \ddots & & & & & & \vdots \\ \vdots & & 0 & h'_{(N-m)(N-m-1)} & \cdots & \cdots & \cdots & h'_{(N-m)N} \\ \vdots & & \vdots & \vdots & & & & \vdots \\ \vdots & & \vdots & \vdots & & & & \vdots \\ \vdots & & \vdots & \vdots & & & & \vdots \\ 0 & \cdots & 0 & h'_{N(N-m-1)} & \cdots & \cdots & \cdots & h'_{NN} \end{bmatrix} \begin{bmatrix} P_1 \\ V_1 \\ \vdots \\ P_n \\ V_n \\ V_{B1} \\ \vdots \\ V_{Bm} \end{bmatrix}. \qquad (5.32)$$

The last m+2 rows can now be used to create the required m+2 by m+2 transfer matrix,

$$\begin{bmatrix} P_0 \\ V_0 \\ 0 \\ \vdots \\ 0 \end{bmatrix} = \begin{bmatrix} h'_{(N-m)(N-m-1)} & \cdots & \cdots & \cdots & h'_{(N-m)N} \\ \vdots & & & & \vdots \\ \vdots & & & & \vdots \\ \vdots & & & & \vdots \\ h'_{N(N-m-1)} & \cdots & \cdots & \cdots & h'_{NN} \end{bmatrix} \begin{bmatrix} P_n \\ V_n \\ V_{B1} \\ \vdots \\ V_{Bm} \end{bmatrix}. \tag{5.33}$$

Thus, as in Section 5.2.3 and 5.2.4, a standardised transfer matrix can be obtained using row operations.

This implies that the whole sub-system can be modelled as a sub two-port element consisting of a 2+m by 2+m transfer matrix. Hence, sequential multiplication of transfer matrices either side of the sub-system can occur. As a result of the ability to include non-primary radiations within any general reduction technique of sub-systems, any exhaust system which consists of multiple tailpipes can be reduced, such as the example shown in Figure 5. 5.

5.3 Multiple radiation points with multiple time-variant sources

5.3.1 Exhaust systems without a balance pipe

The obvious progression in software capability from Section 5.2.1 is to include multiple, time-variant source interaction with multiple radiation points, for example, the system shown in Figure 5. 7. Although the example in this section considers a manifold/exhaust system with twin outlets, the algorithm and generality of the code are such that general multiple radiations can be analysed. The source model presented in Chapter 3 enables the interaction between multiple, time-variant sources to be characterized by one matrix

equation that relates the acoustic variables at the outlet of the manifold, 'Point m'. Thus, if $\{\mathbf{v}\}_m$ defines the acoustic mass velocity vector out of the junction indicated on Figure 5. 7 towards the exhaust, then

$$\{\mathbf{v}\}_m = [\mathbf{G}]_m \{\mathbf{S}\}_m + [\mathbf{H}]_m \{\mathbf{P}\}_m, \tag{5.34}$$

see equations (3.40) to (3.51). A silencer system which has multiple radiation points can always be reduced to a (r+1) by (r+1) transfer matrix for a single frequency, where r is the total number of radiation points.

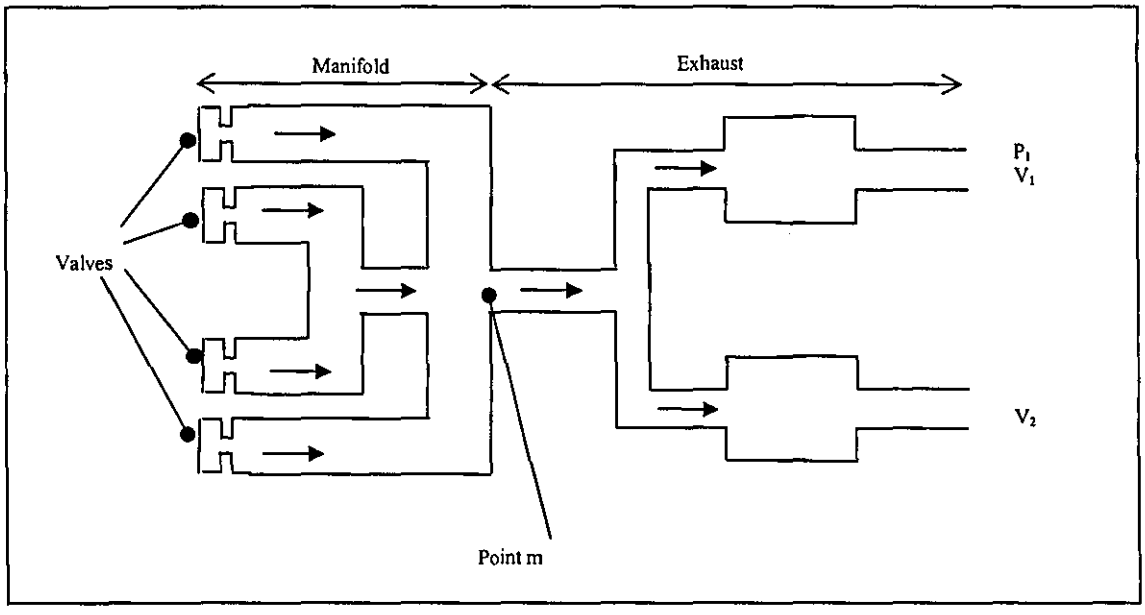

Figure 5. 7 Multiple inlets and outlets

Hence, in this example, the acoustic variables at 'Point m' can be related to those at the radiation points, at an individual frequency, say ω, by a standardised three by three transfer matrix

$$\begin{bmatrix} P_{m_o} \\ V_{m_o} \\ 0 \end{bmatrix}_\omega = \begin{bmatrix} a & b & 0 \\ d & e & 0 \\ g & h & 1 \end{bmatrix}_\omega \begin{bmatrix} P_1 \\ V_1 \\ V_2 \end{bmatrix}_\omega . \tag{5.35}$$

A similar relationship can be gained for each frequency from $-\omega N$ to ωN in frequency steps of ω, where N is the number of harmonics. Therefore, as in Chapter 3, the coefficients in equation (5.35) can each be inserted into a square diagonal matrix, for example

$$[\mathbf{a}]=\begin{bmatrix} a_{-N} & \dots & 0 & \dots & 0 \\ \dots & \dots & \dots & \dots & \dots \\ 0 & \dots & a_0 & \dots & 0 \\ \dots & \dots & \dots & \dots & \dots \\ 0 & \dots & 0 & \dots & a_N \end{bmatrix}, \tag{5.36}$$

referred to as a coefficient matrix.

Therefore, a relationship between the acoustic variables at 'Point m' and those at the primary radiation point can be acquired in conjunction with equations (3.24) to (3.33), (5.35) and (5.36),

$$\{\mathbf{v}\}_1 = ([\mathbf{e}]-[\mathbf{H}]_m[\mathbf{b}])^{-1}[\mathbf{G}]_m\{\mathbf{S}\}_m + ([\mathbf{e}]-[\mathbf{H}]_m[\mathbf{b}])^{-1}([\mathbf{H}]_m[\mathbf{a}]-[\mathbf{d}])\{\mathbf{P}\}_1, \tag{5.37}$$

see Section 3.2.3. Now, let

$$[\mathbf{H}]_1=([\mathbf{e}]-[\mathbf{H}]_m[\mathbf{b}])^{-1}([\mathbf{H}]_m[\mathbf{a}]-[\mathbf{d}]) \tag{5.38}$$

and

$$[\mathbf{G}]_1 = ([\mathbf{e}]-[\mathbf{H}]_m[\mathbf{b}])^{-1}[\mathbf{G}]_m, \tag{5.39}$$

then

$$\{\mathbf{v}\}_1 = [\mathbf{G}]_1\{\mathbf{S}\}_m + [\mathbf{H}]_1\{\mathbf{P}\}_1. \tag{5.40}$$

The radiation impedance at an individual frequency is calculable and can be expressed as a diagonal square matrix similar to equation (5.36). Each radiation point has an individual diagonal impedance matrix denoted by the subscript. Therefore, the system shown in Figure 5. 7 has two matrices $[\mathbf{Z}]_1$ and $[\mathbf{Z}]_2$. These impedance matrices can be used to evaluate $\{\mathbf{v}\}_1$ by using

$$\{\mathbf{P}\} = [\mathbf{Z}]\{\mathbf{v}\} \tag{5.41}$$

in conjunction with equation (5.40) to find the primary velocity vector

$$\{\mathbf{v}\}_1 = ([\mathbf{I}] - [\mathbf{H}]_1[\mathbf{Z}]_1)^{-1}[\mathbf{G}]_1\{\mathbf{S}\}_m. \tag{5.42}$$

Now, the link equation that appears for all frequencies in equation (5.35) allows a subsequent matrix equation to be formed

$$0 = [\mathbf{g}]\{\mathbf{P}\}_1 + [\mathbf{h}]\{\mathbf{v}\}_1 + \{\mathbf{v}\}_2, \tag{5.43}$$

alternatively

$$\{\mathbf{v}\}_1 = -[\mathbf{h}]^{-1}[\mathbf{g}]\{\mathbf{P}\}_1 - [\mathbf{h}]^{-1}\{\mathbf{v}\}_2. \tag{5.44}$$

Equation (5.44) can be written in a general format by letting

$$[\mathbf{H}]_{1R_1} = -[\mathbf{h}]^{-1}[\mathbf{g}] \tag{5.45}$$

and

$$[\mathbf{J}]_{IR_1} = -[\mathbf{h}]^{-1}, \tag{5.46}$$

where R_1 relates to the first radiation equation connecting the primary radiation point to the first secondary radiation. These equations will be termed as connection equations. This allows a general matrix equation connection from the primary radiation pressure and velocity to the non-primary velocity vectors, hence the connection equation is

$$\{\mathbf{v}\}_1 = [\mathbf{H}]_{IR_1}\{\mathbf{P}\}_1 + [\mathbf{J}]_{IR_1}\{\mathbf{v}\}_2. \tag{5.47}$$

The evaluated primary vector can be used with equation (5.42) at the connection equation (5.48) to evaluate non-primary velocity vectors,

$$\{\mathbf{v}\}_2 = [\mathbf{J}]^{-1}_{IR_1}\left([\mathbf{I}] - [\mathbf{H}]_{IR_1}[\mathbf{Z}]_1\right)\{\mathbf{v}\}_1. \tag{5.48}$$

Now $\{\mathbf{v}\}_2$ is known, $\{\mathbf{P}\}_2$ can be evaluated by

$$\{\mathbf{P}\}_2 = [\mathbf{Z}]_2\{\mathbf{v}\}_2. \tag{5.49}$$

The process of using a set of three-by-three transfer matrices to acquire velocity vectors at V_1 and V_2, with respect to Figure 5. 7, is essentially that of moving along one sub two-port element. This can be achieved as the secondary radiation can be modelled as a termination/closed end with a connection equation joining the radiations. However, the example in Figure 5. 7 is simple, as the valves all converge to a single junction/fork at 'Point m' and the exhaust has a sole inlet. Equations (5.34) to (5.49) explain essentially how to progress to a general matrix equation, that encompasses time-variant properties, in order to obtain the velocity vectors at all the radiation points.

The same methodology as described through the equation steps (5.34) to (5.49) can be applied to manifold/exhaust systems with any number of radiation points.

5.3.2 Exhaust systems with a balance pipe

A schematic of the most complex manifold/exhaust system that has a balance pipe and is produced commercially is shown in Figure 5. 8. Manifold and exhaust designs that have a balance pipe consist of two separate systems which each involve a valve bank, manifold and an exhaust. These systems are connected by a balance pipe to maximise the cancellation of out-of-phase pressure pulses in each system, thus reducing noise. This section considers the system within the Figure 5. 8 and demonstrates the new matrix manipulation that is needed to model a balance pipe. The additional algorithmic process is kept general, but is not created for any general system with any number of balance pipes. There is no fundamental change to the hybrid algorithm concerned with sub-system reduction and the matrix manipulation of general equations that describe time-variant sources. The only change occurs when general equations that describe multiple, time-variant, source behaviour at the inlet of a junction are combined into a single, general equation; this happens when one or more of the general equations have an associated connection equation.

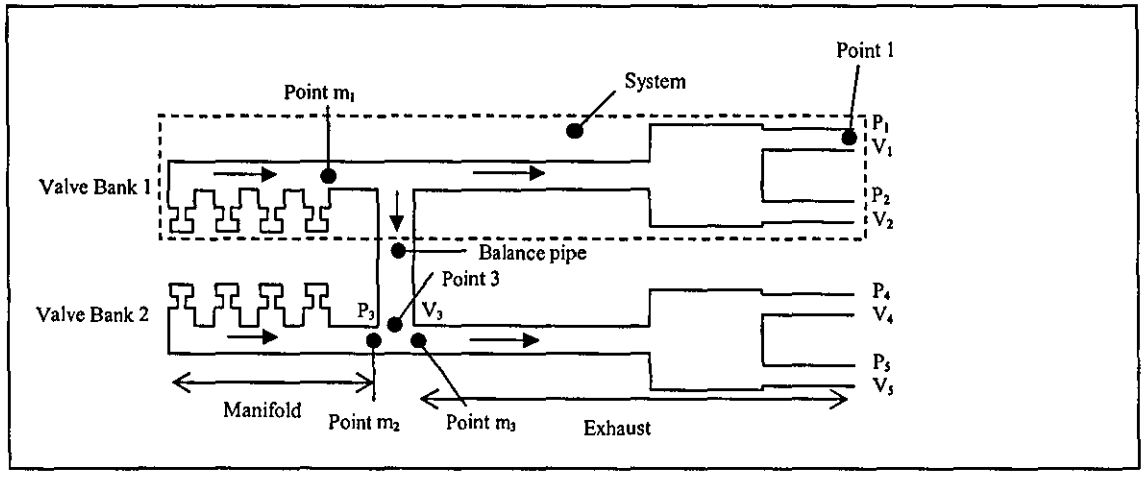

Figure 5. 8 Balance pipe interactions

Section 5.3.1 focused on systems without a balance pipe, but multiple radiations. This involved adapting the link equations once all the time-variant sources have been expressed through a single, general equation, see equations (3.29) and (5.40). Now, a

balance pipe can be modelled as a general pipe which is described generally by a two-by-two transfer matrix. Thus, an exhaust system with a balance pipe can be modelled by standardised transfer matrices. The problem associated with analysing systems that have a balance pipe occurs at junctions where two or more general equations need to be combined into one equation, see Section 3.3.

The equations in Chapter 3 explain how a group of time-varying valves can be characterized by a matrix equation, see the general format in equation (5.34). Also secondary radiations can be characterized as a termination/closed end. Therefore, the system between 'Point m_1' and P_1, V_1, P_2, V_2, P_3 and V_3, with respect to Figure 5. 8, can be characterized as a standardised transfer matrix which has two link equations and is simplified to

$$\begin{bmatrix} P_{m_1} \\ V_{m_1} \\ 0 \\ 0 \end{bmatrix}_\omega = \begin{bmatrix} a & b & 0 & 0 \\ e & f & 0 & 0 \\ i & j & 1 & 0 \\ m & n & 0 & 1 \end{bmatrix}_\omega \begin{bmatrix} P_3 \\ V_3 \\ V_1 \\ V_2 \end{bmatrix}_\omega , \tag{5.50}$$

for every angular frequency ω. Note that P_{m_1} is the pressure at 'Point m_1' on Figure 5. 8 and V_{m_1} is the acoustic mass velocity out of the fork denoted by 'Point m_1' towards the balance pipe. Therefore, equation (5.50), in conjunction with the general equation that describes Valve Bank 1, namely

$$\{\mathbf{v}\}_{m_1} = [\mathbf{G}]_{m_1}\{\mathbf{S}\}_{m_1} + [\mathbf{H}]_{m_1}\{\mathbf{P}\}_{m_1}, \tag{5.51}$$

results in

$$\{\mathbf{v}\}_3 = [\mathbf{G}]_3\{\mathbf{S}\}_{m_1} + [\mathbf{H}]_3\{\mathbf{P}\}_3, \tag{5.52}$$

where

$$[\mathbf{H}]_3 = \left([\mathbf{f}] - [\mathbf{H}]_{m_1}[\mathbf{b}]\right)^{-1}\left([\mathbf{H}]_{m_1}[\mathbf{a}] - [\mathbf{e}]\right) \tag{5.53}$$

and

$$[\mathbf{G}]_3 = \left([\mathbf{f}] - [\mathbf{H}]_{m_1}[\mathbf{b}]\right)^{-1}[\mathbf{G}]_{m_1}, \tag{5.54}$$

see previous section.

In addition to equation (5.52) there are two connection equations

$$\{\mathbf{v}\}_3 = [\mathbf{G}]_{3R_1}\{\mathbf{S}\}_{m_1} + [\mathbf{H}]_{3R_1}\{\mathbf{P}\}_3 + [\mathbf{J}]_{3R_1}\{\mathbf{v}\}_1 \tag{5.55}$$

and

$$\{\mathbf{v}\}_3 = [\mathbf{G}]_{3R_2}\{\mathbf{S}\}_{m_1} + [\mathbf{H}]_{3R_2}\{\mathbf{P}\}_3 + [\mathbf{K}]_{3R_2}\{\mathbf{v}\}_2, \tag{5.56}$$

where in this case

$$[\mathbf{G}]_{3R_1} = [\mathbf{G}]_{3R_2} = [0] \tag{5.57}$$

and

$$[\mathbf{H}]_{3R_1} = -[\mathbf{i}]^{-1}[\mathbf{j}], \tag{5.58}$$

$$[\mathbf{J}]_{3R_1} = -[\mathbf{i}]^{-1}, \tag{5.59}$$

$$[\mathbf{H}]_{3R_2} = -[\mathbf{m}]^{-1}[\mathbf{n}], \tag{5.60}$$

and

$$[\mathbf{K}]_{3R_2} = -[\mathbf{m}]^{-1}. \tag{5.61}$$

Note that all the matrices containing lower case letters define a coefficient matrix as in equation (5.36). R_1 and R_2 are labels for the first and second connection equations. The lower case emboldened letters used in equations (5.53) to (5.61) are constructed from the coefficients of the transfer matrix in equation (5.50).

At 'Point m_2', with respect to Figure 5. 8, the interaction between the valves in 'Valve Bank 2' can be characterized acoustically by equation

$$\{\mathbf{v}\}_{m_2} = [\mathbf{G}]_{m_2}\{\mathbf{S}\}_{m_2} + [\mathbf{H}]_{m_2}\{\mathbf{P}\}_{m_2}. \tag{5.62}$$

Where subscript m_2 defines the acoustic vector/matrix position into the fork labelled 'Point m_2' from the direction of 'Valve Bank 2', with respect to Figure 5. 8.

The normal relationship for acoustic pressure and mass velocity at a fork withstands, so variables between 'Point 3', 'Point m_2' and 'Point m_3' can be related. Since equations (5.51) and (5.62), do not have vectors $\{\mathbf{v}\}_1$ and $\{\mathbf{v}\}_2$ contained within them, the normal addition of matrix equations can proceed, as in Chapter 3. Now the connection equations which are presently dependent on the unknowns $\{\mathbf{P}\}_3$ and $\{\mathbf{v}\}_3$ need to be dependent on $\{\mathbf{P}\}_{m_3}$ and $\{\mathbf{v}\}_{m_3}$. Where $\{\mathbf{v}\}_{m_3}$ is defined as the velocity out of the fork at 'Point m_3' with respect to Figure 5. 8. Pressure is assumed to be constant at a fork, therefore

$$\{\mathbf{P}\}_3 = \{\mathbf{P}\}_{m_2} = \{\mathbf{P}\}_{m_3}, \tag{5.63}$$

also the sum of acoustic mass velocities into a fork is equal to the sum out, so

$$\{\mathbf{v}\}_{m_3} = \{\mathbf{v}\}_{m_2} + \{\mathbf{v}\}_3, \tag{5.64}$$

thus by substituting equations (5.52) and (5.62) into equation (5.64) using (5.63)

$$\{\mathbf{v}\}_{m_3} = [\mathbf{G}]_3 \{\mathbf{S}\}_{m_1} + [\mathbf{G}]_{m_2} \{\mathbf{S}\}_{m_2} + ([\mathbf{H}]_3 + [\mathbf{H}]_{m_2}) \{\mathbf{P}\}_{m_3}. \tag{5.65}$$

Thus, one can write a general matrix equation that describes the acoustic behaviour at the outlet of the junction at the 'Point m_3'

$$\{\mathbf{v}\}_{m_3} = [\mathbf{G}]_{m_3} \{\mathbf{S}\}_{m_3} + [\mathbf{H}]_{m_3} \{\mathbf{P}\}_{m_3}. \tag{5.66}$$

Now the velocity vector $\{\mathbf{v}\}_3$ in connection equations (5.55) and (5.56) can be eliminated to produce

$$\{\mathbf{v}\}_{m_3} = [\mathbf{G}]_{3R_1} \{\mathbf{S}\}_{m_1} + [\mathbf{G}]_{m_2} \{\mathbf{S}\}_{m_2} + ([\mathbf{H}]_{3R_1} + [\mathbf{H}]_{m_2}) \{\mathbf{P}\}_3 + [\mathbf{J}]_{3R_1} \{\mathbf{v}\}_1 \tag{5.67}$$

and

$$\{\mathbf{v}\}_{m_3} = [\mathbf{G}]_{3R_2} \{\mathbf{S}\}_{m_1} + [\mathbf{G}]_{m_2} \{\mathbf{S}\}_{m_2} + ([\mathbf{H}]_{3R_2} + [\mathbf{H}]_{m_2}) \{\mathbf{P}\}_3 + [\mathbf{K}]_{3R_2} \{\mathbf{v}\}_2. \tag{5.68}$$

The vectors and matrices in equations (5.67) and (5.68) can be grouped together to give

$$\{\mathbf{v}\}_{m_3} = [\mathbf{G}]_{4R_1} \{\mathbf{S}\}_{m_3 R1} + [\mathbf{H}]_{4R_1} \{\mathbf{P}\}_3 + [\mathbf{J}]_{3R_1} \{\mathbf{v}\}_1 \tag{5.69}$$

and

$$\{\mathbf{v}\}_{m_3} = [\mathbf{G}]_{4R_2} \{\mathbf{S}\}_{m_3 R2} + [\mathbf{H}]_{4R_2} \{\mathbf{P}\}_3 + [\mathbf{K}]_{3R_2} \{\mathbf{v}\}_2. \tag{5.70}$$

Obtaining a general equation at the primary radiation, i.e. the one labelled as '5' on Figure 5. 8, is exactly the same as moving from 'Point m' to the primary radiation as in Figure 5. 7, see Section 5.3.1. The primary difference is that there are more connection equations.

There is a matrix equation that relates the pressure and velocity vectors at 'Point m_3' towards the exhaust, to the primary and third secondary radiation,

$$\begin{bmatrix} P_{m_3} \\ V_{m_3} \\ 0 \end{bmatrix}_\omega = \begin{bmatrix} a & b & 0 \\ d & e & 0 \\ g & h & 1 \end{bmatrix}_\omega \begin{bmatrix} P_5 \\ V_5 \\ V_4 \end{bmatrix}_\omega , \tag{5.71}$$

for every angular frequency ω. Note that the coefficients in equation (5.71) are different to those in equation (5.50). In addition, there are two connection equations that relate the pressure and velocity vectors to the first two secondary radiation vectors $\{\mathbf{v}\}_1$ and $\{\mathbf{v}\}_2$ via equations (5.69) and (5.70). Thus, from equation (5.71)

$$\{\mathbf{P}\}_{m_3} = [\mathbf{a}]\{\mathbf{P}\}_5 + [\mathbf{b}]\{\mathbf{v}\}_5 \tag{5.72}$$

and

$$\{\mathbf{v}\}_{m_3} = [\mathbf{d}]\{\mathbf{P}\}_5 + [\mathbf{e}]\{\mathbf{v}\}_5 . \tag{5.73}$$

Therefore $\{\mathbf{v}\}_{m_3}$ and $\{\mathbf{P}\}_{m_3}$ in equations (5.65), (5.69) and (5.70) can be substituted to give

$$\{\mathbf{v}\}_5 = [\mathbf{G}]_5 \{\mathbf{S}\}_{m_3} + [\mathbf{H}]_5 \{\mathbf{P}\}_5 , \tag{5.74}$$

$$\{\mathbf{v}\}_5 = [\mathbf{G}]_{5R_1} \{\mathbf{S}\}_{m_3} + [\mathbf{H}]_{5R_1} \{\mathbf{P}\}_5 + [\mathbf{J}]_{5R_1} \{\mathbf{v}\}_1 , \tag{5.75}$$

and

$$\{\mathbf{v}\}_5 = [\mathbf{G}]_{5R_2}\{\mathbf{S}\}_{m_3} + [\mathbf{H}]_{5R_2}\{\mathbf{P}\}_5 + [\mathbf{K}]_{5R_2}\{\mathbf{v}\}_2. \tag{5.76}$$

Where

$$[\mathbf{H}]_5 = ([\mathbf{e}] - [\mathbf{H}]_{m_3}[\mathbf{b}])^{-1}([\mathbf{H}]_{m_3}[\mathbf{a}] - [\mathbf{d}]), \tag{5.77}$$

$$[\mathbf{G}]_5 = ([\mathbf{e}] - [\mathbf{H}]_{m_3}[\mathbf{b}])^{-1}[\mathbf{G}]_{m_3}, \tag{5.78}$$

$$[\mathbf{H}]_{5R_1} = ([\mathbf{e}] - [\mathbf{H}]_{4R_1}[\mathbf{b}])^{-1}([\mathbf{H}]_{4R_1}[\mathbf{a}] - [\mathbf{d}]), \tag{5.79}$$

$$[\mathbf{G}]_{5R_1} = ([\mathbf{e}] - [\mathbf{H}]_{4R_1}[\mathbf{b}])^{-1}[\mathbf{G}]_{4R_1}, \tag{5.80}$$

$$[\mathbf{H}]_{5R_2} = ([\mathbf{e}] - [\mathbf{H}]_{4R_2}[\mathbf{b}])^{-1}([\mathbf{H}]_{4R_2}[\mathbf{a}] - [\mathbf{d}]), \tag{5.81}$$

$$[\mathbf{G}]_{5R_2} = ([\mathbf{e}] - [\mathbf{H}]_{4R_2}[\mathbf{b}])^{-1}[\mathbf{G}]_{4R_2}, \tag{5.82}$$

likewise for matrices $[\mathbf{J}]_{3R_1}$ and $[\mathbf{K}]_{3R_2}$ as for $[\mathbf{G}]_{4R_1}$ and $[\mathbf{G}]_{4R_2}$ Since there is another secondary vector $\{\mathbf{v}\}_4$, that originates from the unknown V_4 in equation (5.71), there has to be a third connection equation

$$\{\mathbf{v}\}_5 = [\mathbf{H}]_{5R_3}\{\mathbf{P}\}_5 + [\mathbf{L}]_{5R_3}\{\mathbf{v}\}_4, \tag{5.83}$$

where

$$[\mathbf{H}]_{5R_3} = -[\mathbf{h}]^{-1}[\mathbf{g}] \tag{5.84}$$

and

$$[\mathbf{L}]_{SR_3} = -[\mathbf{h}]^{-1}. \tag{5.85}$$

5.4 Capability to include intermediate sources

As seen in Section 3.8.1, discontinuity of cross-sectional duct areas, or an obstruction to flow within a duct, produces non-primary noise sources called Flow Generated Noise (FGN), within duct systems. Exhaust system designers and engineers often know where the FGN originates; therefore, this type of noise can be modelled theoretically as a pressure disturbance in a duct, which constitutes a dipole source. Alternatively, an injection of acoustic mass velocity constitutes a monopole source. This type of source has the capability of modelling loudspeakers which are used for active noise cancellation. Dipole and monopole sources are modelled in the hybrid code as an intermediate source (IS) element.

5.4.1 Intermediate source in a straight duct

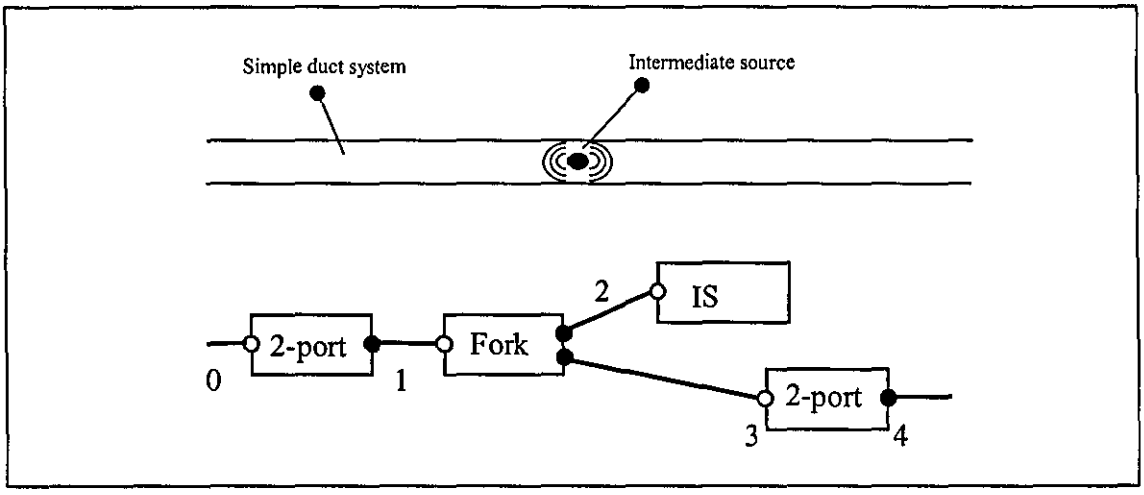

Figure 5. 9 Simple system with an intermediate source element

Intermediate sources can be modelled as a separate acoustic element attached to any part of the exhaust system via the use of a fork element, as in Figure 5. 9. FGN sources are incoherent with primary noise sources of a combustion engine and with each other.

A monopole source, at say x=0, gives the same pressure as $x=0^+$ and $x=0^-$, where $x=0^+$ is immediately downstream of the fork. However, the acoustic mass velocity at $x=0^+$ is equal in magnitude, but opposite in sign to that of $x=0^-$, where $x=0^-$ is immediately upstream of the fork. This complies with the properties of a fork, i.e. all pressures are constant and the summation of acoustic mass velocities into the junction equate to those out. Therefore, it is simple to add the software capability to the current software. The path fraction analysis concerned with intermediate sources is exactly the same as for closed ends, see Section 2.5.4. Note that the strength of a source is known. Thus, the transfer matrix that relates points *1* and *3* for a monopole type intermediate source, see Figure 5. 9, is

$$\begin{bmatrix} P_1 \\ V_1 \end{bmatrix} = \begin{bmatrix} 1 & 0 & 0 \\ 0 & 1 & -1 \end{bmatrix} \begin{bmatrix} P_3 \\ V_3 \\ V_2 \end{bmatrix}, \tag{5.86}$$

where V_2 is the strength of the source. Now, with respect to Figure 5. 9, let

$$\begin{bmatrix} P_0 \\ V_0 \end{bmatrix} = \begin{bmatrix} a_{01} & b_{01} \\ c_{01} & d_{01} \end{bmatrix} \begin{bmatrix} P_1 \\ V_1 \end{bmatrix} \tag{5.87}$$

and

$$\begin{bmatrix} P_3 \\ V_3 \end{bmatrix} = \begin{bmatrix} a_{34} & b_{34} \\ c_{34} & d_{34} \end{bmatrix} \begin{bmatrix} P_4 \\ V_4 \end{bmatrix}. \tag{5.88}$$

Then from equations (5.86) and (5.87),

$$\begin{bmatrix} P_0 \\ V_0 \end{bmatrix} = \begin{bmatrix} a_{01} & b_{01} & -b_{01} \\ c_{01} & d_{01} & -d_{01} \end{bmatrix} \begin{bmatrix} P_3 \\ V_3 \\ V_2 \end{bmatrix}. \tag{5.89}$$

Equation (5.88) can be rearranged to give

$$\begin{bmatrix} P_3 \\ V_3 \\ V_2 \end{bmatrix} = \begin{bmatrix} a_{34} & b_{34} & 0 \\ c_{34} & d_{34} & 0 \\ 0 & 0 & 1 \end{bmatrix} \begin{bmatrix} P_4 \\ V_4 \\ V_2 \end{bmatrix}. \tag{5.90}$$

Therefore, equations (5.89) and (5.90) give

$$\begin{bmatrix} P_0 \\ V_0 \end{bmatrix} = \begin{bmatrix} a_{01}a_{34} + b_{01}c_{34} & a_{01}b_{34} + b_{01}d_{34} & -b_{01} \\ c_{01}a_{34} + d_{01}c_{34} & c_{01}b_{34} + d_{01}d_{34} & -d_{01} \end{bmatrix} \begin{bmatrix} P_4 \\ V_4 \\ V_2 \end{bmatrix}. \tag{5.91}$$

Equation (5.91) shows that the addition of one intermediate source increases the number of columns within a transfer matrix by one. A system with n intermediate sources can always be reduced to a 2 by 2+n transfer matrix.

In contrast to the monopole source, a dipole source gives the same acoustic mass velocity at $x=0^+$ and $x=0^-$, but the actual pressures at $x=0^+$ and $x=0^-$ are equal in magnitude, but are of opposite signs. The dipole source nature of the intermediate source element, as seen in Figure 5. 9, can be characterised in transfer matrix format as

$$\begin{bmatrix} P_1 \\ V_1 \end{bmatrix} = \begin{bmatrix} 1 & 0 & 1 \\ 0 & 1 & 0 \end{bmatrix} \begin{bmatrix} P_3 \\ V_3 \\ P_2 \end{bmatrix}, \tag{5.92}$$

where P_2 is related to the dipole source strength. The logical procedure to relate pressures and mass velocities at points *0* to *4* is similar to those in equation steps (5.87) to (5.91).

As dipole sources are dependent on the pressure fluctuation caused by an obstruction in the duct, the associated coefficients are different. An example of this is the transfer matrix relation equation between points *0* and *3*, hence, instead of obtaining the matrix of coefficients as in equation (5.89) for a dipole source, one obtains

$$\begin{bmatrix} P_0 \\ V_0 \end{bmatrix} = \begin{bmatrix} a_{01} & b_{01} & a_{01} \\ c_{01} & d_{01} & c_{01} \end{bmatrix} \begin{bmatrix} P_3 \\ V_3 \\ P_2 \end{bmatrix}. \tag{5.93}$$

Similarly, the transfer matrix equation which relates points *0* and *4* is now

$$\begin{bmatrix} P_0 \\ V_0 \end{bmatrix} = \begin{bmatrix} a_{01}a_{34} + b_{01}c_{34} & a_{01}b_{34} + b_{01}d_{34} & a_{01} \\ c_{01}a_{34} + d_{01}c_{34} & c_{01}b_{34} + d_{01}d_{34} & c_{01} \end{bmatrix} \begin{bmatrix} P_4 \\ V_4 \\ P_2 \end{bmatrix}. \tag{5.94}$$

5.4.2 General intermediate source (GIS) algorithm

The GIS algorithm is an adaptation of the GRASB algorithm to include the capability of multiple, intermediate sources within a duct combined with multiple radiations. The introduction of an intermediate source to an acoustic sub-system requires an additional column within a transfer matrix, see Section 5.4.1; whereas a radiation requires an additional column and row. Therefore, the GIS algorithm concentrates on the adaptation and resizing of transfer matrices of any size to encompass intermediate sources. The algorithm is used when the hybrid algorithm encounters an intermediate source element.

Consider an intermediate source inserted between two two-port elements, as shown in Figure 5. 9. The two-port element connected to the inlet of the fork in Figure 5. 9 could have a standardised transfer matrix of any size, say m by m, see equation (5.15). The GIS algorithm would insert a column after the first two columns and adapt the first two rows of that column. For a monopole source the transfer matrix is

$$\begin{bmatrix} P_0 \\ V_0 \\ 0 \\ \vdots \\ \vdots \\ 0 \end{bmatrix} = \begin{bmatrix} f_{11} & f_{12} & -f_{12} & 0 & \cdots & \cdots & 0 \\ f_{21} & f_{22} & -f_{22} & 0 & \cdots & \cdots & 0 \\ \vdots & \vdots & 0 & 1 & \ddots & & 0 \\ \vdots & \vdots & \vdots & 0 & \ddots & \ddots & \vdots \\ \vdots & \vdots & \vdots & \vdots & \ddots & \ddots & 0 \\ f_{m1} & f_{m2} & 0 & 0 & \cdots & 0 & 1 \end{bmatrix} \begin{bmatrix} P_1 \\ V_1 \\ V_s \\ V_2 \\ V_3 \\ \vdots \\ V_{(m-1)} \end{bmatrix}, \tag{5.95}$$

where V_s is the acoustic mass velocity associated with the monopole source. Likewise for the dipole source,

$$\begin{bmatrix} P_0 \\ V_0 \\ 0 \\ \vdots \\ \vdots \\ 0 \end{bmatrix} = \begin{bmatrix} f_{11} & f_{12} & f_{11} & 0 & \cdots & \cdots & 0 \\ f_{21} & f_{22} & f_{21} & 0 & \cdots & \cdots & 0 \\ \vdots & \vdots & 0 & 1 & \ddots & & 0 \\ \vdots & \vdots & \vdots & 0 & \ddots & \ddots & \vdots \\ \vdots & \vdots & \vdots & \vdots & \ddots & \ddots & 0 \\ f_{m1} & f_{m2} & 0 & 0 & \cdots & 0 & 1 \end{bmatrix} \begin{bmatrix} P_1 \\ V_1 \\ P_s \\ V_2 \\ V_3 \\ \vdots \\ V_{(m-1)} \end{bmatrix}, \tag{5.96}$$

where P_s is the pressure associated with that source. The inclusion of intermediate sources has introduced non-square matrices. If multiple intermediate sources are required, then columns are added after the first two columns. Thus, in general, if there was a sub two-port element with an associated transfer matrix that represented *m-2* secondary radiation points and *n* intermediate sources, the standardised transfer matrix would be

$$\begin{bmatrix} P_0 \\ V_0 \\ 0 \\ \vdots \\ \vdots \\ 0 \end{bmatrix} = \begin{bmatrix} f'_{11} & f'_{12} & f'_{13} & \cdots & f'_{1(n+2)} & 0 & \cdots & \cdots & 0 \\ f'_{21} & f'_{22} & f'_{23} & \cdots & f'_{1(n+2)} & 0 & \cdots & \cdots & 0 \\ \vdots & \vdots & \vdots & & \vdots & 1 & \ddots & & 0 \\ \vdots & \vdots & \vdots & & \vdots & 0 & \ddots & \ddots & \vdots \\ \vdots & \vdots & \vdots & & \vdots & \vdots & \ddots & \ddots & 0 \\ f'_{m1} & f'_{m2} & f'_{m3} & \cdots & f'_{m(n+2)} & 0 & \cdots & 0 & 1 \end{bmatrix} \begin{bmatrix} P_1 \\ V_1 \\ P_{s1} \mid V_{s1} \\ \vdots \\ P_{sn} \mid V_{sn} \\ V_{r1} \\ \vdots \\ V_{r(m-2)} \end{bmatrix} \quad (5.97)$$

Here $P_{s1}|V_{s1}$ to $P_{sn}|V_{sn}$ are either the pressures or acoustic mass velocities associated with each of the intermediate sources. Also, V_{r1} to $V_{r(m-2)}$ represent the acoustic mass velocities at the secondary radiation points.

5.4.3 Intermediate sources in a side-branch

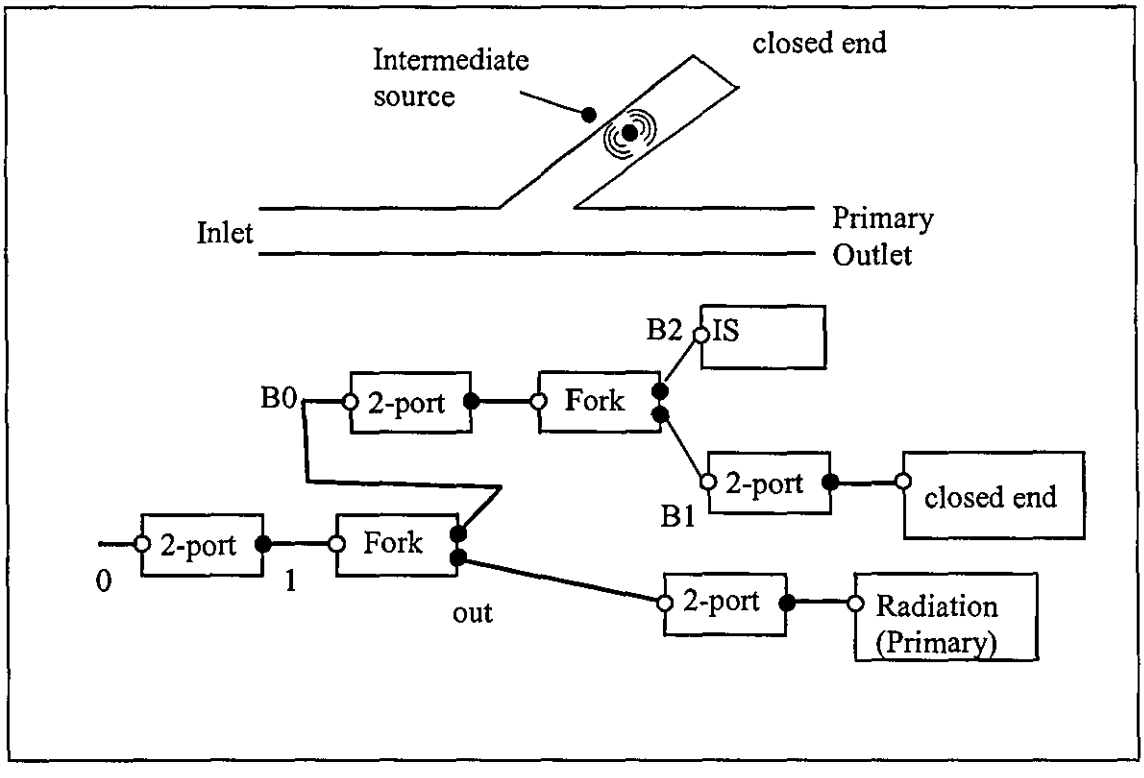

Figure 5. 10 Side-branch with an intermediate source

Noise cancellation systems are often located within a side-branch, or at the wall of a resonator, or expansion box inside an exhaust system. Therefore, the hybrid algorithm has to be able to analyse these types of systems. A side-branch that contains an intermediate source, say a monopole, see Figure 5. 10, can be explained generally as

$$\begin{bmatrix} P_{B0} \\ V_{B0} \end{bmatrix} = \begin{bmatrix} a & b & c \\ d & e & f \end{bmatrix} \begin{bmatrix} P_{B1} \\ V_{B1} \\ V_{B2} \end{bmatrix} = \begin{bmatrix} aZ_{B1}+b & c \\ dZ_{B1}+e & f \end{bmatrix} \begin{bmatrix} V_{B1} \\ V_{B2} \end{bmatrix}, \tag{5.98}$$

see equation (5.89). Here P_{B1} and V_{B1} are the pressure and acoustic mass velocity respectively at the termination/closed end, with known radiation impedance, Z_{B1}. Also, P_{B0} and V_{B0}, describe the acoustic behaviour at the inlet to the side-branch and V_{B2} is the acoustic mass velocity at the intermediate monopole source. The acoustic properties of the fork element to the side-branch, with inlet point *1* and outlets *B1* and '*out*', then result in the transfer matrix

$$\begin{bmatrix} P_1 \\ V_1 \\ 0 \end{bmatrix} = \begin{bmatrix} 1 & 0 & 0 & 0 \\ 0 & 1 & dZ_{B1}+e & f \\ -1 & 0 & aZ_{B1}+b & c \end{bmatrix} \begin{bmatrix} P_{out} \\ V_{out} \\ V_{B1} \\ V_{B2} \end{bmatrix}. \tag{5.99}$$

Further reduction can be obtained by using the third row in equation (5.99) to express V_{B1} in terms of P_{out} and V_{B2}, hence

$$\begin{bmatrix} P_1 \\ V_1 \end{bmatrix} = \begin{bmatrix} 1 & 0 & 0 \\ \dfrac{dZ_e+e}{aZ_e+b} & 1 & -\dfrac{dZ_e+e}{aZ_e+b}c+f \end{bmatrix} \begin{bmatrix} P_{out} \\ V_{out} \\ V_{B2} \end{bmatrix}. \tag{5.100}$$

Note that equation (5.100) conforms with the standardised form as shown in equation (5.97). This routine, from equations from equation (5.98) to (5.100), can be achieved for dipole sources.

5.4.4 General intermediate source and radiation side-branch (GISRSB) algorithm

The GISRSB algorithm is an extension of the GMRASB algorithm. The extension includes the option of having any number of intermediate sources and radiation points within a side-branch. The GISRSB algorithm is used whenever there is one intermediate source with a side-branch. Note that GIS algorithm will not work if there are intermediate sources located within a side-branch, hence the need for this GISRSB algorithm.

Consider a general, standardised transfer matrix, see equation (5.97). Let that matrix relate the acoustic relationship between the inlet, point *B0*, and the closed end, point *B1* of side-branch, where n is the number of intermediate sources and m is the number of radiation points. Thus, the standardised transfer matrix of the side-branch is

$$\begin{bmatrix} P_{B0} \\ V_{B0} \\ 0 \\ \vdots \\ \vdots \\ 0 \end{bmatrix} = \begin{bmatrix} f_{11} & f_{12} & f_{13} & \cdots & f_{1(n+2)} & 0 & \cdots & \cdots & 0 \\ \vdots & \vdots & f_{23} & \cdots & f_{2(n+2)} & 0 & \cdots & \cdots & 0 \\ \vdots & \vdots & \vdots & & \vdots & 1 & \ddots & & 0 \\ \vdots & \vdots & \vdots & & \vdots & 0 & \ddots & \ddots & \vdots \\ \vdots & \vdots & \vdots & & \vdots & \vdots & \ddots & \ddots & 0 \\ f_{(m+2)1} & f_{(m+2)2} & f_{(m+2)3} & \cdots & f_{(m+2)(n+2)} & 0 & \cdots & 0 & 1 \end{bmatrix} \begin{bmatrix} P_{B1} \\ V_{B1} \\ P_{s1} \mid V_{s1} \\ \vdots \\ P_{sn} \mid V_{sn} \\ V_{r1} \\ \vdots \\ V_{rm} \end{bmatrix}. \quad (5.101)$$

Also, $P_{s1}|V_{s1}$ to $P_{s1}|V_{s1}$ are the pressures or acoustic mass velocities associated with the intermediate sources and V_{r1} to V_{rm} are velocities associated with secondary radiation

points. Now at point *B1* the impedance, Z_{B1}, is known. Therefore, P_{B1} can be eliminated, hence

$$\begin{bmatrix} P_{B0} \\ V_{B0} \\ 0 \\ \vdots \\ \vdots \\ 0 \end{bmatrix} = \begin{bmatrix} f_{11}Z_1 + f_{12} & f_{13} & \cdots & f_{1(n+2)} & 0 & \cdots & \cdots & 0 \\ \vdots & f_{23} & \cdots & f_{2(n+2)} & 0 & \cdots & \cdots & 0 \\ \vdots & \vdots & & \vdots & 1 & \ddots & & 0 \\ \vdots & \vdots & & \vdots & 0 & \ddots & \ddots & \vdots \\ \vdots & \vdots & & \vdots & \vdots & \ddots & \ddots & 0 \\ f_{(m+2)1}Z_1 + f_{(m+2)2} & f_{(m+2)3} & \cdots & f_{(m+2)(n+2)} & 0 & \cdots & 0 & 1 \end{bmatrix} \begin{bmatrix} V_{B1} \\ P_{s1} \mid V_{s1} \\ \vdots \\ P_{sn} \mid V_{sn} \\ V_{r1} \\ \vdots \\ V_{rm} \end{bmatrix}. \tag{5.102}$$

Now, let point *B0* in this section be attached to a junction and the inlet of a side-branch, where the junction is a fork element that has two outlets and one inlet, see Figure 5. 10. Let the two-port element attached to the inlet of the junction have a transfer matrix of size (M +2) by (M+N +2), $M \geq 0$ and $N \geq 0$, where N represents the number of previous intermediate sources, $\sigma 1$ to σN, likewise R represents the number of previous radiation points, *R1* to *RM*. Thus, the transfer matrix can be characterised by a standardised matrix, say

$$\begin{bmatrix} P_0 \\ V_0 \\ 0 \\ \vdots \\ \vdots \\ 0 \end{bmatrix} = \begin{bmatrix} h_{11} & h_{12} & h_{13} & \cdots & h_{1(N+2)} & 0 & \cdots & \cdots & 0 \\ \vdots & \vdots & h_{23} & \cdots & h_{2(N+2)} & 0 & \cdots & \cdots & 0 \\ \vdots & \vdots & \vdots & & \vdots & 1 & \ddots & & 0 \\ \vdots & \vdots & \vdots & & \vdots & 0 & \ddots & \ddots & \vdots \\ \vdots & \vdots & \vdots & & \vdots & \vdots & \ddots & \ddots & 0 \\ h_{(M+2)1} & h_{(M+2)2} & h_{(M+2)3} & \cdots & h_{(M+2)(N+2)} & 0 & \cdots & 0 & 1 \end{bmatrix} \begin{bmatrix} P_1 \\ V_1 \\ P_{\sigma 1} \mid V_{\sigma 1} \\ \vdots \\ P_{\sigma N} \mid V_{\sigma N} \\ V_{R1} \\ \vdots \\ V_{RM} \end{bmatrix}, \tag{5.103}$$

see Figure 5. 10. Points *0* and *1* represent the inlet and outlet of this two-port element respectively.

All the pressures at a junction are constant, i.e. $P_I=P_{B0}=P_{out}$, where P_{out} is the pressure at the remaining outlet of the junction. Also, the sum of acoustic mass velocity into the junction is equal to the sum out, $V_I=V_{B0}+V_{out}$, thus, a matrix adaptation to the one in equation (5.102) using equation (5.103) can occur. The GIMRSB algorithm firstly enlarges the matrix in equation (5.103) by $m+n+2$ columns and $m+2$ rows. Then, the algorithm inserts the matrix equation (5.102) into columns $M+N+3$ to $M+N+m+n+4$, hence

$$\begin{bmatrix} P_0 \\ V_0 \\ 0 \\ \vdots \\ \vdots \\ \vdots \\ \vdots \\ \vdots \\ \vdots \\ \vdots \\ 0 \end{bmatrix} = \begin{bmatrix} h_{11} & h_{23} & h_{13} & \cdots & h_{1(N+2)} & 0 & \cdots & \cdots & \cdots & \cdots & \cdots & \cdots & \cdots & \cdots & \cdots & \cdots & \cdots & 0 \\ \vdots & \vdots & h_{23} & \cdots & h_{1(N+2)} & 0 & \cdots & \cdots & 0 & 1 & 0 & \cdots & \cdots & \cdots & \cdots & \cdots & \cdots & 0 \\ \vdots & \vdots & \vdots & & \vdots & 1 & \ddots & & \vdots & 0 & \vdots & & & & & & & \vdots \\ \vdots & \vdots & \vdots & & \vdots & 0 & \ddots & \ddots & \vdots & \vdots & \vdots & & & & & & & \vdots \\ \vdots & \vdots & \vdots & & \vdots & \vdots & \ddots & \ddots & 0 & \vdots & \vdots & & & & & & & \vdots \\ h_{1(M+2)} & h_{2(M+2)} & h_{3(M+2)} & \cdots & h_{(N+2)(M+2)} & 0 & \cdots & 0 & 1 & 0 & 0 & \cdots & \cdots & \cdots & \cdots & \cdots & \cdots & 0 \\ -1 & 0 & \cdots & \cdots & \cdots & \cdots & \cdots & \cdots & 0 & 0 & f_{11}Z_{B1}+f_{12} & f_{13} & \cdots & f_{1(n+2)} & 0 & \cdots & \cdots & 0 \\ 0 & \cdots & \cdots & \cdots & \cdots & \cdots & \cdots & \cdots & 0 & -1 & f_{21}Z_{B1}+f_{22} & f_{23} & \cdots & f_{2(n+2)} & 0 & \cdots & \cdots & 0 \\ \vdots & & & & & & & & \vdots & 0 & \vdots & \vdots & & \vdots & 1 & \ddots & & \vdots \\ \vdots & & & & & & & & \vdots & \vdots & \vdots & \vdots & & \vdots & 0 & \ddots & \ddots & \vdots \\ \vdots & & & & & & & & \vdots & \vdots & \vdots & \vdots & & \vdots & \vdots & & \ddots & 0 \\ 0 & \cdots & \cdots & \cdots & \cdots & \cdots & \cdots & \cdots & 0 & 0 & f_{(m+2)1}Z_{B1}+f_{(m+2)2} & f_{(m+2)3} & \cdots & f_{(m+2)(n+2)} & 0 & \cdots & 0 & 1 \end{bmatrix} \begin{bmatrix} P_{out} \\ V_{out} \\ P_{o1} \mid V_{o1} \\ \vdots \\ P_{oN} \mid V_{oN} \\ V_{R1} \\ \vdots \\ V_{RM} \\ V_{B0} \\ V_{B1} \\ P_{s1} \mid V_{s1} \\ \vdots \\ P_{sn} \mid V_{sn} \\ V_{r1} \\ \vdots \\ V_{rm} \end{bmatrix}. \tag{5.104}$$

Rows (M+3) and (M+4) of equation (5.104) allows variables V_{B0} and V_{B1} to be eliminated. Thus, in doing so and rearranging the columns to create the transfer matrix format

$$\begin{bmatrix} P_0 \\ V_0 \\ 0 \\ \vdots \\ \vdots \\ \vdots \\ \vdots \\ 0 \end{bmatrix} = \begin{bmatrix} h_{11} & h_{12} & h_{13} & \cdots & h_{1(N+2)} & 0 & \cdots & \cdots & \cdots & \cdots & \cdots & \cdots & \cdots & \cdots & \cdots & 0 \\ \frac{f_{21}Z_{B1}+f_{22}}{f_{11}Z_{B1}+f_{12}}+h_{21} & \vdots & h_{23} & \cdots & h_{2(N+2)} & -\frac{(f_{21}Z_{B1}+f_{22})f_{13}}{f_{11}Z_{B1}+f_{12}}+f_{23} & \cdots & -\frac{(f_{21}Z_{B1}+f_{22})f_{1(n+2)}}{f_{11}Z_{B1}+f_{12}}+f_{2(n+2)} & 0 & \cdots & \cdots & \cdots & \cdots & \cdots & \cdots & 0 \\ h_{31} & \vdots & \vdots & & \vdots & 0 & \cdots & 0 & 1 & 0 & \cdots & \cdots & \cdots & \cdots & \cdots & 0 \\ \vdots & \vdots & \vdots & & \vdots & 0 & \cdots & \cdots & 0 & \ddots & \ddots & & & & & \vdots \\ \vdots & \vdots & \vdots & & \vdots & \vdots & & & & \ddots & \ddots & \ddots & & & & \vdots \\ h_{(M+2)1} & h_{(M+2)2} & h_{(M+2)3} & \cdots & h_{(M+2)(N+2)} & 0 & \cdots & \cdots & \cdots & \cdots & 0 & \ddots & \ddots & & & \vdots \\ \frac{f_{31}Z_{B1}+f_{32}}{f_{11}Z_{B1}+f_{12}} & 0 & \cdots & \cdots & 0 & -\frac{(f_{31}Z_{B1}+f_{32})f_{13}}{f_{11}Z_{B1}+f_{12}}+f_{33} & \cdots & -\frac{(f_{31}Z_{B1}+f_{32})f_{1(n+2)}}{f_{11}Z_{B1}+f_{12}}+f_{3n} & 0 & \cdots & \cdots & 0 & \ddots & \ddots & & \vdots \\ \vdots & \vdots & & & \vdots & \vdots & & \vdots & \vdots & & & \ddots & \ddots & \ddots & \vdots & \vdots \\ \vdots & \vdots & & & \vdots & \vdots & & \vdots & \vdots & & & & \ddots & \ddots & \ddots & \vdots \\ \vdots & \vdots & & & \vdots & \vdots & & \vdots & \vdots & & & & & \ddots & \ddots & 0 \\ \frac{f_{(m+2)1}Z_{B1}+f_{(m+2)2}}{f_{11}Z_{B1}+f_{12}} & 0 & \cdots & \cdots & 0 & -\frac{(f_{(m+2)1}Z_{B1}+f_{(m+2)2})f_{13}}{f_{11}Z_{B1}+f_{12}}+f_{(m+2)3} & \cdots & -\frac{(f_{(m+2)1}Z_{B1}+f_{(m+2)2})f_{1(n+2)}}{f_{11}Z_{B1}+f_{12}}+f_{(m+2)n} & 0 & \cdots & \cdots & \cdots & \cdots & \cdots & 0 & 1 \end{bmatrix} \begin{bmatrix} P_{out} \\ V_{out} \\ P_{s1} \mid V_{s1} \\ \vdots \\ P_{sN} \mid V_{sN} \\ P_{s1} / V_{s1} \\ \vdots \\ P_{sn} \mid V_{sn} \\ V_{R1} \\ \vdots \\ \vdots \\ V_{RM} \\ V_{rt} \\ \vdots \\ \vdots \\ V_{rm} \end{bmatrix}$$

(5.105)

Note that rows (M+3) and (M+4) and columns (M+N+3) and (M+N+4) have been deleted, i.e. the matrix equation (5.104) has been reduced. Hence, equation (5.105) conforms to the standardised transfer matrix form. However, if V_{B0} relates to the associated velocity of a secondary radiation point, then V_{B0} should not be eliminated and the row which contains that variable should be moved to the last row. Also, when this occurs the column that contains V_{B0}, see equation (5.104), should be moved to column (M+N+m+n+2).

5.4.5 General matrix multiplication concerned with intermediate sources and radiations (GMMIR) algorithm

The GMMIR algorithm is an extension of the GMMR algorithm. The GMMIR algorithm is used when the transfer matrices of two consecutively sequenced sub two-port elements, as in Figure 5. 4, are reduced. The GMMIR algorithm is required when one or both of these matrices have one or multiple intermediate sources associated with them. This algorithm is capable of evaluating any pair of transfer matrices with any varying sizes due to multiple intermediate sources and radiation points.

Let the first sub two-port element with n intermediate sources and m radiation points, such that it is characterised by an $m+2$ by $m+n+2$ transfer matrix, be

$$\begin{bmatrix} P_0 \\ V_0 \\ 0 \\ \vdots \\ \vdots \\ 0 \end{bmatrix} = \begin{bmatrix} f_{11} & f_{12} & f_{13} & \cdots & f_{1(n+2)} & 0 & \cdots & \cdots & 0 \\ \vdots & \vdots & f_{23} & \cdots & f_{2(n+2)} & 0 & \cdots & \cdots & 0 \\ \vdots & \vdots & \vdots & & \vdots & 1 & \ddots & & 0 \\ \vdots & \vdots & \vdots & & \vdots & 0 & \ddots & \ddots & \vdots \\ \vdots & \vdots & \vdots & & \vdots & \vdots & \ddots & \ddots & 0 \\ f_{(m+2)1} & f_{(m+2)2} & f_{(m+2)3} & \cdots & f_{(m+2)(n+2)} & 0 & \cdots & 0 & 1 \end{bmatrix} \begin{bmatrix} P_1 \\ V_1 \\ P_{s1} \mid V_{s1} \\ \vdots \\ P_{sn} \mid V_{sn} \\ V_{r1} \\ \vdots \\ V_{rm} \end{bmatrix}, \tag{5.106}$$

where $P_{s1}|V_{s1}$ to $P_{sn}|V_{sn}$ are the acoustic pressures or mass velocities associated with the intermediate sources. Also, V_{r1} to V_{rm} represent the acoustic mass velocities associated with the secondary radiation points. Similarly, the second sub two-port element with N intermediate sources and M radiation points can be characterised by an $(M+2)$ by $(M+N+2)$ transfer matrix,

$$\begin{bmatrix} P_1 \\ V_1 \\ 0 \\ \vdots \\ \vdots \\ 0 \end{bmatrix} = \begin{bmatrix} h_{11} & h_{12} & h_{13} & \cdots & h_{1(N+2)} & 0 & \cdots & \cdots & 0 \\ \vdots & \vdots & h_{23} & \cdots & h_{2(N+2)} & 0 & \cdots & \cdots & 0 \\ \vdots & \vdots & \vdots & & \vdots & 1 & \ddots & & 0 \\ \vdots & \vdots & \vdots & & \vdots & 0 & \ddots & \ddots & \vdots \\ \vdots & \vdots & \vdots & & \vdots & \vdots & \ddots & \ddots & 0 \\ h_{(M+2)1} & h_{(M+2)2} & h_{(M+2)3} & \cdots & h_{(M+2)(N+2)} & 0 & \cdots & 0 & 1 \end{bmatrix} \begin{bmatrix} P_2 \\ V_2 \\ P_{\sigma 1} \mid V_{\sigma 1} \\ \vdots \\ P_{\sigma N} \mid V_{\sigma N} \\ V_{R1} \\ \vdots \\ V_{RM} \end{bmatrix}, \tag{5.107}$$

where $P_{\sigma 1} \mid V_{\sigma 1}$ to $P_{\sigma N} \mid V_{\sigma N}$ are the acoustic pressures or mass velocities associated with the intermediate sources. Also, V_{R1} to V_{RM} represent the acoustic mass velocities with respect to the secondary radiation points.

Now, every pressure and acoustic mass velocity within the first sub-system is known in terms of P_1 and V_1. Equation (5.107) has a simple relationship for P_1 and V_1 in terms of P_2 and V_2. Thus, the GMMIR algorithm combines equations (5.106) and (5.107) and eliminates variables P_1 and V_1. The algorithm first creates a new null matrix of size $(m+M+2)$ by $(m+n+M+N+2)$. In the first $m+2$ rows, each row r is written with the first two columns as $f_{r1}h_{11}+f_{r2}h_{21}$ and $f_{r1}h_{12}+f_{r2}h_{22}$ respectively, to eliminate P_1 and V_1. Secondly, the algorithm copies the values in rows 1 to $m+2$ of equation (5.106) from the third column to the n^{th} column and places them in the new matrix, starting at the first row, third column. Now, the algorithm adapts the cell values between the third and $(N+2)^{nd}$ columns of rows one and two in the matrix equation (5.107) to be in terms of P_0 and V_0 as opposed to P_1 and V_1 and inserts them into the first two rows of the new matrix after column $n+2$. Thus, column c of rows one and two become $f_{11}h_{1c}+f_{12}h_{2c}$ and $f_{21}h_{1c}+f_{22}h_{2c}$ respectively, and they are placed in the top two rows of the new matrix, starting at $n+2$, given that c represents the column. Next, the first two columns of the second matrix are copied straight into the last M rows of the enlarged matrix, except for the top two rows. The third to $(N+2)^{nd}$ rows of the equation (5.107) are copied directly into the new matrix, beginning at row $m+2+1$, column n+2+1. Lastly, the GMMIR algorithm inserts the value 1 into the diagonal components of the enlarged matrix, except for the top two rows. Hence

$$\begin{bmatrix} P_0 \\ V_0 \\ 0 \\ \vdots \\ \vdots \\ \vdots \\ \vdots \\ \vdots \\ \vdots \\ 0 \end{bmatrix} = \begin{bmatrix} f_{11}h_{11}+f_{12}h_{21} & f_{11}h_{12}+f_{12}h_{22} & f_{13} & \cdots & f_{1(n+2)} & f_{11}h_{13}+f_{12}h_{23} & \cdots & f_{11}h_{1(N+2)}+f_{12}h_{2(N+2)} & 0 & \cdots & \cdots & \cdots & \cdots & \cdots & \cdots & 0 \\ f_{21}h_{11}+f_{22}h_{21} & f_{21}h_{12}+f_{22}h_{22} & f_{23} & \cdots & f_{2(n+2)} & f_{21}h_{13}+f_{22}h_{23} & \cdots & f_{21}h_{1(N+2)}+f_{22}h_{2(N+2)} & 0 & \cdots & \cdots & \cdots & \cdots & \cdots & \cdots & 0 \\ \vdots & \vdots & \vdots & & \vdots & 0 & \cdots & 0 & 1 & \ddots & & & & & & \vdots \\ \vdots & \vdots & \vdots & & \vdots & \vdots & & \vdots & 0 & \ddots & \ddots & & & & & \vdots \\ \vdots & \vdots & \vdots & & \vdots & \vdots & & \vdots & \vdots & \ddots & \ddots & \ddots & & & & \vdots \\ f_{(m+2)1}h_{11}+f_{(m+2)2}h_{21} & f_{(m+2)1}h_{12}+f_{(m+2)2}h_{22} & f_{(m+2)3_{22}} & & f_{(m+2)(n+2)} & 0 & \cdots & 0 & \vdots & & \ddots & \ddots & \ddots & & & \vdots \\ h_{31} & h_{32} & 0 & \cdots & 0 & h_{33} & \cdots & h_{1(N+2)} & \vdots & & & \ddots & \ddots & \ddots & & \vdots \\ \vdots & \vdots & \vdots & & \vdots & \vdots & & \vdots & \vdots & & & & \ddots & \ddots & \ddots & \vdots \\ \vdots & \vdots & \vdots & & \vdots & \vdots & & \vdots & \vdots & & & & & \ddots & \ddots & 0 \\ h_{(M+2)1} & h_{(M+2)2} & 0 & \cdots & 0 & h_{(M+2)3} & \cdots & h_{(M+2)(N+2)} & 0 & \cdots & \cdots & \cdots & \cdots & \cdots & 0 & 1 \end{bmatrix} \begin{bmatrix} P_2 \\ V_2 \\ P_{s1} \mid V_{s1} \\ \vdots \\ P_{sn} \mid V_{sn} \\ P_{o1} \mid V_{o1} \\ \vdots \\ P_{oN} / V_{oN} \\ V_{1r} \\ \vdots \\ \vdots \\ V_{mr} \\ V_{R1} \\ \vdots \\ \vdots \\ V_{RM} \end{bmatrix} . \tag{5.108}$$

5.4.6 General reduction concerned with intermediate sources and radiations (GRIR)

The path fraction analysis for intermediate sources and secondary radiation points is exactly the same as in Section 2.5.4 since it analyses all one-port elements using the same analysis technique. Any general sub-system can be represented by a general standardised transfer matrix, see equation (5.106); thus, this element could be a part of a larger system which requires a sub-system reduction, see Section 2.7. A reduction matrix must be able to reduce sub-systems that have any number of intermediate sources and secondary radiation points.

Consider the sub-system in Figure 5. 6 and the example used in Section 5.2.7. Now, let the sub-system between points *3* and *7* be characterised by a standardised transfer matrix with any number of intermediate sources, say n, and secondary radiation points, say m. Hence

$$\begin{bmatrix} P_3 \\ V_3 \\ 0 \\ \vdots \\ \vdots \\ 0 \end{bmatrix} = \begin{bmatrix} g_{11} & g_{12} & g_{13} & \cdots & g_{1(n+2)} & 0 & \cdots & \cdots & 0 \\ g_{21} & g_{22} & g_{23} & \cdots & g_{2(n+2)} & 0 & \cdots & \cdots & 0 \\ \vdots & \vdots & \vdots & & \vdots & 1 & \ddots & & 0 \\ \vdots & \vdots & \vdots & & \vdots & 0 & \ddots & \ddots & \vdots \\ \vdots & \vdots & \vdots & & \vdots & \vdots & \ddots & \ddots & 0 \\ g_{(m+2)1} & g_{(m+2)2} & g_{(m+2)3} & \cdots & g_{(m+2)(n+2)} & 0 & \cdots & 0 & 1 \end{bmatrix} \begin{bmatrix} P_7 \\ V_7 \\ P_{s1} \mid V_{s1} \\ \vdots \\ P_{sn} \mid V_{sn} \\ V_{r1} \\ \vdots \\ V_{rm} \end{bmatrix} \tag{5.109}$$

where $P_{s1}|V_{s1}$ to $P_{sn}|V_{sn}$ are the pressures or acoustic mass velocities associated with the intermediate sources. Also, V_{r1} to V_{rm} represent the acoustic mass velocities with the secondary radiations. Equation (5.109) can be re-written in a similar form as to equation (5.28). The acoustic relationship between the other points in Figure 5. 6 remains

the same, as stated in Section 5.2.7. Therefore, an enlarged matrix can be created as explained in Section 5.2.7, where the only difference here occurs due to the extra columns as a result of n intermediate sources. The rows and columns are re-ordered using the same technique as in Section 2.7, see equation (5.30), to produce the matrix equation

$$\begin{bmatrix} 0 \\ \vdots \\ \vdots \\ \vdots \\ \vdots \\ \vdots \\ \vdots \\ \vdots \\ P_0 \\ V_0 \\ 0 \\ \vdots \\ \vdots \\ \vdots \\ 0 \end{bmatrix} = \begin{bmatrix} -1 & 0 & f_{11} & f_{12} & 0 & 0 & 0 & 0 & 0 & 0 & 0 & \cdots & 0 & 0 & \cdots & \cdots & 0 \\ 0 & -1 & f_{21} & f_{22} & 0 & 0 & 0 & 0 & 0 & 0 & 0 & \cdots & 0 & 0 & \cdots & \cdots & 0 \\ 0 & 0 & 0 & 0 & -1 & 0 & g_{11} & g_{12} & 0 & 0 & g_{13} & \cdots & g_{1(n+2)} & 0 & \cdots & \cdots & 0 \\ 0 & 0 & 0 & 0 & 0 & -1 & g_{21} & g_{22} & 0 & 0 & g_{23} & \cdots & g_{2(n+2)} & 0 & \cdots & \cdots & 0 \\ 1 & 0 & 0 & 0 & -1 & 0 & 0 & 0 & 0 & 0 & 0 & \cdots & 0 & 0 & \cdots & \cdots & 0 \\ 0 & 0 & 1 & 0 & 0 & 0 & -1 & 0 & 0 & 0 & 0 & \cdots & 0 & 0 & \cdots & \cdots & 0 \\ 0 & 0 & 0 & 0 & 0 & 0 & 1 & 0 & 1 & 0 & 0 & \cdots & 0 & 0 & \cdots & \cdots & 0 \\ 0 & 0 & 0 & -1 & 0 & 0 & 0 & -1 & 0 & 1 & 0 & \cdots & 0 & 0 & \cdots & \cdots & 0 \\ 1 & 0 & 0 & 0 & 0 & 0 & 0 & 0 & 0 & 0 & 0 & \cdots & 0 & 0 & \cdots & \cdots & 0 \\ 0 & 1 & 0 & 0 & 1 & 0 & 0 & 0 & 0 & 0 & 0 & \cdots & 0 & 0 & \cdots & \cdots & 0 \\ 0 & 0 & 0 & 0 & 0 & 0 & g_{31} & g_{32} & 0 & 0 & g_{33} & \cdots & g_{3(n+2)} & 1 & \ddots & & \vdots \\ \vdots & \vdots & \vdots & \vdots & \vdots & \vdots & \vdots & \vdots & \vdots & \vdots & \vdots & & \vdots & 0 & \ddots & \ddots & \vdots \\ \vdots & \vdots & \vdots & \vdots & \vdots & \vdots & \vdots & \vdots & \vdots & \vdots & \vdots & & \vdots & \vdots & \ddots & \ddots & 0 \\ 0 & 0 & 0 & 0 & 0 & 0 & g_{(m+2)1} & g_{(m+2)2} & 0 & 0 & g_{(m+2)3} & \cdots & g_{(m+2)(n+2)} & 0 & \cdots & 0 & 1 \end{bmatrix} \begin{bmatrix} P_1 \\ V_1 \\ P_2 \\ V_2 \\ P_3 \\ V_3 \\ P_7 \\ V_7 \\ P_6 \\ V_6 \\ P_{s1} \mid V_{s1} \\ \vdots \\ P_{sn} \mid V_{sn} \\ V_{r1} \\ \vdots \\ V_{rm} \end{bmatrix}.$$

(5.110)

Equation (5.110) represents a reduction matrix that can be manipulated by row operations to produce a standardised transfer matrix relating P_0, V_0 to P_6, V_6, $P_{s1}|V_{s1}$ to $P_{sn}|V_{sn}$ and V_{r1} to V_{rm}. Hence, the GRIR algorithm must produce a reduction matrix similar to the one in equation (5.110) for any sub-system. Consider a general reduction matrix with m secondary radiation points and n intermediate sources, that connects $q+1$ ports, where 0 is the inlet port and q is the outlet port. The matrix will have a size $Q=2q+m$ by $Q+n$

$$\begin{bmatrix} 0 \\ \vdots \\ 0 \\ P_0 \\ V_0 \\ 0 \\ \vdots \\ 0 \end{bmatrix} = \begin{bmatrix} h_{11} & \cdots & \cdots & \cdots & \cdots & \cdots & \cdots & h_{1(Q+n)} \\ \vdots & & & & & & & \vdots \\ \vdots & & & & & & & \vdots \\ h_{(Q-m-1)1} & \cdots & \cdots & \cdots & \cdots & \cdots & \cdots & h_{(Q-m-1)(Q+n)} \\ h_{(Q-m)1} & \cdots & \cdots & \cdots & \cdots & \cdots & \cdots & h_{(Q-m)(Q+n)} \\ h_{(Q-m+1)1} & \cdots & \cdots & \cdots & \cdots & \cdots & \cdots & h_{(Q-m+1)(Q+n)} \\ \vdots & & & & & & & \vdots \\ h_{Q1} & \cdots & \cdots & \cdots & \cdots & \cdots & \cdots & h_{Q(Q+n)} \end{bmatrix} \begin{bmatrix} P_1 \\ V_1 \\ \vdots \\ P_q \\ V_q \\ P_{s1} \mid V_{s1} \\ \vdots \\ P_{sn} \mid V_{sn} \\ V_{r1} \\ \vdots \\ V_{rm} \end{bmatrix}. \quad (5.111)$$

Therefore, the final step is to find a $m+2$ by $m+n+2$ transfer matrix relationship between P_0, V_0, and P_k, V_k, the intermediate source variables $P_{s1}|V_{s1}$ to $P_s|V_{sn}$ and the radiation variables V_{r1} to V_{rm}, by row operations. This can always be achieved since the variables of each inlet and outlet of the sub-system only appear once, each in a separate equation. This final step of matrix manipulation starts with finding the maximum value within the first Q-m-2 rows in the first column. Let the largest value be in row 4, say $h_{4,1}$; now interchange rows 4 and 1. This partial pivoting is vitally important as many of the coefficients are zero. The last $2+m$ rows in equation (5.111) cannot be interchanged. The factors within row 1 are now subtracted from rows 2 to Q to force the coefficients in the first column, of these rows, to have the value zero. This is the Gauss-Jordan method with partial pivoting. The method is repeated in column 2 to force the coefficients in rows 3 to n to equal zero, this is repeated until column Q-m-2 is reached. The method is general and will work on any Q by $(Q+n)$ matrix which describes a sub-system with a single inlet and multiple outlets.

$$\begin{bmatrix} 0 \\ \vdots \\ 0 \\ P_0 \\ V_0 \\ 0 \\ \vdots \\ 0 \end{bmatrix} = \begin{bmatrix} h'_{11} & \cdots & \cdots & \cdots & \cdots & \cdots & \cdots & h'_{1(Q+n)} \\ 0 & \ddots & & & & & & \vdots \\ \vdots & \ddots & \ddots & & & & & \vdots \\ \vdots & & 0 & h'_{(Q-m)(Q-m-1)} & \cdots & \cdots & \cdots & h'_{(Q-m-1)(Q+n)} \\ \vdots & & \vdots & \vdots & & & & \vdots \\ \vdots & & \vdots & \vdots & & & & \vdots \\ \vdots & & \vdots & \vdots & & & & \vdots \\ 0 & \cdots & 0 & h'_{Q(Q-m-1)} & \cdots & \cdots & \cdots & h'_{Q(Q+n)} \end{bmatrix} \begin{bmatrix} P_1 \\ V_1 \\ \vdots \\ P_q \\ V_q \\ P_{s1} \mid V_{s1} \\ \vdots \\ P_{sn} \mid V_{sn} \\ V_{r1} \\ \vdots \\ V_{rm} \end{bmatrix}. \tag{5.112}$$

The last m +2 rows can now be used to create the required m+2 by m+n+2 transfer matrix,

$$\begin{bmatrix} P_0 \\ V_0 \\ 0 \\ \vdots \\ 0 \end{bmatrix} = \begin{bmatrix} h'_{(Q-m)(Q-m-1)} & \cdots & \cdots & \cdots & h'_{(Q-m-1)(Q+n)} \\ \vdots & & & & \vdots \\ \vdots & & & & \vdots \\ \vdots & & & & \vdots \\ h'_{Q(Q-m-1)} & \cdots & \cdots & \cdots & h'_{Q(Q+n)} \end{bmatrix} \begin{bmatrix} P_1 \\ V_1 \\ \vdots \\ P_q \\ V_q \\ P_{s1} / V_{s1} \\ \vdots \\ P_{sn} / V_{sn} \\ V_{r1} \\ \vdots \\ V_{rm} \end{bmatrix}. \tag{5.113}$$

Thus, as in Section 5.2.4, a standardised transfer matrix can be obtained using row operations.

This implies that the whole sub-system can be modelled as a sub two-port element consisting of a 2+m by 2+m+n transfer matrix. Hence, sequential multiplication of transfer matrices either side of the sub-system can occur. As a result of the ability to include non-primary radiation points and intermediate sources within any general

reduction technique of sub-systems, any exhaust system which consists of multiple tailpipes, active noise cancellation systems and known FGN sources can be reduced.

5.5 Algorithmic adaptation

(All flowcharts concerned with this chapter are at the back of the chapter)

The earlier flowchart for single-port elements, Flowchart 2.3, is replaced by Flowchart 5.1 in order to accommodate the new single-port elements that are associated with intermediate sources and secondary radiation points. Flowchart 5.2 explains how transfer matrix multiplication proceeds when the size of either matrix is not two-by-two. Flowchart 5.2 replaces the decision box 'Multiply previous transfer matrix with current one' on Flowchart 2.2.

5.5.1 Extended single-port algorithm, Flowchart 5.1

This algorithm receives a single-port element from the 'Main' algorithm, refer to Flowchart 2.1. It then asks a list of questions in order to identify the type of single-port element. If the element is a closed end element, a wall admittance is calculated. Also, if the closed end is attached to a sub two-port element, where the associated matrix has two rows and columns, then the overall admittance is calculated. Thus, if the side-branch is connected to a three-port fork element, the admittance of the side-branch is used to adapt the transfer matrix associated with the sub two-port element, see Section 2.5.4. However, if the sub two-port element has associated secondary radiation points, or IS elements, then the GMRASB or GIS algorithm is used. Note, that the GMRASB algorithm is only used when there are no intermediate sources present.

Alternatively, if the received single-port element is a secondary radiation, the GMRASB algorithm is used to reduce the elements in the immediate area. The process is similar to that of a closed end. Note, that the 'Extended single-port' will record the transfer matrix linking the single-port element to the multi-port element for post-reduction analysis. However, if there is an intermediate source associated with either of the sub two-port elements, as with the closed end procedure, then the GISRSB algorithm is used. However, if the received single-port element is an intermediate source attached to the network by a fork, then 'Extended single-port' algorithm will use the GISR algorithm to adapt the transfer matrices surrounding the fork. Also, when there is a side-branch with intermediate sources within it, the GISRSB algorithm is always used.

Lastly, if any of the side-branches are attached to the system by a three-port fork element, the pointers are realigned to exclude the side-branch as described in Chapter 2. If procedures fail in the 'Extended single-port' algorithm, then the algorithm aborts and subsequently returns the single-port for further analysis by other algorithms.

5.5.2 Transfer matrix multiplication algorithm, Flowchart 5.2

The algorithm receives two transfer matrices from the two-port algorithm, Flowchart 2.2, and condenses the information into the 'current' transfer matrix and returns it, see Flowchart 5.2. Now the algorithm checks if both transfer matrices, associated with the 'previous' and 'current' elements, have two-by-two dimensions. If so, they are multiplied and the resultant is stored within the 'current' matrix and returned. If not, the algorithm checks if either of the transfer matrices have a differing number of rows to columns. When there are differing number of rows to columns, then intermediate sources are present and the GMMIR algorithm is used. However, if the rows and columns of both transfer matrices are equal, then the GMMR algorithm can be used. The resulting matrix is then associated with the 'current' element and returned.

5.5.3 Multiple time-variant source reduction with multiple radiations algorithm, Flowchart 5.3

This flowchart replaces Flowchart 3.2 and is almost the same, except that it can analyse time-varying exhaust systems with the added complication of multiple radiation points. Flowchart 5.3 differs from Flowchart 3.2 when the algorithm adds or manipulates connection equations, see Section 5.3.1. This only occurs when the algorithm encounters either of the process boxes 'Move along sub two-port element' or 'Add velocity whilst keeping pressures the same'. When the box 'Move along sub two-port element' is encountered, the algorithm reverts to Flowchart 5.4. Likewise, Flowchart 5.5 is used when the box 'Add velocity whilst keeping pressures the same' is encountered.

5.5.4 Sub two-port progression with time-variant sources and multiple radiations algorithm, Flowchart 5.4

This algorithm encompasses the process needed to relate matrix equations that are presently characterising the acoustic behaviour between pressure and velocity at a sole inlet of a sub two-port element to the multiple outlets.

The algorithm starts by querying if the sub two-port element has an associated radiation equation, see Section 5.3. If so, the matrices are adapted. An example of this for a transfer matrix with one link equation is demonstrated by equations (5.34) to (5.40) for the adaptation of matrices [**G**] and [**H**], followed by the creation of a connection equation, see equations (5.43) to (5.47). Another example of this adaptation of matrices [**G**] and [**H**] and connection equations is shown by equations (5.50) to (5.61). However, if the sub two-port element along which the algorithm is moving only has a set of two-by-two transfer matrices to describe the acoustical behaviour, then it adapts matrices [**G**] and [**H**] as

described in Section 3.3. However, if the sub two-port element does not contain a link equation, but the previous general equation is associated with a connection equation, then all the matrices [G] and [H], despite their subscripts, are adapted see Section 3.3 and equations (5.71) to (5.85).

5.5.5 Fork calculations for time-varying reduction with multiple radiations algorithm, Flowchart 5.5

This algorithm adds together the velocity vectors whilst keeping the pressure variables within the pressure vectors constant. The algorithm occurs when general equations characterising the inlets of a fork need to be combined. The algorithm detects if any of the matrix equations originating from the inlet of the fork have associated connection equations. If they do not, the summations of [G] and [H] occur, as described in Section 3.3. However, if there are connection equations present, then a series of matrix manipulations are required to create the main matrix and connection equations, these are described by equations (5.62) to (5.70).

5.6 Evaluation of exhaust systems with multiple radiation points and intermediate sources

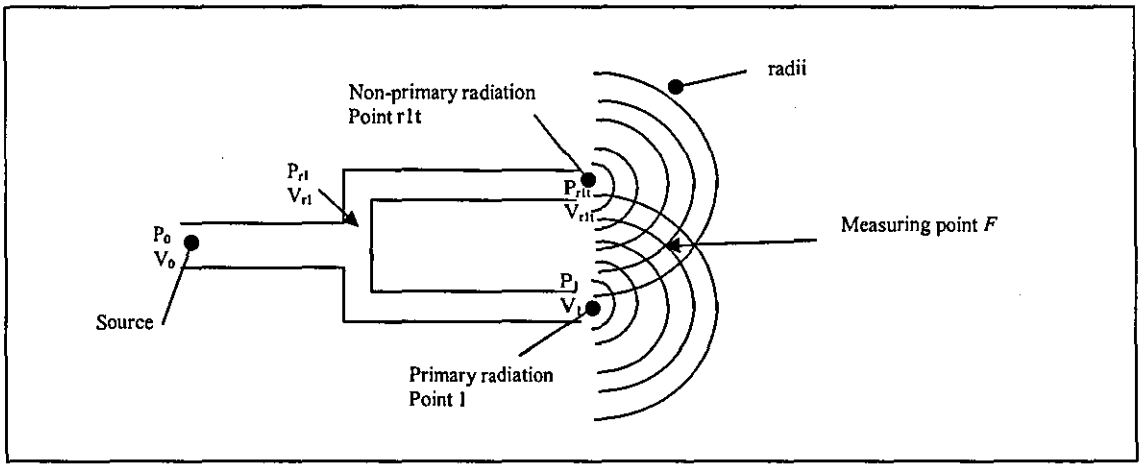

Figure 5. 11 Multiple radiation interference pattern

Consider a general exhaust system, with n intermediate sources and m secondary radiation points, such that the transfer matrix of the system is

$$\begin{bmatrix} P_0 \\ V_0 \\ 0 \\ \vdots \\ \vdots \\ 0 \end{bmatrix} = \begin{bmatrix} f_{11} & f_{12} & f_{13} & \cdots & f_{1(n+2)} & 0 & \cdots & \cdots & 0 \\ \vdots & \vdots & f_{23} & \cdots & f_{2(n+2)} & 0 & \cdots & \cdots & 0 \\ \vdots & \vdots & \vdots & & \vdots & 1 & \ddots & & 0 \\ \vdots & \vdots & \vdots & & \vdots & 0 & \ddots & \ddots & \vdots \\ \vdots & \vdots & \vdots & & \vdots & \vdots & \ddots & \ddots & 0 \\ f_{(m+2)1} & f_{(m+2)2} & f_{(m+2)3} & \cdots & f_{(m+2)(n+2)} & 0 & \cdots & 0 & 1 \end{bmatrix} \begin{bmatrix} P_1 \\ V_1 \\ P_{s1} \mid V_{s1} \\ \vdots \\ P_{sn} \mid V_{sn} \\ V_{r1} \\ \vdots \\ V_{rm} \end{bmatrix}, \tag{5.115}$$

where $P_{s1}|V_{s1}$ to $P_{sn}|V_{sn}$ are the pressures or acoustic mass velocities associated with the intermediate sources. Also, V_{r1} to V_{rm} represent the acoustic mass velocities associated

with the secondary radiation points. The primary radiation point *1* is assumed to have a known radiation impedance, Z_1, such that

$$\begin{bmatrix} P_0 \\ V_0 \\ 0 \\ \vdots \\ \vdots \\ 0 \end{bmatrix} = \begin{bmatrix} f_{11}Z_1 + f_{12} & f_{13} & \cdots & f_{1(n+2)} & 0 & \cdots & \cdots & 0 \\ \vdots & f_{23} & \cdots & f_{2(n+2)} & 0 & \cdots & \cdots & 0 \\ \vdots & \vdots & & \vdots & 1 & \ddots & & 0 \\ \vdots & \vdots & & \vdots & 0 & \ddots & \ddots & \vdots \\ \vdots & \vdots & & \vdots & \vdots & \ddots & \ddots & 0 \\ f_{(m+2)1}Z_1 + f_{(m+2)2} & f_{(m+2)3} & \cdots & f_{(m+2)(n+2)} & 0 & \cdots & 0 & 1 \end{bmatrix} \begin{bmatrix} V_1 \\ P_{s1} \mid V_{s1} \\ \vdots \\ P_{sn} \mid V_{sn} \\ V_{r1} \\ \vdots \\ V_{rm} \end{bmatrix}. \tag{5.115}$$

At the source of a multiple radiation exhaust system, see Figure 5. 11, the inlet pressure, P_0, velocity, V_0, or the source impedance, P_0/V_0, is known. Then, if the strengths of all the intermediate sources, from $P_{s1}|V_{s1}$ to $P_{sn}|V_{sn}$, are known and are coherent with the engine source; the velocity at point *1* is

$$V_1 = \frac{P_0 - \sum_{k=1}^{n} \left(f_{1(k+2)} P_{sk} \mid V_{sk} \right)}{f_{11}Z_1 + f_{12}}. \tag{5.116}$$

Similarly, if the velocity at point *0* is known, then

$$V_1 = \frac{V_0 - \sum_{k=1}^{n} \left(f_{2(k+2)} P_{sk} \mid V_{sk} \right)}{f_{21}Z_1 + f_{22}}. \tag{5.117}$$

However, if neither P_0 or V_0 is known, but the source impedance, Z_0, is known, then an expression for P_0 can be formed using the second row of equation (5.115)

$$P_0 = \left(f_{21}Z_1 + f_{22} \right) Z_0 V_1 + \sum_{k=1}^{n} \left(f_{2(k+2)} Z_0 P_{sk} \mid V_{sk} \right). \tag{5.118}$$

Thus, equation (5.118) can be used to replace P_0 in equation (5.116) to give

$$V_1 = \frac{\sum_{k=1}^{n}\left(\left(f_{2(k+2)}Z_0 - f_{1(k+2)}\right)P_{sk} \mid V_{sk}\right)}{\left(f_{11}Z_1 + f_{12} - f_{21}Z_0Z_1 - f_{22}Z_0\right)}. \tag{5.119}$$

Once V_1 is known, then the velocities V_{r1} to V_{rm} can be calculated by

$$V_{rq} = -\left(\left(f_{(q+2)1}Z_1 + f_{(q+2)2}\right)V_1 + \sum_{k=1}^{n}\left(f_{(q+2)(k+2)}\ P_{sk} \mid V_{sk}\right)\right), \tag{5.120}$$

where q is an integer between 1 and m. Obtaining the velocity or pressure at each secondary radiation point requires the transfer matrix which describes the acoustic behaviour of the side-branch. An example of such a transfer matrix is equation (5.1) when considering the side-branch with respect to Figure 5. 2. Now, let point rq be attached to the inlet of a side-branch which is described with a sub two-port element, thus it can be characterised by a transfer matrix of size (M+2) by (M+N+2), $M \geq 0$ and $N \geq 0$. Where N represents the number of previous intermediate sources, $\sigma 1$ to σN, likewise R represents the number of previous radiation points, $R1$ to RM. Thus, the general standardised transfer matrix of the side-branch can be characterised by

$$\begin{bmatrix} P_{rq} \\ V_{rq} \\ 0 \\ \vdots \\ \vdots \\ 0 \end{bmatrix} = \begin{bmatrix} h_{11} & h_{12} & h_{13} & \cdots & h_{1(N+2)} & 0 & \cdots & \cdots & 0 \\ \vdots & \vdots & h_{23} & \cdots & h_{2(N+2)} & 0 & \cdots & \cdots & 0 \\ \vdots & \vdots & \vdots & & \vdots & 1 & \ddots & & 0 \\ \vdots & \vdots & \vdots & & \vdots & 0 & \ddots & \ddots & \vdots \\ \vdots & \vdots & \vdots & & \vdots & \vdots & \ddots & \ddots & 0 \\ h_{(M+2)1} & h_{(M+2)2} & h_{(M+2)3} & \cdots & h_{(M+2)(N+2)} & 0 & \cdots & 0 & 1 \end{bmatrix} \begin{bmatrix} P_{rqt} \\ V_{rqt} \\ P_{\sigma 1} \mid V_{\sigma 1} \\ \vdots \\ P_{\sigma N} \mid V_{\sigma N} \\ V_{R1} \\ \vdots \\ V_{RM} \end{bmatrix}, \tag{5.121}$$

where *rqt* is the termination of the side-branch. Now, the impedance at the secondary radiation point is also known, Z_{rqt}, therefore

$$V_{rqt} = \frac{V_{rq} - \sum_{k=1}^{N} \left(h_{2(k+2)} + P_{ok} \mid V_{ok} \right)}{h_{21} Z_{rqt} + h_{22}}. \qquad (5.122)$$

Thus, for every secondary radiation point, the associated standardised transfer matrix linking the point to the junction, combined with the radiation impedance, needs to be stored for post system reduction analysis. This is possible as each secondary radiation point is given an identification number that can be associated with a transfer matrix and radiation impedance at a specified frequency. Thus, finally the radiation impedance at each radiation point can be used to obtain the pressure at each point, if required.

However, if the intermediate sources are not coherent with the engine source, or with each other, the velocity and pressure at all the radiation points are evaluated for each source in turn by assuming that only one of the sources is producing noise. This is achieved by setting all the intermediate sources to zero magnitude and modelling the engine with a source impedance, see equation (5.119).

Previous work in the thesis evaluated the effectiveness of an exhaust system by comparing two systems, focusing on insertion loss. This was achieved by keeping the noise source and the distance between the observation point and the radiation point constant. When an exhaust system with multiple radiation points is compared to another exhaust system, the position of the observation in relationship to all of the radiation points is vitally important.

The radiating sound wave from a single radiation point of an exhaust system can be modelled as a point source. Point sources propagate spherically into a free field. The pressure, P_F, at some point, with respect to Figure 5. 11, *F*, at distance *l* from the source is given by [43]

$$P_F = \frac{P_r e^{i\omega \frac{l}{\bar{c}}}}{4\pi r^2}, \tag{5.123}$$

where $\bar{c}$ is the mean speed of sound at the radiation point, P_r is the pressure at the radiation point and ω is the angular frequency. Now, let there be M radiation points with known pressures at each radiation point, say P_{rk}, k=1...m. Also, let radiation point be the distance l_k away from the field point, F. Hence, the pressure at the field point, P_F, is

$$P_F = \sum_{k=1}^{k=M} \frac{P_{rk} e^{i\omega \frac{l_k}{\bar{c}_k}}}{4\pi l_k^2} \tag{5.124}$$

The effect of the ground plane can be included by the usual technique of image sources.

5.7 Multiple radiation validation

In order to validate the inclusion of the multiple radiation algorithm within the code, a selection of analytical tests have been applied, as given below. Unfortunately, there are no known published experimental results that include multiple radiation points with which to make a comparison.

5.7.1 Validation test 1

The first validation test considers the simplest symmetrical duct network with two radiation points, see Figure 5. 12, and verify that the same acoustic waves propagate out of each radiation point. The figure shows a simple rigid pipe of length 500mm and a diameter of 40√2mm connected to two tailpipes, each of length 500mm and diameter

40mm. Let the temperature throughout the duct be 350°C and in the surrounding atmosphere be 20°C. This pipe network can be reduced to a three-by-three transfer matrix similar to equation (5.11). The duct network in Figure 5. 12 is characterised by the same type of elements as in Figure 5. 11. Since the radiation impedance can be calculated [1] and a simplistic source model is used, say the inlet acoustic mass velocity has a constant V_0=0.1m/s with infinite source impedance, the velocity at the primary radiation can be obtained, V_1, see equation (5.117). Now, equations (5.120) and (5.122) are used to calculate the velocity at the secondary radiation V_{r1t}. Finally, the radiation impedance is used to obtain the pressure at each radiation point.

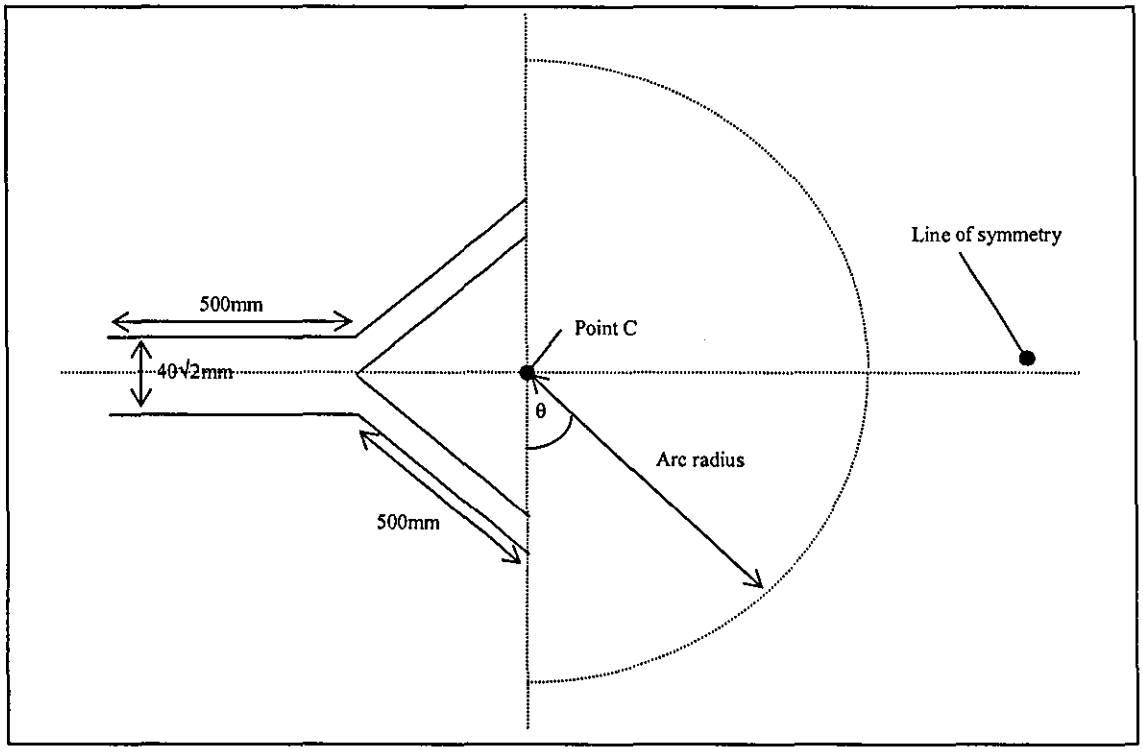

Figure 5. 12 Simple twin radiation network

The calculated pressure and velocity at the two radiation points were exactly the same, as to be expected. Figure 5. 13 shows the real and imaginary components of the pressure at the radiation points. The figure also shows resonances at 125Hz, 375Hz, 625Hz and 875Hz which are characteristic of a closed-open pipe [1]. The resonances when the length of the duct is an odd quarter multiple of the wavelength.

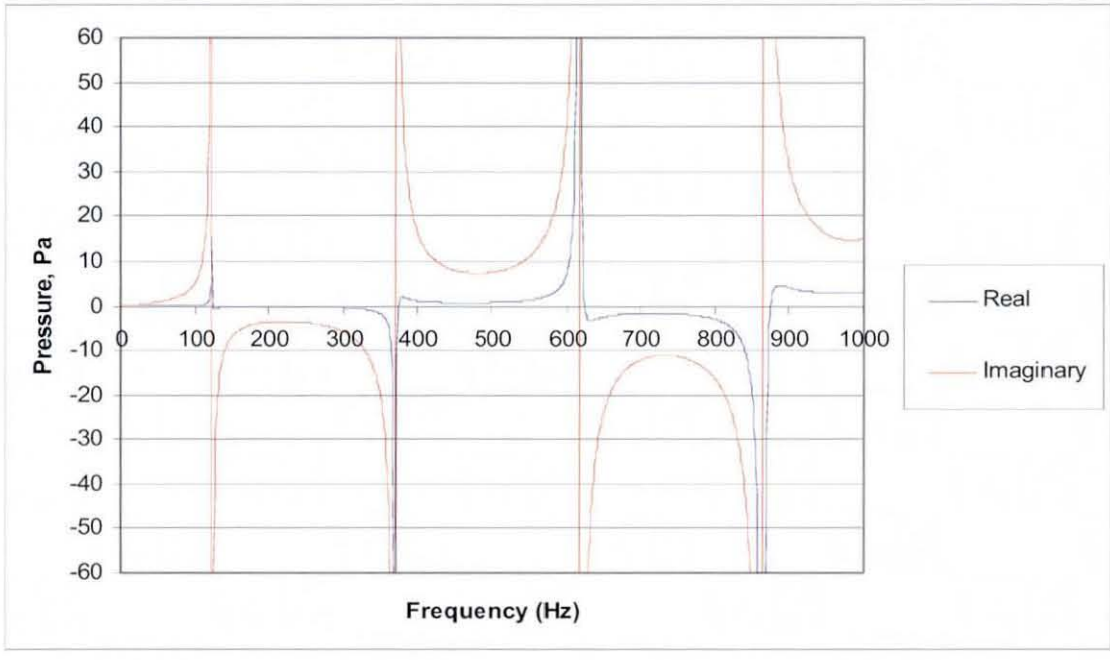

Figure 5. 13 Real and imaginary components of pressure at the radiation points

5.7.2 Validation test 2

Another validation test to ensure that the code models correctly the sound waves at the outlet of the ducts is to observe the behaviour of the interaction between the sound waves in the free field along an arc, see Figure 5. 12, with pipe lengths of 1000mm. Let the arc constitute half of a circle with its centre at 'Point C' on the line of symmetry, where the point is 500mm from each tailpipe exit.

Figure 5. 14 shows the calculated pressure at angle θ, $0 < \theta < \pi$, along the arc, at 200Hz. The pressures at the two radiation points are calculated using the same method as in the first validation test and the arc radius was chosen to be 3000mm. Figure 5. 14 shows that as θ progresses from zero to π, wave interaction occurs and there is the expected symmetry about $\theta/2$, or the 'Line of symmetry' with respect to Figure 5. 12. There will be no absolute cancelling of both waves when the two pressure waves are half a wavelength

out of phase, since the magnitude of the pressure from each radiation point is different, as the distances from the two radiation points are not the same. However, it is found that the magnitude of the pressure along the arc is at a minimum at positions where the path difference is half a wavelength.

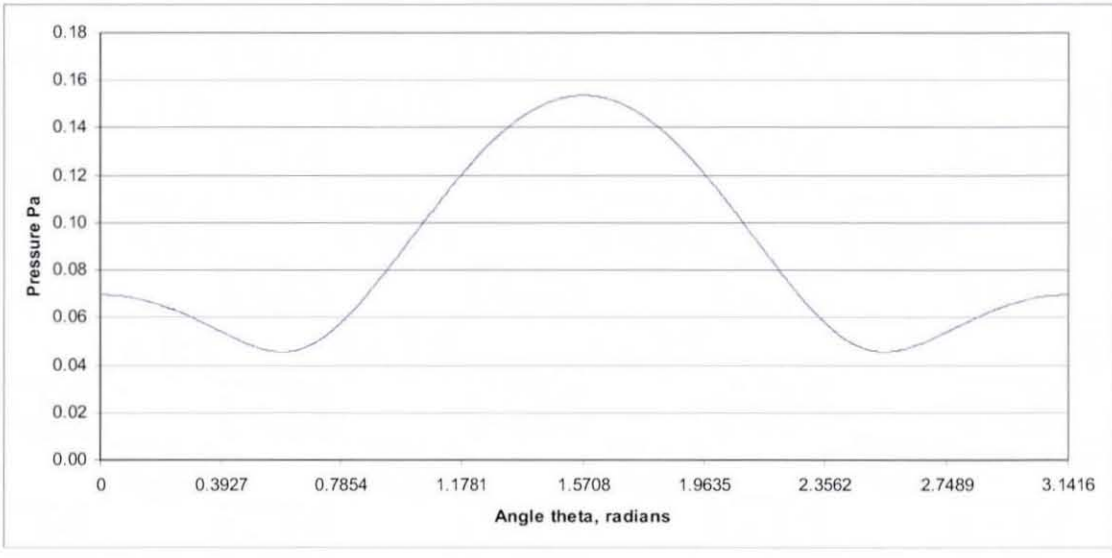

Figure 5. 14 Pressure evaluated along the 'Arc' as in Figure 5. 12, at 200Hz

5.7.3 Validation test 3

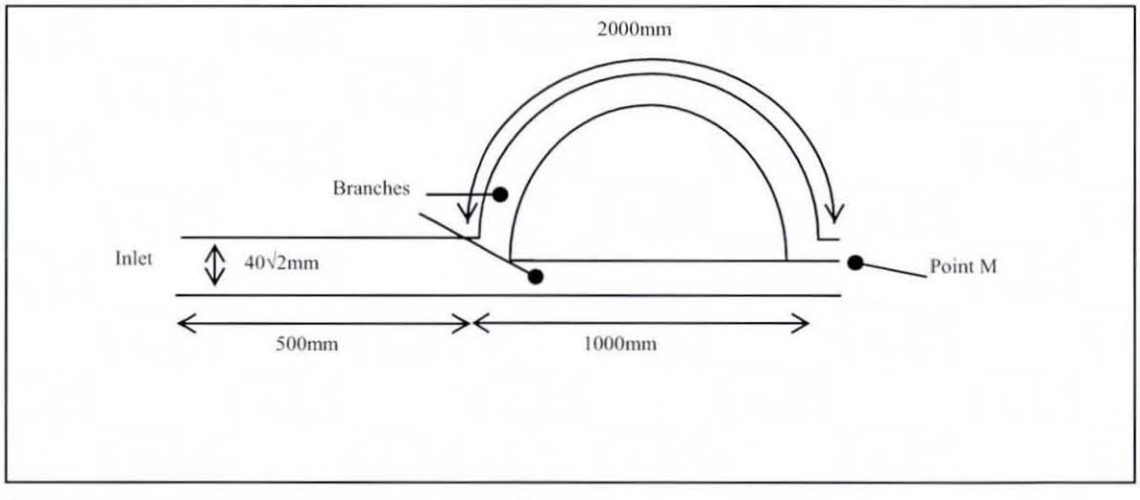

Figure 5. 15 Pipe network to verify total cancellation

Another exercise to check that multiple radiation points are modelled correctly is to model the pipe system of Figure 5. 15, a network with one inlet and two outlets. The cross sectional areas of the branches are half the area of the inlet pipe. Let the acoustic mass velocity at the inlet be V_0=0.1m/s, thus, equations (5.117) and (5.120) can be used to acquire the velocities at the radiation points. Now, the radiation impedance of both points can be used to obtain the respective pressures, at 'Point M' with respect to Figure 5. 15. Two radiation points cannot be located physically at exactly the same point in space, however, for verification purposes, it is assumed that they are. The temperature within the duct is taken to be 350°C, such that the speed of sound is 500 m/s. Since the difference in path lengths is 1m, there will be a path difference of half a wavelength and hence complete cancellation of sound at frequencies 250Hz, 750Hz, 1250Hz etc. The inputs for this verification example are calculated by the same method as for the first validation test.

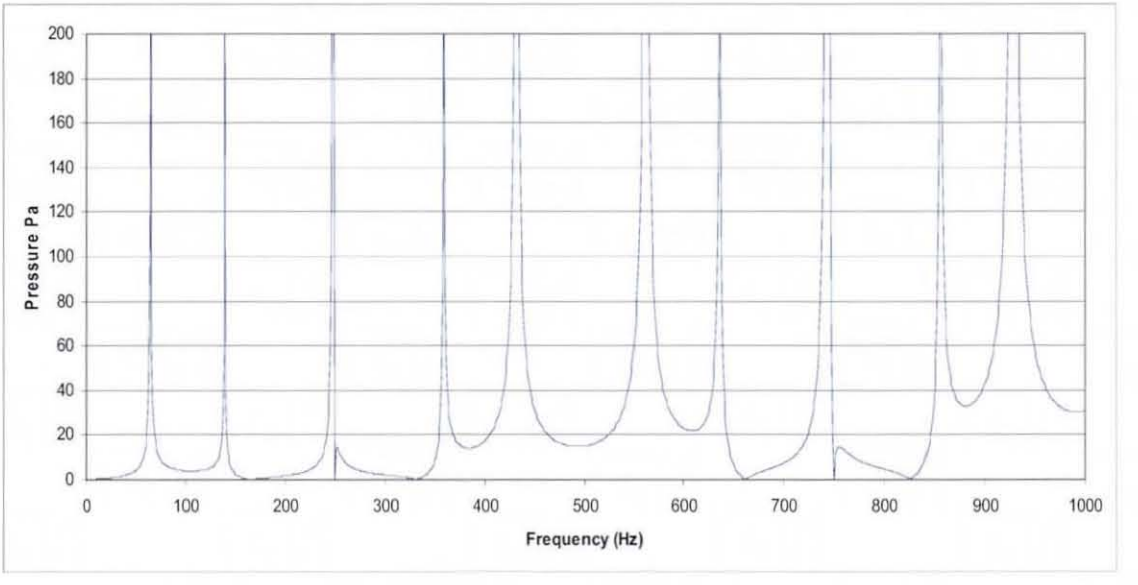

Figure 5. 16 Pressure evaluated at 'Point M', as on Figure 5. 15

Figure 5. 16 illustrates the varying magnitude of pressure at 'Point M' with frequency. As expected, the radiated pressure magnitude is seen to be zero at 250Hz and 750Hz.

However, there are many other features to be observed in Figure 5. 16. An analytical solution of the simple network is given below to achieve full validation of this test case.

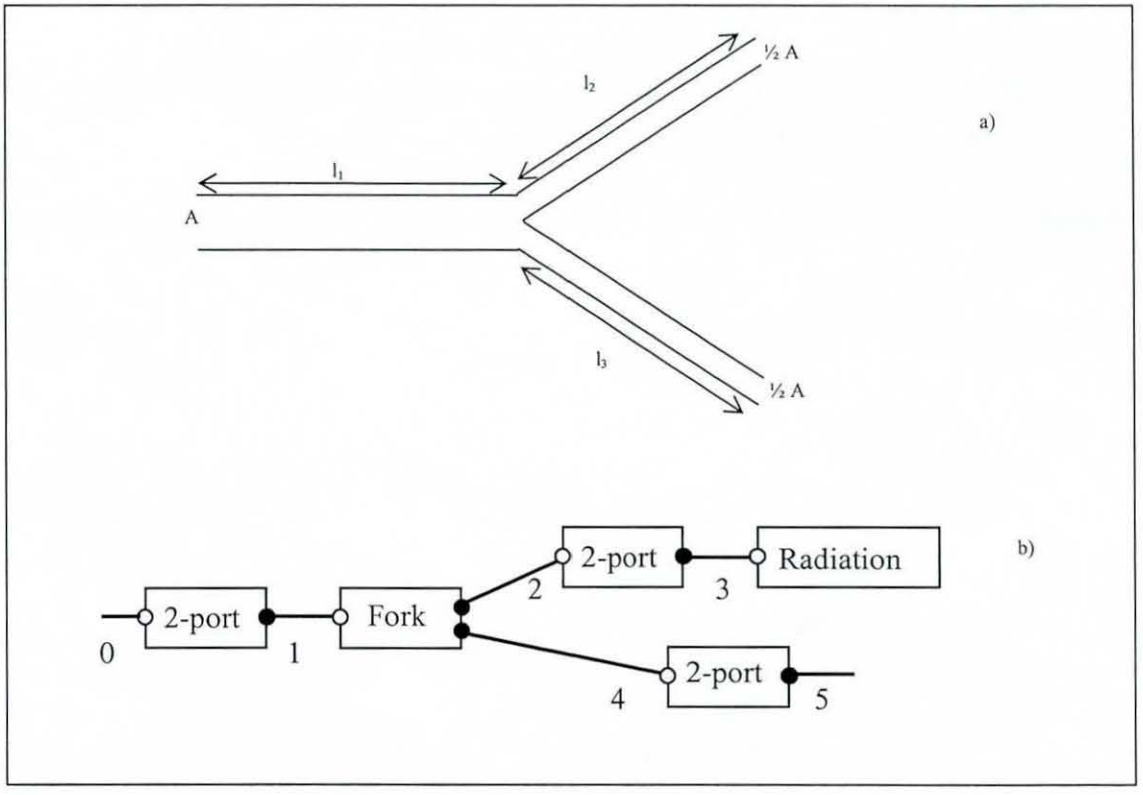

Figure 5. 17 Simple Twin Radiation model

Consider the general representation of the system of Figure 5. 17 as given in Figure 5. 15. The network in Figure 5. 17a can be represented by a system of acoustic elements, as shown by Figure 5. 17b, therefore the acoustic properties between the numbered positions are described as

$$\begin{bmatrix} P_0 \\ V_0 \end{bmatrix} = \begin{bmatrix} \cos(kl_1) & \frac{i}{A_d}\sin(kl_1) \\ iA_d \sin(kl_1) & \cos(kl_1) \end{bmatrix} \begin{bmatrix} P_1 \\ V_1 \end{bmatrix} \tag{5.125}$$

$$\begin{bmatrix} P_2 \\ V_2 \end{bmatrix} = \begin{bmatrix} \cos(kl_2) & i\frac{2}{A_d}\sin(kl_2) \\ i\frac{A_d}{2}\sin(kl_2) & \cos(kl_2) \end{bmatrix} \begin{bmatrix} P_3 \\ V_3 \end{bmatrix}, \tag{5.126}$$

and

$$\begin{bmatrix} P_4 \\ V_4 \end{bmatrix} = \begin{bmatrix} \cos(kl_3) & i\frac{2}{A_d}\sin(kl_3) \\ i\frac{A_d}{2}\sin(kl_3) & \cos(kl_3) \end{bmatrix} \begin{bmatrix} P_5 \\ V_5 \end{bmatrix}. \tag{5.127}$$

Where k is the wave number ω/c_o, ω is the angular frequency and A_d is the admittance A/c_o. The radiation impedance at position 3, with respect to Figure 5. 1, can be defined as [1]

$$Z_r = 0.5\left(k\sqrt{\frac{A}{\pi}}\right)^2 + i0.6k\sqrt{\frac{A}{\pi}}. \tag{5.128}$$

Therefore the impedance, Z_2, at position number 2, is

$$Z_2 = \frac{2}{A_d}\frac{Z_r\cos(kl_2)+i\sin(kl_2)}{Z_r i\sin(kl_2)+\cos(kl_2)}. \tag{5.129}$$

Let the two-by-two transfer matrix which relates the properties at position 0 to that of position 5 be

$$\begin{bmatrix} P_0 \\ V_0 \end{bmatrix} = \begin{bmatrix} a_{05} & b_{05} \\ c_{05} & d_{05} \end{bmatrix} \begin{bmatrix} P_5 \\ V_5 \end{bmatrix}, \tag{5.130}$$

such that

$$\begin{bmatrix} a_{05} & b_{05} \\ c_{05} & d_{05} \end{bmatrix} = \begin{bmatrix} \cos(kl_1) & \frac{i}{A_d}\sin(kl_1) \\ iA_d\sin(kl_1) & \cos(kl_1) \end{bmatrix} \begin{bmatrix} 1 & 0 \\ \frac{1}{Z_2} & 1 \end{bmatrix} \begin{bmatrix} \cos(kl_3) & i\frac{2}{A_d}\sin(kl_3) \\ i\frac{A_d}{2}\sin(kl_3) & \cos(kl_3) \end{bmatrix}, \tag{5.131}$$

or

$$\begin{bmatrix} a_{05} & b_{05} \\ c_{05} & d_{05} \end{bmatrix} = \begin{bmatrix} \cos(kl_1) + \frac{i}{Z_2 A_d}\sin(kl_1) & \frac{i}{A_d}\sin(kl_1) \\ iA_d \sin(kl_1) + \frac{1}{Z_2}\cos(kl_1) & \cos(kl_1) \end{bmatrix} \begin{bmatrix} \cos(kl_3) & i\frac{2}{A_d}\sin(kl_3) \\ i\frac{A_d}{2}\sin(kl_3) & \cos(kl_3) \end{bmatrix}. \tag{5.132}$$

Now resonance occurs when there is a non-trivial solution for a null input, which in this case implies $V_o = 0$. Thus from equation (5.130) resonance should occur when

$$\frac{2}{A_d} c_{05} Z_r + d_{05} = 0. \tag{5.133}$$

Now substitute c_{05} and d_{05} from equation (5.133) with known algebraic expressions from equation (5.132)

$$\begin{aligned} &\left(\left(iA_d \sin(kl_1) + \frac{1}{Z_2}\cos(kl_1)\right)\cos(kl_3) + i\frac{A_d}{2}\cos(kl_1)\sin(kl_3)\right)\frac{2Z_r}{A_d} + \\ &\left(iA_d \sin(kl_1) + \frac{1}{Z_2}\cos(kl_1)\right)\frac{2i}{A_d}\sin(kl_3) + \cos(kl_1)\cos(kl_3) = 0 \end{aligned}, \tag{5.134}$$

further reduction of equation (5.134) gives

$$\begin{aligned} &\left(2i\sin(kl_1) + \frac{iZ_r \sin(kl_2) + \cos(kl_2)}{Z_r \cos(kl_2) + i\sin(kl_2)}\cos(kl_1)\right)(i\sin(kl_3) + Z_r \cos(kl_3)) + \\ &\cos(kl_1)(iZ_r \sin(kl_3) + \cos(kl_3)) = 0 \end{aligned}. \tag{5.135}$$

Let the left-hand side of this equation be termed *VC*. The blue series on Figure 5.20 shows |VC| as a function of frequency for the network of Figure 5.16.

$$VC(f)=\left|\begin{array}{c}\left(2i\sin\left(\frac{2\pi f}{c_0}l_1\right)+\frac{iZ_r\sin\left(\frac{2\pi f}{c_0}l_2\right)+\cos\left(\frac{2\pi f}{c_0}l_2\right)}{Z_r\cos\left(\frac{2\pi f}{c_0}l_2\right)+i\sin\left(\frac{2\pi f}{c_0}l_2\right)}\cos\left(\frac{2\pi f}{c_0}l_1\right)\right)\\ \left(i\sin\left(\frac{2\pi f}{c_0}l_3\right)+Z_r\cos\left(\frac{2\pi f}{c_0}l_3\right)\right)+\\ \cos\left(\frac{2\pi f}{c_0}l_1\right)\left(iZ_r\sin\left(\frac{2\pi f}{c_0}l_3\right)+\cos\left(\frac{2\pi f}{c_0}l_3\right)\right)\end{array}\right|, \tag{5.136}$$

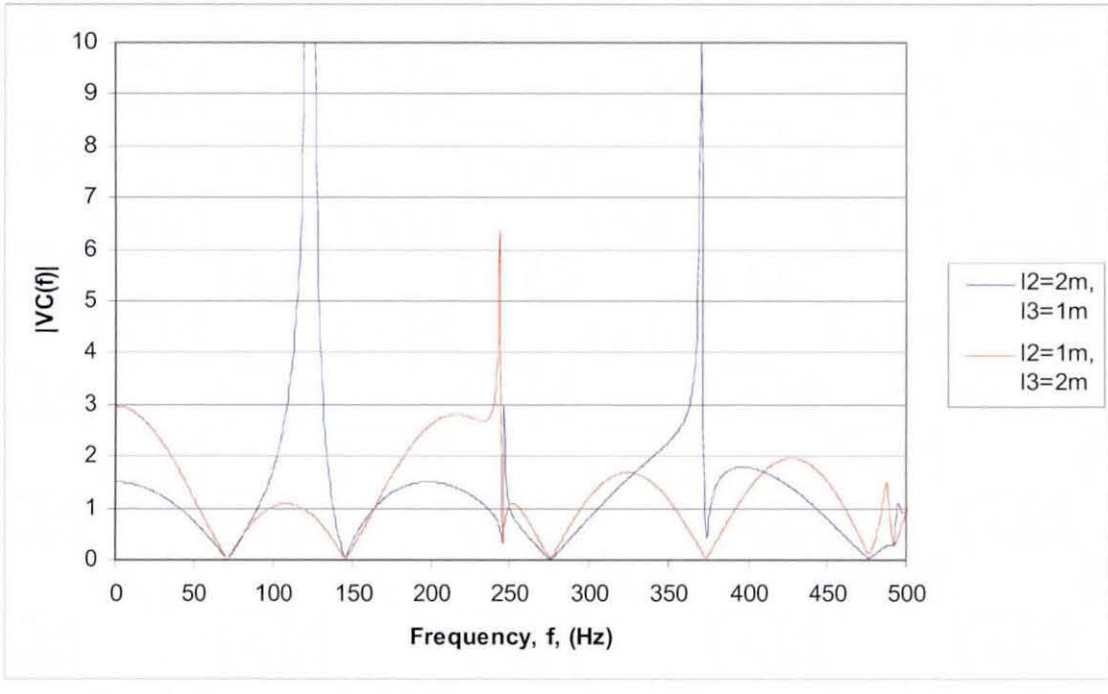

Figure 5. 18 Variation of the function VC(*f*)

The red series illustrates the behaviour of the same duct network with a reclassification of l_2=1m and l_3=2m. The zeros of Figure 5. 18, which relate to in-duct resonances, for example at 75Hz, 146Hz, 250Hz etc., correlate with the resonant features seen in Figure 5. 16. It may also be observed that essentially the same in-duct resonances are present whichever way around the pipes are modelled, i.e. the red and blue series, although of

course the function $VC(f)$ is different for the two cases. Note that the function $|VC(f)|$ is not the same as the sum of velocities at some external 'Point M' in Figure 5. 15.

5.7.4 Validation test 4

The purpose of this test is to validate the modelling of the multiple time-varying sources coupled with multiple radiations. The test will consist of the Arvin Meritor manifold, see Figure 3. 13 and Figure 3. 14, attached to an adapted version of silencer 'IA00085', say 'IA00085b' see Figure 5. 19, which has a twin radiation configuration. This silencer will be compared with silencer IA00085, thus illustrating the change in radiated sound pressure level between the two exhaust silencers, given the same manifold and source.

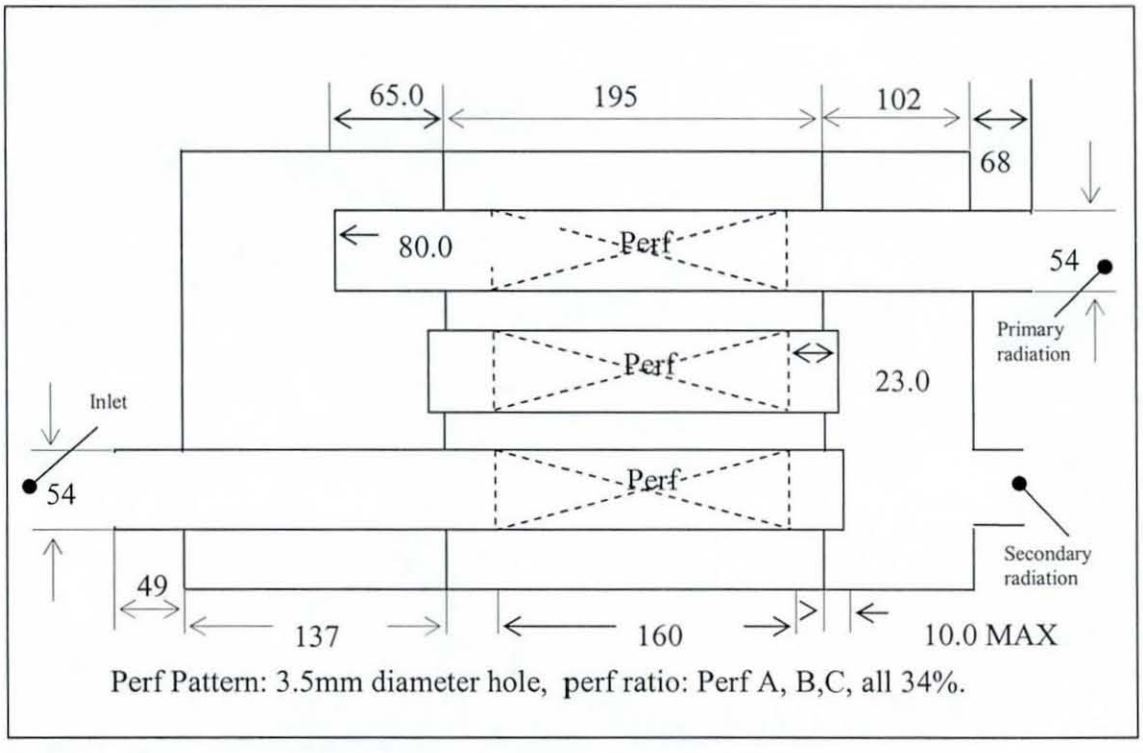

Figure 5. 19 Triple pass resonator with a twin outlet, silencer IA00085b

The running conditions of the engine, harmonics, valve timing, interconnecting pipe, manifold and cylinder/valves have the same configuration as described in Section 3.6.

Specific conditions, such as 1000RPM engine speed and constant in-cylinder pressure of 10Pa are the same as stated in Section 3.8.1. Since there are two acoustic outlets in one system and one outlet in the other, the sum of all the radiated pressure at every outlet of a given system constitutes an effective measurement of radiated sound. Thus, this summation of pressure over m radiation points is compared to a reference pressure, $P_{REF}=2\cdot10^{-5}$Pa, enabling the radiated sound pressure level [1] to be calculated,

$$SPL = 10\log_{10}\left(\frac{\left|\sum_{k=1}^{m} P_k^{\,2}\right|}{P_{\mathrm{Re}f}^2}\right), \tag{5.137}$$

where P_k is the pressure at the outlet k. A measurement of the total sound pressure level enables the measurement of sound without the decay and phase relationship between each radiation point and a field point occurring as a factor, see Section 5.6.

Section 3.2.3 illustrates the method required to obtain a velocity vector from a general matrix equation, thus by using equation (3.39) in conjunction with equation (3.38) the pressure can be acquired for each harmonic. Section 5.2.7 describes how a secondary radiation located within a network of ducts that are not consecutively sequenced, as in Figure 5. 19, can be reduced to a three-by-three transfer matrix for each individual frequency. Hence, if a general matrix equation is known at the inlet of the silencer in Figure 5. 19, then two velocity vectors can be acquired to describe the acoustic output at the radiations, see Section 5.6. Application of equation (3.38) to each of the velocity vectors will produce pressure vectors, thus allowing radiated noise to be calculated.

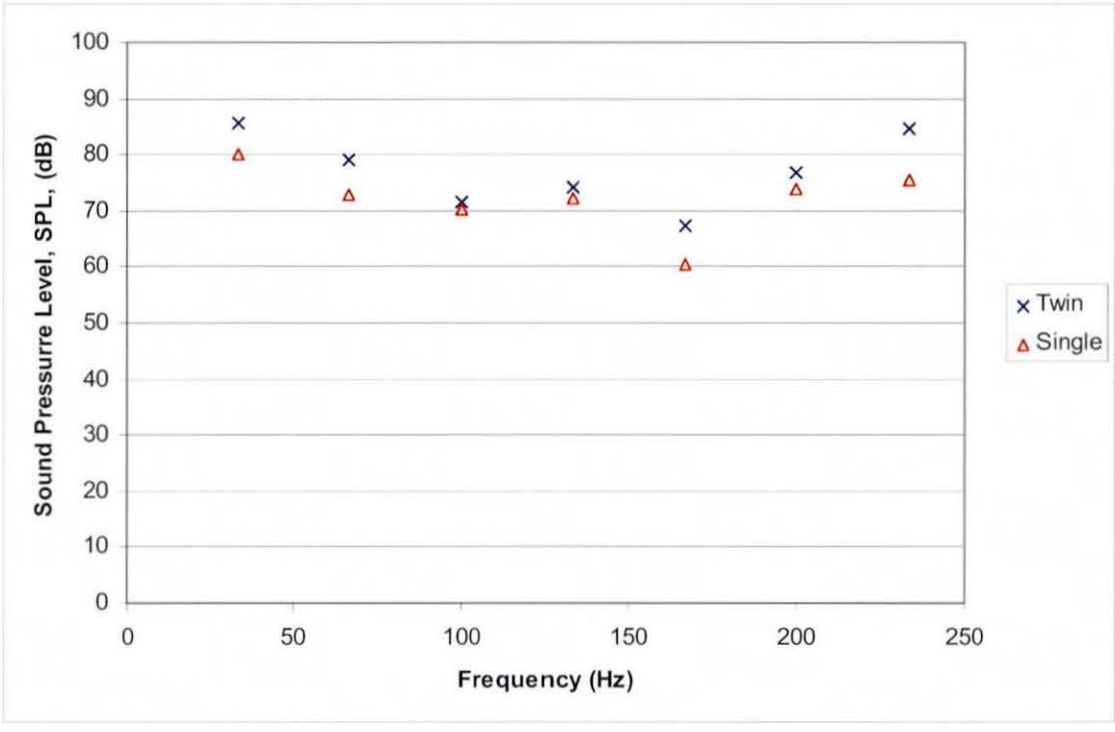

Figure 5. 20 Radiated sum of sound pressure levels from single and twin radiation exhaust systems

Figure 5. 20 shows radiated noise levels at multiples of the firing frequency, 33.33Hz. Since the manifold is symmetrical, there is wave cancellation at every multiple of valve frequency, except those which coincide with multiples of firing frequency, i.e. every fourth harmonic of the valve frequency. The radiated power at firing frequency from the twin radiation exhaust system is seen to be greater than that from the single radiation exhaust system. Furthermore, the greatest contribution to the overall radiated power is from the firing frequency. Both of these predictions concur with present knowledge and experience of twin exhaust systems. They are known [97] to increase the radiated noise, but are sometimes used in order to reduce back-pressure at high flow rates. Thus, at least this validation test shows that the algorithm and mathematical matrix manipulation used to analyse twin radiation exhaust systems, with time-variant sources, works for a realistic system and produces sensible results.

5.7.5 Validation test 5

The fifth validation test concerns exhaust systems which comprise of two symmetrical silencer systems connected by a balance pipe. The addition of a balance pipe requires new manipulation procedures of the general matrix equations, hence this validation test was undertaken to help verify the mathematics in Section 5.3.2 and subsequent coding of the algorithm.

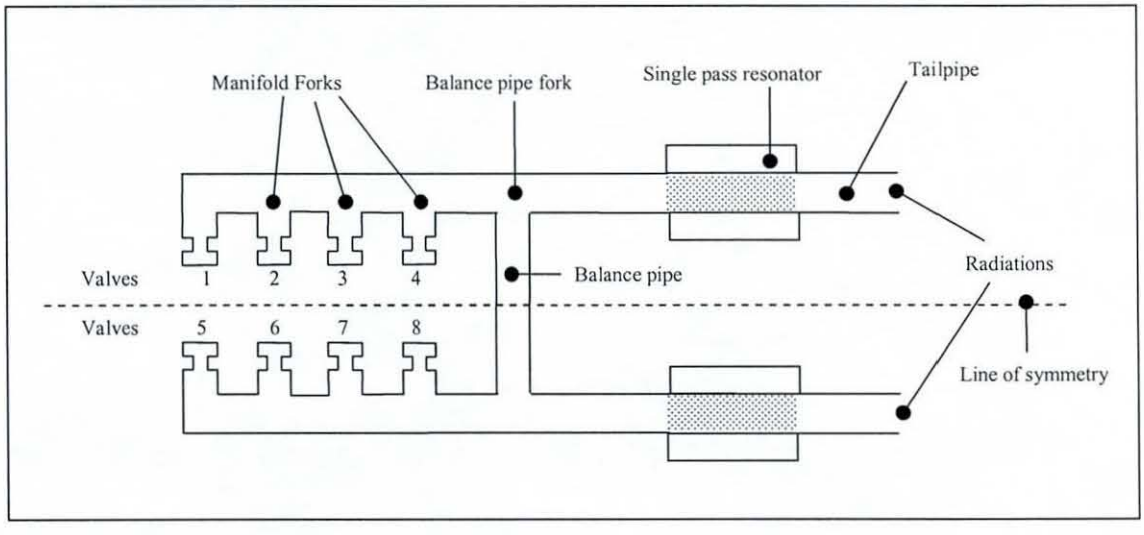

Figure 5. 21 Exhaust system with a balance pipe and single pass resonators

This validation test reviews the radiated noise at the radiation of the manifold and silencer system as shown in Figure 5. 21. All the straight and rigid pipes within this system have a consistent diameter of 40mm and the temperature throughout the system remains constant at 350°C. The pipes between each valve and manifold fork have equal lengths of 100mm. The balance pipe has a length of 750mm, the pipe between the manifold fork and balance pipe has a length of 1000mm, likewise for the pipes between the balance pipe and single pass resonators. The straight-through, single-pass resonators in Figure 5. 21 are both exactly the same with a length of 210mm, a casing with a cross-sectional area of 26624mm^2 and a perforated pipe of 34% porosity. The tailpipe has a length of 150mm. All the valves have exactly the same time-variant, open area curves given by function $A(t)$, as described in equation (4.48), with a maximum open area of 100mm^2. The constant

in-cylinder pressure is 100Pa. Exactly the same geometric configuration is present above and below the 'Line of symmetry', with respect to Figure 5. 21. The valve frequency in this test is 8.33Hz.

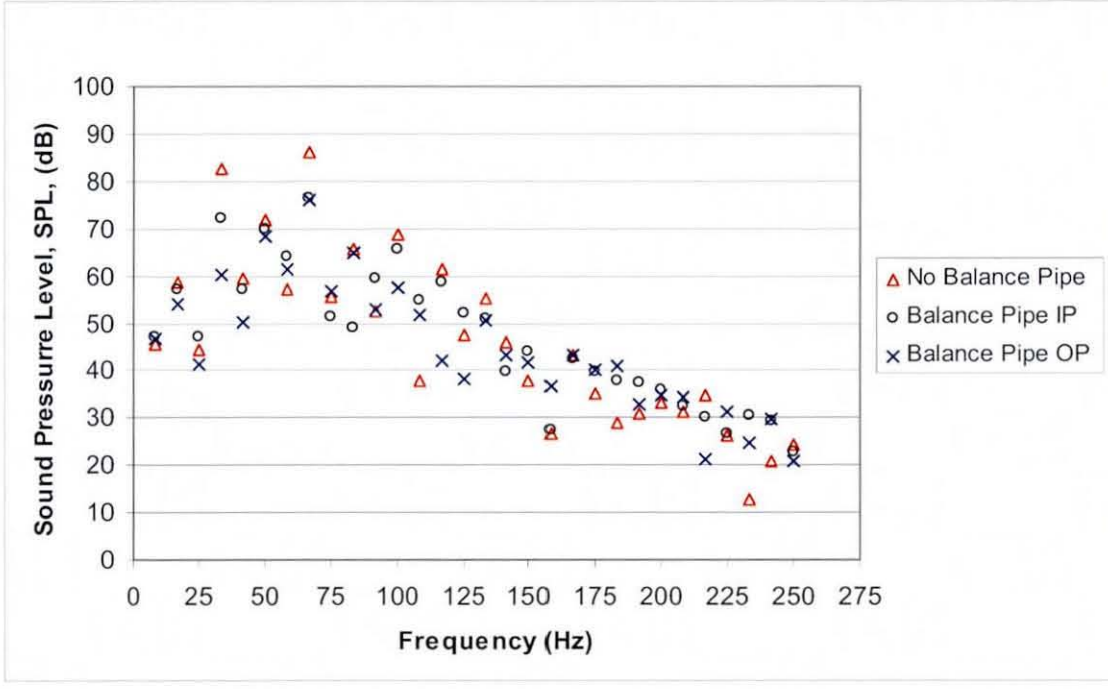

Figure 5. 22 Radiated sum of sound pressure levels from the system shown in Figure 5. 21 at multiples of valve frequency

The exhaust system shown in Figure 5. 21 comprises of two identical exhaust systems connected via a balance pipe. Thus, in order to validate the balance pipe calculations and algorithm procedure, the radiated sound pressure level for one exhaust system, without the involvement of a balance pipe, should be known in order to make a comparison, i.e. a control. The 'No Balance Pipe' series on Figure 5. 22 illustrates this radiated noise level, increased by 3dB to account for the separated identical systems. The valve firing order starts with valve 1, followed by valve 3, valve 2 and lastly valve 4, each separated by a quarter of the time period for one complete valve cycle.

The second series 'Balance Pipe IP', in Figure 5. 22, includes both of the identical exhaust systems which are connected via a balance pipe, see Figure 5. 21. The firing order in this series is; valves 1 and 5 fire first, followed by valves 3 and 7, then valves 2 and 6, lastly

valves 4 and 8. Each pair of valves fire together and each pair are separated by a quarter of the time period for one complete valve cycle. Note that this firing sequence would not be used commercially, however, it provides a valuable theoretical comparison here. Since there are two radiations, the addition of radiated noise level will occur as in Section 5.7.4.

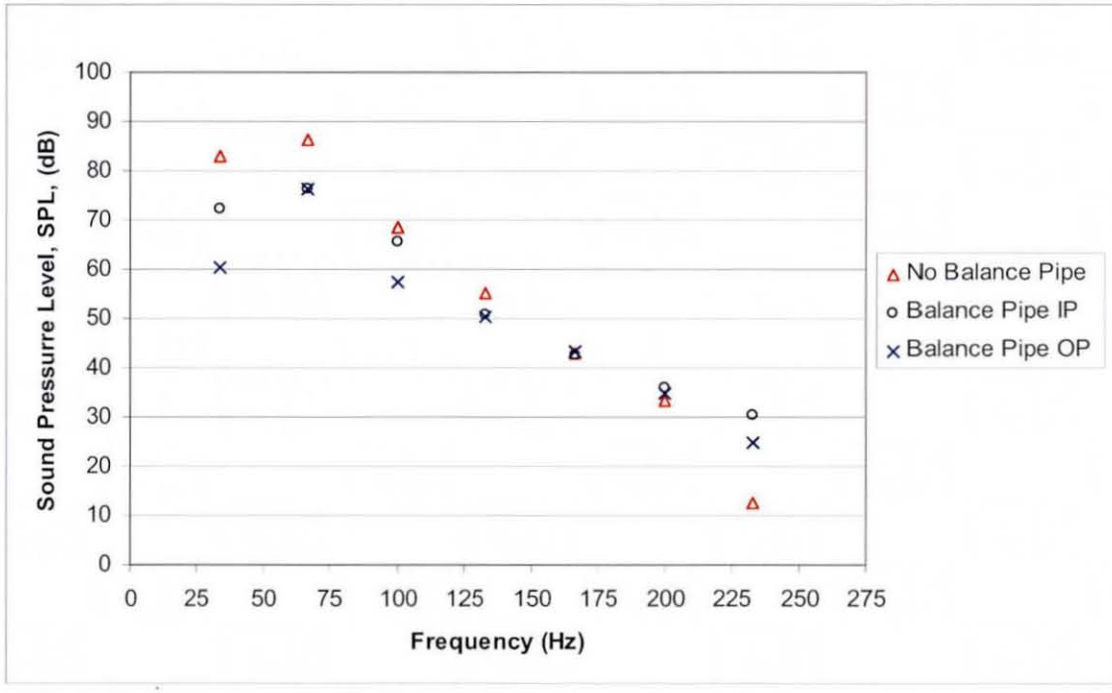

Figure 5. 23 Radiated sum of sound pressure levels from the system shown in Figure 5. 21 at multiples of firing frequency

Lastly, the only difference between 'Balance Pipe OP' and 'Balance Pipe IP' series, in Figure 5. 22, is that 'Balance Pipe OP' has a different firing order, namely valve 1, fires first followed by valves 5, 3, 7, 2, 6, 4 and then lastly valve 8. Each of the cylinders fire with an eighth of the time period for one complete valve cycle between them. Thus, the firing frequency is actually twice that of the other two systems shown in this figure and occurs at 66.66Hz. Again, since there are two radiations, the addition of radiated noise level will occur as in Section 5.7.4.

The predicted results shown in Figures 5.22 and 5.23 are sensible. The radiated noise levels are higher at multiples of firing frequency than in between, where noise cancellation should occur, and are highest at low engine orders. Furthermore, the

inclusion of a balance pipe is seen to reduce the maximum contributions to the overall radiated noise, as found in practice [97]. The reduction is slightly greater for the 'Balance Pipe OP' than the 'Balance Pipe IP' series, as might be expected [97]. Furthermore, the benefits of extra phase cancellation from the 'normal' firing sequence represented by the 'Balance Pipe OP' series is seen very clearly in Figure 5. 22 at odd multiples of the firing frequency, 33.33Hz, which are actually half-orders for this series. Again, the test at least serves to demonstrate that the algorithm and mathematical modelling of manifold/exhaust systems that involve balance pipes works for this complex system and produces results that are sensible.

5.8 Intermediate source validation test

Introducing an additional IS element requires validation of the acoustic modelling of both monopole and dipole sources. The simplest pipe network is a single straight pipe, the modelling of this is well known. Therefore, the additional behaviour of an intermediate source (IS) can be observed and compared to that of a uniform, straight pipe with an engine source of infinite impedance, see Figure 5. 24.

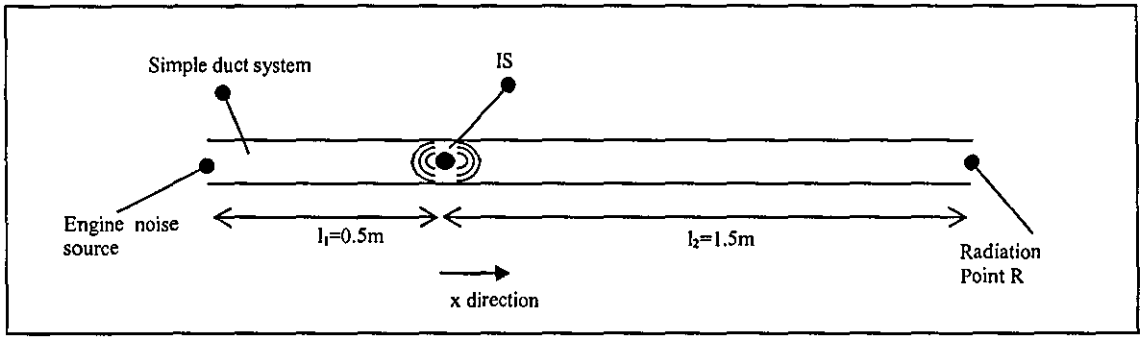

Figure 5. 24 Simple network with an intermediate source attached to an engine noise source

Figure 5. 24 illustrates a simple network with an added IS source located somewhere within the pipe, defined by lengths l_1 and l_2. The network in this figure can be characterised by a two-by-three transfer matrix, see Section 5.4.1. Let the intermediate

source strength be, say, P_{sk}=0.1m/s or V_{sk}=0.1m/s and incoherent with the engine source which has an infinite impedance, Z_s. Thus, equation (5.116) can be adapted to give the pressure at the radiation point

$$|P_r| = \left| \frac{\sum_{k=1}^{n} \left(f_{1(k+2)} P_{sk} \mid V_{sk} \right)}{f_{11} Z_r + f_{12}} Z_r \right|, \tag{5.138}$$

where Z_r is the radiation impedance. This is possible by setting point *1*, in conjunction with equation (5.116), to point *R* and using the relationship P_r=$Z_r V_r$, see Figure 5. 24. Now, let the intermediate source be placed 0.5m downstream of the engine source and 1.5m upstream of the radiation point. The temperature throughout the duct network is 350°C.

A valid comparison, or control, to the network in Figure 5. 24 with a non-zero intermediate source strength is achieved by setting that strength to zero and the velocity, V_0, at the engine source, to 0.1m/s and observing the pressure magnitude at the radiation point. The pressure at the radiation point is calculated by using equation (5.117), in conjunction with the relationship P_r=$Z_r V_r$. Figure 5. 25 and Figure 5. 26 show radiated pressure at the radiation point for monopole and dipole type intermediate sources respectively. A series that represents the control is also plotted on each graph.

A closed-open, uniform straight pipe resonates when the wavelength is any odd quarter multiple of the length of the pipe. Therefore, when l_1=0.5m and l_2=1.5, with respect to Figure 5. 24, where there is zero intermediate source strength and a known engine source strength with an infinite source impedance; then the pipe will resonate at 62.5Hz, 187.5Hz, 312.Hz etc. This is shown by the 'Control' series in Figure 5. 25.

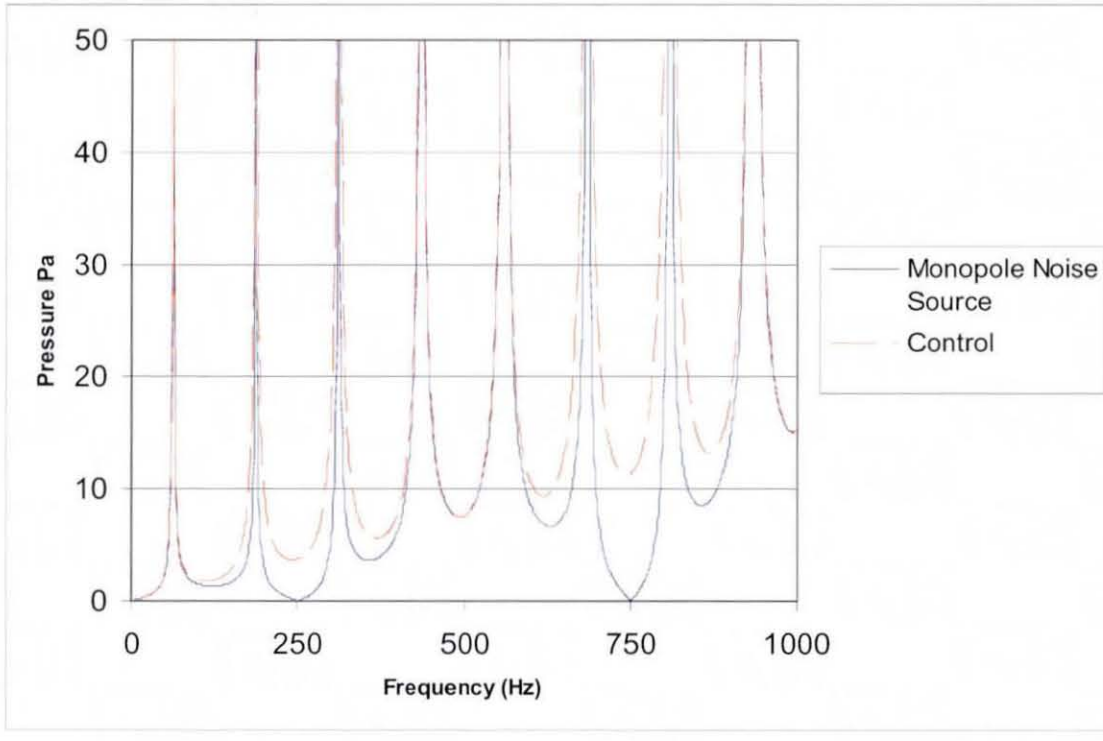

Figure 5. 25 Monopole results for the network shown in Figure 5. 24

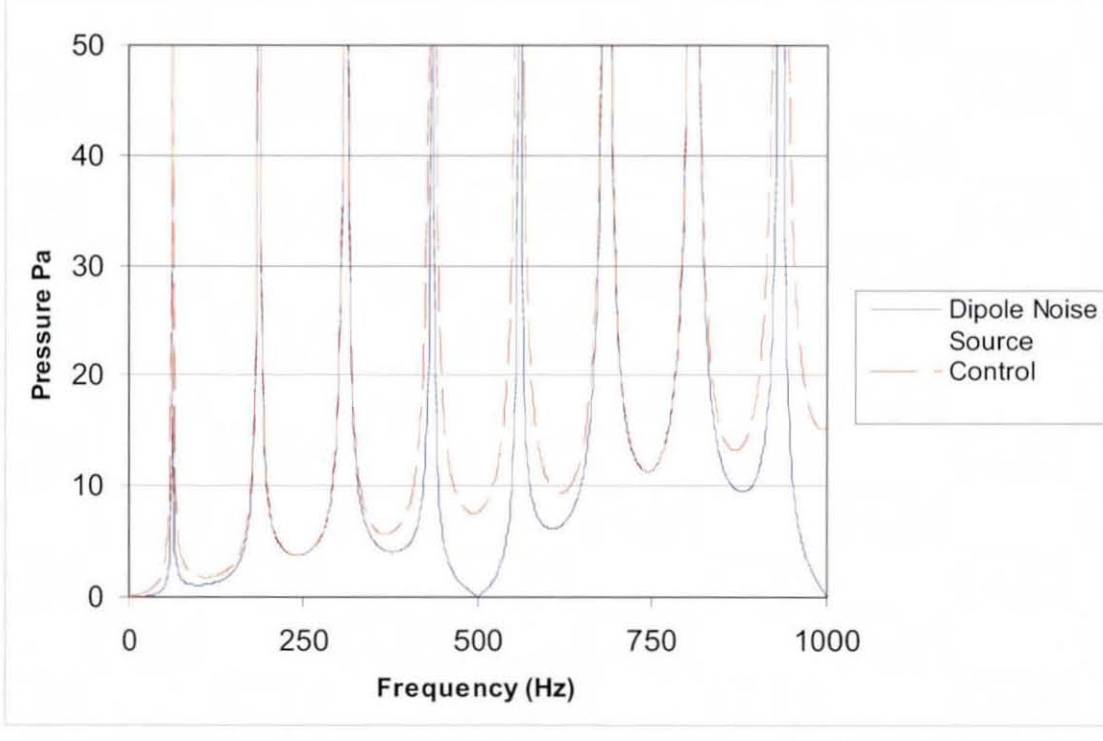

Figure 5. 26 Dipole results for the network shown in Figure 5. 24

When a monopole source is added 0.5m upstream of the engine source, exact cancellations occur when the wavelength is at odd quarter multiples of L_1. This occurs due to the reflective monopole source rebounding from the engine source, cancelling itself out when the acoustic wave reaches the intermediate source location. This is shown clearly on Figure 5. 25 where the evaluated pressure at 250Hz and 750Hz is zero, hence validating the monopole source modelling.

A dipole source acting within a straight pipe, see Figure 5. 24, creates a positive wave travelling in the 'x direction' and the negative wave travelling in the negative 'x direction'. Therefore, if the wave travelling towards the engine source has a wavelength of any half multiple of L_1, it will be exactly out of phase with the positive wave when it returns to the IS location; hence exact cancellation of the positive wave. An example of the code modelling this behaviour is shown in Figure 5. 26, where the evaluated pressure at 500Hz and 1000Hz is zero, hence validating the dipole source modelling.

5.9 Conclusion

The inclusion of multiple radiation points into the software capability of the hybrid algorithm has enhanced its usefulness and application area as a linear code for general silencer analysis. In addition, the ability to place non-primary radiation points anywhere in an exhaust system, which is connected to a manifold and thence to multiple time-variant sources, has demonstrated the versatility and flexibility of the hybrid algorithm. Even the inclusion of a balance pipe connecting two exhaust systems has been shown to be possible. Validation tests have verified that the algorithms work on complex as well as simple systems and the code generates sensible results.

Although the quantity of validation tests for intermediate sources are limited, the simple tests on monopole and dipole sources verify that the hybrid algorithm models these features correctly. Thus, the hybrid algorithm now admits the capability to model the

effects of flow generated noise and active noise control systems, although in the first instance, both the location and strength of all FGN sources would have to be known.

Flowchart 5.1, Extended single algorithm

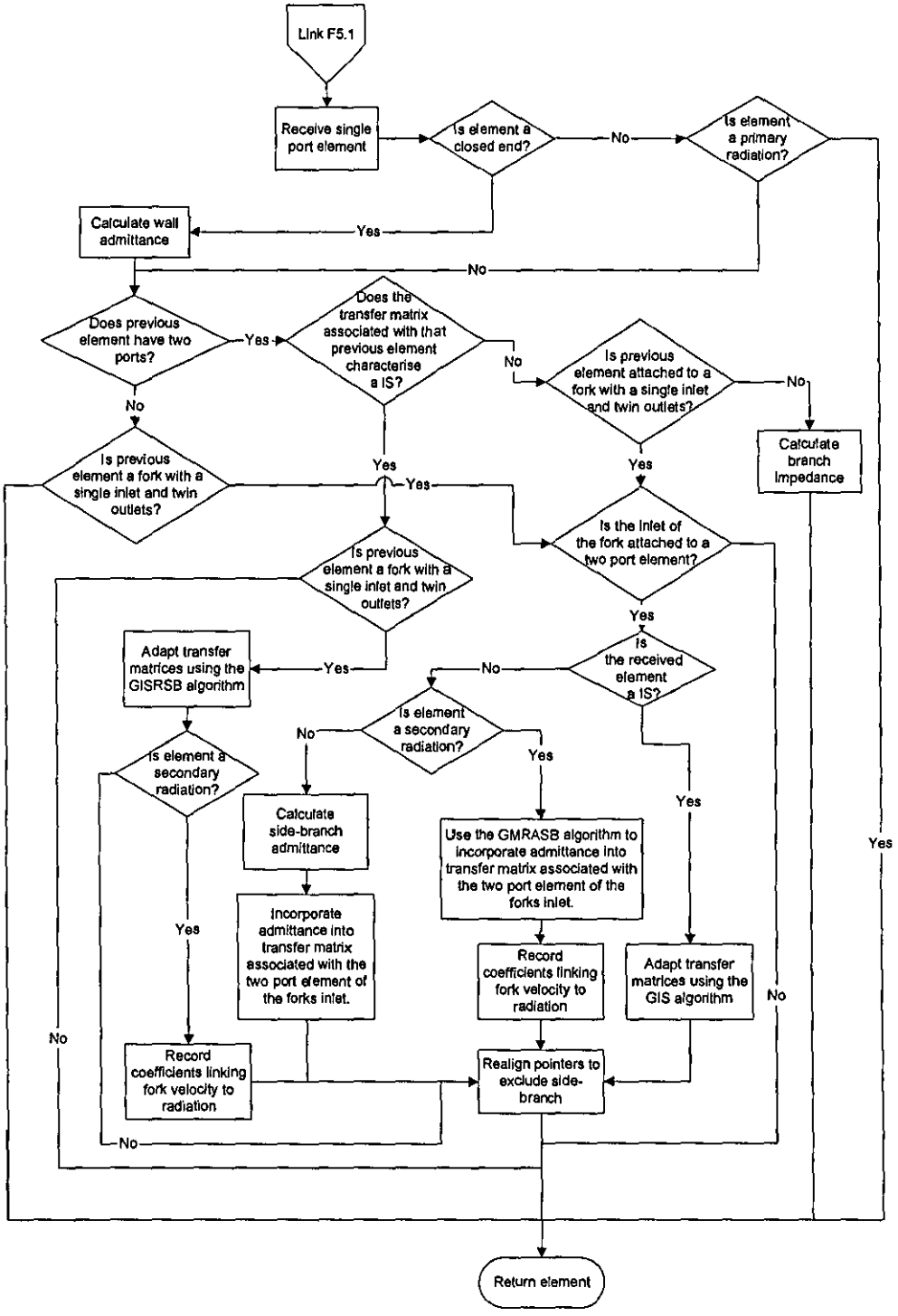

Flowchart 5.2, Transfer matrix multiplication algorithm

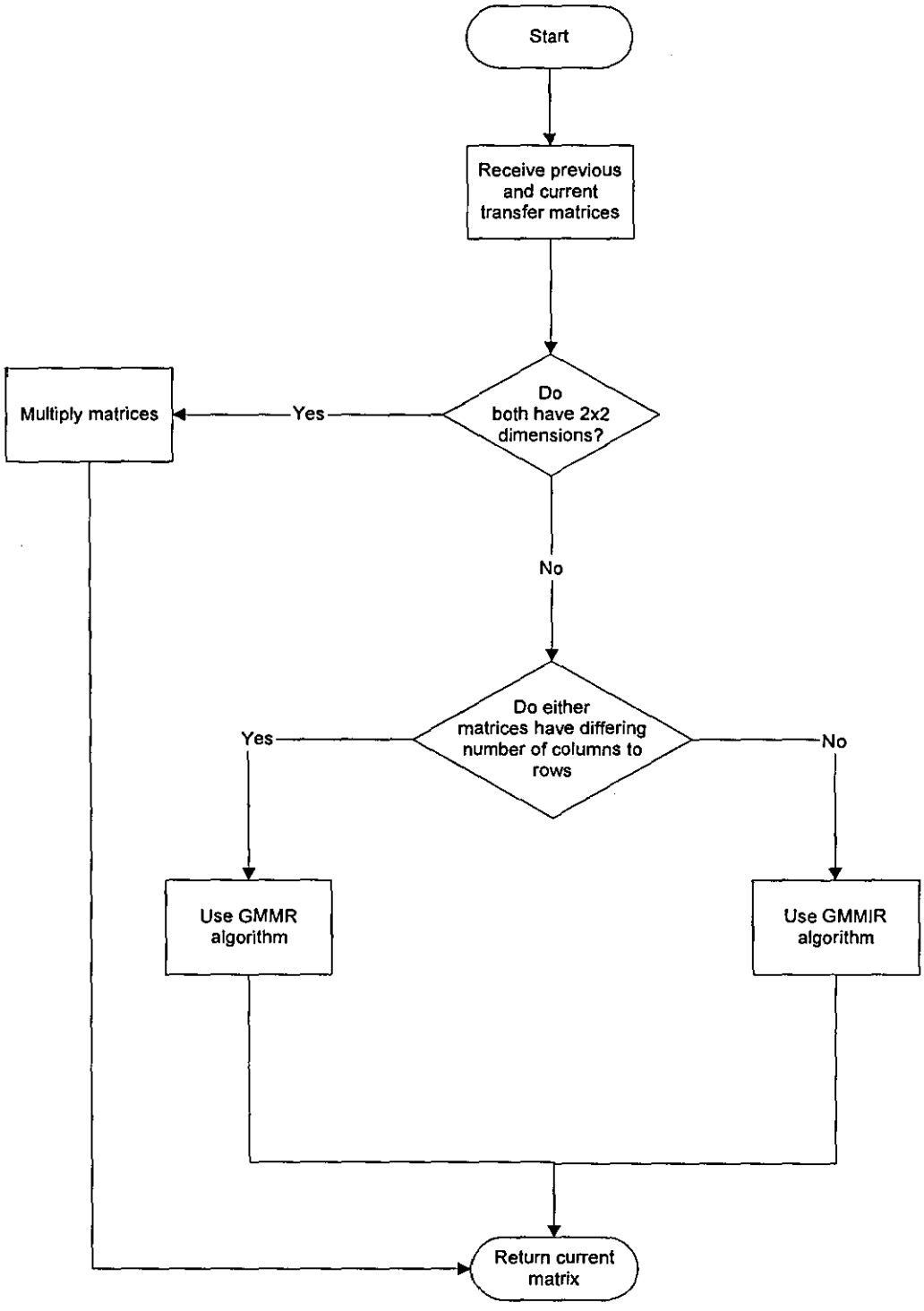

Flowchart 5.3, Multiple time-variant source reduction with multiple radiations algorithm

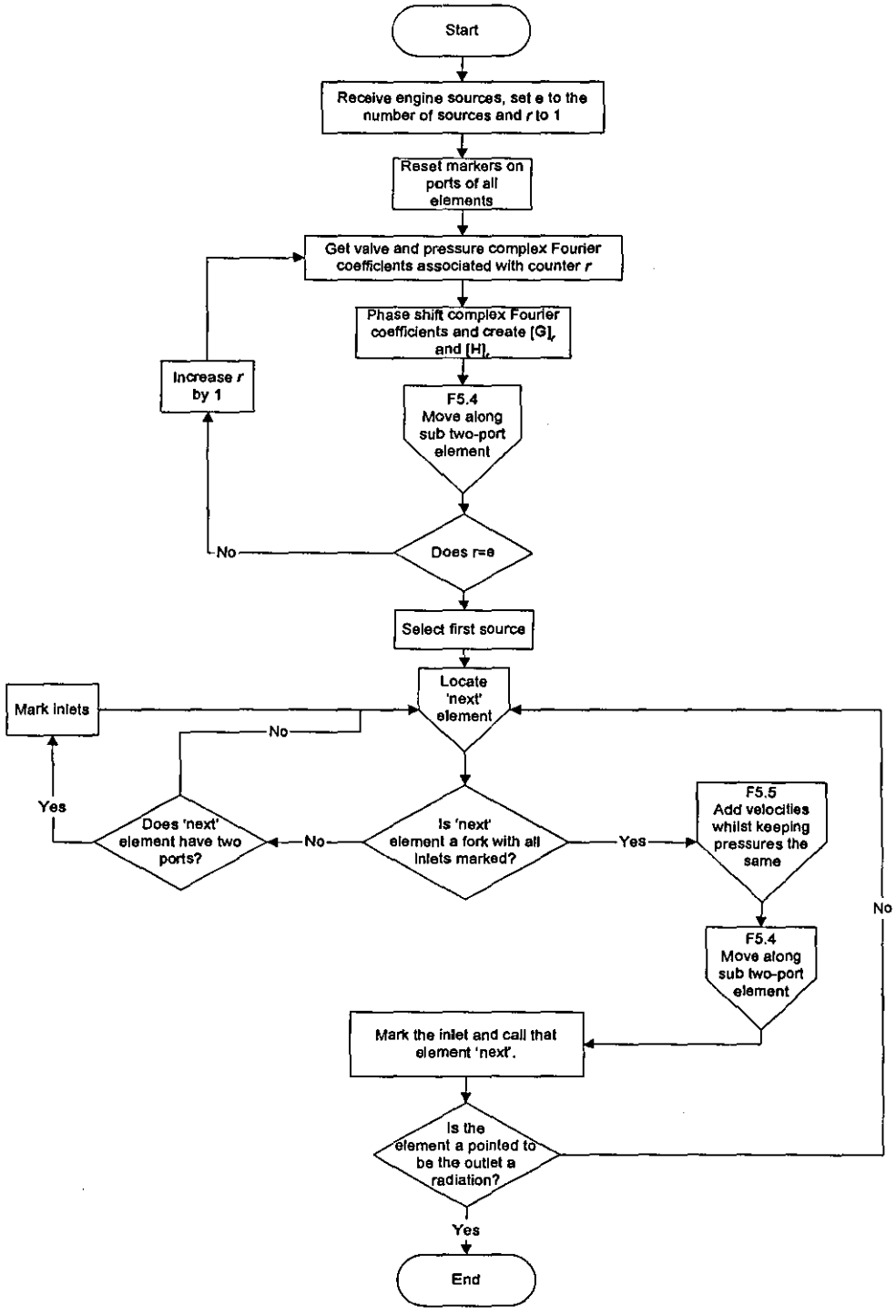

Flowchart 5.4, Sub two-port progression with time-variant sources and multiple radiations algorithm

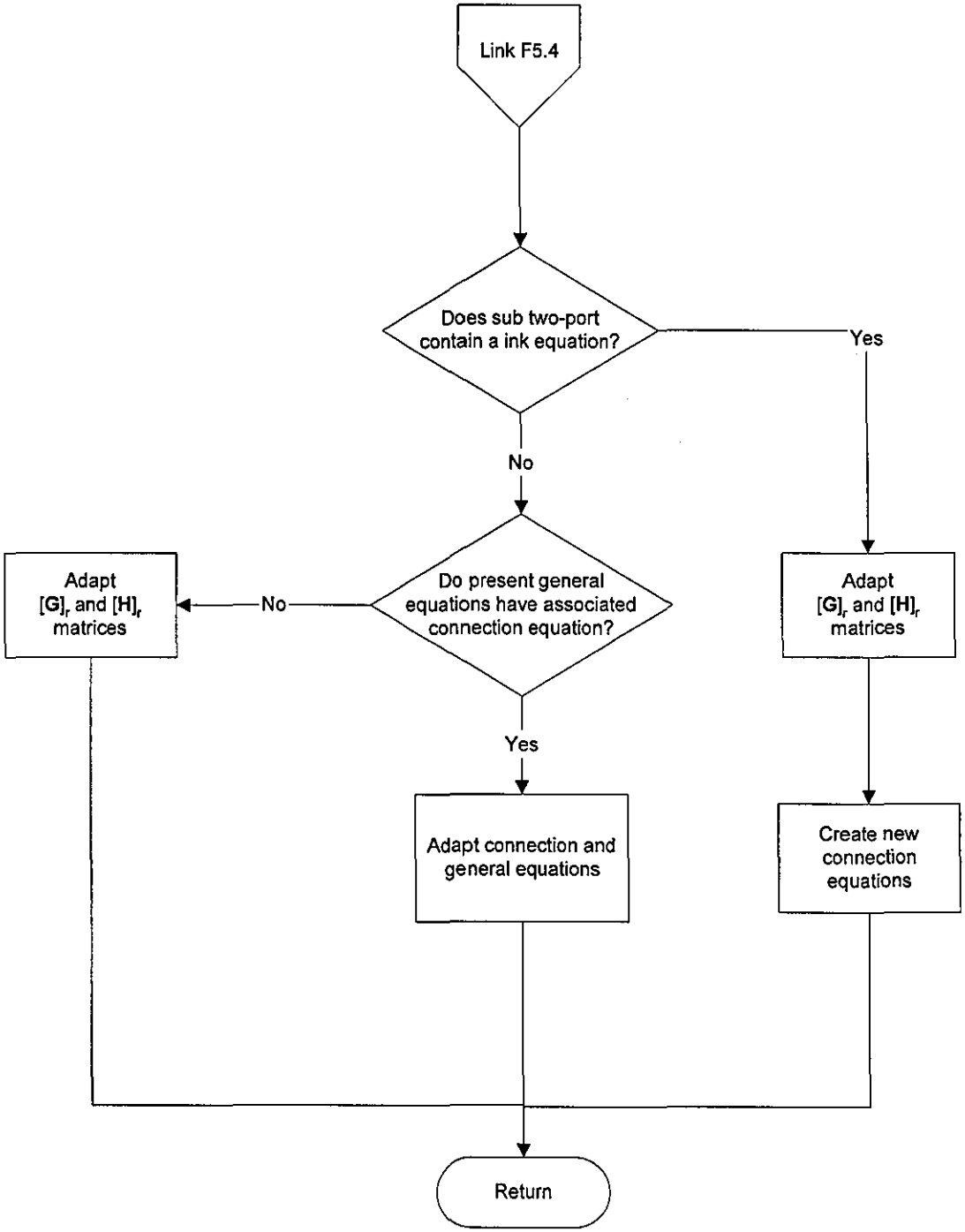

Flowchart 5.5, Fork calculations for time-varying reduction with multiple radiations algorithm

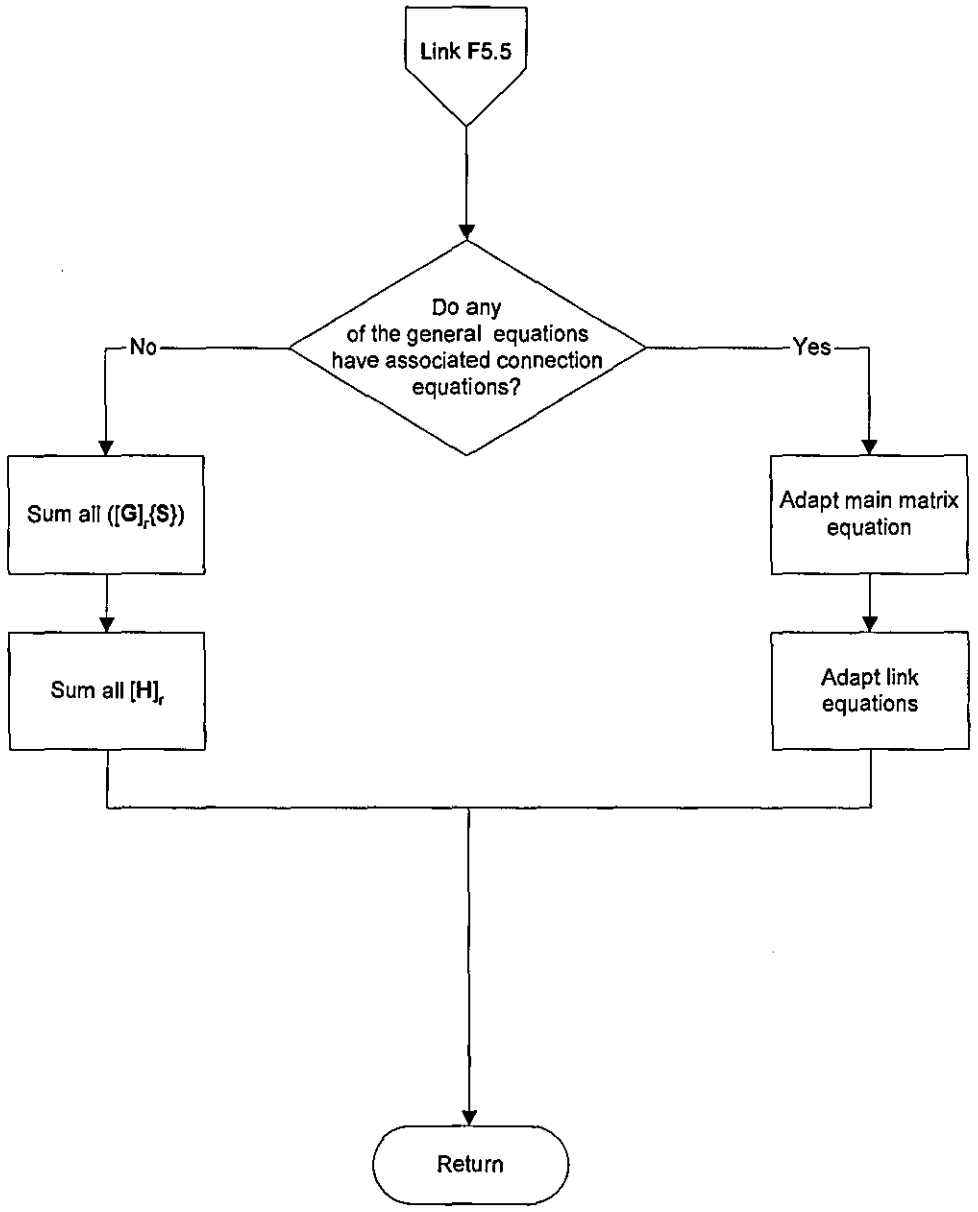

CHAPTER 6

Conclusions and Suggestions for Further Work

Prior to the work of the thesis, there was an existing software package, LAMPS [11], this was capable of modelling the frequency domain, linear, acoustics of exhaust systems. This software had dedicated algorithms that were capable of modelling a wide range of silencer geometries. Although the software algorithms were not general, they were fast. The commercial software package was also restricted by algorithmic constraints, such that exhaust systems had to have a sole inlet and outlet.

There was an alternative software processing program that addressed the problem of the non-generalities concerned with the conventional code of LAMPS. However, the alternative global code [15] was exceptionally slow. The hybrid algorithm developed within the thesis adopted the advantages of both the conventional [11,12] and global codes to maximise computational efficiency, whilst maintaining generality [9,10]. Thus, the use of C++ has utilised the flexibility, versatility and generality of object oriented programming [91] when writing linear, mathematical, acoustical software for manifold/exhaust systems. The identification of consecutively sequenced two-by-two exhaust components aided the simplification and speed of obtaining results; the use of path fractions to identify the smallest possible sub-systems was a key element in this work.

Transmission loss calculations do not require the use of source impedance, whereas they are necessary for insertion loss and external noise reduction calculations. LAMPS models the inlet of an exhaust system with an estimation for source impedance as an empirical constant. However, the characterisation of an inlet of an exhaust is time-dependent [72]; therefore, the concept of it being constant is flawed. In the thesis a method to model multiple, phase related, time-variant, engine sources within the

linear, frequency domain and an algorithm that incorporates any general manifold geometry [69] have been developed. General matrix equations were derived to relate the time-variant properties of an acoustic source at the inlet of a two-port element to that of the outlet.

A general equation was also derived to sum the incoming waves to a junction that resulted in one outward propagating wave. As the sources from the exhaust valves of the engine were coherent, summation of the waves could ensue, hence wave cancellation could occur. Complete wave cancellation was demonstrated in the work. This has provided a powerful analysis tool that has the ability to analyse any general manifold/exhaust system that has any general, time-variant valve and in-cylinder pressure.

A time-invariant source impedance is required when analysing the performance of exhaust systems, particularly when optimisation studies are required, as many thousands of exhaust system designs are evaluated during this process. Thus, improved characterisation and measurement methods of source impedance are required. Thus, the thesis investigated source impedance measurement methods. Both the indirect [71] and direct [72] measurement methods were modelled analytically. This showed that the entire concept of a single, complex value to characterise source impedance for a given frequency is flawed. The flaws are attributed to previous assumptions that the source impedance was considered time-invariant and is independent of the acoustic load. Even with the improved modelling capability of including multiple, time-variant sources, the analytical modelling of source impedance, via the indirect measurement method, yielded totally load dependent results.

The valve model for an idealized, inertial, linear, time-variant source was discovered to be modelled incorrectly. Thus, since there were no available experimental results to compare against results generated by the direct measurement method, a new, correct valve model for such a source was developed. The work, within the thesis, on the direct measurement method of source impedance also assessed the numerical effects of neglecting Fourier coefficients associated with the valve open area when $A_{\pm j}, j>N$.

This was found to increase the variations of results to those with non-zero $A_{\pm j}, j>N$, hence the results are more unstable. The analysis of the direct measurement method also confirmed that the resultant source impedance is highly dependent on the acoustic load.

New algorithmic capabilities were also developed to include the capability of reducing any exhaust system with multiple radiation points, monopole and dipole intermediate sources, thus widening the application area of this software code. The incorporation of multiple radiations, combined with time-variant multiple sources and the inclusion of a balance pipe, has created the potential for the software to analyse any manifold/exhaust without inlet and outlet restrictions. The inclusion of the capability to analyse intermediate sources, within the hybrid algorithm, has enabled the effect of flow generated noise and active noise cancellation sources within exhaust systems to be modelled.

Throughout work on this thesis, there have been areas of research that could have been investigated further to gain more efficiency, generality and modelling techniques. However, due to time, these possibilities have not been pursued. Therefore, these areas constitute possible further work, which could be achieved by the author or other researchers.

The algorithmic efficiency work focused on the algorithmic procedures and manipulation of data within a chosen programming language where C++ object oriented programming was used. The development of the program focused largely on the identification of consecutively sequenced and sub-systems of exhaust components, or objects, which were analysed repetitively. The fundamental change between each analysis was a single frequency variable change. Theoretical logs were created to track each procedure for subsequent analysis after the first analysis, this involved large copying functions. Further work to increase the computational efficiency of the hybrid algorithm could involve the exclusion of logs and copying functions. This work would involve the evaluation of transfer matrices for all required frequencies at the same time. Hence, each reduction of consecutively sequenced transfer matrices, two-port sub-systems and the complete exhaust system would happen for all frequencies

consecutively. This would be fundamentally different to the reduction of a whole exhaust system at a sole frequency, followed by the same analysis executed with a single variable change of frequency. A large amount of computer memory will be required to hold a significant amount of transfer matrix coefficients; however, this would be balanced by the shorter time required to hold the parameters for each exhaust component. Also, once a reduction or transfer matrix multiplication has occurred, there will be one or more objects that can be destructed [91].

The source models used for insertion loss calculations and for the indirect measurement method of source impedance both used a simplistic valve model. An obvious improvement is to implement the same idealized, inertial, linear, time-variant valve model in these areas, as was used in the work concerning the direct measurement method of source impedance. The work should consider the computational efficiency costs incurred, compared to the level of improved experimental prediction that it provides. The work concerning the prediction of insertion loss using a linear, time-variant engine source model could be extended to assess where a source model should be employed, as opposed to a single value that characterises the source impedance. This extension would observe the balance of accuracy and computational efficiency.

Non-linear modelling of the in-cylinder pressure is well researched [23,36] and achieves a good level of prediction. The source model in Chapter 3 requires a source vector which models a constant or known time-variant pressure curve. The source modelling research could be extended to incorporate a linearised version of the non-linear, in-cylinder pressure model; this would define the Fourier coefficients of the source pressure vector associated with the valve.

Since the thesis has included and validated the use of multiple radiations in conjunction with a balance pipe and multiple time-variant sources, comparisons of theoretical and experimental results are now needed; hence constituting further work. There is now a need for experimental results to provide data to compare with results from the theoretical work achieved within this thesis.

Algorithmic advances developed have included intermediate sources. Thus, if an exhaust system designer knows where a flow generated noise source is being produced, then the inclusion of a monopole, intermediate source in the software could allow a calculation of the affect that the source has on the noise at the radiation point. This would allow designers to separate the noise caused by the engine from that of the flow generated noise; however, more work is needed to calibrate various intermediate source parameters. Within exhaust systems, flow generated noise occurs primarily within perforated pipes of resonators; however, there is no experimental data to provide validation tests or comparisons. Thus, this experimental area of research needs to be developed in order to gain the full benefits of the algorithm capability developed in this thesis.

Further theoretical work could investigate active noise cancellation systems without the financial and labour cost incurred when building such systems. The addition of algorithmic theory to include monopole sources can allow exhaust system designers to evaluate theoretically the best position and strengths for loudspeakers within an exhaust system. These loudspeakers would be used in active noise cancellation systems.

The thesis has produced and implemented many algorithms that add new features and increased the efficiency and generality of the software package. However, the work has only considered the processing application. The implementation of the work to provide a useful scientific software package will require pre-processor and post-processor applications with graphical user interfaces. After the process application has analysed the exhaust system, there are many different types of outputs, Fourier coefficients, transfer matrices of different sizes, pressure or source impedance measurements etc. Thus, the post-processor application needs to know these types of results and how the processor stores these within various files. Eventually, once the three applications function cohesively, a commercially viable software package could be produced.

References

1. M.L.Munjal, 'Acoustics of Ducts and Mufflers with Application to Exhaust and Ventilation System Design', Wiley-Interscience Publication, New York, (1987).
2. BS ISO 362:1998 'Acoustics - Measurement of Noise Emitted by Accelerating Road Vehicles - Engineering Method', British Standard Institute (1998).
3. J.R.Smith(Edit.), 'Mathematics in the Automotive Industry', Clarendon Press, Oxford(1992).
4. R.G.White and J.G.Walker (Editors), 'Noise and Vibration', Ellis Horwood Ltd, Chichester England (1982)
5. F.P.Mechel(Editor), 'Formulas of Acoustics', Springer-Verlag, New York(2002).
6. D.E.Winterbone and R.J.Pearson, 'Theory of Engine Manifold Design. Wave Action Methods for I.C. Engines', Prof. Eng. Publications Ltd., London(2000).
7. I.Arbuckle, S.Naylor and M.Worthington, 'Optimization Strategies Applied to Exhaust System Design', SEA Paper 2002-01-0812.
8. A.Jackson and I.Arbuckle, 'Exhaust System Optimization for Drive by Noise', Proceedings of the I.Mech.E C605/006/2002.
9. J.F.Dowling and K.S.Peat, 'An Efficient and General Algorithm for the Acoustic Analysis of Silencers', Proceedings of InterNoise 2003, Cheju, Korea (2003), Paper N182.
10. J.F.Dowling and K.S.Peat, 'An Algorithm for the Efficient Acoustic Analysis of Silencers of Any General Geometry', Applied Acoustics (2004), 65, pp 211-227.
11. K.S.Peat, 'LAMPS Software for the Acoustic Analysis of Silencers', Proceedings of Euro-noise (1995), Lyon, France, pp 791-796
12. R.Glav PhD Thesis, 'On Acoustic Modelling of Silencer', Department of Vehicle Engineering, Royal Institute of Technology, Stockholm (1994)
13. J. Xia PhD Thesis, Loughborough University [to be published]
14. K.S.Peat and J.Xia, 'Accuracy of Linear Plane Wave Acoustic Modelling of Silencers', Proceedings of InterNoise 2003, Cheju, Korea (2003), Paper N172.

15. K.S.Peat, 'Computer Aided Design Development in Silencers', (LAMPS 3), Technical Report on LINK, Inland Surface Transport Programme, Project IST 046, Dept. of Aeronautical and Automotive Eng. Loughborough University (2003).
16. D.E.Winterbone and R.J.Pearson, 'A Solution of the Wave Equations Using Real Gases', Int. Journ. Mech. Sci.(1992), 34(12), pp 917-932.
17. Y.Sathyanarayana and M.L.Munjal, 'A Hybrid Approach for Aeroacoustic Analysis of the Engine Exhaust System', Applied Acoustics(2000), 60, pp 425-450.
18. K.S.Peat, 'Computational Prediction of Exhaust Noise' Proceedings of 6th International Congress, Zurich, Switzerland (1992), pp 77-80
19. P.O.A.L.Davis and M.F.Harrison 'Hybrid Systems for I.C. Engine Breathing Noise Synthesis', Proceedings Institute of Acoustics Southampton, Southampton (1993), pp 369-374
20. C.W.S.To, 'The Acoustic Simulation and Analysis of Complicated Reciprocating Compressor Piping Systems I : Analysis Technique and Parameter Matrices of Acoustic Elements', JSV(1984), 96(2), pp 175-194.
21. C.W.S.To, 'The Acoustic Simulation and Analysis of Complicated Reciprocating Compressor Piping Systems II : Program Structure and Applications', JSV(1984), 96(2), pp 195-205.
22. R.Singh and W.Soedal, 'Mathematical Modeling of Multi-cylinder Compressor Discharge System Interactions', JSV(1979), 63(1), pp 125-143.
23. R.S.Benson, 'The Thermodynamics and Gas Dynamics of Internal Combustion Engines', Vol I Edit. J.H.Horlock and D.E.Winterbone, Oxford Science Publications, O.U.P. (1982).
24. E.Jenny, 'Unidimensional Transient Flow with Consideration of Friction, Heat Transfer and Change of Section', Brown Boveri Rev. (1950), 37, pp 447-461.
25. R.J.Pearson and D.E.Winterbone, 'A Rapid Synthesis Technique for Intake Manifold Design', Int. Journ. of Vehicle Design (1989), 10(6), pp 659-686.
26. R.S.Benson, 'The Effects of Excess Scavenge Air on the Pressure Drop in the Cylinder of a Two-Stoke Cycle Engine During Exhaust Blow-down', J. R. Aero. Soc. Technical Notes (1955), 59, pp 773-778.
27. F.J.Wallace and G.Boxer, 'Wave Action Diffusers for Exhaust Pipe Systems, with Special Reference to the Scavenging of Two-Stroke Engines' Proc. Inst. Mech. Engrs. (1956), 170, pp 1131-1150.

28. R.S.Benson and W.A.Woods, 'Wave Action in the Exhaust of a Supercharged Engine Model', Int. J. Mech. Sci. (1960), 1, pp253-281.
29. M.Goyal, G.Scharpf and G.Borman, 'The Simulation of Similarly Cylinder Intake and Exhaust Systems', SEA(1967), paper 650451.
30. Courant and Fredrichs, 'Supersonic Flow and Shock Waves', Interscience Publishers, New York (1948)
31. R.J.Pearson and D.E.Winterbone, 'The Simulation of Gas Dynamics in Engine Manifolds Using Non-Linear Symmetric Difference Schemes', Proc.Inst.Mech. Eng.(1997), 211(part C), pp 601-613.
32. F.Payri, M.D.Chust and A.J.Torregrosa, 'Application of MacCormack Schemes to I.C. Engine Exhaust Noise Prediction', JSV(1996), 195(5), pp 757-773.
33. R.J.Pearson and D.E.Winterbone, 'Calculating the Effects of Variations in Composition on Wave Propagation in Gases', Int. Journ. Mech. Sci. (1993), 35(6), pp 517-537.
34. R.J.Pearson and D.E.Winterbone, 'A Rapid Wave Action Simulation Technique for Intake Manifold Design', SEA (1990), paper 900676
35. G.P.Blair, 'The Basic Design of Two-stroke Engines' Society of Automotive Engineers, USA (1990).
36. J.H.Horlock and D.E.Winterbone, 'The Thermodynamics and Gas Dynamics in Internal Combustion Engines - Vol II', Clarendon Press, Oxford, (1986).
37. A.D.Jones and G.L. Brown, 'Determination of Two-stroke Engine Exhaust Noise by the Method of Characteristics', JSV(1982), 82(3), pp 305-327.
38. AVL Website http://tec.avl.com
39. Ricardo Wave Website http://software.ricardo.com
40. GT-Power Website http://www.gtisoft.com/broch_gtpower.html
41. Lotus CFD Website http://www.cd-adapco.com/news/22/lotuscfd.htm
42. R.J.Pearson, M.D.Bassett, N.P.Fleming and T.Rodemann, 'An Approach to Model-Based Design', Lotus Engineering Software, Hethel UK, www.softscout.com
43. M.J.Crocker, 'Handbook of Acoustics', Wiley-Interscience Publication, New York (1988).
44. E.Dokumaci, 'An Exact Transfer Matrix Formulation of Plane Sound Wave Transmission in Inhomogeneous Ducts', JSV(1998), 217(5), pp 869-882.

45. P.O.A.L.Davies, 'Flow-Acoustic Coupling in Ducts', JSV (1981), 77(2), pp 191-209.
46. P.O.A.L.Davies, 'Practical Flow Duct Acoustics', JSV(1988), 124(1), pp 91-115.
47. R.J.Alfredson and P.O.A.L.Davies, 'Performance of Exhaust Silencer Components', JSV (1971), 15(2), pp 175-196.
48. S.Nygard, 'Low Frequency Modelling of Complex Duct Networks', Dept. of Vehicle Eng. Marcus Wallenberg Laboratory for Sound and Vibration Research, Stockholm(1999).
49. M.L.Munjal, 'Velocity Ratio-cum-Transfer Matrix Method for the Evaluation of a Muffler with Mean Flow', JSV(1975), 39(1), pp 105-119.
50. K.S.Peat, 'Transfer Matrix of a Uniform Duct with a Linear Temperature Gradient', JSV(1998), 123, pp 43-53
51. E.Dockumaci, 'On Transmission of Sound in a Non-uniform Duct Carrying a Subsonic Compressible Flow', JSV(1998), 210, pp 391-401.
52. V.Easwaran, M.L.Munjal, 'Plane Wave Analysis of Conical and Exponential Pipes with Incompressible Flow', JSV(1992), 152, pp73-93
53. K.S.Peat, 'The Acoustical Impedance at Discontinuities of Ducts in the Presence of Mean Flow', JSV(1998), 127, pp 123-132
54. M.L.Munjal and P.T.Thawani, 'Acoustic Performance of Hoses– A Parametric Study', Noise Control Engineering Journal (1996), 44, pp 274-278.
55. K.S.Peat, 'A First Approximation to the Effects of Mean Flow on Sound Propagation Through Cylindrical Capillary Tubes', JSV(1994), 175, pp 475-489
56. S.Allam and M.Abom, 'On Transmission of Sound in Diesel Particulate Filters (DPF:s)', Tenth International Congress on Sound and Vibration, Stockholm (2003), pp 3187-3194
57. P.M.Morse and K.U.Ingard, 'Theoretical Acoustics', Mcgraw-Hill Inc., New York (1968).
58. S.N.Rscheukin, 'A Course of Lectures on The Theory of Sound', Pergamon Press, London (1963).
59. J.W.Sullivan and M.J.Crocker, 'Analysis of Concentric-Tube Resonators Having Unpartitioned Cavities', JASA(1978), 64(1), pp 207-215.
60. K.S.Peat, 'A Numerical Decoupling Analysis of Perforated Pipe Silencer Elements', JSV(1988), 123(2), pp 199-212.

61. J.W.Sullivan, 'A Method for Modeling Perforated Tube Muffler Components. I. Theory', JASA(1979), 66(3), pp 772-777.
62. J.W.Sullivan, 'A Method for Modeling Perforated Tube Muffler Components. II. Applications', JASA(1979), 66(3), pp 779-788
63. K.Jayaraman and K.Yam, 'Decoupling Approach to Modeling Perforated Tube Muffler Components', JASA(1981), 69(2), pp 390-396.
64. P.T.Thawani and K.Jayaraman, 'Modeling and Applications of Straight-Through Resonators', JASA(1983), 73(4), pp 1387-1389.
65. M.L.Munjal,B.K.Behera and P.T.Thawani, 'Transfer Matrix Model for the Reverse-Flow, Three-Duct Open End Perforated Element Muffler', Journ Applied Acoustics (1998), 54(3), pp 229-238
66. G.D. Callow and K.S. Peat, 'Insertion Loss of Engine Intake and Exhaust Silencers' Proceedings of the I.Mech.E., C19/88, (1988), pp 39-46
67. K.S. Peat, G.D. Callow and P.A. Bannister, 'Improving the Acoustic Performance of an Intake System', Proceedings of the I.Mech.E., C420/021, (1990), pp 119-127
68. A.Frid, 'Fluid Vibration in Piping Systems - A Structural Mechanics Approach, I : Theory. II : Applications', JSV(1989), 133(3), pp 423-438 and pp 439-448.
69. J.F.Dowling and K.S.Peat, 'Source Impedance Model', Proceedings of the Eleventh International Congress on Sound and Vibration, ICSV11, St Petersburg, Russia (2004), Paper 691, pp 1-5.
70. W.M.Wang, 'Acoustical Analysis of a Multi-Cylinder Engine Air-Induction System', JASA(1967), 42(6), pp 1244-1249.
71. K.S.Peat and J.-G.Ih, 'An Analytical Investigation of the Indirect Measurement Method of Estimating the Acoustic Impedance of a Time-Varying Source', JSV(2001), 244(5), pp 821-835.
72. K.S.Peat, 'An analytical Investigation of the Direct Measurement Method of Estimating the Acoustic Impedance of a Time-varying Source', JSV(2002), 256(2), pp 271-285
73. W.M.Wang, 'Matrix Formulation in Acoustical Analysis of Mechanically Driven Fluid Systems', JASA(1967), 41(6), pp 1418-1423.
74. J.Lavrentjev and M.Abom, 'Characterization of Fluid Mechanics as Acoustic Multi-Port Sources', JSV(1996), 1971(1), pp 1-16.
75. H.Boden, 'Error Analysis for the Two-Load Method Used to Measure the Source Characteristics of Fluid Machines', JSV(1988), 126(1), pp 173-177.

76. M.G.Prasad, 'A Four Load Method for Evaluation of Acoustical Source Impedance in a Duct', JSV(1987), 114(2), pp 347-356.
77. H.Boden, 'On Multi-Load Methods for Determination of the Source Data of Acoustic One-Port Sources', JSV(1995), 180(5), pp 725-743.
78. L.Desmons and J.Hardy, 'A Least Squares Method for Evaluation of Characteristics of Acoustical Sources', JSV(1994), 175(3), pp 365-376.
79. H.Boden, 'The Multiple Load Method for Measuring the Source Characteristics of the Time-Variant Sources', JSV(1991), 148(3), pp 437-453.
80. S.-H.Jang and J.-G.Ih, 'Refined Multi-Load Method for Measuring Acoustical Source Characteristics of an Intake or Exhaust System', JASA(2000), 107(6), pp 3217-3225.
81. H.Boden PhD Thesis, 'Characterization of Fluid Machines as Sources of Fluid Borne Noise', Dept. Tech. Acoustics, Royal Inst. of Tech. Stockholm (1989).
82. K.S.Peat and J.Xia, 'The Influence of Mean Flow on the Characterisation and Effect of Flow-Generated Noise Sources', Proc.9th Int.Cong.Sound and Vibration, Florida(2002), Paper 251, pp 1-8.
83. E.I.Iudin, 'The Acoustic Power of the Noise Created by Air Duct Elements', Soviet Physics-Acoustics 1, 383-398. (1955)
84. C.G.Gordon, 'Spoiler Generated Noise I The experiment', JASA(1968), 43, pp 1041-1048.
85. CG.Gordon, 'Spoiler Generated Noise II Results', JASA(1969), 45, pp 214-223.
86. D.J.Oldham and A.U.Ukpoho, 'A Pressure-based Technique for Predicting Regenerated Noise Levels in Ventilation Systems', JSV(1990), 140, pp 259-272.
87. D.C. Waddington and D.J.Oldham, 'Generalized Flow Noise Prediction Curves for Air Duct Elements', JSV(1999), 222, 163-169.
88. F.H.Kunz, 'Semi-empirical Modal for Flow Noise Prediction on Intake and Exhaust System', SAE Technical Paper(1999), 99NV-68.
89. F.Kunz and P.Garcia, 'Simulation and Measurement of Hot Exhaust Gas Flow Noise With a Cold Air Flow Bench', SAE Technical Paper(1995), 950546.
90. C.F.Gerald and P.O.Wheatley, 'Applied Numerical Analysis', Addison-Wesley (6th Edition), Harlow, U.K. (1997).
91. H.Schildt, 'C++ The Complete Reference', Osborne, McGraw-Hill(1998), 3rd Edition, New York.

92. K.R.Irvine, 'C++ and Object-Orientated Programming', (Int. Edition), Prentice-Hall Inc., New Jersey (1997).
93. Arvin Meritor Website http://www.arvinmeritor.com
94. J.-G.Ih and K.S.Peat, 'On the Causes of Negative Source Impedance in the Measurement of Intake and Exhaust Noise Sources', Applied Acoustics(2002), 63, pp 153-171.
95. K.T.Hogskolan, Final technical report 'Acoustic Research on Turbo-charged Engine Modelling of Exhaust and Inlet Systems', Contract N° G3RD-2001-00511, Project N° GRD1-2000-25507, Date of issue 31/08/2004
96. K.S.Peat, A.J.Torregrosa, A.Broatch and T.Fernández, 'A Linear Acoustic Model of the Passive Effect of the Turbine of an Automotive', Journal of Sound and Vibration, Submitted 2004.
97. 'Private communications to Dr Peat at Loughborough University and Arvin Meritor'

Publications

Thus far, three publications have been based on the work in this thesis, namely:

- J.F.Dowling and K.S.Peat, 'An Efficient And General Algorithm For The Acoustic Analysis Of Silencers', Proceedings of InterNoise 2003, Cheju, Korea (2003), Paper N182.
- J.F.Dowling and K.S.Peat, 'An Algorithm for the Efficient Acoustic Analysis of Silencers of Any General Geometry', Applied Acoustics (2004), 65, pp 211-227.
- J.F.Dowling and K.S.Peat, 'Source impedance model', Proceedings of the Eleventh International Congress on Sound and Vibration, ICSV11, St. Petersburg, Russia (2004), Paper 691, pp 1-5.